

Archived in Dspace@nitr
<http://dspace.nitrkl.ac.in/dspace>

AN ANALYSIS OF STRAIN IN CHIP BREAKING USING SLIP-LINE FIELD THEORY WITH ADHESION FRICTION AT CHIP/TOOL INTERFACE

A DISSERTATION SUBMITTED TO
THE DEPARTMENT OF MECHANICAL ENGINEERING
NATIONAL INSTITUTE OF TECHNOLOGY,
ROURKELA (INDIA)



IN PARTIAL FULFILMENT OF THE REQUIREMENTS
FOR THE DEGREE OF
DOCTOR OF PHILOSOPHY

UNDER THE GUIDANCE OF

Prof. N S Das

and

Dr. C K Biswas

By

Balbeer Singh Chawla

July 2005

AN ANALYSIS OF STRAIN IN CHIP BREAKING USING
SLIP-LINE FIELD THEORY WITH ADHESION
FRICTION AT CHIP/TOOL INTERFACE

A DISSERTATION SUBMITTED TO
THE DEPARTMENT OF MECHANICAL ENGINEERING
NATIONAL INSTITUTE OF TECHNOLOGY,
ROURKELA (INDIA)



IN PARTIAL FULFILMENT OF THE REQUIREMENTS
FOR THE DEGREE OF
DOCTOR OF PHILOSOPHY

UNDER THE GUIDANCE OF

Prof. N S Das

and

Dr. C K Biswas

By

Balbeer Singh Chawla

July 2005

CERTIFICATE

This is to certify that the thesis titled “**An Analysis of Strain in Chip Breaking using Slip-Line Field Theory with Adhesion Friction at Chip/Tool Interface**” being submitted by Mr. Balbeer Singh Chawla to the National Institute of Technology, Rourkela for the award of the degree of DOCTOR OF PHILOSOPHY is a record of bonafide research carried out by him under our guidance and supervision. Mr. Chawla has worked for about five years on the above problem and the work has reached the standard fulfilling the requirements and the regulations relating to the degree. To the best of our knowledge the work incorporated in this thesis has not been submitted to any other University or Institute for the award of any other degree or diploma.

Dr. N. S. Das,
Professor Emeritus,
Mechanical Engineering Department,
National Institute of Technology,
Rourkela (India)

Dr. C. K. Biswas,
Asstt. Professor,
Mechanical Engineering Department,
National Institute of Technology,
Rourkela (India)

ACKNOWLEDGEMENT

The author expresses his deep sense of gratitude and indebtedness to his thesis supervisors, Prof. N S Das and Dr. C K Biswas, for providing valuable guidance, inspiring discussions and constant supervision throughout the course of this work.

He thanks Prof. B K Nanda, present Head of the Department and QIP Coordinator and former Heads and Q I P Coordinators Prof. N Kavi, Prof. A K Behera and Prof. P K Kar of Mechanical Engineering Department for providing various facilities for completion of this work.

The author would also like to thank Prof. Sunil Kumar Sarangi, former Director, NIT Rourkela and Prof. A K Mohanty, former Principal, REC, Rourkela for creating healthy working environment at NIT campus and for the timely help he received from them.

He is extremely grateful to Dr. S C Haldar, Mr. Alok Satpathy , Dr. C R Patra and Mrs. Simantini Behera for their inspiration and good company during these years. He remains obliged to Prof. K R Patel, Dr. S K Acharya, Dr. K P Maity and all other staff members of the Mechanical Engg. Department for their useful suggestions and for the help rendered to him in carrying out this work.

He will carry in his memory the company of Dr. P K Mahanta, Mr. S T Dundur, Mr. Naresh Prasad and Mr. S D Patle, all QIP Research Scholars at NIT Rourkela.

He is immensely grateful to Dr. U K Mohanty, former Head, Central Workshop and his staff for their cooperation and support in conducting the metal cutting experiments.

The author also expresses his gratitude to Dr. S Adak and Dr. J Bera of Ceramic Engg. Department for the help and encouragement extended to him during the time of experimentation.

Thanks are also due to his colleagues in the department of Mechanical Engineering, Government Engineering College, Bilaspur for their whole hearted support and

cooperation during the course of this work.

Author is also indebted to his mother and other near and dear ones for their blessings to carry out this work. He expresses his deep sense of gratitude to Prof. (Mrs.) P Das and Mrs. S Biswas for the affection showered by them during his stay at Rourkela. He shall remain indebted to Ms Ani for her selfless support, guidance and inspiration.

He is extremely grateful to his wife Mani and daughters Gagan and Prithvi for their tolerance, sacrifice, support and encouragement.

Finally, He wishes to acknowledge the financial support given to him by the Ministry of Human Resource Development, Government of India during his tenure of stay at National Institute of Technology, Rourkela and the Higher Education Department (Technical Education), Govt. of Chhattisgarh, for granting study leave to carry out this research work at NIT, Rourkela.

(Balbeer Singh Chawla)

ABSTRACT

Despite rapid growth in the applications of metal machining in manufacturing, a comprehensive analysis of the problem of chip control has always been a difficult task. This is because of the complex mechanism of the chip formation process and a lack of knowledge of the factors that influence chip form/chip breakability under a given set of input machining conditions such as work material properties, tool geometry, chip breakers and cutting conditions. Consequently, the solution to the problem has been approached empirically with a limited degree of success.

In the present investigation, an attempt has been made to examine chip breaking by a step-type chip breaker using the rigid-plastic slip-line field theory. Orthogonal machining is assumed and the deformation mode is analysed using the solutions proposed earlier by Kudo and Dewhurst. The rake face friction is represented by the adhesion friction law suggested by Maekawa *et al.* The fields are constructed and analysed by the matrix operational procedure developed by Dewhurst and Collins. Limit of validity of the fields has been determined from the consideration of overstressing of the rigid vertices at the chip and the workpiece and also from the consideration that friction angle along the tool face nowhere becomes negative. The extent of 'material damage' is assessed by computing the cumulative shear strain suffered by the material in passing through the primary shear line and secondary deformation zones, by a method due to Atkins *et al.* Variation of total strain, breaking strain and the chip curl radius as a function of the chip breaker height and its distance from the cutting edge is studied. The variation of strain across the chip thickness is estimated. The accuracy of prediction of the degree of chip breaking by some of the breakability criterion is examined in the light of rigid-perfectly plastic slip-line field theory.

It is found that as the chip breaker moves away from the cutting edge the radius of chip curvature (R_{chip}/t_0), tool-chip contact length (l_n/t_0), specific cutting energy (F_c/t_0), cutting ratio ζ and total strain ϵ_t in the chip increase while the breaking

strain and the secondary strain decrease. This observation is found to be influenced both by uncut chip thickness t_0 and tool rake angle γ . The cutting force increases as WTR increases and rake angle γ decreases, however, the reverse trend is exhibited by chip breaker force F_b . The amount of shear strain in the secondary deformation zone is found to be about 10 to 15 % of total strain. The trend of variation of total strain ϵ_t , specific cutting energy (F_c/t_0) and the breaking strain ϵ_b with chip breaker position supports the view that chip breaking is governed mainly by the breaking strain and not by “material damage” or by specific cutting energy consumed during machining.

Experimental investigation has been carried out to validate the theoretical observations. Orthogonal machining tests were carried out on mild steel tubes using HSS tools with 10 % cobalt. Chip breaking was accomplished using a step-type chip breaker. Chip thickness and chip curl radius were measured using an image analyser. For the chips, the shift in the position of the neutral axis from the centre was calculated using the theory of bending of curved beams. The chip curl radius before breaking was determined taking into account the elastic recovery of the chips. Breaking strain was calculated from a simplified formula, $\epsilon_b = t_{chip}/(2 R_{chip})$ and this was correlated with the degree of chip breaking. A procedure for chip breaker design to achieve effective breaking is also suggested.

It is seen that chip breakability criteria based on t_0 , t_{chip} and R_{chip} predict the effectiveness of chip breaking more accurately than those based on specific cutting energy and material damage.

NOMENCLATURE

B_0	=	Linear coefficient
CL	=	Linear Coulomb/adhesion friction operator
$\bar{\mathbf{c}}$	=	Column vector representing a circle of unit radius of curvature
d	=	Depth of cut
E	=	Modulus of elasticity of work piece
F_x, F_y	=	Traction components along cartesian coordinate directions
$F_{\bar{x}}, F_{\bar{y}}$	=	Traction components along moving coordinate directions
F_b	=	Chip breaker force
F_b/t_0	=	Normalised Chip breaker force
F_1, F_2	=	Forces perpendicular and parallel to chip breaker force
F_c	=	Cutting force
F_c/t_0	=	Specific cutting energy
H	=	Height of the chip breaker
HTR	=	H/t_0
I	=	Unit matrix
l_{chip}	=	Length of the chip
l_n	=	Contact length of the chip tool interface
l_n/t_0	=	Normalised contact length
M	=	Moment exerted by the slip-lines AB and BC
n	=	Index of stress distribution or constant based on material properties of the tool and work piece combinations
G, K, J, M	=	Matrix operators

(continued on next page)

$\mathbf{P}, \mathbf{Q}, \mathbf{P}^*, \mathbf{Q}^*$,	=	Standard matrix operators
$\mathbf{R}, \mathbf{S}, \mathbf{T}$		
p_C, p_D	=	Hydrostatic pressure at points C and D
R_{chip}^*	=	Radius of the chip curvature without spring back correction
R_{chip}	=	Radius of the chip curvature
R_{chip}/t_0	=	Normalised radius of curvature
R_L	=	Radius of the chip curvature when fracture occurs
R_o, R_i	=	Outer and inner radii of chip curvature
t_0	=	Uncut chip thickness i.e. Feed (in case of orthogonal cutting)
t_{chip}	=	Chip thickness
V_c	=	Cutting speed
W	=	Position of the chip breaker from the cutting edge of tool
WTR	=	W/t_0
X, Y	=	Cartesian coordinates
\bar{X}, \bar{Y}	=	Moving coordinates
α_1, α_2	=	Angles made by the primary shear line with free surfaces
$\epsilon_b, \epsilon_p, \epsilon_s, \epsilon_t$	=	Breaking, Primary, Secondary and Total shear strains
γ	=	Orthogonal rake angle of cutting tool
κ	=	Yield stress in shear of the work material
λ	=	Shear plane angle
μ	=	Low stress level friction coefficient
η_s	=	Chip side-flow angle
$\eta, \beta, \theta, \psi, \nu$	=	Slip-line field angles
ω	=	Angular velocity of chip curl
ϕ_C, ϕ_D, ϕ_E	=	Friction angles between slip-lines and tool's rake face
ρ	=	Scale parameter representing the geometrical scale of the field
ρ_u, ρ_s	=	Chip up-curl and side-curl radii
σ_0	=	Yield Stress

(continued on next page)

- $\sigma_1, \sigma_2, \sigma_3, \sigma_4$ = Column vectors representing slip-line curves
- σ_n = Normal stress
- τ = Shear stress
- ζ = Cutting ratio = t_{chip}/t_0

CONTENTS

<i>Certificate</i>	ii
<i>Acknowledgement</i>	iii
<i>Abstract</i>	v
<i>Nomenclature</i>	vii
1. <i>INTRODUCTION</i>	1
2. <i>SLIP-LINE FIELD CONSTRUCTION BY MATRIX METHOD</i>	30
2.1 Introduction	30
2.2 Series representation for radius of curvature of slip-line curves	33
2.3 Matrix representation of slip-line fields	34
2.4 Calculation of coordinates, traction and moment	39
2.4.1 Coordinates	39
2.4.2 Traction	40
2.4.3 Moment	41
2.5 Straight rough boundary operator	42
2.6 Adhesion operator	43
2.7 Subroutines	45
3. <i>SLIP-LINE FIELD ANALYSIS OF STRESSES AND STRAINS IN CHIPS ASSUMING NO SINGULARITY AT TOOL TIP</i>	46
3.1 Introduction	46
3.2 Slip-line field solutions	52
3.3 Method of solution	54
3.4 Streamline Plotting and Strain Estimation in Chips	61

3.4.1	Streamline Plotting	61
3.4.2	Strain estimation	65
3.5	Breaking strain estimation	71
3.6	Results and Discussion	71
3.7	Conclusions	94
4.	<i>AN EVALUATION OF CHIP BREAKABILITY CRITERIA USING SLIP- LINE FIELD ANALYSIS</i>	97
4.1	Introduction	97
4.2	Slip-line field solution	103
4.3	Method of solution	107
4.4	Streamline Plotting and Strain Estimation	110
4.4.1	Plotting of Streamline	110
4.4.2	Strain estimation	112
4.5	Results and Discussion	114
4.6	Evaluation of chip breakability criterion	138
4.7	Conclusions	141
5.	<i>PARTIAL EXPERIMENTAL VALIDATION OF MODEL</i>	142
5.1	Introduction	142
5.2	Experimental Setup and Procedure	143
5.3	Correction due to spring back	145
5.4	Correction due to shifting of neutral axis	151
5.5	Results and discussion	151
5.6	Chip breaker design	161
5.7	Conclusions	161
6.	<i>CONCLUSIONS</i>	178
	<i>Appendix</i>	180
A.	<i>Determination of linear coefficient</i>	181
B.	<i>Hill's criteria to check over-stressing of vertices</i>	183

C. Correction of breaking strain due to shifting of neutral axis 185

D. Determination of Aspect Ratio 188

Publications 201

Biodata 202

LIST OF TABLES

4.1	Chip Breakability Criterion	100
4.1	Chip Breakability Criterion (Contd.)	101
4.1	Chip Breakability Criterion (Contd.)	102
5.1	Specifications of items related with experimental work	144
5.1	Specifications of items related with experimental work (Contd.)	145
5.2	Experimental observations	166
5.2	Experimental observations (Contd.)	167
5.2	Experimental observations (Contd.)	168
5.2	Experimental observations (Contd.)	169
5.2	Experimental observations (Contd.)	170
5.2	Experimental observations (Contd.)	171
5.2	Experimental observations (Contd.)	172
5.3	Comparison of results of breaking strain ϵ_b with and without correction due to neutral axis shift	173
5.4	Experimentally determined chip breaking parameters	174
5.4	Experimentally determined chip breaking parameters (Contd.)	175
5.4	Experimentally determined chip breaking parameters (Contd.)	176
5.4	Experimentally determined chip breaking parameters (Contd.)	177

LIST OF FIGURES

1.1	Helix as a compound of two orthogonal circular arcs (a) Chip helix (b) Orthogonal circular arcs in XOY and YOZ planes	5
1.2	Up-curling	6
1.3	The motion of chip	8
1.4	Side-curling	9
1.5	Straight chip	10
1.6	Chips with no sidecurling (a) $\eta =$ positive (b) $\eta =$ zero (c) $\eta =$ negative	11
1.7	Chips with the sidecurling of normal direction (a) $\eta =$ positive (b) $\eta =$ zero (c) $\eta =$ negative	12
1.8	Chips with the sidecurling of opposite direction (a) $\eta =$ positive (b) $\eta =$ zero (c) $\eta =$ negative	13
1.9	Variation of chip form by upcurling and sidecurling when $\eta = 0$. . .	14
1.10	Variation of chip form by upcurling and sidecurling when $\eta = 15$. . .	15
1.11	Chip forms produced in machining operations	17
1.12	Chip breaking by sidecurling	20
1.13	Chip breaking by upcurling	20
1.14	Chip breaking by contact with tool flank in 3-D machining	21
1.15	Groove-type chip breaker	21
1.16	Step-type chip breaker	22
1.17	Ramp-type chip breaker	22
2.1	Physical plane showing stress system in plane plastic flow	31
2.2	A slip-line field net for demonstrating Hencky's theorems	32
2.3	A slip-line field net for series representation of radius of curvature . .	34
2.4	A slip-line field net for matrix representation of slip-line curves	35
2.5	Matrix operators generating singular field on the convex side of a slip-line curve	36

2.6	Shifting the origin of a slip-line curve	37
2.7	A slip-line field net for showing relation between radius of curvature of slip-line curves	38
2.8	Smooth boundary operator generating field between slip-line curve and straight frictionless boundary	39
2.9	Calculation of co-ordinates, traction and moment	40
2.10	Slip-line field adjacent to a straight rough boundary	42
2.11	Slip-line field adjacent to a curved boundary	43
2.12	Coulomb operator	44
3.1	(a) Merchant's shear plane model (b) Velocity field for corresponding model	47
3.2	Lee and Shaffer's model	48
3.3	Kudo's field for chip streaming	50
3.4	Kudo's field for chip curling	50
3.5	Dewhurst slip-line field	51
3.6	(a) Solution I with chip-breaker (b) Hodograph for corresponding field (not to scale)	55
3.7	Solution II with chip-breaker (b) Hodograph for corresponding field (not to scale)	56
3.8	Forces acting on chip in case of Solution I	58
3.9	Forces acting on chip in case of Solution II	59
3.10	Calculation of distance 'd' and radius of curvature R_{chip}	60
3.11	(a) Streamlines in the workpiece and chip (b) Construction for estimation of strain along the primary shear line (not to scale)	62
3.12	Construction for plotting of streamlines in the secondary deformation zone. (a) Slip-line field (b) Hodograph	64
3.13	Solution I with streamlines (Chip breaker not shown)	66
3.14	Flow zones for plotting of streamlines for solution II	69
3.15	Solution II showing streamlines of flow (Chip breaker not shown)	70
3.16	Variation of total strain ϵ_t and ϵ_p with chip-breaker position and feed, N= Negative friction angle limit	73

3.17	Variation of total strain ϵ_t and ϵ_p with chip-breaker position and feed, N= Negative friction angle limit	74
3.18	Variation of total strain ϵ_t and specific cutting energy (F_c/t_0) with chip-breaker position and rake angle γ , N= Negative friction angle limit	75
3.19	Variation of total strain ϵ_t and specific cutting energy (F_c/t_0) with chip-breaker position and rake angle γ , N= Negative friction angle limit	76
3.20	Variation of ϵ_t , ϵ_p , ϵ_s and ϵ_b with chip-breaker position, N= Negative friction angle limit	77
3.21	Variation of ϵ_t , ϵ_p , ϵ_s and ϵ_b with chip-breaker position , N= Negative friction angle limit	78
3.22	Variation of cutting ratio ζ with chip-breaker position and feed, N= Negative friction angle limit	79
3.23	Variation of cutting ratio ζ with chip-breaker position and feed, N= Negative friction angle limit	80
3.24	Variation of breaking strain ϵ_b with chip-breaker position and rake angle γ , N= Negative friction angle limit	82
3.25	Variation of breaking strain ϵ_b with chip-breaker position and feed, N= Negative friction angle limit	83
3.26	Variation of breaking strain ϵ_b with chip-breaker position and feed, N= Negative friction angle limit	84
3.27	Variation of breaking strain ϵ_b with chip-breaker position and friction coefficient, N= Negative friction angle limit μ	85
3.28	Variation of non-dimensionalized outer radius of chip curvature with chip-breaker position and rake angle γ , N= Negative friction angle limit	86
3.29	Variation of non-dimensionalized outer radius of chip curvature with chip-breaker position and feed, N= Negative friction angle limit . . .	87
3.30	Variation of non-dimensionalized outer radius of chip curvature with chip-breaker position and feed, N= Negative friction angle limit . . .	88
3.31	Variation of outer radius of chip curvature with chip-breaker position and feed, N= Negative friction angle limit	89
3.32	Variation of non-dimensionalized outer radius of chip curvature with total strain ϵ_t and feed, N= Negative friction angle limit	90

3.33	Variation of cutting ratio ζ with chip-breaker position and rake angle γ , N= Negative friction angle limit	91
3.34	Variation of non-dimensionalized contact length with chip-breaker position and rake angle γ , N= Negative friction angle limit	92
3.35	Variation of non-dimensionalized contact length with chip-breaker position and feed, N= Negative friction angle limit	93
3.36	Variation of non-dimensional chip breaker force with chip breaker position and feed, N= Negative friction angle limit	94
3.37	Variation of non-dimensional chip breaker force and cutting force with chip breaker position and rake angle γ , N= Negative friction angle limit	95
4.1	Aspect ratio	99
4.2	(a) Dewhurst's slip-line field with the geometry of chip-breaker and cutting tool (b) Hodograph for corresponding slip-line field (not to scale)	105
4.3	Forces acting on chip	106
4.4	Calculation of distance 'd' and radius of curvature R_{chip}	108
4.5	(a) Flow of streamlines in the workpiece and slip-line field (b) Hodograph for estimation of strain along the primary shear line (not to scale)	111
4.6	Dewhurst's slip-line field with streamlines (Chip breaker not shown)	113
4.7	Construction for estimation of strain in secondary deformation zone (not to scale) Ref Fig. 4.2(a) for corresponding slip-line field	115
4.8	Range of variation of radius of curvature with chip-breaker position and feed, N= Negative friction angle limit	116
4.9	Variation of total strain ϵ_t , breaking strain ϵ_b , specific cutting energy F_c/t_0 , cutting ratio ζ , normalized contact length l_n/t_0 with chip radius of curvature , N= Negative friction angle limit	117
4.10	Variation of total strain ϵ_t , breaking strain ϵ_b , specific cutting energy F_c/t_0 , cutting ratio ζ with contact length , N= Negative friction angle limit	118
4.11	Range of variation of breaking strain ϵ_b with chip-breaker position and feed, N= Negative friction angle limit	119
4.12	Range of variation of breaking strain ϵ_b with chip-breaker position and rake angle γ , N= Negative friction angle limit	120

4.13	Variation of total strain ϵ_t , primary shear strain ϵ_p , secondary zone shear strain ϵ_s and breaking strain ϵ_b with chip-breaker position, N= Negative friction angle limit	122
4.14	Range of variation of secondary shear strain ϵ_s with chip-breaker position and feed, N= Negative friction angle limit	123
4.15	Range of variation of secondary shear strain ϵ_s with chip-breaker position and rake angle γ , N= Negative friction angle limit	124
4.16	Range of variation of total strain ϵ_t with chip-breaker position and feed, N= Negative friction angle limit	125
4.17	Range of variation of total strain ϵ_t with chip-breaker position and rake angle γ , N= Negative friction angle limit	126
4.18	Range of variation of cutting ratio ζ with chip-breaker position and feed, N= Negative friction angle limit	127
4.19	Range of variation of cutting ratio ζ with chip-breaker position and rake angle γ , N= Negative friction angle limit	128
4.20	Range of variation of specific cutting energy (F_c/t_0) with chip breaker position and feed	129
4.21	Range of variation of specific cutting energy (F_c/t_0) with chip breaker position and rake angle γ , N= Negative friction angle limit	130
4.22	Variation of total strain ϵ_t , cutting ratio ζ and specific cutting energy (F_c/t_0) with chip-breaker position and friction coefficient μ	131
4.23	Variation of breaking strain ϵ_b with chip-breaker position and friction coefficient μ , N= Negative friction angle limit	132
4.24	Range of variation of non-dimensionalised contact length with chip-breaker position and feed, N= Negative friction angle limit	133
4.25	Variation of non-dimensionalised contact length with chip-breaker position and rake angle γ , N= Negative friction angle limit	134
4.26	Variation of non-dimensional chip breaker force and cutting force with chip breaker position and rake angle γ , N= Negative friction angle limit	135
4.27	Variation of primary and total strain across the normalized chip thickness with chip breaker position	136
4.28	Variation of total strain across the normalized chip thickness with feed	137

4.29	Comparison of various Chip Breaking Criterion	139
5.1	Turning operation on HMT Lathe	146
5.2	Grinding of tools rake face on CNC surface grinder	147
5.3	Welding of chip breaker on tool rake face	148
5.4	Measurement of chip features	149
5.5	Chip forms produced in machining operations	150
5.6	Chip radius of curvature with and without spring back	151
5.7	Variation of cutting ratio ζ with chip-breaker position for higher feed	152
5.8	Variation of cutting ratio ζ with chip-breaker position for lower feed	153
5.9	Variation of breaking strain ϵ_b with chip-breaker position for higher feed	154
5.10	Variation of breaking strain ϵ_b with chip-breaker position for lower feed	155
5.11	Variation of breaking strain ϵ_b with chip-breaker position with and without spring back (SB) correction	156
5.12	Variation of normalized chip radius of curvature with chip-breaker po- sition	158
5.13	Variation of chip radius of curvature with chip-breaker position with and without spring back (SB) correction	159
5.14	Variation of breaking strain ϵ_b with normalized chip radius of curvature, considering all three fields	160
5.15	Variation of chip breakability parameters with chip breaker position .	162
5.16	Variation of chip breakability parameters with feed	163
5.17	Variation of breaking strain ϵ_b and radius of curvature with chip- breaker position	164
A.1	Angular coordinates of any point on the tool face	181
B.1	Hill's criteria to check over-stressing of vertices	184
C.1	Estimation of breaking strain	186
D.1	Determination of length of chip outside the chip breaker groove . . .	189

1. INTRODUCTION

With the development of advanced manufacturing technology, metal machining operations are now being carried out at high speeds to secure maximum production. The disposal of long continuous chips produced at high cutting speeds has posed a problem for industry. For easy disposal of chips the volume of chips relative to the volume of the same material in bulk should be as low as possible. Long chips curl around the tool and can pose serious hazards to the work piece surface, the operator and the machine-tool operations. The situation becomes more critical with the present day tendency toward achieving increased material removal rates under the environment of automated machine loading and unloading and in-process inspection of the machined parameters of the work piece without close human supervision. This requires very reliable machining processes where, the normal variations of the input parameters of the machining process such as variation in work material properties can be taken care of by the robustness of the system or by suitable monitoring and adaptive control process and effective chip control which aids in the occurrence of acceptable chip forms which can be evacuated easily and reliably from the working zone.

Chip control may be defined as the predictability of chip form/ chip breakability for a given set of input machining conditions including work material properties, tool geometry, chip breakers and cutting conditions. However it is difficult to achieve this with a high degree of accuracy due to a lack of suitable predictive theories or applicable methods. The chip form and size is important for the design of cutting tools such as drill, broach, milling cutters etc., because a poor design brings about clogging of chips resulting in the breakdown of the tool. Higher reliability of chip control is also required in small batch production, automatic selection of cutting tools and conditions by CAPP systems and automated machining processes. Inconvenient chip forms lead to additional costs due to scrap parts, lost machining time and delays

in the delivery of parts. In general, it has been shown that efficient chip control in machining contributes to reliability of the machining process, production of high quality machined surfaces, increased productivity and safety of operation including operator's safety and protection of machine tool and cutting tool.

In metal machining a thin layer of work material is removed from the work piece and is transformed into a chip by the mechanical action of the cutting tool. The principal mechanism in this mode of metal removal has been recognised to be a shearing process which takes place along a shear plane. By the shearing action, the work material is plastically deformed and separated from the work piece. The nature of chip forming process, however, is extremely variable, the exact mechanism or combination of mechanisms depending upon the metallurgical aspects of tool-work piece pair, the undeformed chip thickness, the tool rake angle, the cutting temperature and the sharpness of the tool [1].

The first classification of the chip form on the basis of 'chip appearance' was made by Ernst and Merchant [2]. These investigators recognised only three types of chip forms. These are

- a. continuous or ribbon type chips
- b. discontinuous chips
- c. continuous chips with built-up edge interposed between the chip and the tool in the vicinity of the cutting edge.

This basic classification of chips is termed as 'known classification' in metal cutting.

Loladze [3] classified chips into five different types as

- a. Irregularly shaped chips
- b. Continuous chips (i) no built-up edge (ii) with built-up edge
- c. Elemental chips
- d. Jointed chips or partially continuous chips.

Jawahir *et al.* [4] considered three basic types of chip forms on the basis of their formation mechanism as

- a. Continuous chips based on quasi-static 2-D chip formation models in which continuity of material is maintained and which shows a Pseudo-stationary plastic deformation in the shear zone.
- b. Segmented chips based on dynamic chip formation model which is composed of a number of more or less connected elements usually resulting from a periodic variation of the height of the retarded layer which leads to alternating zones of concentrated but very little shear deformation in the chip.
- c. Elemental chips based on 2-D dynamic model which is predominantly formed in separate (not connected) elements usually resulting from breaking rather than from shearing of the work material.

In two dimensional or orthogonal cutting operations the only variables influencing the chip form are the cutting velocity, chip up-curl and the back flow angle as in restricted contact tools. The chip produced is initially tightly curled but the radius of chip curvature is forced to increase gradually as cutting proceeds. This gradual increase in chip-curvature radius imposes gradually increasing stresses in the chip eventually causing breakage and resulting in ‘spiral’ chips. If the chip does not have a natural curl as in the case at high cutting speeds and no chip breaker is present, ‘straight or ribbon’ type chips are produced that can become ‘snarled’ if the cutting process is continuous. With a chip breaker present, the chip is curled, but because of the restriction imposed on its path it strikes the transient surface of the work piece and continuously breaks into small fragments. These fragments, known as ‘loose arc’ chips often fly off violently from the cutting region and present a hazard to the machine operator.

It has been suggested that the chip form is heavily dependent on tool/chip contact length. Hence factors such as tool material, work material, tool geometry, cutting conditions and cutting fluid that affect the contact length also affect the chip form [5]. This is because in metal machining the chip curl radius that governs the chip form is strongly influenced by chip thickness ratio which in turn depends on tool chip contact length. Hence, variation in contact length as a consequence of the variation in the cutting speed and tool geometry resulting in a variation in chip deformation is considered by some to be the main factor governing the final chip form [5].

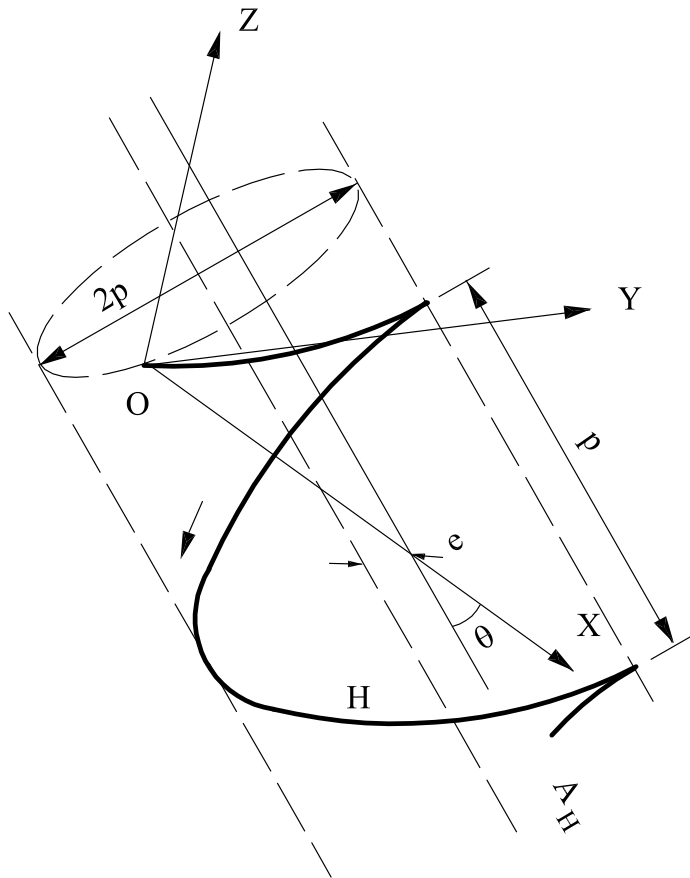
Mechanism of chip formation in three dimensional or oblique cutting process is rather complex. Analysis of chip formation in this mode of cutting has been carried out in the past by a number of investigators such as Kharkevich and Venuvinod [6], Seah, Rahman, Li and Zhang [7], Seethalar and Yellowley [8], Arsecularatne, Mathew and Oxley [9], Rubenstien [10] and Lau and Rubenstein [11]. The work of Nakayama *et al.* [12, 13] however, seems to represent the currently reigning paradigm concerning the geometric features of three dimensional chip forms.

According to Nakayama *et al.* [12, 13] the chip in three dimensional mode of cutting has a screw surface in general if all conditions are kept unchanged. Cylindrical and flat surfaces are included in the family of screw surfaces in its extremity. When the shape and position of a helix on the screw surface are determined in relation to the cutting edge, the real shape of chip and its position relative to cutting tool can be obtained by embodying the helix with the width and thickness of chip. These authors represent each helical trajectory on this screw surface in terms of its radius ρ , pitch p and the angle θ , between the axis of the helix and the tool rake plane (Fig. 1.1). Further, they suggest that the geometric form of the chip is completely determined by the velocity and curl states of the chip at the moment the chip leaves the tool-chip separation line.

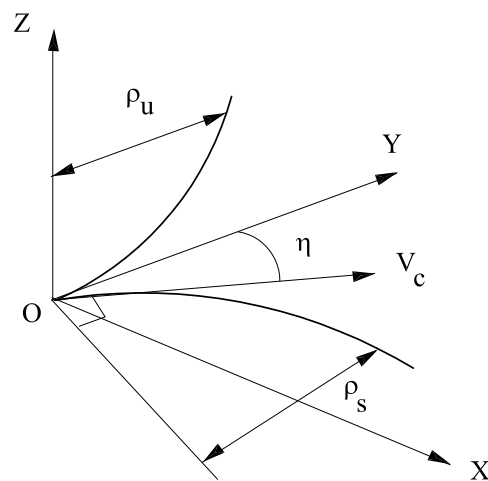
The chip after striking the rake surface curls away from it. The curling may take place either in the plane normal to rake surface which is termed as up-curl, or it may curl in the plane parallel to rake face which is called side-curl. According to Fang [14] a third pattern of chip curl termed as lateral curl may also exist in machining where the chip rotates in a plane perpendicular to the earlier two planes. Nakayama *et al.* [13] however, point out that the chip rotation can have only two components of angular velocity ω_x and ω_z due to up-curl and side-curl respectively and the third component of angular velocity, $\omega_y = 0$.

Most previous theories of natural chip curl have suggested that the chip is curled due to the conditions existing in one or other of the deformation zones. Early theories indicated that chip curl has origins in the primary deformation zone and several mechanisms as to how this is effected have been proposed.

Ernst and Merchant [2] suggested that curl was due to a variation in velocity of different parts of the chip through the primary deformation zone. Lee and Shaffer [15]



(a)



(b)

Fig. 1.1: Helix as a compound of two orthogonal circular arcs (a) Chip helix (b) Orthogonal circular arcs in XOY and YOZ planes

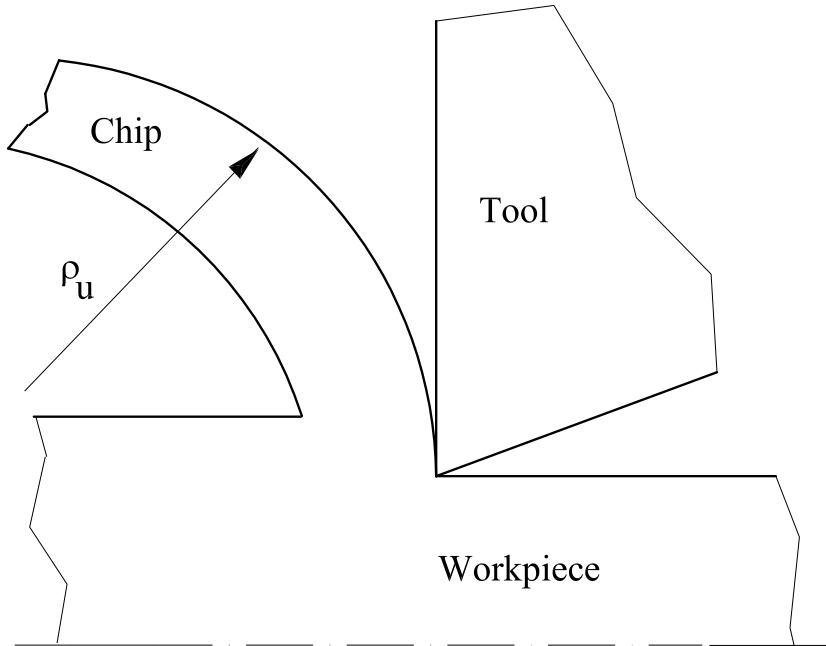


Fig. 1.2: Up-curling

and Hahn [16] ascribed chip curl to the effect of thermal strains and residual stresses set up in this zone. Nakayama *et al.* [17] suggested that under certain cutting conditions the built up layer is triangular in shape with the upper most side concave. It was proposed that the chip followed this contour and was thus curled. Ponshe [18] considered chip curl to be a consequence of the variation of the residual shear strains across the thickness of the chip. Rubenstien [19] and Albrecht [20] were of the opinion that chip curl was due to the non-collinearity of the resultant forces on the tool and the shear plane that results in a bending moment.

Up-curling (Fig. 1.2) takes place due to variation in velocity across the thickness of the chip. This radius of upward curvature is approximately equal to the radius of chip flow circle which is determined by the geometry of the chip former and tool-chip contact length. Actual radius, however, is somewhat larger than this due to the elastic recovery under free state [12].

Radius of chip flow circle in orthogonal machining has been determined by using slip-line field analysis by Kudo [21], Dewhurst [22, 23], Maity and Das [24], Fang [25, 26, 27, 28] for machining with a sharp tool and by Shi and Ramalingam [29] for

machining with a tool with finite flank wear land. Significant contributions in this direction have also been made by Henriksen [30] and Hahn [16]. Up-curl radius in 3D-chip forms has been estimated by Kharkevich *et al.* [6].

The chip curling mechanism has been studied extensively by Jawahir and Oxley [31] for machining with tools with a groove-type chip breaker. For a given undeformed chip thickness these authors observed an increase in chip curvature or a decrease in chip curl radius with decrease in tool restricted contact.

Nakayama [32] in his work observed the chip up-curl as a natural phenomenon and considered the effect of chip breakers and built-up edge. Worthington and Redford [33] considered the chip up-curl as resulting from a stable built-up edge.

In machining it is normally assumed that the tool-chip separation line (TCSL) is parallel to the cutting edge. In actual practice, however, this is not so and TCSL is inclined to the cutting edge at a small angle (Fig. 1.3). When this is the case the velocity of the chip varies across its width giving rise to chip side-curl (Fig. 1.4). Certain cutting conditions and tool geometric parameters cause chip side-curl. Following early models of chip side-curl suggested by Nakayama [12, 13], Bhaktavachalam and Venuvinod [34] it has been shown that several factors influence chip side-curl. These may be summarised as [4]

- a. Cutting edge is not straight
- b. Primary motion is not rectilinear
- c. Cutting edge is not perpendicular to primary motion, and
- d. Chip compression rate varies along the chip width.

The above factors cause variations in the chip velocity along the chip width resulting in chip side-curl. Based on the results of an extensive experimental investigation a direct relationship between the chip side-curl radius and the chip side-flow angle has been reported by Van Luttervelt [4]. The effect of contact length on chip side-curl has been visualised through a simple experiment by De Chiffre [4]. Using a tool having a variable contact length across the rake face, a chip side-curl was produced when machining dry. The use of a lubricant inhibits the side-curling, since a constant

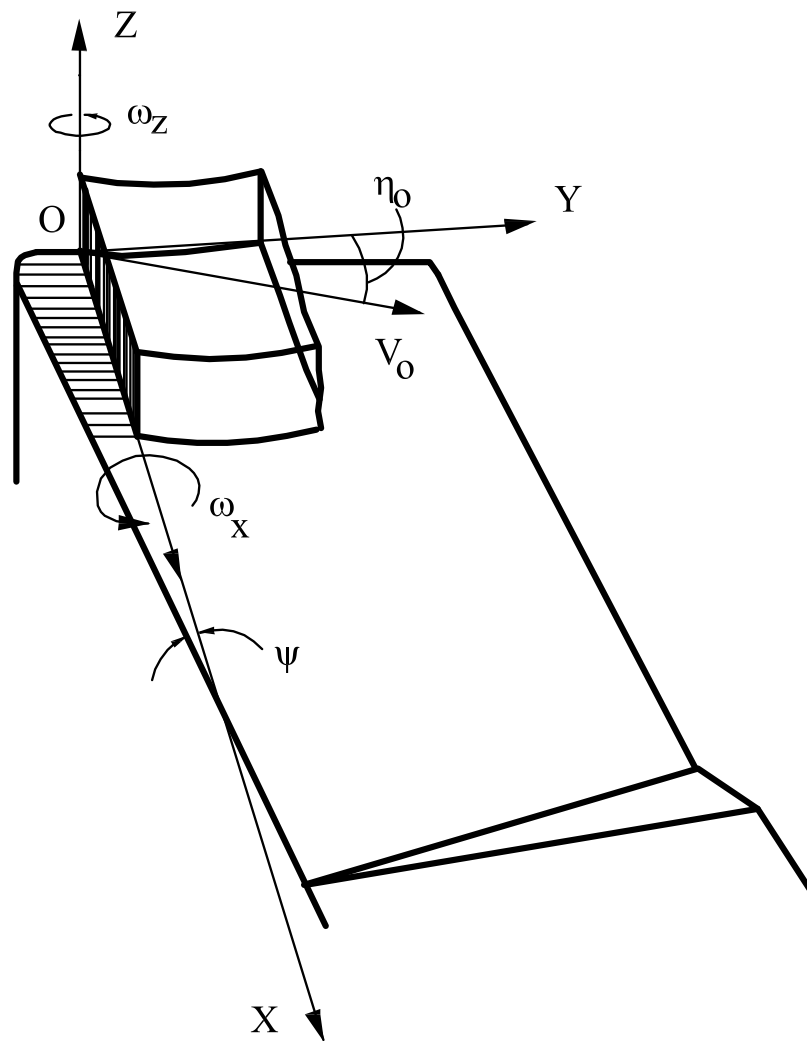


Fig. 1.3: The motion of chip

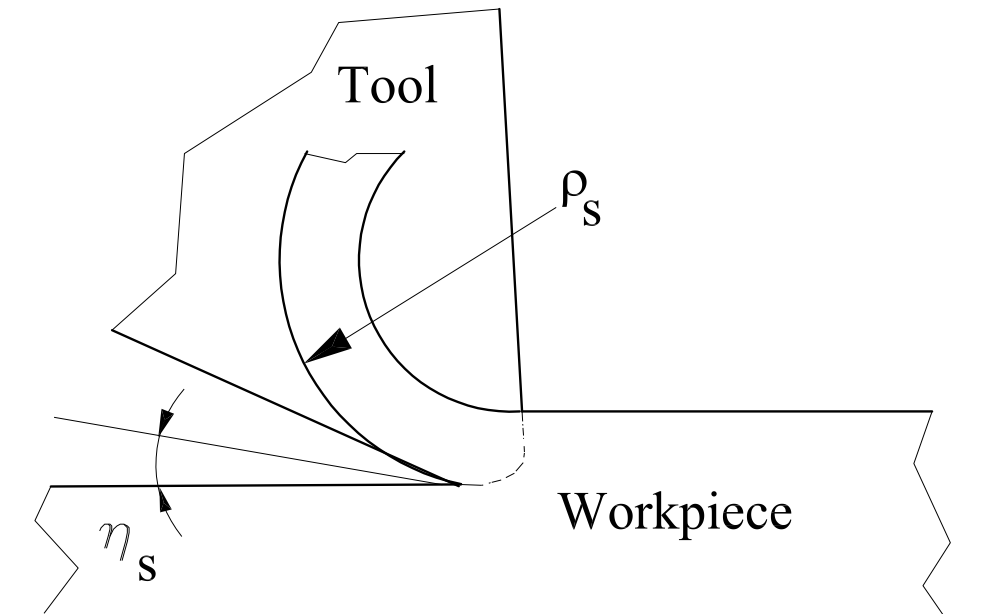


Fig. 1.4: Side-curling

and shorter contact length is obtained under lubricated conditions. In reference [12] Nakayama has indicated that the chip produced in machining may side-curl in the normal direction or in the opposite direction.

Another important variable affecting the chip form in three dimensional machining process is the chip side flow angle (Fig. 1.5). A number of studies has been carried out to predict the side flow angle as may be seen from the review of available literature on this topic presented in reference [4]. The dominant factors influencing chip side flow are known to be

- a. The inclination angle of the major cutting edge
- b. The tool nose radius
- c. The length of contact at auxiliary cutting edge
- d. The magnitude and direction of feed velocity
- e. The direction of resultant friction force on tool face
- f. Depth of cut, and

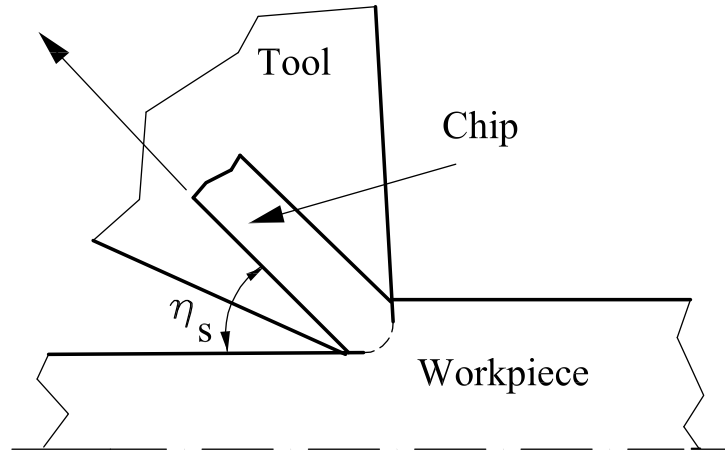


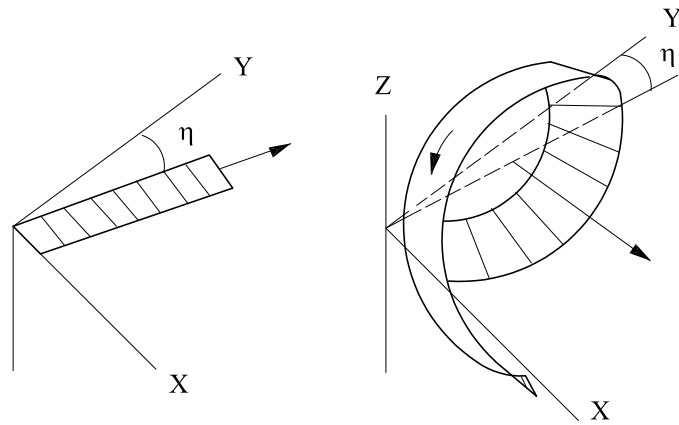
Fig. 1.5: Straight chip

g. Side cutting edge angle.

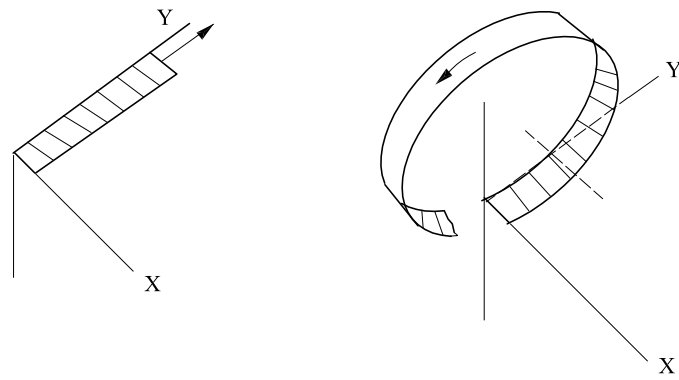
Nakayama *et al.* [12] have demonstrated how the form of a chip at the instance it leaves the tool-chip separation line is dictated by the three basic chip form parameters such as up-curl radius ρ_u , side curl radius ρ_s and side flow angle η_s (Fig. 1.6, 1.7, 1.8, 1.9, 1.10). These authors have also indicated how the angle of inclination θ of chip helix, its radius ρ and pitch 'p' can be calculated from the above chip form parameters.

The majority of unobstructed or lightly obstructed chip forms obtained in continuous cutting operations such as turning are particular cases of 3-D helical chips. For instance a combination of ρ_u and ρ_s usually leads to cylindrical helical chips whereas the addition of η_s to this combination leads to conical helical chips. Suitable combinations of ρ_u , ρ_s and η_s also yields chip forms such as straight ribbon, tubular and corkscrew (washer) as special cases of 3-D helical chips. Spiral and arc chips are considered as helical chips whose progression has been unsteady or arrested due to chip breaking respectively.

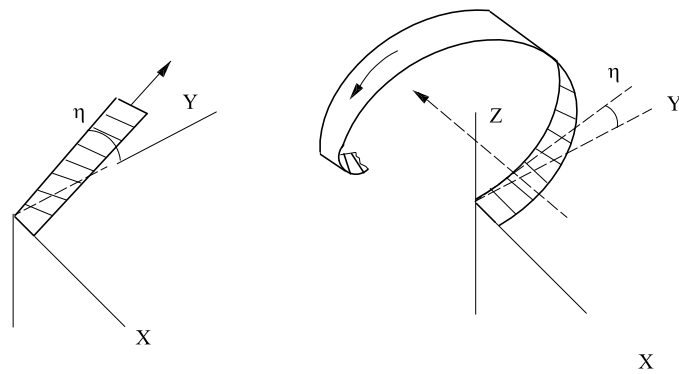
In practice, chip flow is guided by special provisions on the rake face of the tool



(a)

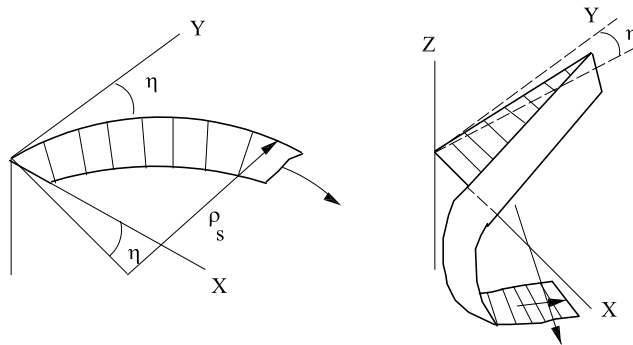


(b)

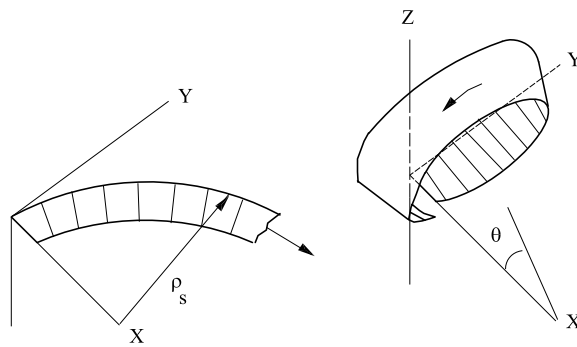


(c)

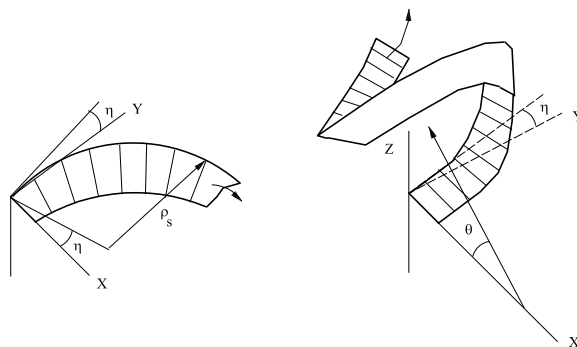
Fig. 1.6: Chips with no sidecurling (a) $\eta = \text{positive}$ (b) $\eta = \text{zero}$ (c) $\eta = \text{negative}$



(a)

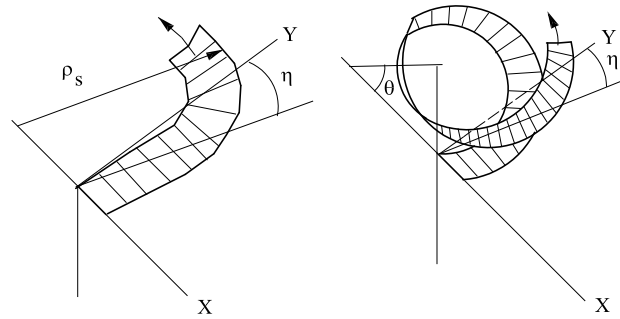


(b)

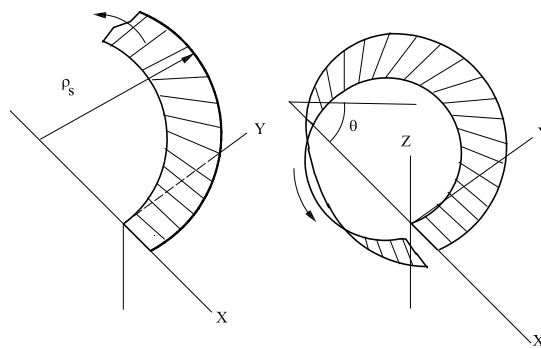


(c)

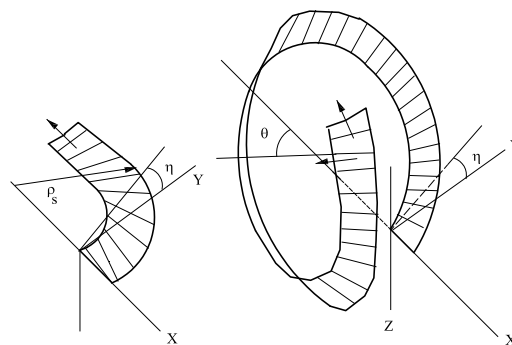
Fig. 1.7: Chips with the sidecurling of normal direction (a) $\eta = \text{positive}$ (b) $\eta = \text{zero}$ (c) $\eta = \text{negative}$



(a)



(b)



(c)

Fig. 1.8: Chips with the sidecurling of opposite direction (a) $\eta = \text{positive}$ (b) $\eta = \text{zero}$ (c) $\eta = \text{negative}$

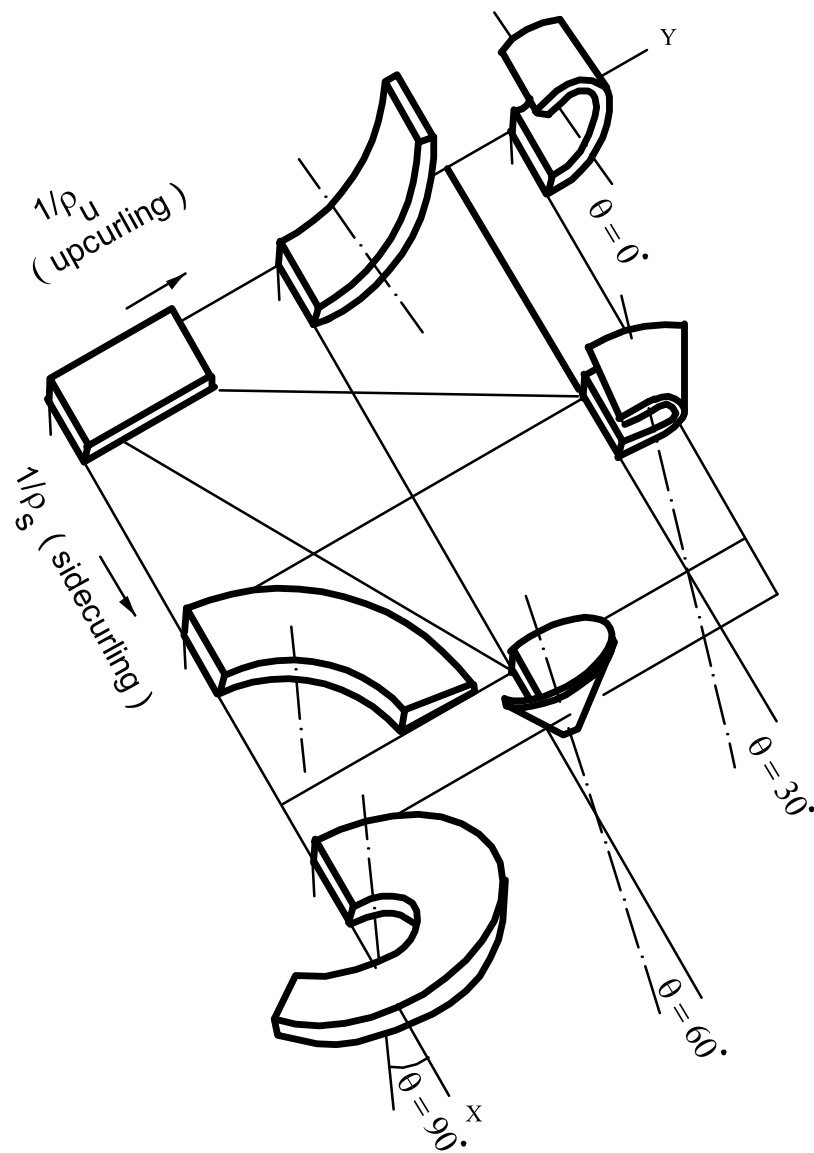


Fig. 1.9: Variation of chip form by upcurling and sidecurling when $\eta = 0$

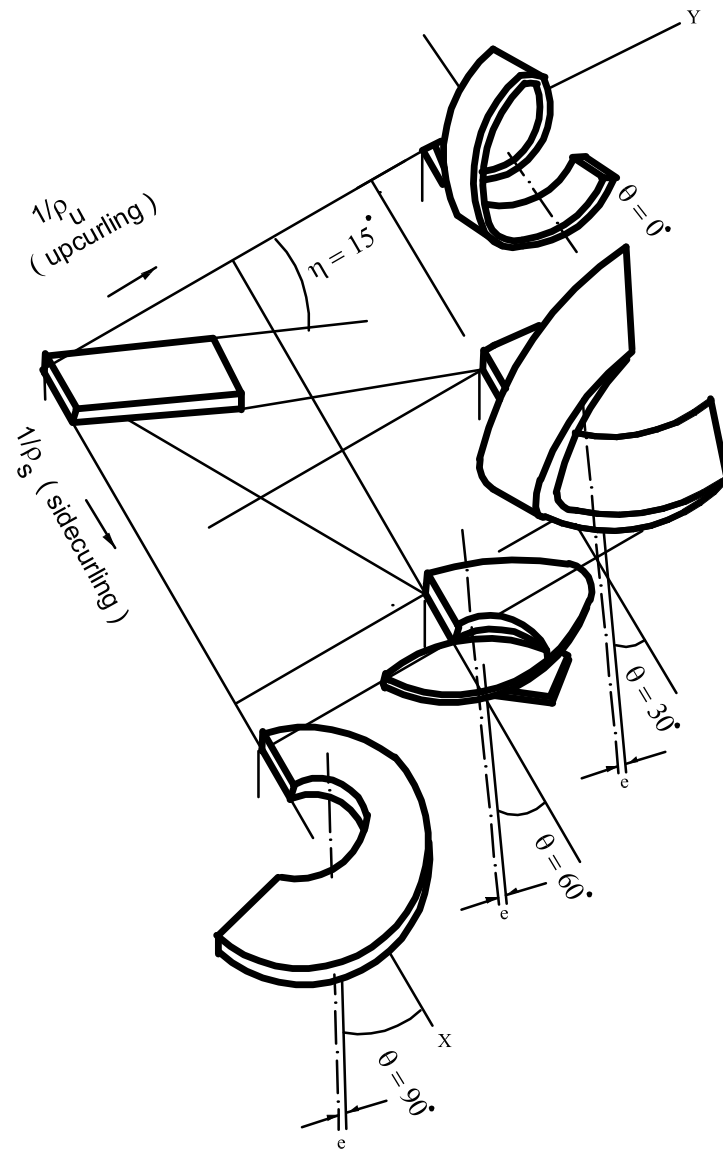


Fig. 1.10: Variation of chip form by upcurling and sidecurling when $\eta = 15$

such as a step or a groove forcing it to make contact with the work piece, the tool, or elements of the machine tool. These obstacles exert forces on the chip causing changes in the chip formation process. Chips of this type are called forced chips.

A lot of effort has been made to classify the chip forms into different groups based on chip shapes and chip sizes. ISO 3685-1977 gives a comprehensive chip form classification based on shape and size [35] for 3-D chips as shown in Fig. 1.11. This classification considers eight different shape groups with further sub-division defining the size and physical condition of chips as given below,

- a. Shapes- Ribbon, Tubular, Spiral, Washer type, conical helical, Arc, Elemental and Needle
- b. Sizes- Long, Short, Flat, Conical etc.
- c. Physical condition- Snarled, Connected

Each shape in the above classification is also identified by a numeral.

Japanese Society for Precision Manufacturing (JSPE) identifies nine different shapes of chip produced in 3-D cutting [36].

Kluft *et al.* [37] classified chips into ten forms. They grouped the chips into two categories on the basis of their acceptability as described below:

- a. Unacceptable- Ribbon, Tangled, Cork screw, Long helical and Tubular
- b. Acceptable- Short tubular, Spiral tubular, Short Spiral, Long and Short comma

The short and long comma types including the ones bearing the geometrical form C, G or E were considered as optimal since they do not pose any difficulty in chip disposal.

Henriksen [30] classified chips on the basis of their breakability into three categories as over broken, efficiently broken and under broken.


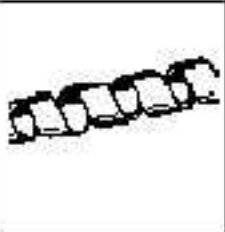
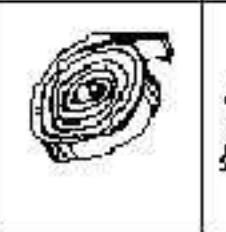



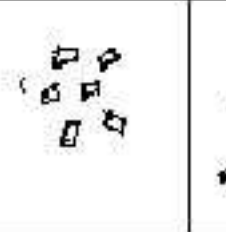
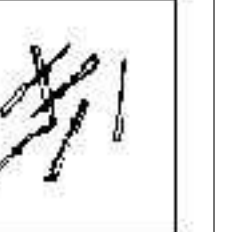

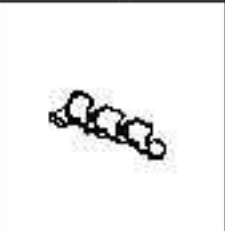

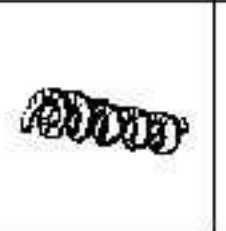
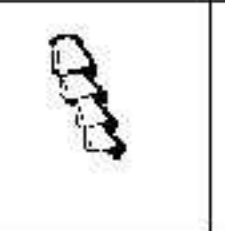
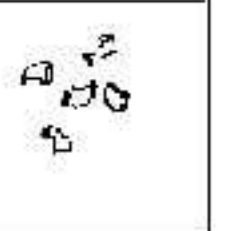
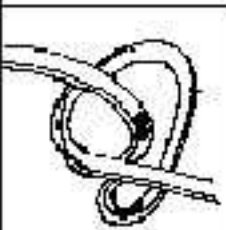


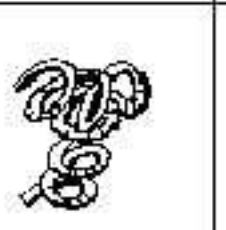




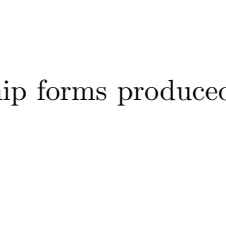
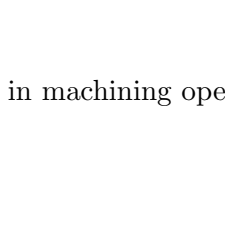
1. Ribbon chips	2. Tubular Chips	3. Spiral Chips	4. Washer type helical chips	5. Conical helical chips	6. Arc chips	7. Elemental chips	8. Needle chips
							
1.1 Long	2.1 Long	3.1 Flat	4.1 Long	5.1 Long	6.1 Connected		
							
1.2 Short	2.2 Short	3.2 Conical	4.2 Short	5.2 Short	6.2 Loose		
							
1.3 Snarled	2.3 Snarled		4.3 Snarled	5.3 Snarled			
							

Fig. 1.11: Chip forms produced in machining operations

Recently Fang, Fie and Jawahir [36] presented a hybrid algorithm for predicting chip form/chip breakability in machining. Yao and Fang [38] have tried to quantify the relationship between chip breakability and tool wear using neural networks and have predicted chip forms successfully in the presence of tool wear.

In most cutting operations, the chip form is rather unstable and varies very easily even when the apparent cutting conditions are kept identical. The main reasons for such variations are as follows [13]:

- a. Variation of the forces acting on chip: With the progress of cutting, the weight of chip increases constantly and the centre of gravity goes away. Obstacles in the way of chip flow such as the chip former add resistant force to the chip. These forces induce a bending moment or non-uniform stress distribution changing the direction of maximum shear stress and that of maximum shear strain at the root of the chip thus resulting in a chip of different geometry.
- b. Transient phenomena in the initial stage of cutting: Before cutting, a tool face is covered with lubricant or absorbed layers of oxygen and other materials. With the progress of cutting these materials are removed and the friction coefficient, the chip thickness and the radius of upward curvature increase gradually. The cutting temperature also goes up and changes the shape and size of built-up edge and, as the result the form of chip.
- c. Variation of tool geometry: It is practically impossible to get a perfectly identical geometry of cutting tools. The geometry is also varied during cutting due to wear and chipping. This is another reason for the instability of chip form.
- d. Non-uniformity of work material: The work material used in industry varies in chemical composition and level of cold working. This varies the shear angle and hence the form of the chip.

It must be emphasized that the present methods of classifying chips are based on the differences in the chip appearance and pay little attention to the chip's physical state including its state of stress and strain, hardness, texture etc. Also neither the cutting regime nor the tool geometry is taken into consideration in these classifications. Hence, these classifications have a post-process rather than helping in

making pre-process decisions about chip breaking [39]. The chip forms also vary significantly with tool wear progression due to alteration in the original tool configuration/geometry [38].

An important aspect of chip control is chip breaking which may be defined as production/ generation of chips of manageable size from long continuous chips so that it can be evacuated easily and reliably from the working zone. Chip breaking is influenced not only by chip shape but also by other factors such as cutting fluid, cutting conditions, machine tool operation, tool geometry, tool and work material properties and process variation [4].

Breaking of chips is accomplished by a chip breaker which is a modification of the rake face of the tool consisting of either an integral groove or an integral/ attached obstruction. A chip breaker acts by controlling the radius of the chip and directing the chip in such a way that it makes contact with some surface of the tool or workpiece and results in breakage of the chip after only a small length has been produced. In 2-D mode of cutting the chip breaks by contact with the surface to the machined (caused by side curling, Fig. 1.12) or by contact with the machined surface (caused by up-curling, Fig. 1.13). In 3-D mode of cutting the chip breaks by anchoring onto tool flank (Fig. 1.14). This mode of chip breaking by contact of chip with tool flank is most common. In both 2-D and 3-D mode of chip breaking using grooved tools it is the chip flow direction and the tool back wall configuration that most directly influences the chip curl and the subsequent chip breaking.

There are basically two types of chip breakers: the groove type (Fig. 1.15) and the obstruction type. The obstruction type chip breaker can further be classified into step type (Fig. 1.16) and ramp type (Fig. 1.17). In obstruction type chip formers with conventional flat faced tools, the naturally curled chip after reaching the tool/chip natural contact length is further curled by the action of the tool face obstruction. In the conventional groove type chip formers the chip flows into the groove owing to the effect of tool restricted contact and then is curled by groove back wall.

The operation of an obstruction type chip breaker depends on the uncut chip thickness or feed, the distance of the chip breaker from the cutting edge and the chip breaker height. Presence of side curl may also influence chip breaking in this type of chip breaker. The operation of grooved chip breakers depends on feed, the length

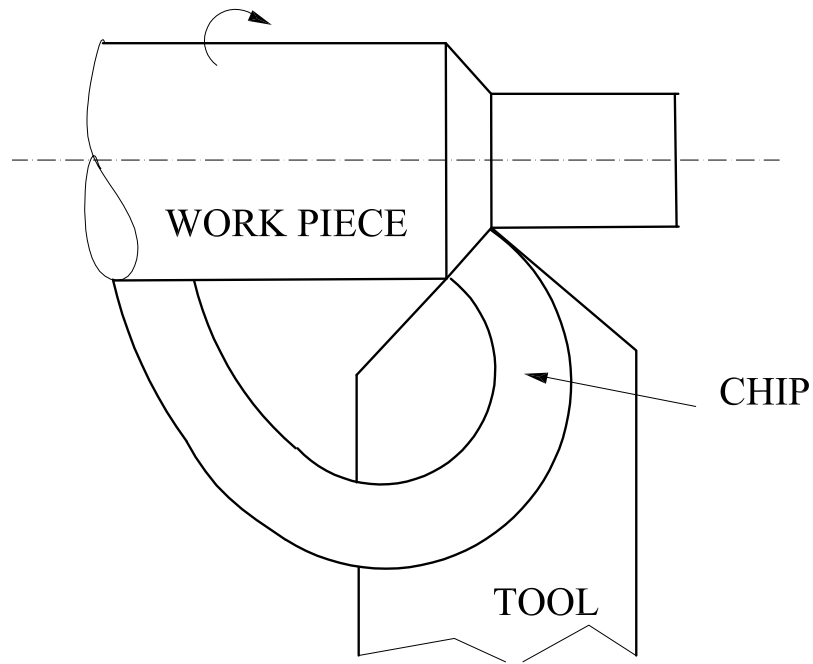


Fig. 1.12: Chip breaking by sidecurling

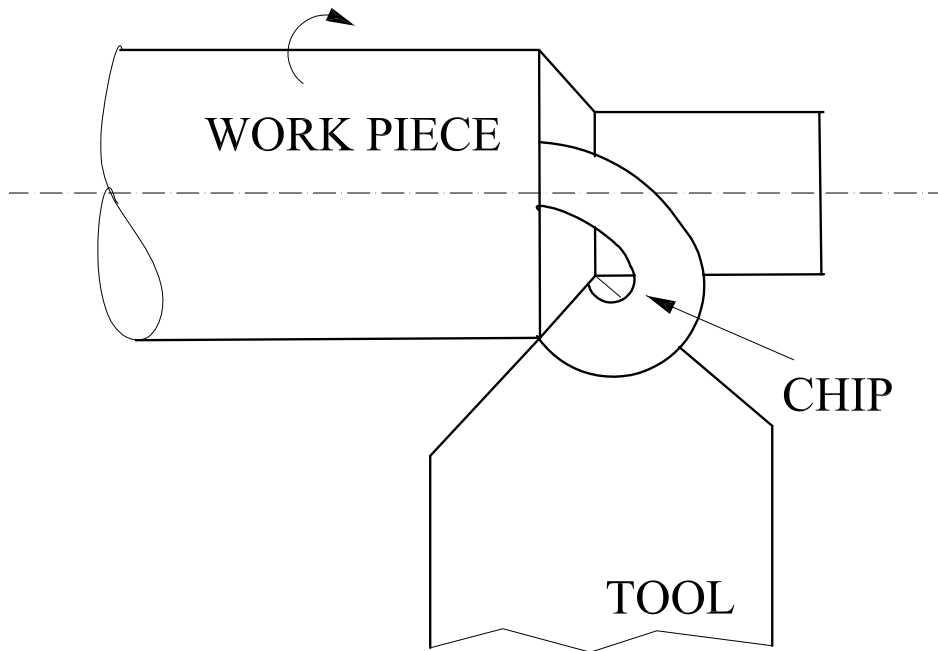


Fig. 1.13: Chip breaking by upcurling

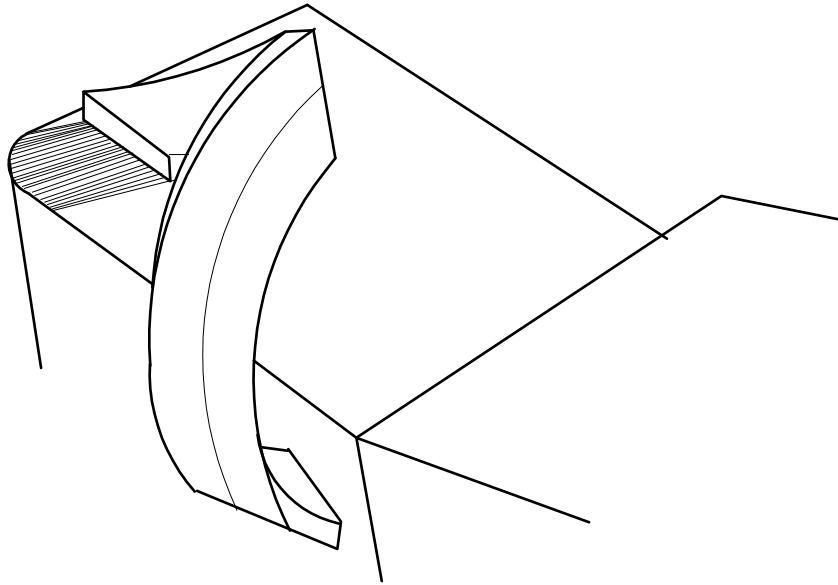


Fig. 1.14: Chip breaking by contact with tool flank in 3-D machining

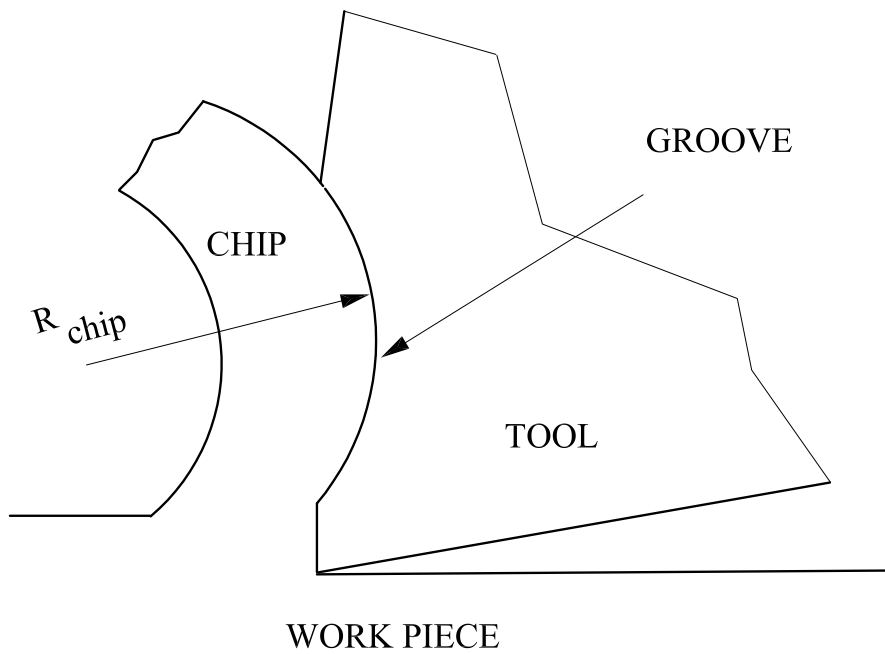


Fig. 1.15: Groove-type chip breaker

of restricted contact and chip groove parameters. Chip flow into the groove occurs as a combination of chip side and back flow. Chip side flow is a measure of the flow on the tool face and is similar to that of a flat faced tool while the chip back flow determines the degree of ‘chip streaming’ into the groove. The ratio of feed to length of restricted contact is seen to be an important parameter in determining chip back flow [17].

The action of a groove type chip former have been studied by Worthington and Redford [33], Worthington [40], Worthington and Rahman [41]. Finite element simulation of 2-D chip breaking from the view point of optimum design of a grooved cutting tool has also been reported by Shinozuka, Obikawa and Shirakashi [42].

The advantages of a groove type chip former has been discussed by Worthington [43]. These include:

- a. The land on the tool can have a high negative rake angle which improves the strength of the tool and hence its performance, particularly with respect to cutting edge chipping.
- b. The tool and chip forming devices are integral and the cost is less as with obstruction type formers the obstruction may need to be changed periodically—typically, this may occur once every 10 inserts used.
- c. The chip breaking efficiency is determined by groove design and does not rely upon the operator positioning the obstruction.
- d. The setting up time is shorter as there is no obstruction to adjust.
- e. Tool life may be increased compared with plane negative rake tools because
 - (i) the tool cuts effectively with a positive rake due to a stable built-up edge forming on the primary land.
 - (ii) contact area on the tool face is reduced thus reducing rake face friction.
- f. The cutting forces are reduced as the rake angle is effectively positive. This is particularly advantageous when machining slender work pieces.

The main disadvantage is that the range of feed over which a particular tool will effectively operate is smaller than that of an obstruction type former as there is no adjustment. Also, if the groove type chip former is incorrectly designed or cutting conditions inappropriately selected, it is possible that cutting forces may be higher, tool life reduced and the surface finish of the machined surface poorer.

The chip breaking process in 2-D machining has been studied by Fang and Jawahir [44] using high speed filming technique. According to these authors chip formation and chip breaking is cyclic in nature and begins with the formation of a new chip and its deflection due to the action of the chip former so that its free end makes floating contact with the rotating work piece. The chip then moves downwards to a certain point along the workpiece surface after which it starts moving upwards, till the chip reaches highest degree of straining and its final up-curl radius and breaks due to the development of fracture from the outer profile of the chip (or from the inner profile of the curled chip). Experimentally measured cutting forces within a chip breaking cycle also exhibit cyclic variation with the amplitude and frequency of force change increasing with undeformed chip thickness [4, 42, 44]. For thicker chips this cyclic variation may induce heavy chatter vibration [4, 42]. Measurement of chip thickness and chip hardness along the length of a broken chip also shows cyclic variation in these parameters within a chip breaking cycle [4, 44].

Nakayama [32] has shown that the efficiency of chip breaking is influenced by only four factors. These are

- a. the bending strain ϵ_b
- b. the chip thickness t_{chip}
- c. the radius of chip flow circle R_o and
- d. the maximum radius of chip curvature R_L just before it breaks.

According to him, the cutting conditions that directly affect these four factors also affect chip breaking. Thus efficiency of chip breaking increases if feed t_0 increases because this results in the increase of chip thickness t_{chip} . Cutting speed has no direct effect on chip breaking, but increase of cutting speed increases the limiting

feed for chip breaking due to the fact that it decreases chip thickness. Depth of cut in the usual range does not affect chip breaking. At very low values of depth of cut, however, limiting chip thickness for chip breaking increases steeply due to change in the direction of chip flow and also due to increase in the radius of chip flow circle. Increasing height of tool flank increases the radius R_L and makes chip breaking easy. Similarly, increasing radius of chip flow circle R_o , increases the limiting feed for chip breaking.

The limiting chip thickness for chip breaking is not affected by tool rake angle in the range of +12 degree to -7 degree. But increasing side cutting edge angle reduces chip thickness and makes the chip hard to break.

Nakayama, Arai and Kondo [17] have suggested the use of tools with curved rake faces for breaking thin chips. A new chip breaking system for mild steel in turning has been developed by Kim and Kweun [45]. Andreason and De chiffre [46] have proposed an automative system for elaboration of chip breaking diagrams. A method for active chip control by varying the position of the tool/chip separation line have been advanced by VenuVinod and Djordiecich [47].

A lot of effort has been undertaken during the last four decades to establish suitable criteria for chip breaking. Studies on chip breaking and chip breakability criteria have been reported by Henriksen [30, 48, 49], Okushima *et al.* [50], Nakayama [51], Takayama *et al.* [52], Jawahir [53], Worthington *et al.* [40], Shinozuka *et al.* [42], Athavale and Strenkowski [54], Grzesik and Kwaitkowska [55], Yang *et al.* [56, 57].

It must be emphasized that the chip breakability criteria referred to above are rather qualitative and can by no means predict with certainty whether a chip will break or not. This is because of the fuzzy nature of the chip formation process and effect of other intervening phenomena such as adiabatic shear heating and thermal effect which makes the prediction of degree of chip breaking difficult. Tool material and interface friction condition is also known to influence the process.

Frictional stresses at chip-tool contact region are developed due to the motion of the deforming material over the tool rake face under high normal stresses. These stresses have profound effect on the chip formation process, chip curling and tool wear. High friction favours formation of chips of large curl radius and increases tool-chip contact length. Under low friction condition the contact length decreases, tool-chip

interface peak pressure increases and chip produced are usually tightly curled.

Different schools of thought have evolved over the years to stipulate the appropriate friction condition that governs the chip-tool contact region. Most analysts looking into the mechanics of chip formation have preferred the linear friction law given by

$$\tau = mk \quad (1.1)$$

where τ is the interface friction stress, m is the friction factor and k is the shear flow stress of the work material. Oxley and Hastings [58] have indicated that the above friction law best represents the friction condition along the tool rake face. Merchant [59], Lee and Shaffer [15], Zorev [60], Childs [61], Kudo [21] and many others, however, have advocated that the rake friction may be adequately represented by a modified Coulomb's law of friction which may be stated as

$$\tau = \mu\sigma \quad (1.2)$$

at low normal pressure ($\mu\sigma \leq k$) and

$$\tau = k \quad (1.3)$$

at high normal pressure ($\mu\sigma \geq k$)

where τ and σ are the interface shear stress and normal stress respectively and μ is the coefficient of friction.

It is now generally recognised that the linear friction law (equation (1.1)) and Coulomb's law (equation (1.2)) of sliding friction do not hold for the tool-chip contact area where high traction/high pressure condition leads to an extreme friction situation. Measurement of contact stress distribution at this interface using split tool dynamometers [62, 63, 64] or photo elastic tools [65, 66, 67] are in general found to be in agreement with this observation. As for friction characteristics at the tool-chip interface, it is likely that adhesion is predominant over abrasion where, the friction force stems from the shear fracture of the bonded asperities. The relation between frictional stress and normal stress under this condition may be written as [68, 69].

$$\tau = k \left[1 - e^{-\left(\frac{\mu\sigma_n}{k}\right)} \right] \quad (1.4)$$

More recently the contact stress distribution at the tool-chip interface was studied by Maekawa, Kitagawa and Childs [70] using a split-tool dynamometer when machining steel with TiN cemented, P20 and K20 carbide tools in dry conditions. These authors demonstrated that the friction stress τ in machining shows a trapezoidal distribution that increases from the chip releasing point to the cutting edge and saturates at the shear flow stress of the chip material, whereas the normal stress σ_n has an exponential distribution that increases monotonically from the chip releasing point towards the cutting edge. Based upon their experimental observations, they proposed a modified equation for the governing friction condition which is stated as

$$\tau = k \left[1 - e^{-\left(\frac{\mu\sigma_n}{k}\right)^n} \right]^{\frac{1}{n}} \quad (1.5)$$

where, τ is the shear stress, k is the yield stress in shear of the work material, σ_n is the normal stress, μ is the low stress level coefficient of friction, and n is a constant whose value depends on tool-work material combination.

It is easily verified that in a lightly loaded condition ($\tau, \sigma \rightarrow 0$) equations (1.4) and (1.5) reduce to Coulomb's law. On the other hand when σ_n becomes large the friction stress τ approaches the shear flow stress k of the chip material. As suggested by Wanheim [71] the above equations provide a smooth transition between the two regimes proposed by Coulomb's law (equation (1.2)).

Despite the rapid growth in the applications of metal machining in manufacturing, a comprehensive analysis of the problem of chip control has always been a difficult task. This is because of the complex mechanism of the chip formation process and a lack of knowledge of the factors that influence chip form/chip breakability under a given set of input machining conditions such as work material properties, tool geometry, chip breakers and cutting conditions. Consequently, the solution to the problem has been approached empirically with a limited degree of success.

In the present investigation, an attempt has been made to examine chip breaking by a step type chip breaker using the rigid-plastic slip-line field theory. Orthogonal machining is assumed and the deformation mode is analysed using the solutions proposed earlier by Kudo [21] and Dewhurst [22]. The rake face friction is represented by the adhesion friction law indicated by equation (1.5). The fields are constructed

by the matrix operational procedure developed by Dewhurst and Collins [72] and Dewhurst [73, 74]. The extent of ‘material damage’ is assessed by computing the cumulative shear strain suffered by the material within a pair of consecutive streamlines in the deforming material and summing the same over all the pairs of streamlines constituting the flow field. The accuracy of prediction of the degree of chip breaking by some of the breakability criteria have also been evaluated. The results are compared with experiments carried out using HSS tools with 10 % cobalt and mild steel as work material.

In Chapter II, a brief account of plane-strain slip-line field theory is presented and the power series and the matrix method of analysis [72, 73, 74] is explained in detail. The structure of the fundamental matrix operators is discussed and equations are presented for calculation of traction and moment for any slip-line curve. The Coulomb friction operator [73, 74] to deal with non-linear boundary value problems such as those involving adhesion friction or curved boundaries is also discussed.

In Chapter III, the slip-line field solutions due to Kudo [21] for orthogonal machining with a step-type chip breaker are analysed in detail. The extent of ‘material damage’ is calculated by a method due to Atkins, Rowe and Johnson [75]. The amount of shear strain in secondary deformation zone is estimated and is found to be about 10-15 % of total strain. The variation of chip thickness ratio as a function of chip breaker height and its distance from the cutting edge is studied. It is shown that the total strain and specific cutting energy increase as the chip breaker moves away from the cutting edge even though the radius of curvature of the formed chip increases and the breaking strain decreases.

Chapter IV reviews in detail the chip breakability criteria proposed by different investigators dealing with machining research to determine the degree of chip breaking. Some of these criteria have been evaluated using the slip-line field solution proposed by Dewhurst [22]. Adhesion friction condition is assumed at chip-tool interface and the field is analysed by the matrix method [72, 73, 74]. Limit of validity of the field has been calculated from the consideration of the overstressing of the rigid vertices at the chip and the workpiece and also from the consideration that the friction angle on tool face nowhere becomes negative. Variation of total strain, breaking strain and the chip curl radius as a function of the chip breaker height and its distance from the

cutting edge is studied. The variation of strain across the chip thickness has been estimated.

Chapter V describes in detail the experimental investigation carried out to validate the theoretical observations. Orthogonal machining tests were carried out on mild steel tubes using HSS tools with 10 % cobalt. Chip breaking was accomplished using a step-type chip breaker. Chip thickness and chip curl radius were measured using an image analyser. For the chips the shift in the position of the neutral axis from the centre was calculated using the theory of bending of curved beams. The exact value of chip curl radius imposed by the chip breaker was determined taking into account the elastic recovery of the chips. Breaking strain was calculated from a simplified formula $\epsilon_b = (t_{chip}/(2R_{chip}))$ and this was correlated with the degree of chip breaking. A procedure for Chip breaker design to achieve effective breaking was also suggested.

Conclusions from the present investigation are finally presented in Chapter VI.

2. SLIP-LINE FIELD CONSTRUCTION BY MATRIX METHOD

2.1 Introduction

The state of stress in a body deforming under conditions of plain strain satisfy the equilibrium equations, which in the absence of body forces is written as

$$\begin{aligned}\frac{\partial \sigma_x}{\partial x} + \frac{\partial \tau_{xy}}{\partial y} &= 0 \quad \text{and} \\ \frac{\partial \tau_{xy}}{\partial x} + \frac{\partial \sigma_y}{\partial y} &= 0\end{aligned}\tag{2.1}$$

and the yield criterion

$$(\sigma_x - \sigma_y)^2 + 4\tau_{xy}^2 = 4\kappa^2\tag{2.2}$$

The yield criterion is satisfied by the stresses in the Cartesian coordinate direction as

$$\begin{aligned}\sigma_x &= -p - \kappa \sin 2\phi \\ \sigma_y &= -p + \kappa \sin 2\phi \quad \text{and} \\ \tau &= \kappa \cos 2\phi\end{aligned}\tag{2.3}$$

where, $-p = \frac{1}{2}(\sigma_x + \sigma_y)$ is the hydrostatic part of the stress tensor and $(\phi + \pi/4)$ is the anti-clockwise rotation of the direction of the algebraically greatest principal stress from the positive direction of the x axis as shown in Fig. 2.1.

Substitution of equation (2.3) in equation (2.1) gives

$$\begin{aligned}\frac{-\partial p}{\partial x} - 2\kappa \cos 2\phi \left(\frac{\partial \phi}{\partial x}\right) - 2\kappa \sin 2\phi \left(\frac{\partial \phi}{\partial y}\right) &= 0 \quad \text{and} \\ \frac{-\partial p}{\partial y} - 2\kappa \sin 2\phi \left(\frac{\partial \phi}{\partial x}\right) + 2\kappa \cos 2\phi \left(\frac{\partial \phi}{\partial y}\right) &= 0\end{aligned}\tag{2.4}$$

Equations (2.4) are hyperbolic and yield two families of characteristics inclined to the x -axis at angles ϕ and $(\phi + \frac{\pi}{2})$ respectively, thus forming an orthogonal network

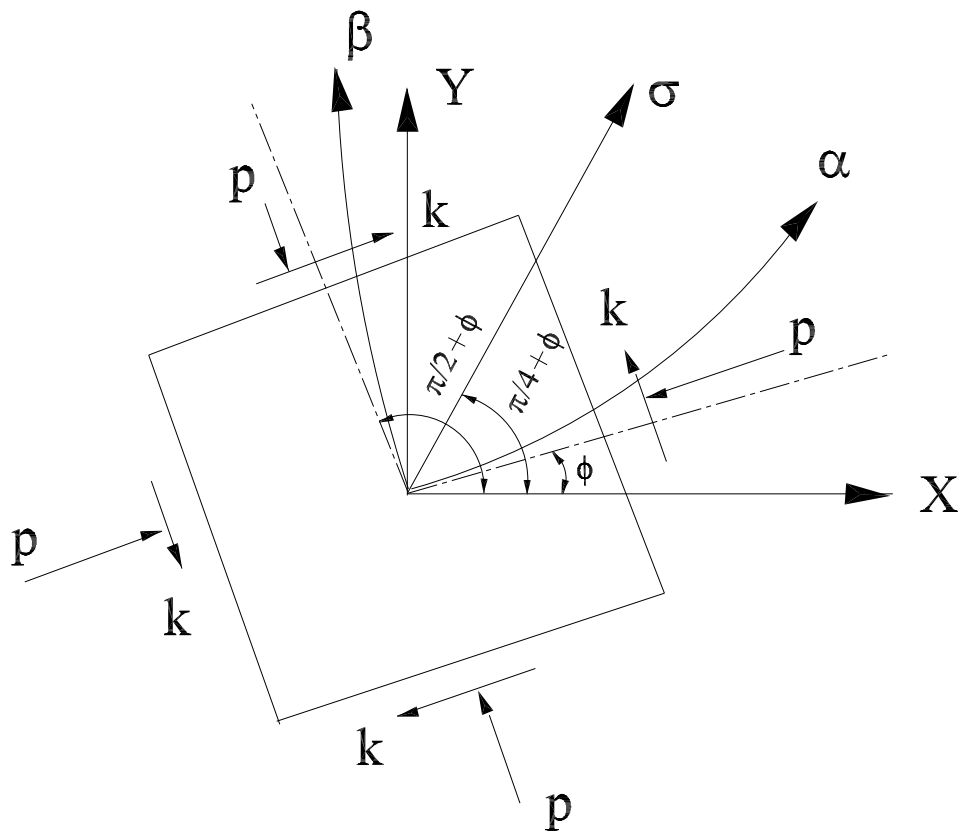


Fig. 2.1: Physical plane showing stress system in plane plastic flow

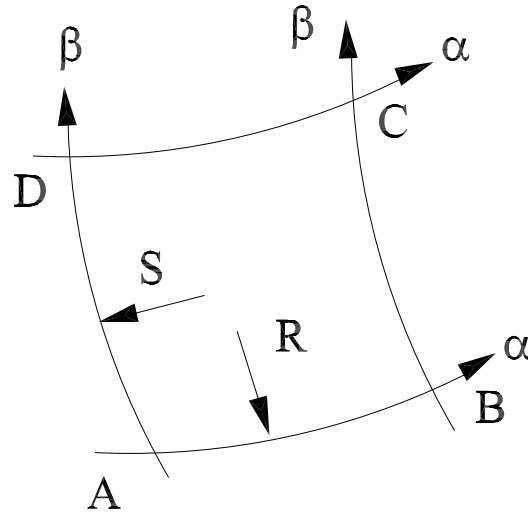


Fig. 2.2: A slip-line field net for demonstrating Hencky's theorems

known as slip-lines [76]. The members of the family given by the parameter ϕ are, by convention, called the α -lines and those given by the parameter $(\phi + \frac{\pi}{2})$, the β -lines. Evidently, the α -lines and β -lines coincide with the trajectories of maximum shear stress.

The hydrostatic pressures along the slip-lines satisfy Hencky's equations, which in the absence of work-hardening may be expressed as:

$$p + 2\kappa\phi = \text{constant along an } \alpha\text{-line, and}$$

$$p - 2\kappa\phi = \text{constant along a } \beta\text{-line.}$$

The velocities along the slip-lines are related by Geiringer's equations written as,

$$du - v \cdot d\phi = 0 \quad \text{on an } \alpha\text{-line, and}$$

$$dv - u \cdot d\phi = 0 \quad \text{on a } \beta\text{-line}$$

where, u and v are the velocity components in the α and β directions respectively.

A field of slip-lines possesses several geometrical properties, which are enunciated in the two theorems due to Hencky [77]. Hencky's first theorem states that the angle between two slip-lines of one family, where they are intersected by a pair of slip-lines of the other family, is constant along their length. Thus referring to Fig. 2.2, we have

$$\phi_D - \phi_A = \phi_C - \phi_B, \quad \text{or}$$

$$\phi_C - \phi_D = \phi_B - \phi_A$$

Hencky's second theorem states that as we move along a slip-line, the radius of

curvature of the slip-line of the other family at the points of intersection changes by the distance traveled. Thus, referring to Fig. 2.2, we have

$$\begin{aligned} dS + Rd\phi &= 0 \quad \text{along an } \alpha\text{-line, and} \\ dR - Sd\phi &= 0 \quad \text{along a } \beta\text{-line.} \end{aligned}$$

Solution to boundary value problems by analytic integration of the plain strain equations is possible only in a few simple cases. Hence, construction of the slip-line network is usually carried out by the graphical procedure suggested by Hill [77] or Prager [78, 79]. When applied to indirect or mixed boundary value problems, however, this method of analysis becomes very cumbersome. Such problems are more readily solved by the matrix method [80], where the construction of slip-line field is achieved through the use of some standard matrix operators and superposition principle [72, 81].

2.2 Series representation for radius of curvature of slip-line curves

The sign convention for the series representation of the radius of curvature of the slip-line curves is same as the approach adopted by Dewhurst and Collins [72], so that the slip-line field construction is independent of whether it is an α -line or β -line.

- a. The inclination of a slip-line is always reckoned from the tangent to the slip-line at its base point and is always taken as positive irrespective of the sense of rotation.
- b. The radius of curvature ρ of a slip line is defined by $\frac{1}{\rho} = \pm \frac{d\psi}{ds}$ where, ψ is the inclination of the local tangent to that at the base point and ds is the differential arc length. The plus or minus sign is taken according as whether it increases in an anti-clockwise or clockwise sense along the slip-line.

With this sign convention, Hencky's second theorem for the slip-line network shown in Fig. 2.3 is given as:

$$\begin{aligned} \frac{\partial R}{\partial \beta} &= -S \quad \text{and} \\ \frac{\partial S}{\partial \alpha} &= -R \end{aligned} \tag{2.5}$$

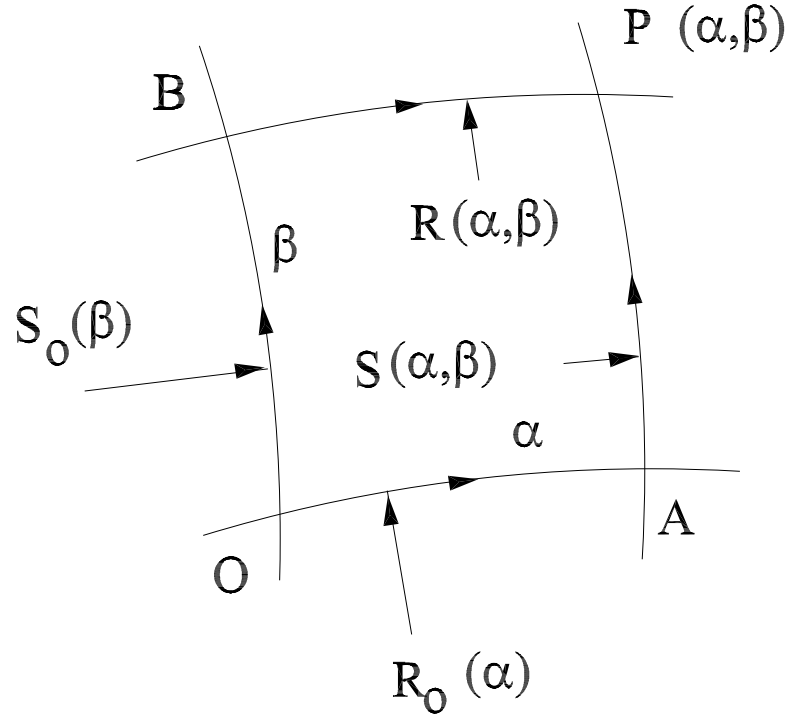


Fig. 2.3: A slip-line field net for series representation of radius of curvature

Referring to the Fig. 2.3, if the radii of curvature of the two given slip-lines OA and OB are expanded in a power series in terms of the angular co-ordinates such that

$$\begin{aligned} R_o(\alpha) &= \sum_{n=0}^{\infty} a_n \frac{\alpha^n}{n!} \quad \text{and} \\ S_o(\beta) &= \sum_{n=0}^{\infty} b_n \frac{\beta^n}{n!} \end{aligned} \quad (2.6)$$

Then, the radii of curvature at the general point $P(\alpha, \beta)$ are given by (Ewing [82]),

$$\begin{aligned} R(\alpha, \beta) &= \sum_{m,n=0}^{\infty} \left[a_n \cdot \frac{\alpha^{m+n}}{(m+n)!} \cdot \frac{\beta^m}{m!} - b_n \cdot \frac{\alpha^m}{m!} \cdot \frac{\beta^{m+n+1}}{(m+n+1)!} \right] \quad \text{and} \\ S(\alpha, \beta) &= \sum_{m,n=0}^{\infty} \left[-a_n \cdot \frac{\alpha^{m+n+1}}{(m+n+1)!} \cdot \frac{\beta^m}{m!} + b_n \cdot \frac{\alpha^m}{m!} \cdot \frac{\beta^{m+n}}{(m+n)!} \right] \end{aligned} \quad (2.7)$$

It may be seen with reference to equation (2.3) that the radii of curvature of α -line and β -line through $P(\alpha, \beta)$ are obtained by algebraic addition of two terms, which in essence is the mathematical formulation of superposition principle.

2.3 Matrix representation of slip-line fields

The series solutions given by Ewing [82] were developed into matrix formulation by Collins [80] and Dewhurst and Collins [72] using principle of linear algebra. Referring

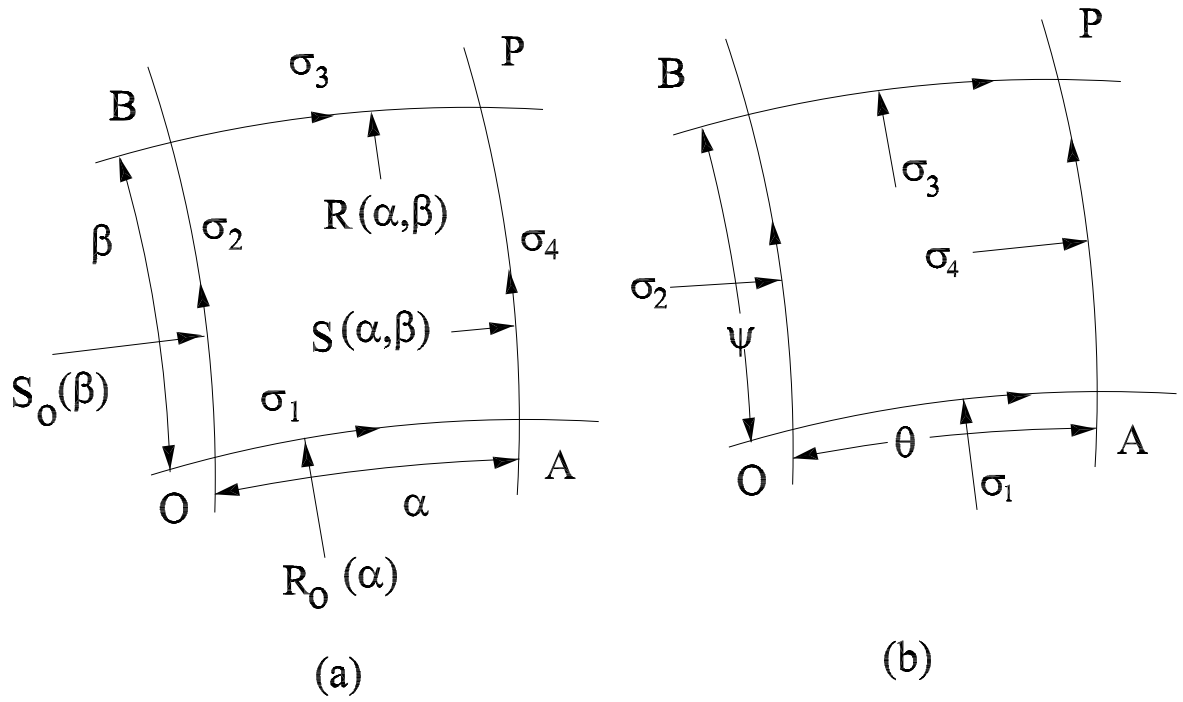


Fig. 2.4: A slip-line field net for matrix representation of slip-line curves

to Fig. 2.4, let the radius of curvature of the base slip-lines OA and OB through O be represented by the column vectors σ_1 and σ_2 respectively where, the elements of the column vectors are the coefficients in the power series expansion of the radius of curvature of the slip-lines (equation (2.6)). Then, as shown by Dewhurst and Collins [72], the column vectors σ_3 and σ_4 representing the radius of curvature of the slip-lines BP and AP are given by the relations,

$$\begin{aligned}\sigma_3 &= \mathbf{P}_\psi^* \sigma_1 + \mathbf{Q}_\psi^* \sigma_2 \quad \text{and} \\ \sigma_4 &= \mathbf{P}_\theta^* \sigma_2 + \mathbf{Q}_\theta^* \sigma_1\end{aligned}\tag{2.8}$$

where,

$$\mathbf{P}_\phi^* = \begin{vmatrix} \phi_0 & 0 & 0 & \dots \\ \phi_1 & \phi_0 & 0 & \dots \\ \phi_2 & \phi_1 & \phi_0 & \dots \\ \dots & \dots & \dots & \dots \end{vmatrix}$$

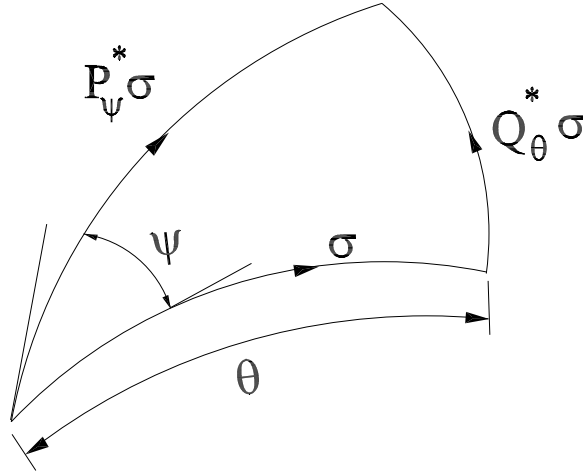


Fig. 2.5: Matrix operators generating singular field on the convex side of a slip-line curve

and

$$\mathbf{Q}_\phi^* = - \begin{vmatrix} \phi_1 & \phi_2 & \phi_3 & \dots \\ \phi_2 & \phi_3 & \phi_4 & \dots \\ \phi_3 & \phi_4 & \phi_5 & \dots \\ \dots & \dots & \dots & \dots \end{vmatrix} \quad (2.9)$$

where

$$\phi_m = \frac{\phi^m}{m!} \quad (2.10)$$

is the reduced power of ϕ and \mathbf{P}^* and \mathbf{Q}^* are the matrix operators that generate the singular fields on the convex side of a given slip-line (Fig. 2.5).

The other basic operators are the reversion matrix operator \mathbf{R}_ϕ , un-starred operators \mathbf{P} and \mathbf{Q} , the shift operator \mathbf{S}_ϕ and the smooth boundary operator \mathbf{T}_ϕ . It may be noted that the direction of the arrows in the slip-lines in Fig. 2.4 indicate the intrinsic direction in which the inclination of the slip-line increases from zero at the base point. The reversion matrix operator \mathbf{R}_ϕ reverses the intrinsic direction of a given slip-line with angular span ϕ . Thus, referring to Fig. 2.6 if slip-line curve OA is represented by σ , the curve AO is given as,

$$AO = \mathbf{R}_\theta \cdot \sigma \quad (2.11)$$

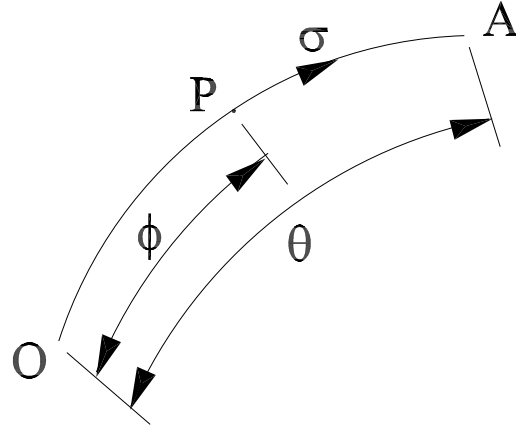


Fig. 2.6: Shifting the origin of a slip-line curve

where the reversion operator \mathbf{R}_ϕ is given by the square matrix [72],

$$\mathbf{R}_\phi = - \begin{vmatrix} \phi_0 & \phi_1 & \phi_2 & \dots \\ 0 & -\phi_0 & -\phi_1 & \dots \\ 0 & 0 & \phi_0 & \dots \\ \vdots & \vdots & \vdots & \dots \end{vmatrix} \quad (2.12)$$

where ϕ_m is as given in equation (2.10).

The shift operator \mathbf{S}_ϕ shifts the origin of a slip-line through an angular distance ϕ in the intrinsic direction (Fig. 2.6). Thus, if OA is represented by σ , PA is given as,

$$PA = \mathbf{S}_\phi \cdot \sigma \quad (2.13)$$

where the shift operator is written in the matrix form as [72],

$$\mathbf{S}_\phi = \begin{vmatrix} \phi_0 & \phi_1 & \phi_2 & \dots \\ 0 & \phi_0 & \phi_1 & \dots \\ 0 & 0 & \phi_0 & \dots \\ \vdots & \vdots & \vdots & \dots \end{vmatrix} \quad (2.14)$$

The un-starred \mathbf{P} and \mathbf{Q} operators are defined using the reversion operator as,

$$\begin{aligned} \mathbf{P}_{\theta\psi} &= \mathbf{R}_\theta \mathbf{P}_\psi^* \quad \text{and} \\ \mathbf{Q}_{\theta\psi} &= \mathbf{R}_\psi \mathbf{Q}_\theta^* \end{aligned} \quad (2.15)$$

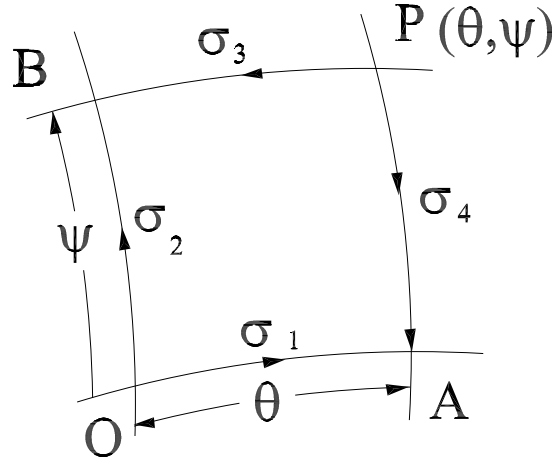


Fig. 2.7: A slip-line field net for showing relation between radius of curvature of slip-line curves

Using the reversion matrix operators, the relation between the radius of curvatures of the slip-lines σ_1 , σ_2 , σ_3 , and σ_4 may be written as (Fig. 2.7)

$$\begin{aligned}\sigma_3 &= P_{\theta\psi}\sigma_1 + Q_{\psi\theta}\sigma_2 \quad \text{and} \\ \sigma_4 &= P_{\psi\theta}\sigma_1 + Q_{\theta\psi}\sigma_2\end{aligned}\quad (2.16)$$

By taking σ_3 (PB) and σ_4 (PA) as base slip-lines, as in Fig. 2.7, the relations for σ_1 and σ_2 may be expressed as,

$$\begin{aligned}\sigma_1 &= P_{\theta\psi}\sigma_3 - Q_{\psi\theta}\sigma_4 \quad \text{and} \\ \sigma_2 &= P_{\psi\theta}\sigma_4 - Q_{\theta\psi}\sigma_3\end{aligned}\quad (2.17)$$

The smooth boundary operator \mathbf{T}_ϕ generates the field between a given slip-line and a straight frictionless boundary (Fig. 2.8). \mathbf{T}_ϕ constructs the field on the concave side of the given slip-line, while it's inverse \mathbf{T}_ϕ^{-1} yields the field on convex side. Thus,

$$BA = \mathbf{T}_\phi OA, \text{ and}$$

$$OA = \mathbf{T}_\phi^{-1} BA$$

where,

$$\begin{aligned}\mathbf{T}_\phi &= -P_{\phi\phi} - Q_{\phi\phi} \quad \text{and} \\ \mathbf{T}_\phi^{-1} &= -P_{\phi\phi} + Q_{\phi\phi}\end{aligned}\quad (2.18)$$

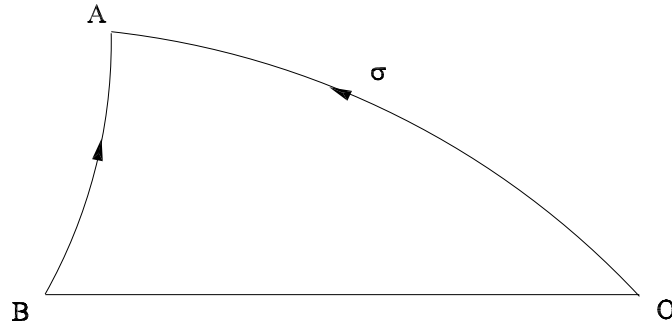


Fig. 2.8: Smooth boundary operator generating field between slip-line curve and straight frictionless boundary

2.4 Calculation of coordinates, traction and moment

2.4.1 Coordinates

Referring to Fig. 2.9, OQ is a slip-line with range ϕ and OX and OY are the Cartesian co-ordinate axes. $O\bar{X}$ and $O\bar{Y}$ are the moving or Mikhlin coordinate axes. At any point P with angular coordinate t , the differential arc length ds can be expressed in terms of its components as,

$$\begin{aligned} d\bar{X} &= ds \cos(\phi - t) \quad \text{and} \\ d\bar{Y} &= -ds \sin(\phi - t) \end{aligned} \quad (2.19)$$

The coordinates of the point Q are, therefore, given by,

$$\bar{X} = \int_0^{\phi} ds \cos(\phi - t) = \int_0^{\phi} R(t) \cos(\phi - t) dt \quad \text{and} \quad (2.20)$$

$$\bar{Y} = - \int_0^{\phi} ds \sin(\phi - t) = - \int_0^{\phi} R(t) \sin(\phi - t) dt \quad (2.21)$$

as $ds = R(t)dt$

If $R(t)$ is expanded as a power series such that

$$R(t) = \sum_{n=0}^{\infty} r_n \cdot \frac{t^n}{n!} \quad (2.22)$$

then \bar{X} and \bar{Y} are given by [72, 82]

$$\begin{aligned} \bar{X} &= \sum_{n=0}^{\infty} t_n \cdot \frac{\phi^n}{n!} \quad \text{and} \\ \bar{Y} &= \mp \sum_{n=0}^{\infty} t_n \cdot \frac{\phi^{n+1}}{(n+1)!} \end{aligned} \quad (2.23)$$

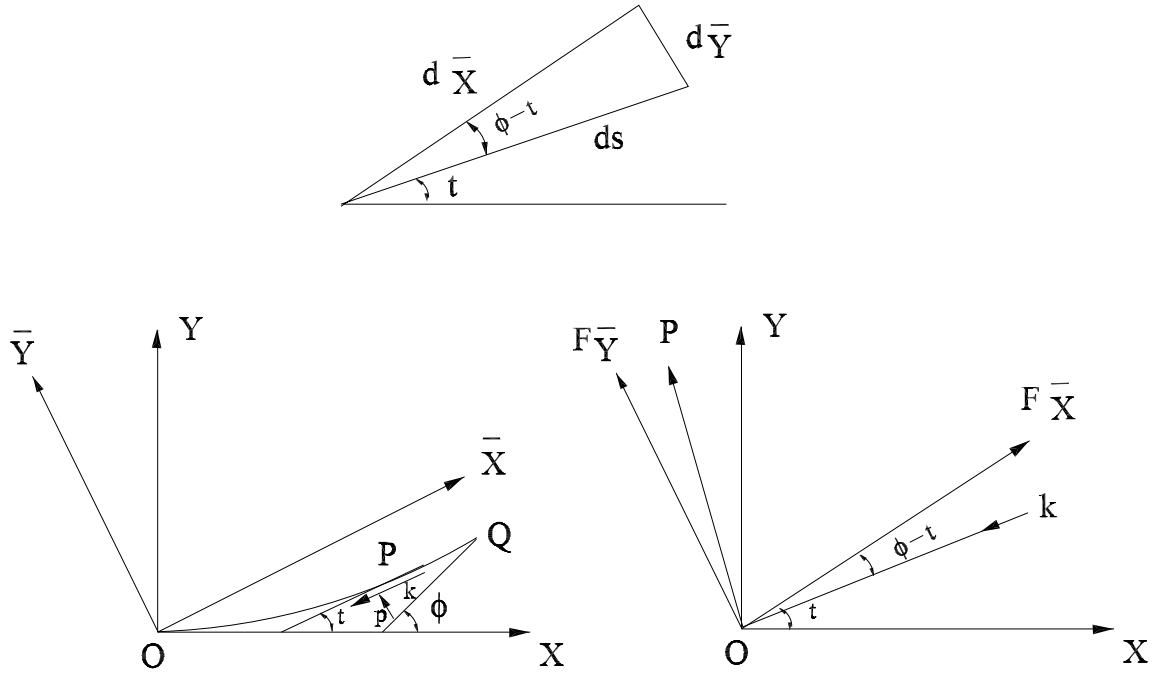


Fig. 2.9: Calculation of co-ordinates, traction and moment

where t_n is given by the recurrence relation,

$$t_{n+1} - t_{n-1} = |r_n|$$

where $t_0 = 0$ and $t_1 = |r_0|$

The minus or plus sign is taken according as whether $R(t)$ is positive or negative. Once the moving co-ordinates of the point Q are known, the Cartesian co-ordinates can be calculated from the relationships,

$$\begin{aligned} X &= \bar{X} \cos \phi - \bar{Y} \sin \phi \quad \text{and} \\ Y &= \bar{X} \sin \phi + \bar{Y} \cos \phi \end{aligned} \quad (2.24)$$

2.4.2 Traction

Referring to Fig. 2.9, if p_0 is the hydrostatic pressure at the origin, the hydrostatic pressure at the point P is given by

$$p = p_0 \pm 2\kappa t$$

the negative or positive sign being chosen according as whether the slip-line is an α -line or a β -line and κ is the yield stress in shear. The tractions along the Mikhlin

directions at the point P are given by,

$$\begin{aligned} dF_{\bar{x}} &= (p_0 \pm 2\kappa t)ds \sin(\phi - t) \pm kds \cos(\phi - t) \quad \text{and} \\ dF_{\bar{y}} &= (p_0 \pm 2\kappa t)ds \cos(\phi - t) \mp kds \sin(\phi - t) \end{aligned} \quad (2.25)$$

where ds is the differential arc length.

Integrating equation (2.24) and substituting $ds=R(t) dt$, the total traction for the slip-line is given by,

$$\begin{aligned} F_{\bar{x}} &= -p_0\bar{Y} \pm k\bar{X} \pm 2k \int_0^\phi t \sin(\phi - t)R(t)dt \quad \text{and} \\ F_{\bar{y}} &= p_0\bar{X} \pm k\bar{Y} \pm 2k \int_0^\phi t \cos(\phi - t)R(t)dt \end{aligned} \quad (2.26)$$

Using equation (2.22) for the power series expansion of $R(t)$, the integration finally yields,

$$\begin{aligned} \int_0^\phi t \cos(\phi - t)R(t)dt &= \sum_{n=0}^{\infty} C_n \frac{\phi^n}{n!} \quad \text{and} \\ \int_0^\phi t \sin(\phi - t)R(t)dt &= \sum_{n=0}^{\infty} C_{n-1} \frac{\phi^n}{n!} \end{aligned} \quad (2.27)$$

where, the coefficients C_n 's are given by the recurrence relations [72, 82],

$$\begin{aligned} C_{n+1} &= n|r_{n-1}| - C_{n-1} \quad \text{and} \\ C_0 &= C_{-1} = 0 \end{aligned}$$

2.4.3 Moment

Unfortunately, a series representation for the moment M does not lead to any simple recurrence relation and recourse must be made to numerical integration. However, the required integrand takes a particularly simple form when expressed in terms of the Mikhlin co-ordinates (\bar{X}, \bar{Y}) .

For the positive α -line shown in Fig. 2.9 the moment M is given by [82].

$$\frac{M}{\kappa} = \int_0^\phi \left[\left(\frac{p_0}{\kappa} - 2t \right) \bar{X}(t) + \bar{Y}(t) \right] R(t)dt \quad (2.28)$$

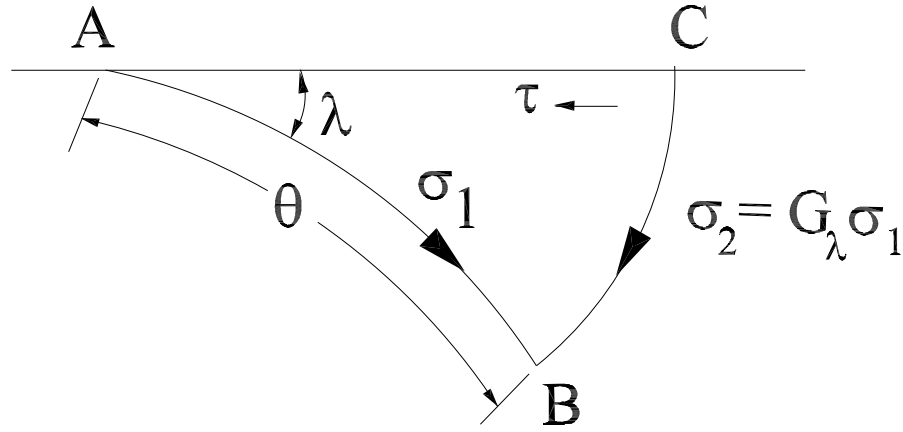


Fig. 2.10: Slip-line field adjacent to a straight rough boundary

2.5 Straight rough boundary operator

Let σ_1 and σ_2 be the vector representation of the bounding slip-lines of deforming region ABC (Fig. 2.10).

AC is a straight rough boundary with constant shear stress τ . Thus the families of α -lines and β -lines in ABC meet CA at constant angles of λ and $(\frac{\pi}{2} - \lambda)$ respectively, where

$$\lambda = \frac{1}{2} \cos^{-1}\left(\frac{\tau}{\kappa}\right).$$

Then, as discussed by Dewhurst [22]

$$\begin{aligned} \sigma_2 &= [\mathbf{Q}_{\theta\theta} + \mathbf{P}_{\theta\theta}(\mathbf{I} \cos \lambda - \mathbf{J} \sin \lambda)^{-1}(\mathbf{J} \cos \lambda - \mathbf{I} \sin \lambda)]\sigma_1 = \mathbf{G}_\lambda \sigma_1 \quad \text{and} \\ \sigma_1 &= [-\mathbf{Q}_{\theta\theta} - \mathbf{P}_{\theta\theta}(\mathbf{I} \sin \lambda + \mathbf{J} \cos \lambda)^{-1}(\mathbf{J} \cos \lambda + \mathbf{I} \sin \lambda)]\sigma_2 = \\ &= \mathbf{G}_{(\frac{\pi}{2}-\lambda)}^{-1} \sigma_2 \end{aligned} \quad (2.29)$$

where \mathbf{I} is the unit matrix and \mathbf{J} the integration operator, which is written as

$$\mathbf{J} = \begin{vmatrix} 0 & 0 & 0 & 0 & \dots \\ 1 & 0 & 0 & 0 & \dots \\ 0 & 1 & 0 & 0 & \dots \\ 0 & 0 & 1 & 0 & \dots \end{vmatrix}$$

The two extreme cases are:

- a. The boundary is perfectly smooth so that the slip-lines meet the boundary at angles $\pm\frac{\pi}{4}$. The straight rough boundary operator then is reduced to the smooth boundary operator given by

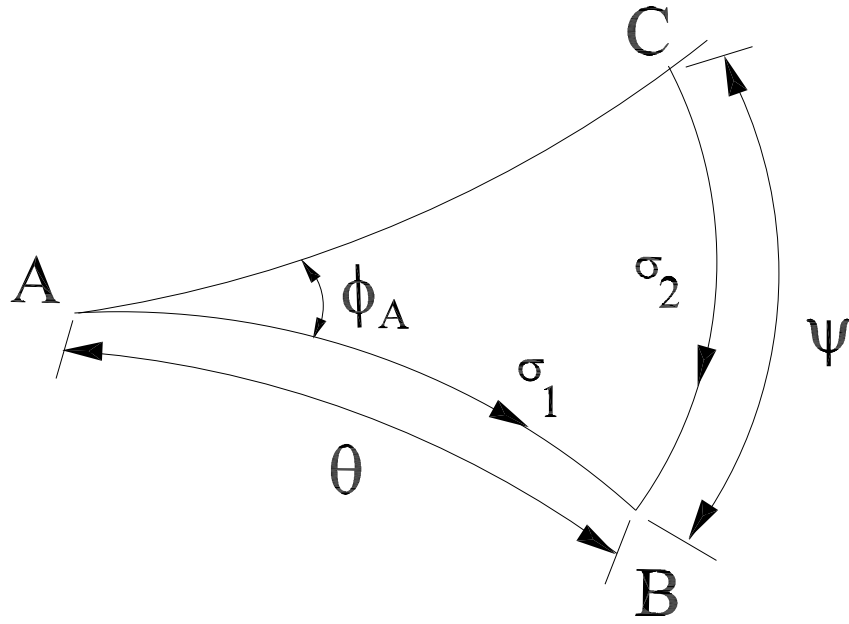


Fig. 2.11: Slip-line field adjacent to a curved boundary

$$\mathbf{G}_{\frac{\pi}{4}} = \mathbf{Q}_{\theta\theta} - \mathbf{P}_{\theta\theta}$$

- b. The boundary is perfectly rough so that the slip-lines meet the boundary at 0 degree and $\frac{\pi}{2}$.

$$\text{Thus, } \mathbf{G}_0 = \mathbf{Q}_{\theta\theta} + \mathbf{P}_{\theta\theta}J$$

2.6 Adhesion operator

Dewhurst [73, 74] has proposed a more general form of matrix operator which generates the slip-line field adjacent to an arbitrary curved surface with constant interfacial shear stress or a flat surface with interfacial shear stress governed by Coulomb's law of friction. In the present investigation the above matrix operator has been used to construct the field when interfacial shear stress follows adhesion friction law (equation (1.5)).

Referring to Fig. 2.11, the boundary is defined by a linear relationship in the slip-line coordinate system,

$$\psi = B_0\theta \quad (2.30)$$

and along the boundary, the angle of intersection of the slip-lines with the bound-

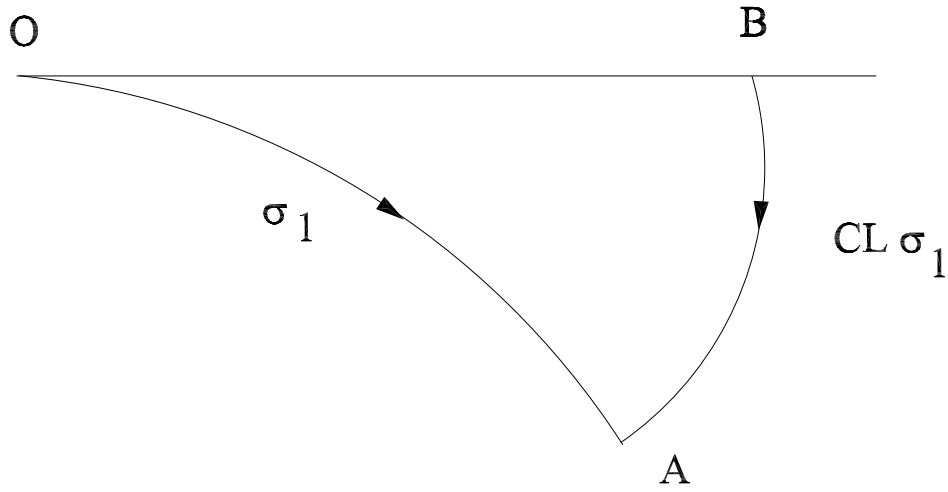


Fig. 2.12: Coulomb operator

ary is given by:

$$\phi = \phi_A + B_1\theta \quad (2.31)$$

Coefficients B_0 and B_1 are constants and ϕ_A is the intersection angle at point A.

Slip-line AB is defined by column vector $a = \{a_n\}$ such that the radius of curvature at any angular position θ from A is given by,

$$R(\theta) = \sum_{n=1}^{\infty} a_n \cdot \frac{\theta^n}{n!} \quad (2.32)$$

Then the radius curvature of line CB is given by,

$$S(\psi) = \sum_{n=1}^{\infty} b_n \cdot \frac{\psi^n}{n!} \quad (2.33)$$

where vector $b = \{b_n\}$ is obtained from a simple matrix transformation:

$$b = \mathbf{CL} a$$

where \mathbf{CL} is the general matrix operator as established by Dewhurst [73] and is given as follows:

$$\mathbf{CL} = \mathbf{Q}_{\theta(B\theta)} + \mathbf{P}_{(B\theta)\theta} (\mathbf{K}_\phi \mathbf{MJ} - m_0 \mathbf{K}_{(\phi+\frac{\pi}{2})} \mathbf{M})^{-1} (\mathbf{K}_\phi - B_0 \mathbf{K}_{(\phi+\frac{\pi}{2})} \mathbf{J}) \quad (2.34)$$

where \mathbf{P} and \mathbf{Q} are the un-starred matrix operators defined earlier (equation 2.15)

and \mathbf{J} and \mathbf{M} are matrices given as,

$$\mathbf{J} = \begin{vmatrix} 0 & 0 & 0 & - & - \\ 1 & 0 & 0 & - & - \\ 1 & 1 & 0 & - & - \\ 1 & 1 & 1 & 0 & - \\ 1 & 1 & 1 & 1 & 0 \end{vmatrix} \quad (2.35)$$

$$\mathbf{M} = \begin{vmatrix} 1 & 0 & 0 & - & - \\ 0 & B_0 & 0 & - & - \\ 0 & 0 & B_0^2 & 0 & - \\ - & - & - & - & - \end{vmatrix} \quad (2.36)$$

and \mathbf{K} is a lower triangular matrix whose general term k_{ij} at row i and column j is given by,

$$\begin{aligned} k_{ij} &= \sum_{p=0}^{\text{int}\left(\frac{i-j}{2}\right)} \binom{i}{j+2p} M_1^{(i-j-2p)} \sin^{(i-j-2p)} \phi_A \binom{j+2p}{p} M_0^p & \text{for } i \geq j \\ &= 0 & \text{for } i < j \end{aligned} \quad (2.37)$$

2.7 Subroutines

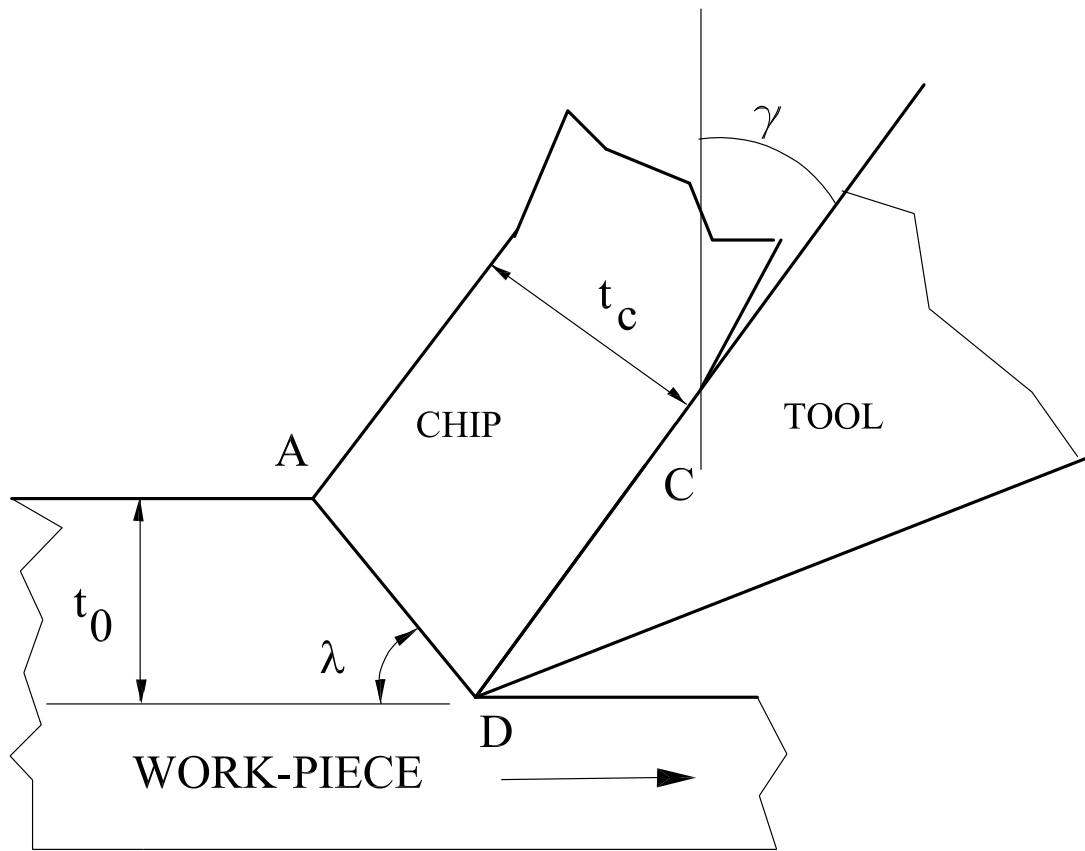
The subroutines used for the present slip-line field analysis were similar to those given in references [72, 73, 74].

3. SLIP-LINE FIELD ANALYSIS OF STRESSES AND STRAINS IN CHIPS ASSUMING NO SINGULARITY AT TOOL TIP

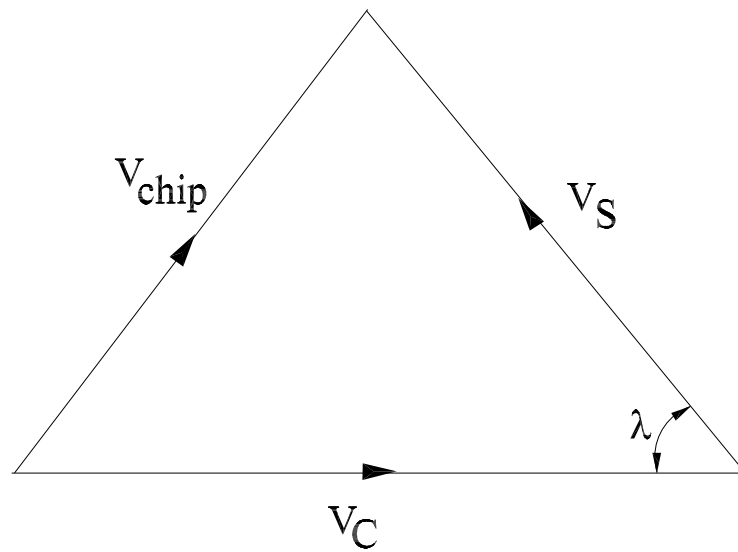
3.1 Introduction

The recent industrial trends towards automated machining systems has led to increased demand for cutting tools that break chips reliably. This in turn requires better predictability of chip form and accurate knowledge of stress and strain distribution in the chip body as a function of the cutting geometry and regime. A comprehensive analysis of metal cutting studies shows that there are several known models of this process resulting in different states of stress and strain in the chip. To make chip breaking process controllable an understanding of the dynamics of chip formation due to these models is vitally important. The earliest model of chip formation was due to Merchant and Ernst [2] who proposed the shear plane model based on the assumption that continuous chip is formed by plastic deformation in a narrow zone (shear plane) that runs from the tool cutting edge to the free surface of the workpiece. The model proposed by them is shown in Fig. 3.1(a) where AD represents the shear plane. Across this plane the work velocity V_c (the tool is assumed stationary) is instantaneously changed to the chip velocity V_{chip} . This requires discontinuity (jump) in the tangential component of velocity across AD equal to V_s as shown in the velocity diagram (Fig. 3.1(b)). Two cardinal principles were established by these authors. These are

- a. Chip equilibrium (the chip can be considered as a rigid body in translational equilibrium under the action of external forces), and
- b. Force velocity co-linearity (the shear and frictional forces at the shear plane and tool-chip contact face are collinear and opposite to the shear and sliding velocities at these two faces respectively).



(a)



(b)

Fig. 3.1: (a) Merchant's shear plane model (b) Velocity field for corresponding model

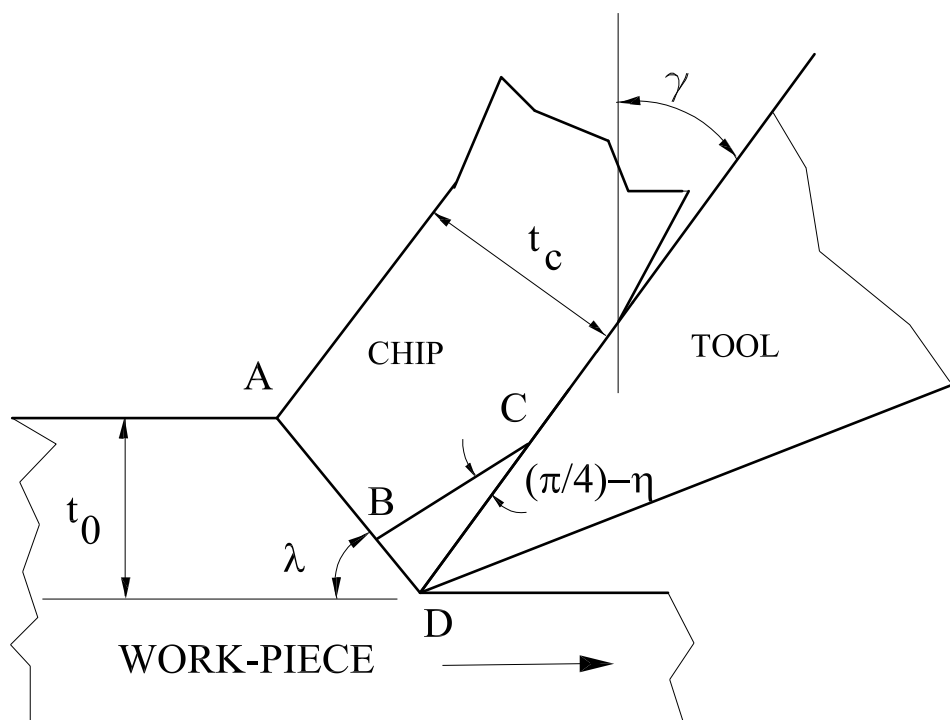


Fig. 3.2: Lee and Shaffer's model

The solution proposed by Merchant is now accepted as an upper bound solution provided the work material could be considered as perfectly plastic. Because of poor agreement of this solution with experimental observations, Merchant [59] introduced the effect of dependency of shear stress on normal stress and proposed a modified shear angle relationship ($2\lambda + \eta - \gamma = \cot^{-1} \kappa, \eta = \tan^{-1} \mu$). Lee and Shaffer [15] applied the slip-line field theory to the problem of metal cutting and assumed a plastic zone in contact with the tool face with uniform stress distribution at the chip-tool interface. This field consisting of straight slip-lines AB, BC and BD is shown in Fig. 3.2. Taking AB and BC as slip-lines of equal length equilibrium of the chip was ensured. Hence, the hydrostatic pressure, equal to the yield stress κ in shear is uniform throughout the field. For this field all the machining parameters are uniquely determined by the tool rake angle γ and rake face friction ratio $\frac{\tau}{\kappa} (= \cos 2\phi_C)$. It may be seen that under high friction condition and with a negative rake tool the shear plane angle λ may be zero or negative which is physically not tenable. Even with low positive rake angle the cutting forces calculated from the above field becomes

extremely high. This led Lee and Shaffer [15] to conclude that under such conditions a small permanent built-up edge similar to a cap of dead metal forms at the tool tip.

After carefully examining the assumptions made in the solutions proposed by Ernst and Merchant and Lee and Shaffer, Shaw, Cook and Finnie [83] draw attention to the inter-relationship between the shear and friction process in metal cutting. The assumption that the shear plane may not lie in the direction of maximum shear stress was incorporated into a slip-line field by these authors. Despite particular anomalies, this approach suggested an important concept, namely, that the compatibility relationship between the shear and friction process is a decisive factor in determining the final steady-state configuration in the cutting process.

The slip-line fields solution due to Lee and Shaffer has been critically examined by Hill [84] who concluded that metal machining may not necessarily ensure a unique solution. In reality, there is always a permissible range of steady state solutions rather than a unique solution. Therefore, a unique state of stress and strain should not be expected in the chip body.

Okushima and Hitomi [85] assumed that shearing takes place within a particular triangular flow region than along a single shear plane. These authors analysed the mechanics of formation of discontinuous chips. However as suggested by Astakhov *et al.*[39] the final strain and stress in the chips calculated using their approach was similar to those obtained using Ernst and Merchant's analysis [2].

Kudo [21] modified Lee and Shaffer's chip streaming solution by introducing a singularity at chip-workpiece intersection point (Fig. 3.4). For the same uncut chip thickness this field yielded lower values of cutting forces compared to those calculated from Lee and Shaffer's solution.

A slip-line field solution for machining involving formation of curled chips was first suggested by Kudo [21]. This field was constructed by replacing the straight slip-lines AB and BC in Lee and Shaffer's solution by a pair of equal and opposite identical circular arcs as shown in Fig. 3.3. This field is associated with the normal stress that decreases continuously from C to D while the shear stress increases.

A non-unique solution for free chip machining assuming stress singularity at tool tip was proposed by Dewhurst [22]. This field, shown in Fig. 3.5 also applies when machining is accompanied by formation of curled chips and degenerates to Lee and

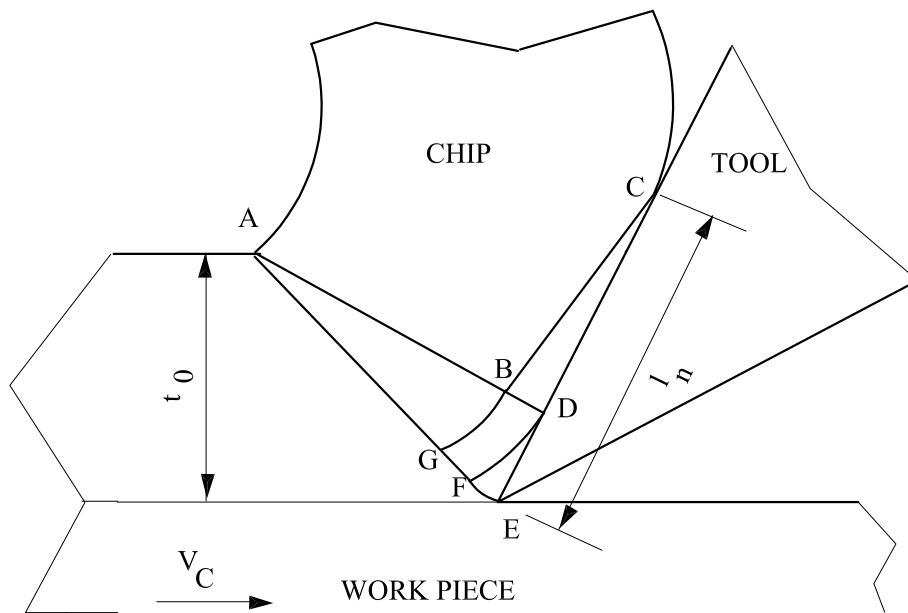


Fig. 3.3: Kudo's field for chip streaming

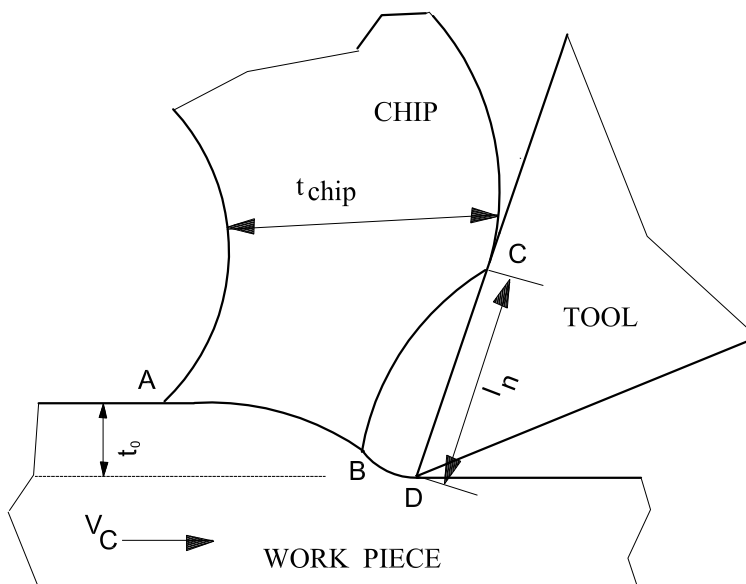


Fig. 3.4: Kudo's field for chip curling

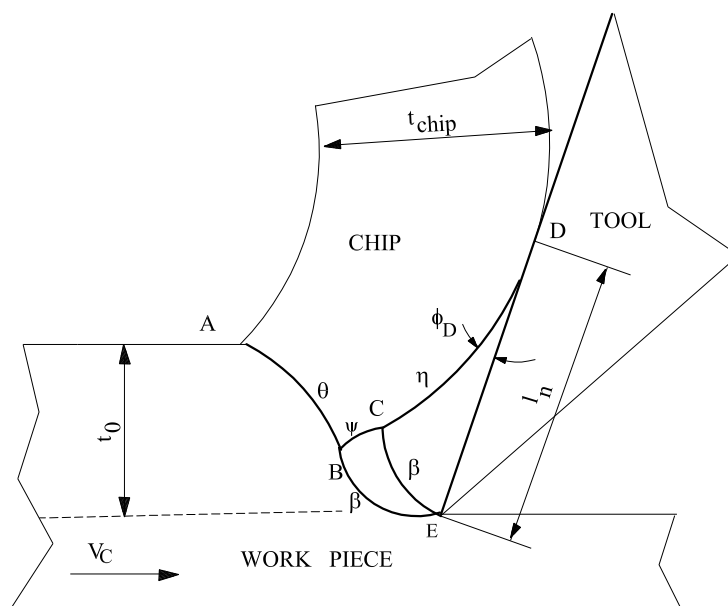


Fig. 3.5: Dewhurst slip-line field

Shaffer's solution with straight slip-lines when the hydrostatic pressure at A equals κ . Dewhurst showed that for any given cutting condition the field parameters computed from this solution remained within a range such that the rigid vertices in the chip or the workpiece were not over-stressed. Free chip solutions involving chip curl has also been proposed by Fang and Jawahir [26] and by Fang [27, 28]. Solutions assuming an elastic contact region has been proposed by Maity and Das [86, 24].

When the rake face is equipped with a chip breaker, the radius of the chip flow circle is modified due to its constraining action. Slip-line field solutions for machining in the presence of a chip breaker constraint has been reported by Shi and Ramalingam [29], Fang [25] for groove type chip breakers, by Dewhurst [23] for ramp type chip breakers and by Maity and Das [87, 88] for step type chip breakers. However, no attempt has been made till date to relate the stresses and strains in the chip as a function of its formation mechanism with efficiency of chip breaking.

In this chapter slip-line field analysis for pure orthogonal cutting is presented when machining with tools with parallel step-type chip breakers. Two slip-line field solutions are proposed. These fields are obtained by modification of chip streaming solutions due to Lee and Shaffer [15] and Kudo [21] discussed earlier. Adhesion

friction (equation (1.5)) at chip-tool interface is assumed and the fields are analysed by the matrix operational procedure developed by Dewhurst and Collins [72] and Dewhurst [73, 74]. For both the fields the cumulative shear strains imparted to the chip material is calculated as a function of the chip breaker height and distance from the cutting edge. The breaking strain is also calculated as ratio of chip thickness to the diameter of chip flow circle. It is shown that as the distance of the chip breaker from the cutting edge increases, the accumulated shear strain in the chip also increases, but the breaking strain decreases thus reducing the tendency for chip breaking.

3.2 Slip-line field solutions

The two slip-line field solutions for metal machining with step-type chip breaker involving chip curl are shown in Fig. 3.6 and 3.7 along with their associated hodographs.

Referring to solution I (Fig. 3.6(a)) it may be seen that the plastically stressed region consists of the primary shear line ABD and the secondary shear zone BCD. The chip boundary is defined by ABC where, BC is the α -line and AB the β -line. Within BCD the deforming material slides on the tool face CD in accordance with the adhesion friction law given by equation (1.5).

Referring to the hodograph shown in Fig. 3.6 (b) it is seen that the material suffers a velocity discontinuity of magnitude ρ on crossing the primary shear-line. Hence, velocity along the slip-line DBA is indicated by the circular arc db in the hodograph, similarly the velocity along slip-line BC is shown by the hodograph curve bc . Since the chip is rotating rigidly with angular velocity ω , the images of lines BA and BC appear in the hodograph, but rotated through 90 degrees in the direction of ω multiplied by the scale factor ω . Thus, the curves ab and bc in the hodograph are geometrically similar to the curves AB and BC in the slip-line field, respectively. Hence, slip-line curve BA is also a circular arc of radius ρ/ω .

It is readily seen that the column vector $\bar{\sigma}$ for the radius of curvature of the slip-line CB is calculated from the relationship:

$$\bar{\sigma} = \left(\frac{\rho}{\omega}\right) \cdot \mathbf{CL}_{\beta\phi_D} \cdot \bar{c} \quad (3.1)$$

where, $\mathbf{CL}_{\beta\phi_D}$ is the linear operator defined by Dewhurst [73, 74] that constructs the

field between the circular arc db and the tool face consistent with the adhesion friction condition given by equation (1.5) and \bar{c} is a column vector representing a unit circle. Slip-line curve BD is similarly calculated from CB using the corresponding operator. Hence, forces and moments on the chip boundary can be calculated.

Solution II shown in Fig. 3.7 is an extension of solution I shown in Fig. 3.6 and consists of the primary shear line AGFE, the secondary shear zones BCD and DEF, a singular field AGB and a quadrilateral region BDFG. The singular field AGB separates the chip from the primary shear line AGFE. Referring to its hodograph, (Fig. 3.7(b)) it is also verified that all velocity boundary conditions are satisfied, namely rigid body rotation of the chip and translational motion along the tool face CDE. Velocity compatibility further requires that efg is a circular arc of radius ρ and that the hodograph curves ba and bc are geometrically similar to their slip-line images BA and BC.

AB and CB are easily calculated from the circular arc efg . Thus,

$$efg = -\rho\bar{c} \quad (3.2)$$

Hence,

$$df = -\rho\mathbf{CL}_{\nu\phi_E}\bar{c} \quad (3.3)$$

and,

$$fd = -\rho\mathbf{R}_\psi\mathbf{CL}_{\nu\phi_E}\bar{c} \quad (3.4)$$

where \mathbf{R} is the reversion operator [72] and ϕ_E is the friction angle at E. db is related to fg and fd by the equation,

$$db = -\rho(\mathbf{P}_\psi^* + \mathbf{Q}_\psi^*\mathbf{R}_\psi\mathbf{CL}_{\nu\phi_E})\bar{c} \quad (3.5)$$

Hence,

$$cb = -\rho\mathbf{CL}_{\beta\phi_D}(\mathbf{P}_\psi^* + \mathbf{Q}_\psi^*\mathbf{R}_\psi\mathbf{CL}_{\nu\phi_E})\bar{c} \quad (3.6)$$

and

$$ab = -\rho\mathbf{S}_\delta(\mathbf{P}_\psi^* + \mathbf{Q}_\psi^*\mathbf{R}_\psi\mathbf{CL}_{\nu\phi_E})\bar{c} \quad (3.7)$$

where, $\delta = (\beta - \theta)$,

$ab = (\omega \text{ AB})$ and

cb = (ω CB)

Hence,

$$AB = -\left(\frac{\rho}{\omega}\right)\mathbf{S}_\delta(\mathbf{P}_\psi^* + \mathbf{Q}_\psi^*\mathbf{R}_\psi\mathbf{CL}_{\nu\phi_E})\bar{c} \quad (3.8)$$

$$CB = -\left(\frac{\rho}{\omega}\right)\mathbf{CL}_{\beta\phi_D}(\mathbf{P}_\psi^* + \mathbf{Q}_\psi^*\mathbf{R}_\psi\mathbf{CL}_{\nu\phi_E})\bar{c} \quad (3.9)$$

In the above equations \mathbf{R} , \mathbf{S} , \mathbf{P}^* and \mathbf{Q}^* are standard matrix operators as discussed by Dewhurst and Collins [72] and ϕ_D and ϕ_E are friction angles at D and E respectively.

It may be seen that the angular coordinates η_i, β_i (Fig. A.1) of any point on the rake face CD (or DE) are related by equation (1.5) through equations,

$$\frac{\sigma}{\kappa} = p_C + 2(\eta_i + \beta_i) + \sin(2(\phi_C + \eta_i - \beta_i)) \quad (3.10)$$

and

$$\frac{\tau}{\kappa} = \cos(2(\phi_C + \eta_i - \beta_i)) \quad (3.11)$$

where, p_C and ϕ_C are the hydrostatic pressure and the friction angle at C respectively. With the assumption of adhesion friction this relation becomes non-linear. Following Dewhurst [73, 74], this non-linear relation was approximated by the linear relation

$$\beta = m_0\eta \quad (3.12)$$

m_0 in equation (3.12) was evaluated by linear regression analysis from angular coordinates of ten discrete points on CD using the relation (refer to Appendix A)

$$m_0 = \frac{\sum_{i=1}^{10} \eta_i^2}{\sum_{i=1}^{10} \eta_i \beta_i} \quad (3.13)$$

This value of m_0 was then utilised to construct the linear operator CL [73, 74].

Under high friction condition (low value of ϕ_C) and high value of η , ($\phi_C + \eta - m_0\eta$) may become negative resulting in negative friction condition at D or E. When this happens, the programme is terminated.

3.3 Method of solution

The slip-line fields shown in Figs 3.6 and 3.7 are of direct type. Hence, these can be constructed when the values of the field variables are known. Both these fields are

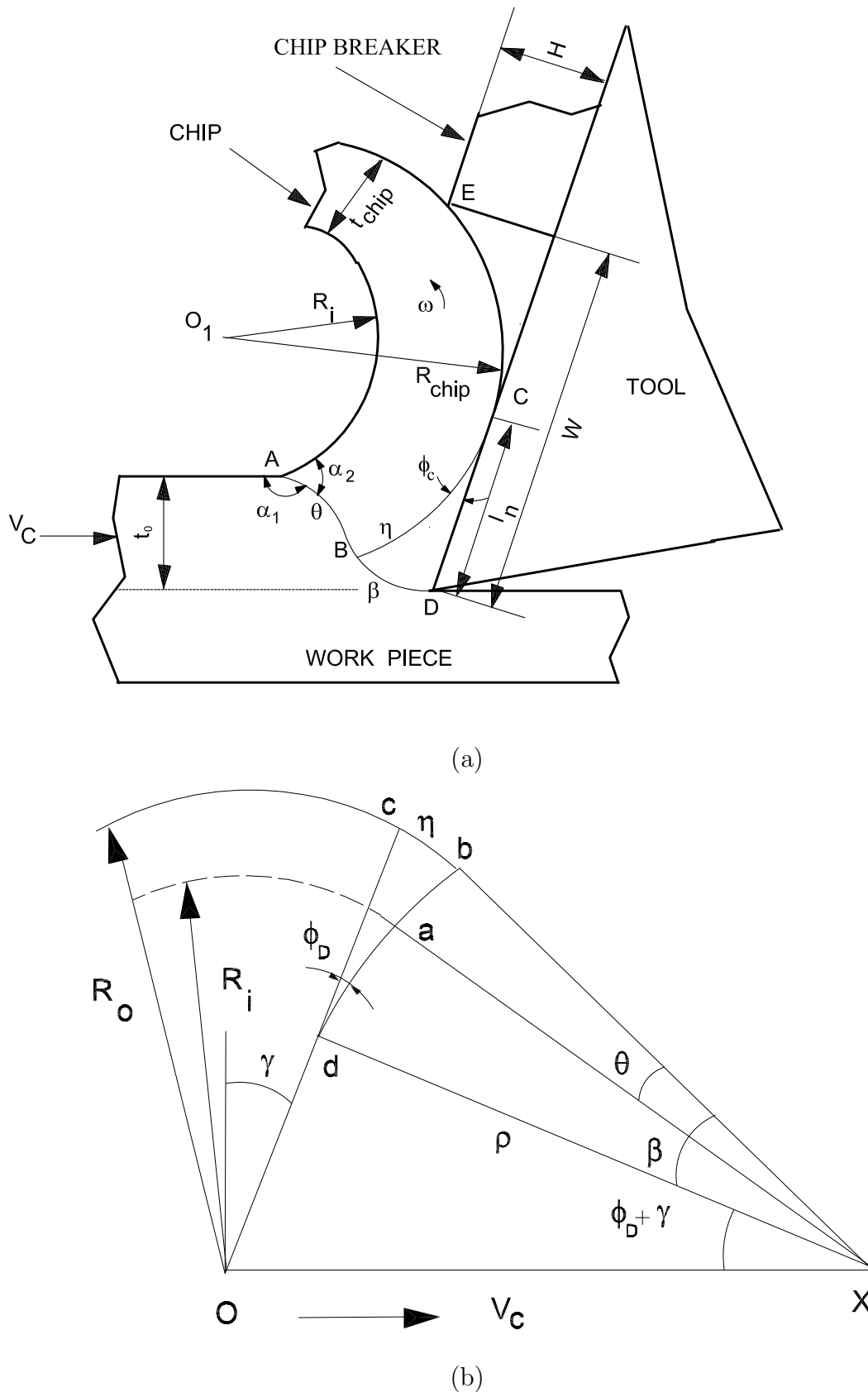
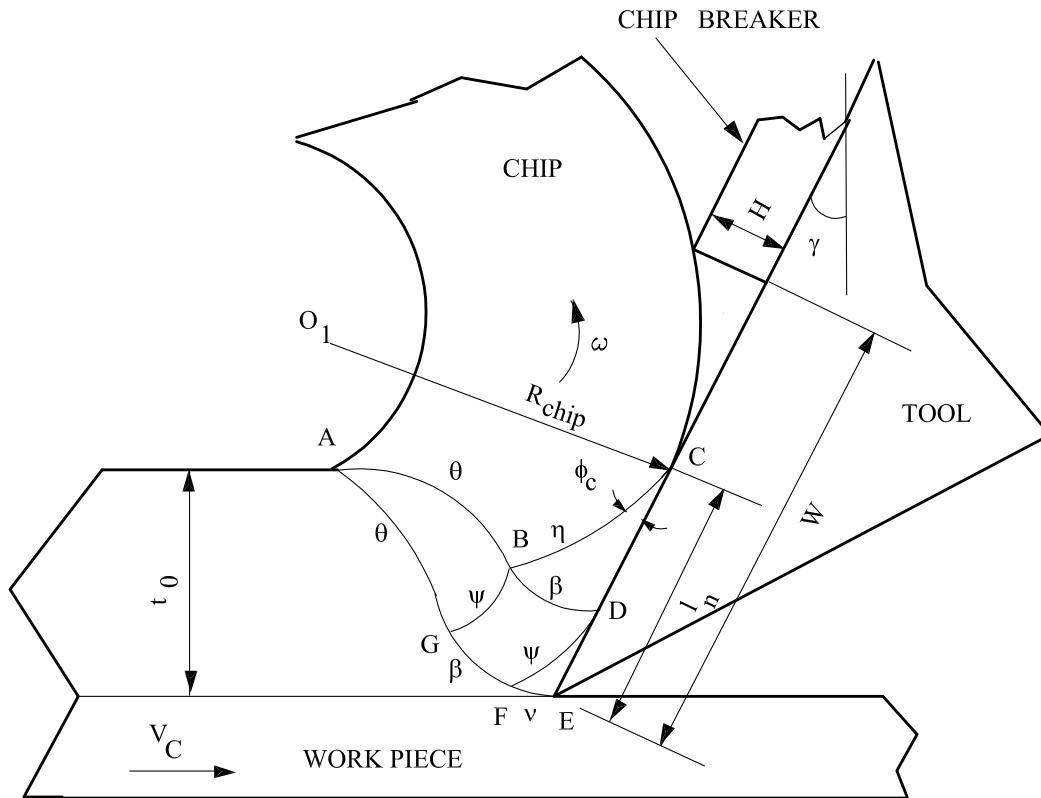
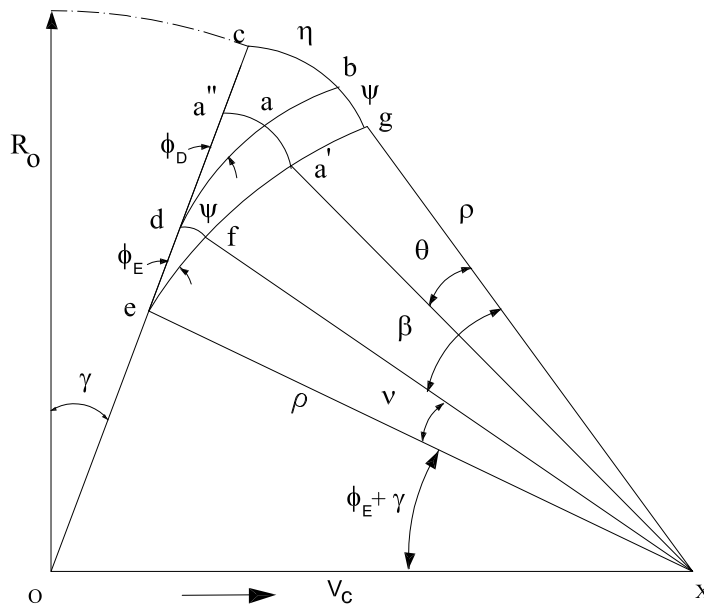


Fig. 3.6: (a) Solution I with chip-breaker (b) Hodograph for corresponding field (not to scale)



(a)



(b)

Fig. 3.7: Solution II with chip-breaker (b) Hodograph for corresponding field (not to scale)

characterised by three degrees of freedom. These are the angular range θ of slip-line AB, the hydrostatic pressure p_C at point C and non-dimensional chip breaker distance WTR ($=W/t_0$) where W is the distance of the chip breaker from the cutting edge and t_0 is the uncut chip thickness. Three conditions also exist from which these three field variables can be determined. These are

- a. The resultant force F_1 perpendicular to the chip breaker must be zero (smooth chip breaker).
- b. The anti-clockwise moment on the chip due to forces on the chip boundary ABC and the chip breaker force F_b must be zero, and
- c. The radius of chip curvature R_{chip} imposed by the chip breaker on the outgoing chip must be equal to that calculated from the hodograph.

Referring to Fig. 3.8 or 3.9 and 3.10 it may be seen that

$$F_2 = F_x \cos(2\alpha - \gamma) + F_y \sin(2\alpha - \gamma) \quad (3.14)$$

$$F_1 = F_y \cos(2\alpha - \gamma) - F_x \sin(2\alpha - \gamma) \quad (3.15)$$

$$d = W - l_n + Y_{BC} \cos(2\alpha - \gamma) - X_{BC} \sin(2\alpha - \gamma) \quad (3.16)$$

$$CE = \sqrt{((W - l_n)^2 + H^2)}$$

$$\sin \alpha = \frac{H}{CE}$$

$$R_{chip} = \frac{CE}{2 \sin \alpha}$$

or,

$$R_{chip} = \frac{(W - l_n)^2}{2H} + \frac{H}{2} \quad (3.17)$$

where, F_x, F_y are the cartesian components of forces at the chip boundary, Y_{BC} and X_{BC} are respectively the vertical and horizontal distances of C from B and l_n is the natural contact length.

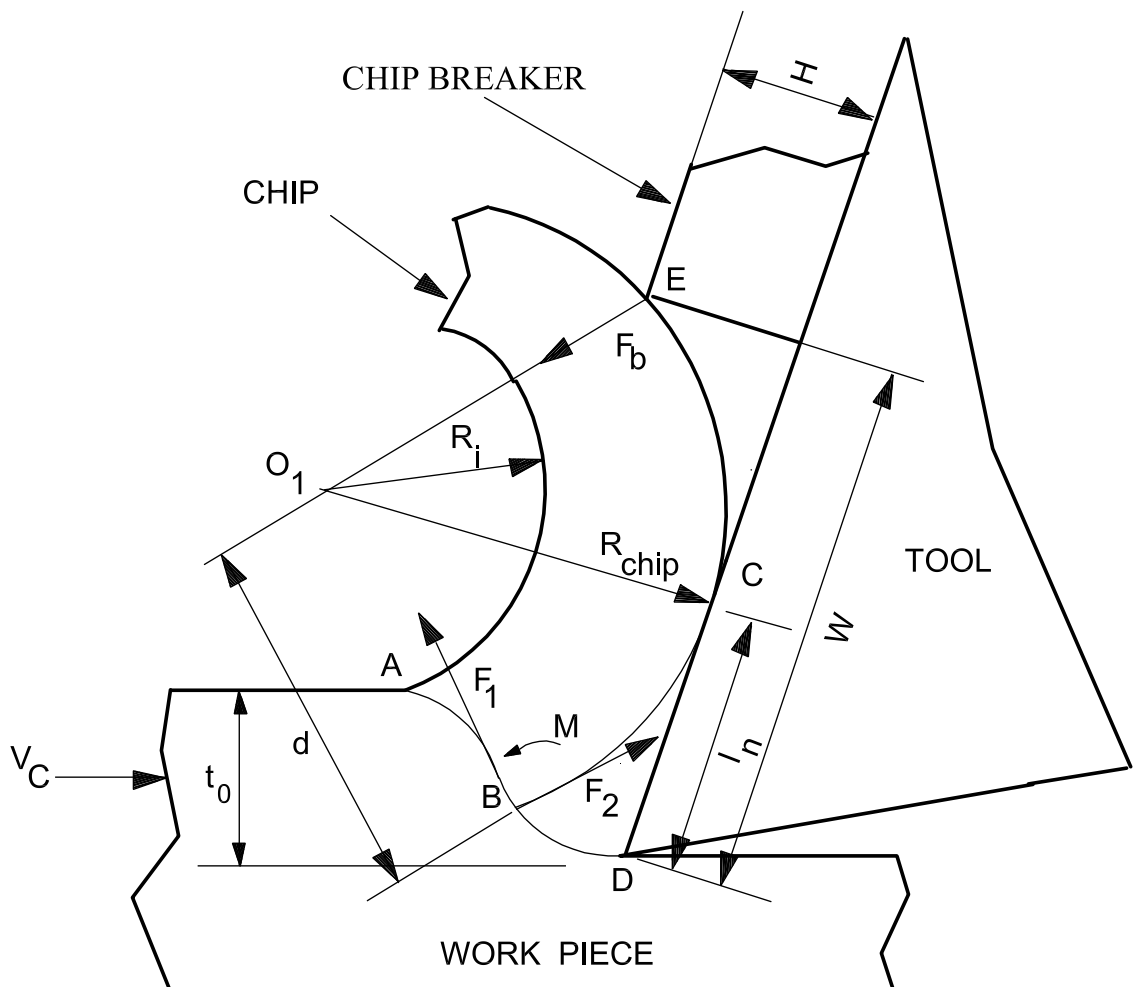


Fig. 3.8: Forces acting on chip in case of Solution I

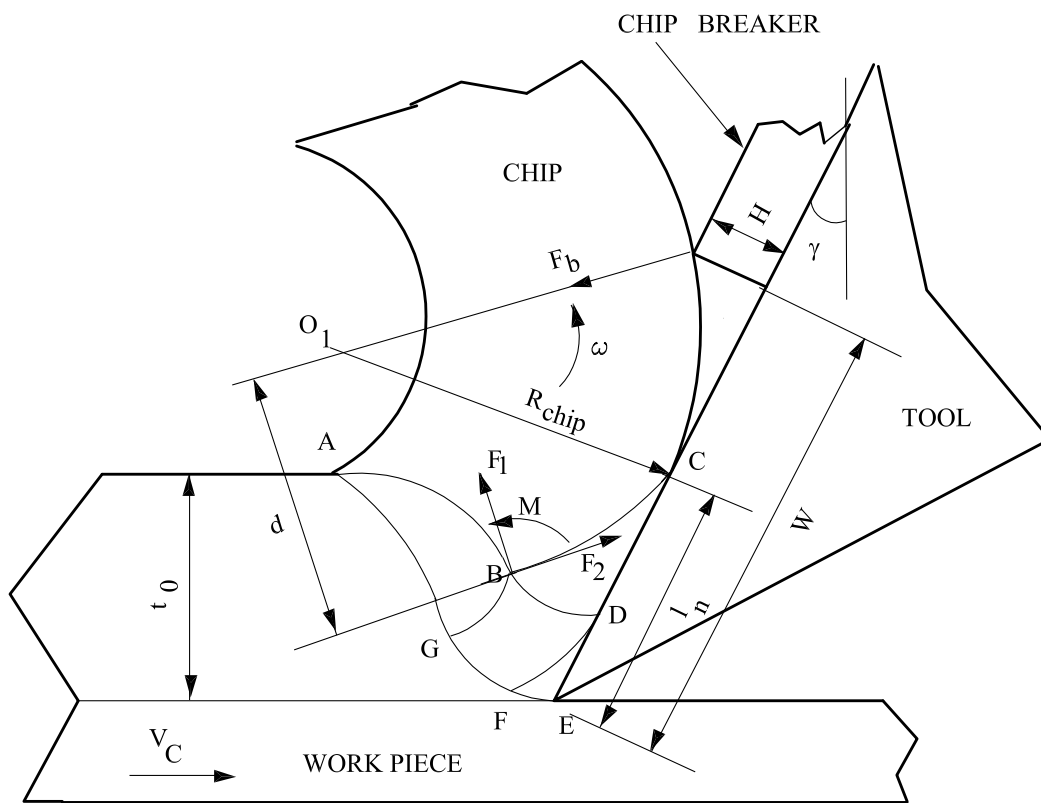


Fig. 3.9: Forces acting on chip in case of Solution II

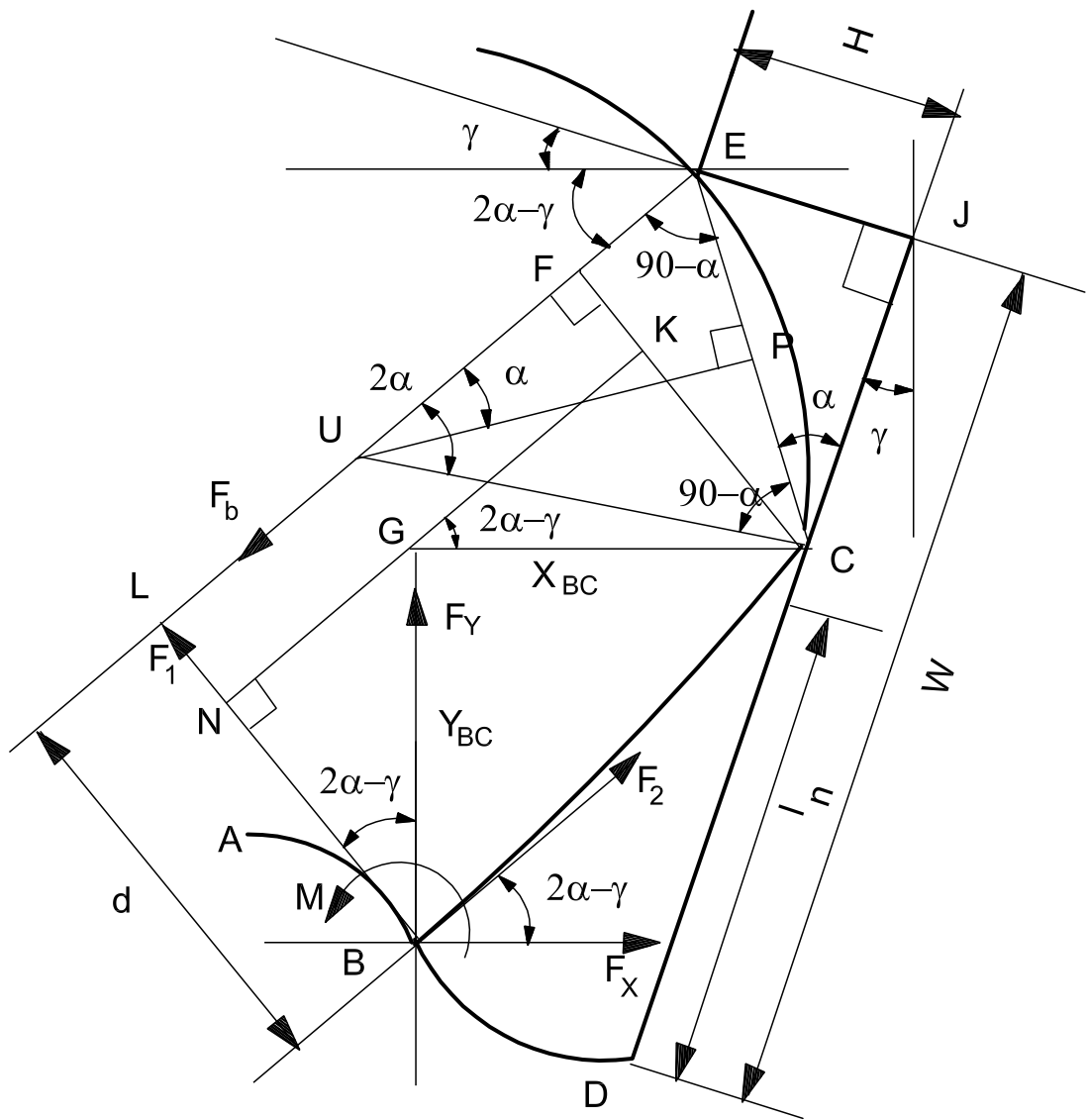


Fig. 3.10: Calculation of distance 'd' and radius of curvature R_{chip}

For inputs of friction parameters μ , n and the angular range η of the base slip-line BC (and fan angle ψ in Fig. 3.7(a)), conditions (a), (b) and (c) result in three non-linear algebraic equations. These may be written as,

$$E_1 = F_1 = 0 \quad (3.18)$$

$$E_2 = M + F_b \cdot d = 0 \quad (3.19)$$

where $F_b = F_2$, and

$$E_3 = R_o - R_{chip} = 0 \quad (3.20)$$

where R_o is the outer radius of chip curvature as determined from the hodographs (Fig. 3.6(b) and Fig. 3.7(b)).

The above equations were solved for θ , p_C and WTR by an algorithm developed by Powell [89] for solution to non-linear algebraic equations with unknown derivatives. θ , p_C and WTR were assumed to be correctly estimated when the sum of the squares of the residuals, $E_1^2 + E_2^2 + E_3^2$ was less than 10^{-10} . These optimised field variables were then used to calculate the cumulative shear strain in the chip.

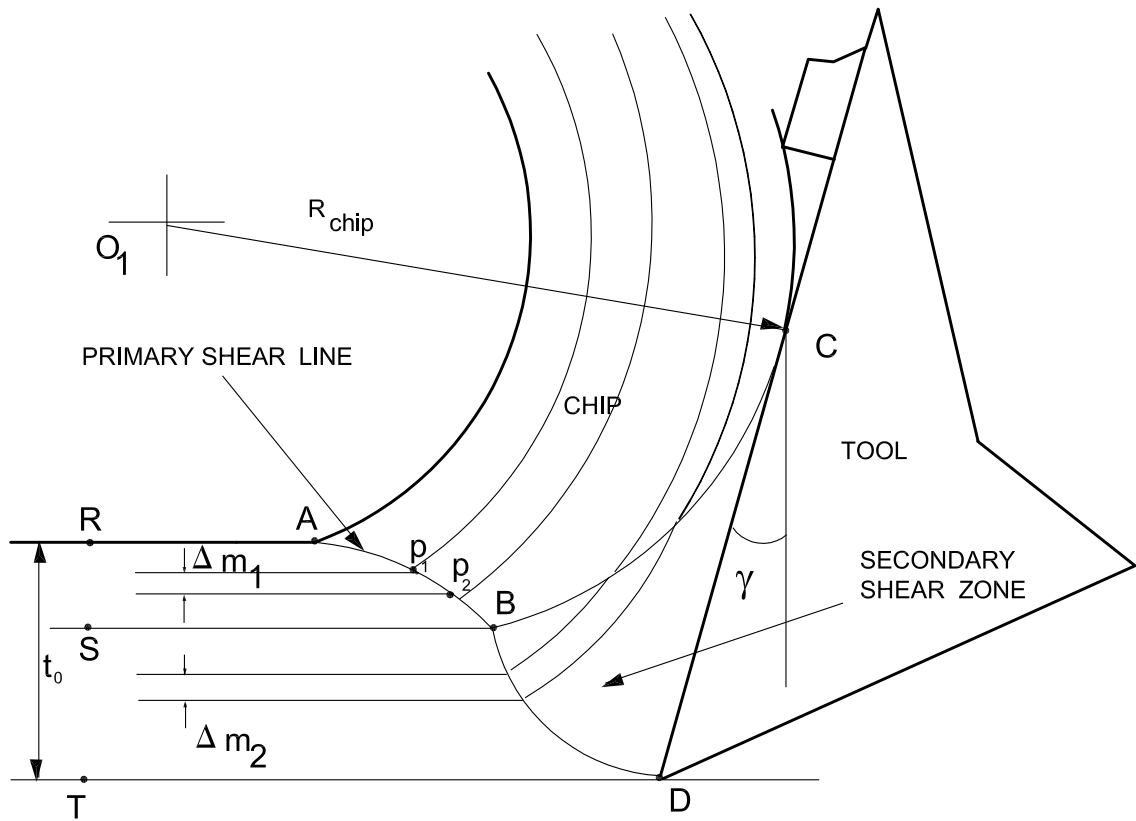
In this manner solutions were generated and machining parameters were computed for a tool with rake angle $\gamma = 5, 10$ and 15 degrees for values of $\mu = 1.0, 2.0, 3.0$, $n = 1.5$ and the non-dimensional chip breaker height HTR ($=H/t_0$) equal to $5, 10$ and 20 . The programme incorporated flatness and mass flux checks as reported in references [87] and [88]. It also contained checks to ensure that the rigid vertices at A are not overstressed by applying Hill's criteria [90] (Refer Appendix B). The programme was terminated when the friction angle at D (or E) became negative or F_b became negative or when l_n was greater than W.

The procedure for determination of θ , p_C and WTR for solution II was identical to that for solution I.

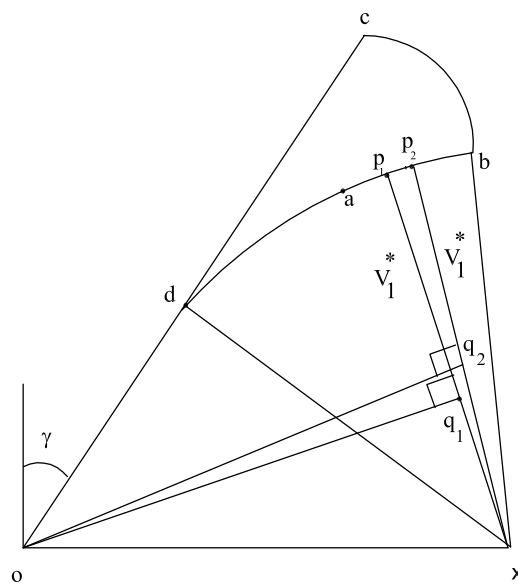
3.4 Streamline Plotting and Strain Estimation in Chips

3.4.1 Streamline Plotting

For the purpose of plotting the streamlines the uncut chip material was divided into regions RS and ST (Fig. 3.11(a)) that experience two different history of deformation.



(a)



(b)

Fig. 3.11: (a) Streamlines in the workpiece and chip (b) Construction for estimation of strain along the primary shear line (not to scale)

The material through RS is strained on crossing the primary line only. The material through ST after being strained by the primary shear line is further strained on passing through the secondary shear zone.

The streamlines through RS (or ST) are horizontal lines before the material undergoes plastic deformation. On crossing the primary shear line AB, the streamlines through RS become circular arcs with centre at O_1 as shown in Fig. 3.11(a).

The region RS is divided into 14 streamtubes with equal mass flow of Δm_1 between two successive streamlines. Similarly, the region ST is discretized into 14 streamtubes with mass flow Δm_2 between two successive streamlines. The material through ST after crossing the primary shear line BD, undergoes further deformation in the secondary shear zone. The streamlines become circular arcs with centre O_1 after crossing the line CB. The method of plotting the streamlines in the secondary deformation zone is discussed in the following section.

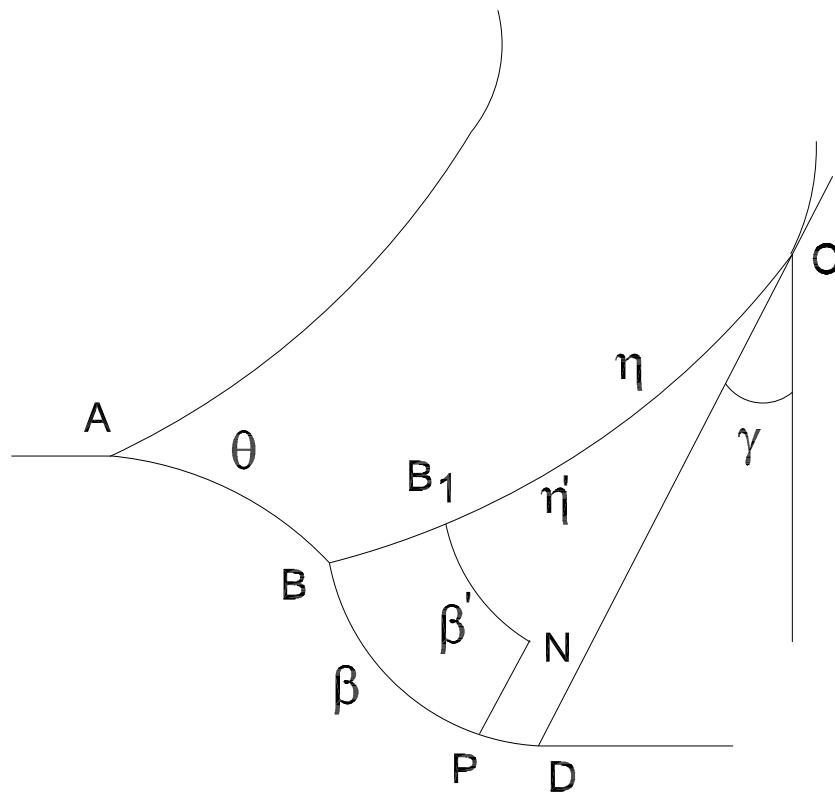
Streamline plotting in secondary deformation zone

The secondary deformation zone is the region formed by the slip-lines CB, BD and tool face CD. The method for plotting of streamlines in this zone [91] is as follows:

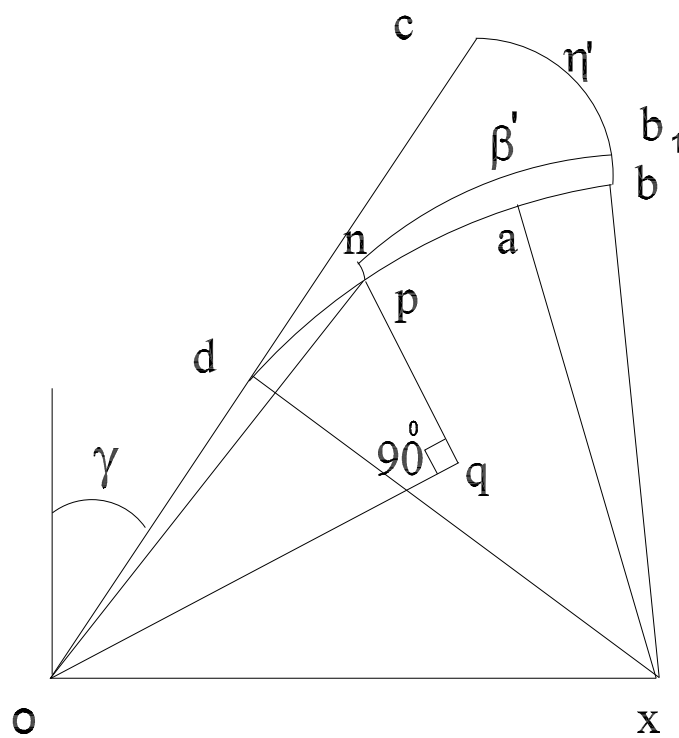
1. For any point P on β -slip-line BD (Fig. 3.12 (a)) the corresponding point 'p' on the hodograph curve bd (Fig. 3.12 (b)) is located.
2. Absolute velocity of point P is obtained from the hodograph, which is equal to 'op'
3. As the work material advances through a distance Δs in a time interval Δt ($\Delta s \rightarrow 0$), the material at P moves through a small distance PN in a direction parallel to the line 'op'. This line represents the newly generated streamline through point P.
4. After a time interval Δt , material reaches point N (Fig. 3.12(a)). Coordinates of point N are calculated from the equations :

$$X_N = X_P + V_X \cdot \Delta t \quad (3.21)$$

$$Y_N = Y_P + V_Y \cdot \Delta t \quad (3.22)$$



(a)



(b)

Fig. 3.12: Construction for plotting of streamlines in the secondary deformation zone. (a) Slip-line field (b) Hodograph

where V_X and V_Y are horizontal and vertical components of velocity at P. The value of time interval, Δt is taken as equal to 0.002 for calculation purpose.

5. To determine the angular coordinates η' and β' of N within the secondary deformation zone an initial guess for the field angles is made and the coordinates X'_N and Y'_N of N are estimated from η' and β' .
6. The exact values of η' and β' are then determined by solution to the two algebraic equations

$$E_4 = (X_N - X'_N) = 0 \quad (3.23)$$

$$E_5 = (Y_N - Y'_N) = 0 \quad (3.24)$$

using Powell's algorithm [89], for sum of square minimization $E_4^2 + E_5^2 \leq 10^{-10}$.

7. In this manner point n corresponding to point N in the secondary deformation zone is located in hodograph(Fig. 3.12(b)).
8. The steps 1 to 7 are repeated by considering the velocity at N till a new point N' is reached. The procedure is continued till the streamline through P reaches the slip-line CB (β' becomes equal to zero). The streamlines in the work material and in the chip for a particular field configuration is shown in Fig. 3.13.

3.4.2 Strain estimation

Strain estimation along primary shear line

The shear strains induced in the material for any given geometry are calculated from the corresponding slip-line field configuration using the method suggested by Atkins *et al.* [75]. For computing the shear strain suffered by the material on crossing the primary shear line, the material flowing through AB or BD is divided into a number of streamtubes (15 numbers each in the present case). If P_1 P_2 are points on a streamtube as shown in Fig. 3.11(a) then the strain $\Delta\epsilon$ suffered by the material flowing through this streamtube may be estimated in the following manner:

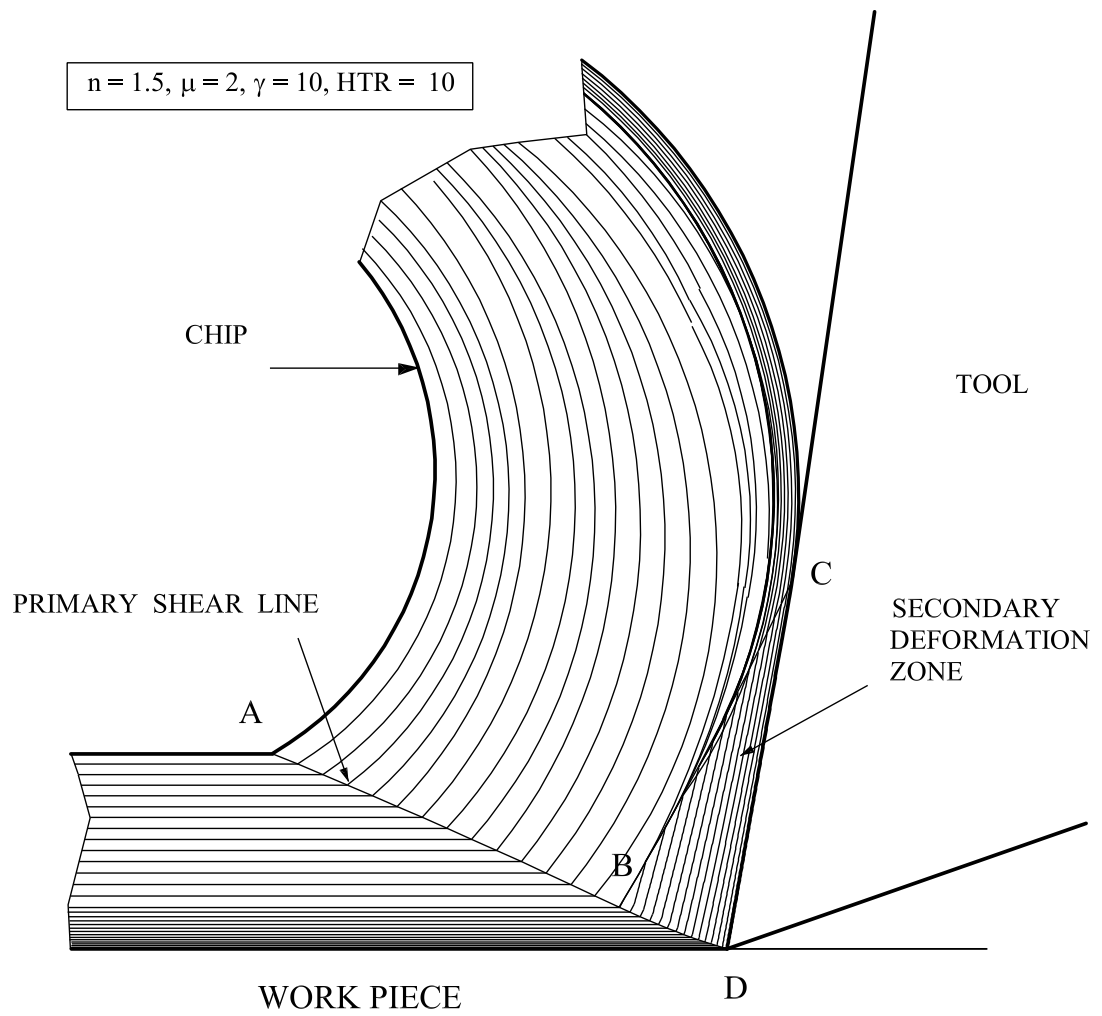


Fig. 3.13: Solution I with streamlines (Chip breaker not shown)

The shear strain $\delta\epsilon_1$ suffered by the material on crossing P_1 is given by [75]

$$\delta\epsilon_1 = \frac{V_1^*}{oq_1} \quad (3.25)$$

Similarly the strain $\delta\epsilon_2$ suffered by the material on crossing P_2 may be written as

$$\delta\epsilon_2 = \frac{V_1^*}{oq_2} \quad (3.26)$$

where V_1^* is the magnitude of velocity discontinuity and oq_1 and oq_2 are perpendicular distances of o from xp_1 and xp_2 respectively(Fig. 3.11(b)). $\Delta\epsilon$ may be assumed as the average of $\delta\epsilon_1$ and $\delta\epsilon_2$ and is given by

$$\Delta\epsilon = \frac{1}{2}(\delta\epsilon_1 + \delta\epsilon_2)$$

On summing up the strain for all streamtubes, the strain ϵ_p for the primary shear lines AB and BD is estimated as

$$\epsilon_p = \frac{\Delta m_1}{t_0} \sum_{i=1}^{14} \left(\frac{\delta\epsilon_i + \delta\epsilon_{i+1}}{2} \right) |_{AB} + \frac{\Delta m_2}{t_0} \sum_{i=1}^{14} \left(\frac{\delta\epsilon_i + \delta\epsilon_{i+1}}{2} \right) |_{BD} \quad (3.27)$$

where, $\delta\epsilon_i$ and $\delta\epsilon_{i+1}$ are respectively the strains as calculated from equations (3.25) and (3.26) for two consecutive streamlines.

Strain estimation in secondary deformation zone

For computing the shear strain in the secondary deformation zone BCD, the material flowing through it was similarly divided in to 14 streamtubes. The shear strains suffered by the material along the i^{th} streamline is calculated at discrete points along this line starting from BD till it crosses slip-line BC as shown in Fig. 3.11(a). The strain suffered by the material in moving from P to N (Fig. 3.12(a)) may be written as,

$$\delta\epsilon_s = \frac{V^*}{oq} \quad (3.28)$$

where V^* = velocity discontinuity 'pn' as shown in Fig. 3.12(b), and oq = perpendicular distance of 'o' from 'pn'. The total strain suffered by the material on moving along this streamline from entry to exit may be written as,

$$\epsilon_s = \sum \frac{V^*}{oq} \quad (3.29)$$

The mean strain values for two successive streamlines is multiplied by the mass flowing through these lines to get the strain for that streamtube. The total shear strain is obtained by summing up of the strain values for all these streamtubes, which can be expressed as:

$$\epsilon_s = \frac{\Delta m_2}{t_0} \sum_{i=1}^{14} \left(\frac{\epsilon_{si} + \epsilon_{s(i+1)}}{2} \right) \quad (3.30)$$

Hence the total strain ϵ_t experienced during the chip formation can be expressed as

$$\epsilon_t = \epsilon_p + \epsilon_s \quad (3.31)$$

The procedure for plotting the streamlines for field II was exactly similar to that for field I. For this case the uncut chip material was divided into three different flow zones RS, ST and TU as shown in Fig. 3.14. The material through RS entered into the deformation zone through AG. Similarly the material through ST moved into the deformation zone through GF and material through TU through FE. For each zone the streamlines were plotted using the procedure as discussed earlier. The streamlines for a particular geometry for this solution is shown in Fig. 3.15.

For solution II (Fig. 3.7), the primary shear strains ϵ_p induced in the material along the primary shear line AGFE in Fig. 3.14 was estimated by the method described earlier. Each of the lines AG, GF and FE were discretised into 14 straight elemental regions. For each element the average normal component of the velocity was obtained from the hodograph and the shear strain was calculated as the ratio of the magnitude of the velocity discontinuity to the normal velocity. On summing up the shear strains for all elements the total strain ϵ_p along the primary shear line AGFE was estimated as

$$\epsilon_p = \frac{\Delta m_1}{t_0} \sum_{i=1}^{14} \left(\frac{\delta\epsilon_i + \delta\epsilon_{i+1}}{2} \right) |_{AG} + \frac{\Delta m_2}{t_0} \sum_{i=1}^{14} \left(\frac{\delta\epsilon_i + \delta\epsilon_{i+1}}{2} \right) |_{GF} + \frac{\Delta m_3}{t_0} \sum_{i=1}^{14} \left(\frac{\delta\epsilon_i + \delta\epsilon_{i+1}}{2} \right) |_{FE} \quad (3.32)$$

The shear strains experienced by the streamtubes while crossing the secondary deformation zones BCD, FDE, AGB and quadrilateral zone GBDF shown in Fig. 3.14 were computed in the manner as discussed with reference to solution I. The total strain ϵ_s due to shear in the secondary deformation zone was calculated by summing up the strains for each streamtubes using the equation given below (Fig. 3.15):

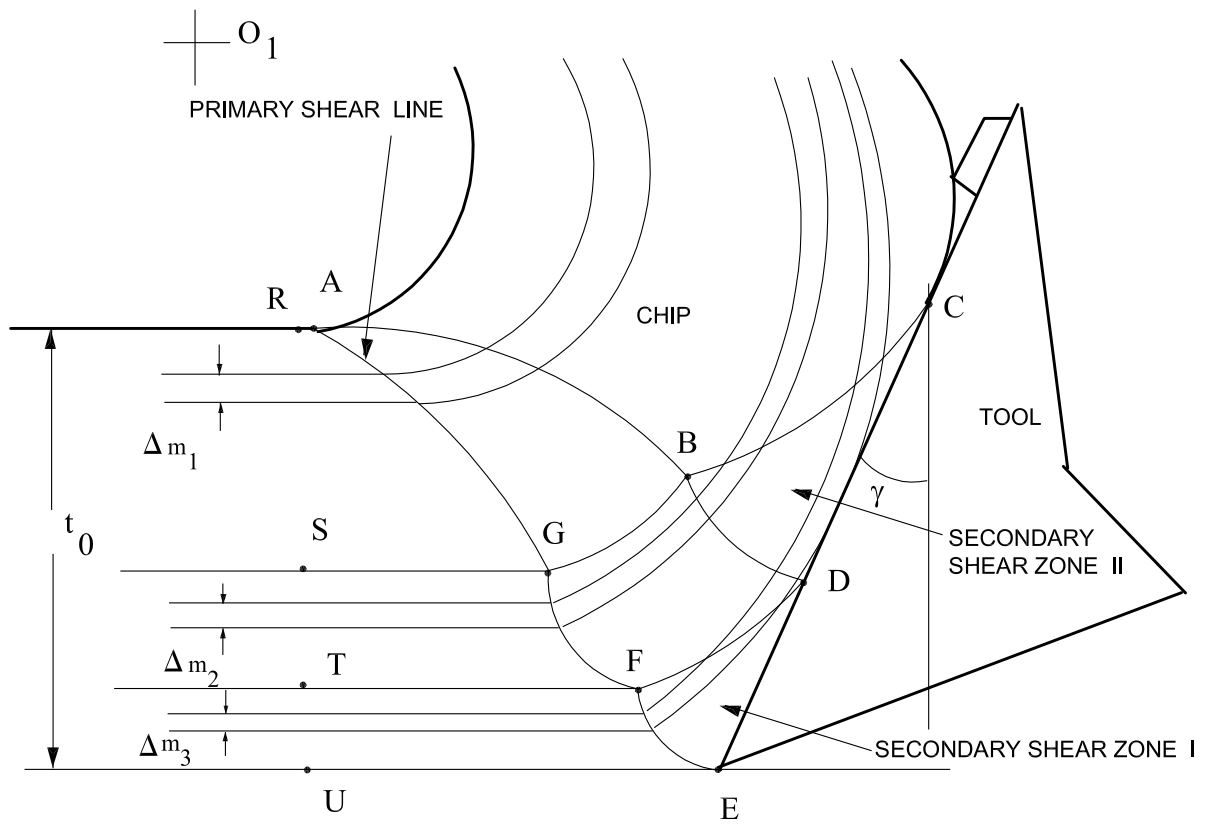


Fig. 3.14: Flow zones for plotting of streamlines for solution II

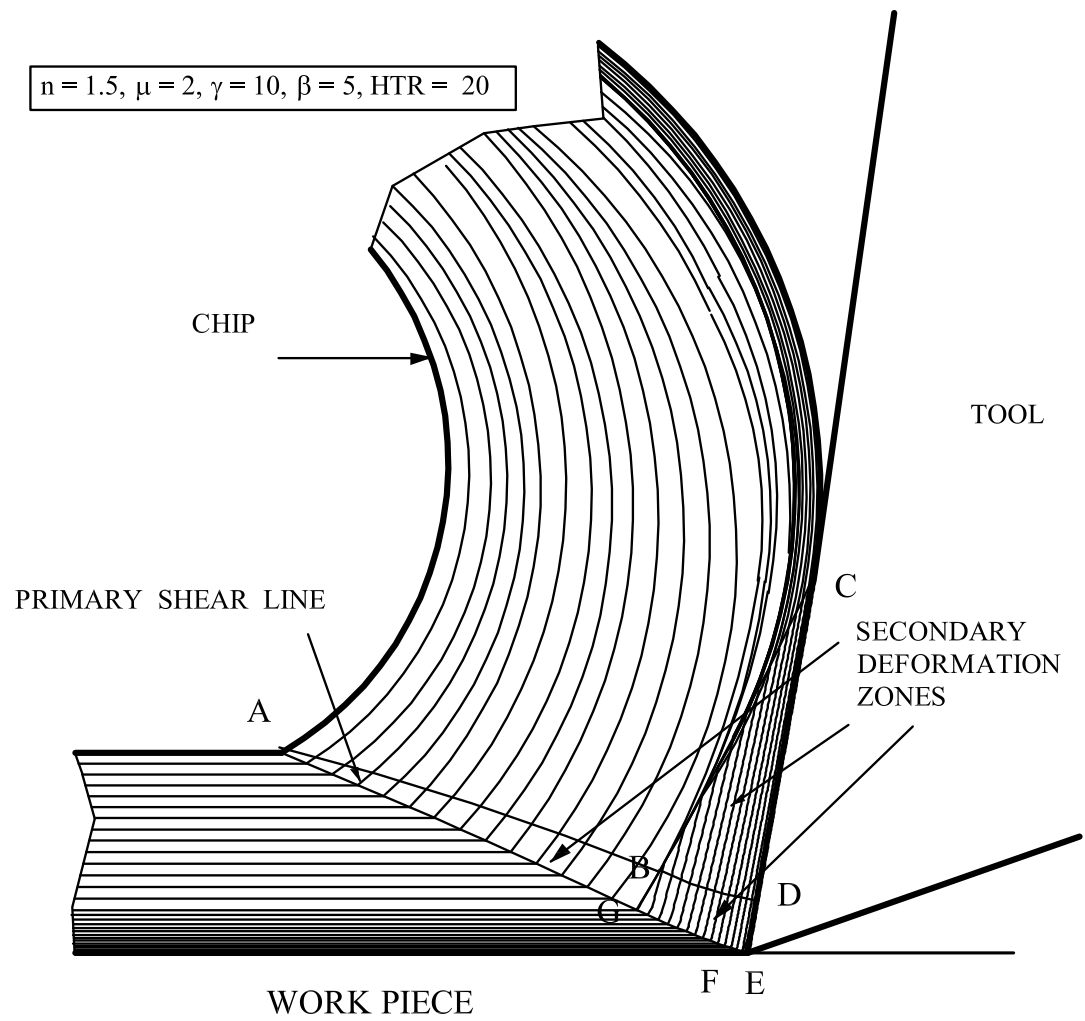


Fig. 3.15: Solution II showing streamlines of flow (Chip breaker not shown)

$$\begin{aligned} \epsilon_s = & \frac{\Delta m_1}{t_0} \sum_{i=1}^{14} \left(\frac{\epsilon_{si} + \epsilon_{s(i+1)}}{2} \right) |_{AGB} + \frac{\Delta m_2}{t_0} \sum_{i=1}^{14} \left(\frac{\epsilon_{si} + \epsilon_{s(i+1)}}{2} \right) |_{GBDF} \\ & + \frac{\Delta m_3}{t_0} \sum_{i=1}^{14} \left(\frac{\epsilon_{si} + \epsilon_{s(i+1)}}{2} \right) |_{FDE} + \frac{(\Delta m_2 + \Delta m_3)}{t_0} \sum_{i=1}^{14} \left(\frac{\epsilon_{si} + \epsilon_{s(i+1)}}{2} \right) |_{BCD} \end{aligned} \quad (3.33)$$

3.5 Breaking strain estimation

Nakayama [32, 51] had shown that the chip breaks when the strain of its skin reaches maximum elongation of the chip material before its tip can escape through the bottom of the tool. This condition is expressed as

$$\epsilon_b = \frac{t_{chip}}{2} \left[\frac{1}{R_{chip}} - \frac{1}{R_L} \right] \quad (3.34)$$

where R_L is maximum radius of chip curvature when fracture occurs, R_{chip} is outer radius of chip flow circle imposed by the chip breaker and t_{chip} is chip thickness (Fig. 3.6(a)).

R_L is usually much larger than R_{chip} . Worthington [41] considered R_L to be about 2 times R_{chip} . However, as indicated by Nakayama [32] R_L has less effect on chip breaking.

Hence, the term $(1/R_L)$ in equation (3.34) has little contribution to breaking strain. On neglecting this term the expression for breaking strain ϵ_b is written as

$$\epsilon_b = \left[\frac{t_{chip}}{2R_{chip}} \right] \quad (3.35)$$

3.6 Results and Discussion

The results of computation from the slip-line field analysis are presented in this section, where the nature of variation of important cutting parameters like cutting ratio ζ , breaking strain ϵ_b , primary strain ϵ_p , secondary strain ϵ_s , chip radius of curvature R_{chip} , contact length l_n , cutting forces and chip breaker force F_b are studied as functions of feed t_0 , chip breaker position W , rake angle γ for different tool/chip interface friction conditions. The cutting and field parameters referred to above are

non-dimensionalised by dividing them with uncut chip thickness t_0 for rational comparison of results obtained from various slip-line fields with experiments presented in the subsequent chapters. The non-dimensional chip breaker parameter HTR in these plots refers to the ratio of height H of the chip breaker to uncut chip thickness t_0 . Thus, for a constant chip breaker height H, a lower value of HTR represents higher feed and vice-versa. WTR is the ratio of distance W of chip breaker position from tool cutting edge to the uncut chip thickness t_0 (Fig. 3.6(a) and 3.7(a)).

The primary strain ϵ_p referred to above indicates the strain imparted to the chip material on crossing the primary shear line. Similarly, the secondary strain ϵ_s corresponds to the strain suffered by the material while crossing the secondary shear zone. Point N in the above graphs represents the limit of solutions beyond which the friction angle at D or E becomes negative.

The predicted variation of total strain $\epsilon_t (= \epsilon_p + \epsilon_s)$ and primary strain ϵ_p with WTR is shown in Fig. 3.16 and 3.17 for solutions I and II respectively. The figures indicate that both ϵ_t and ϵ_p increase with feed and WTR and that $\epsilon_s (= \epsilon_t - \epsilon_p)$ constitutes only an insignificant percent of ϵ_t ($\approx 10 - 15\%$) for the whole range of WTR studied. Thus ϵ_t and ϵ_p can not possibly be correlated with chip breaking since moving the chip breaker away from the cutting edge (High value of WTR) usually results in poor chip breaking even though the absolute values of these strains increase.

It may also be seen that both ϵ_t and specific cutting energy (F_c/t_0) decrease with tool rake angle γ even though they increase with increase in WTR (Fig. 3.18 and 3.19). However, both breaking strain ϵ_b and secondary strain ϵ_s decrease with WTR as may be observed with reference to Fig. 3.20 and 3.21.

It is further demonstrated that the chip thickness ratio ζ increases as WTR and feed increases (Fig. 3.22 and Fig.3.23). Since in metal machining an increased value of ζ is always associated with an increased shear strain, these results are consistent with those shown in Fig. 3.16 to 3.19. The results also agree with the findings of Dewhurst [23] for a ramp type chip breaker. It may further be inferred that since ϵ_s constitutes only a small percentage of total strain ϵ_t , the bulk of the ‘damage’ is experienced by the material when it crosses the primary shear line.

It, therefore, appears that a chip breaking criterion based on specific cutting energy as proposed by Grzesik *et al.* [55] nor that based on total ‘material damage’

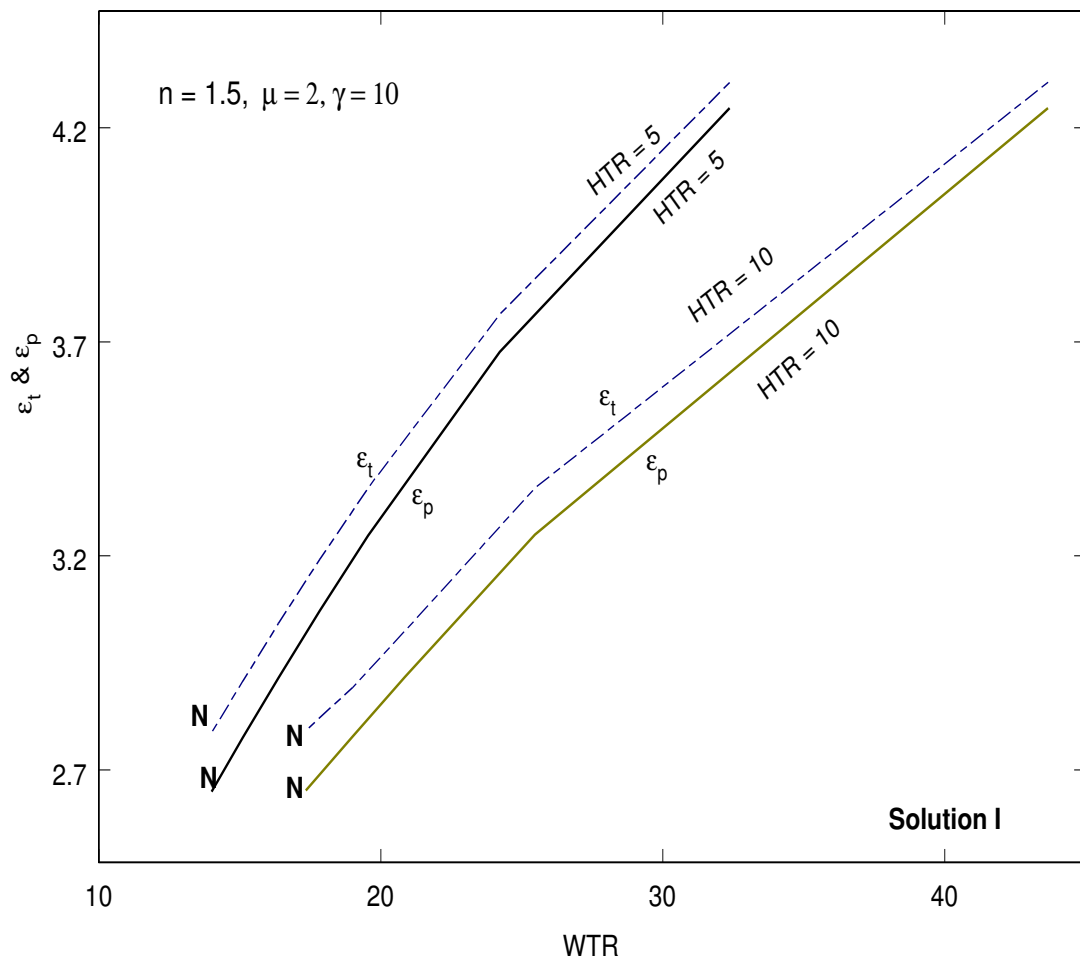


Fig. 3.16: Variation of total strain ϵ_t and ϵ_p with chip-breaker position and feed, N= Negative friction angle limit

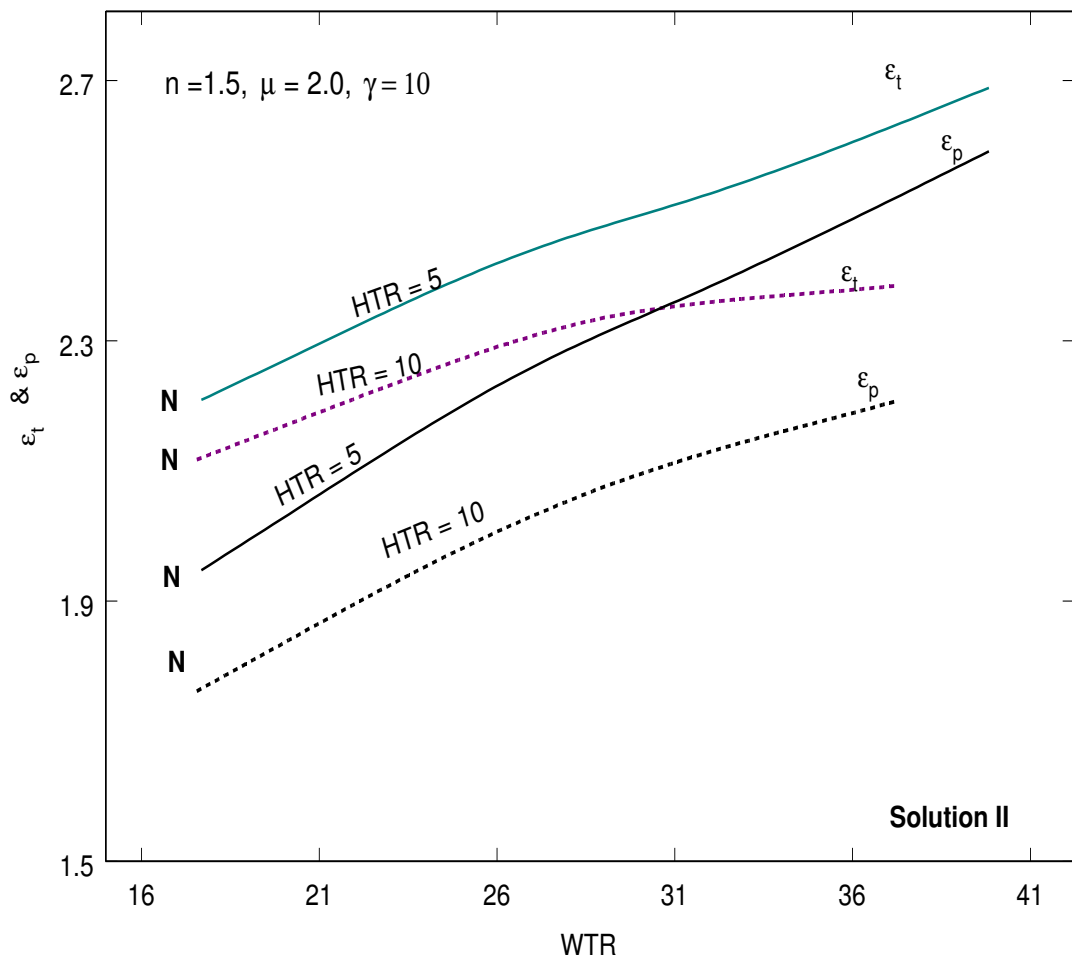


Fig. 3.17: Variation of total strain ϵ_t and ϵ_p with chip-breaker position and feed, N= Negative friction angle limit

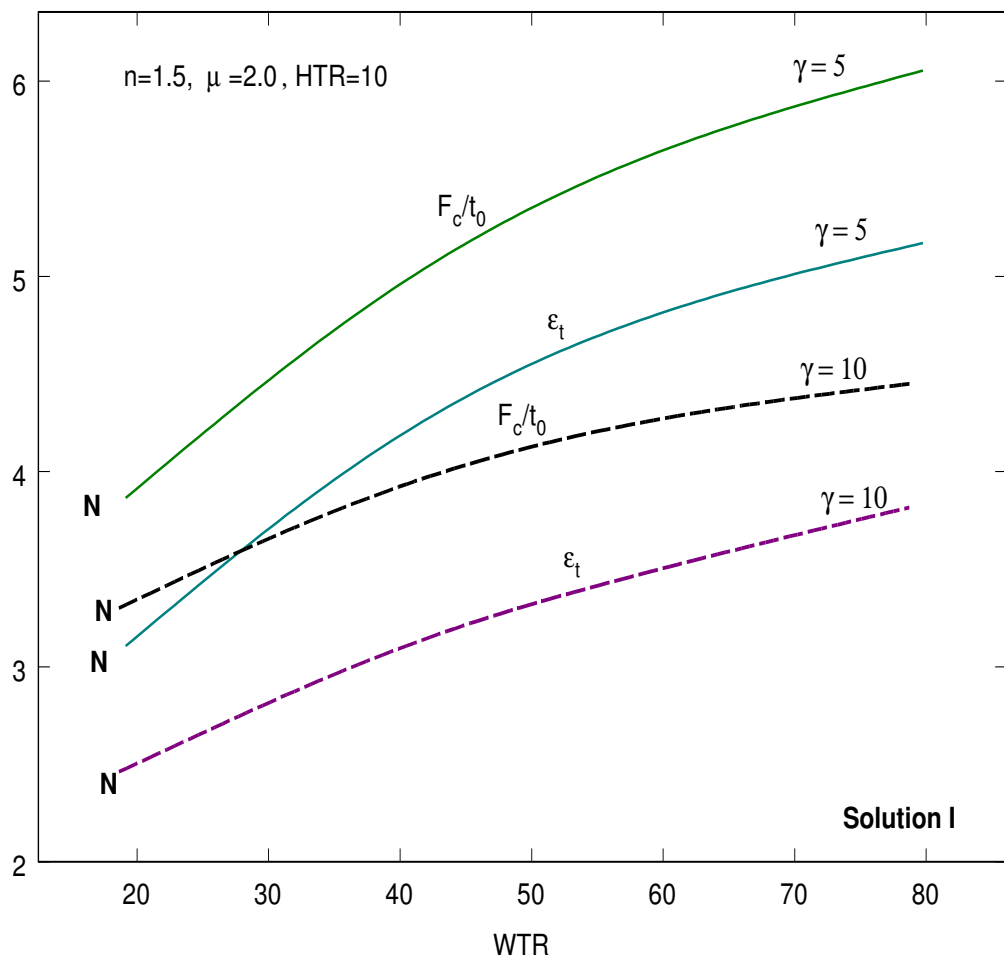


Fig. 3.18: Variation of total strain ϵ_t and specific cutting energy (F_c/t_0) with chip-breaker position and rake angle γ , N= Negative friction angle limit

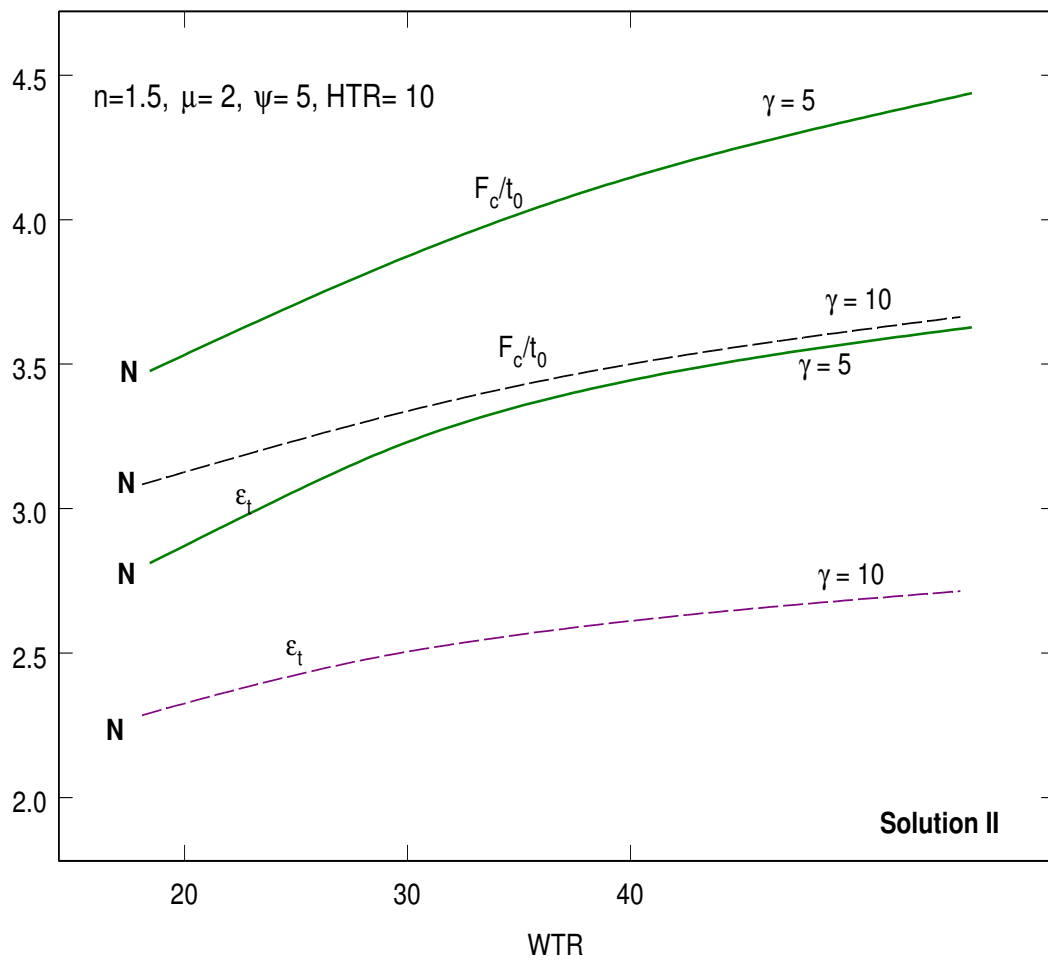


Fig. 3.19: Variation of total strain ϵ_t and specific cutting energy (F_c/t_0) with chip-breaker position and rake angle γ , N= Negative friction angle limit

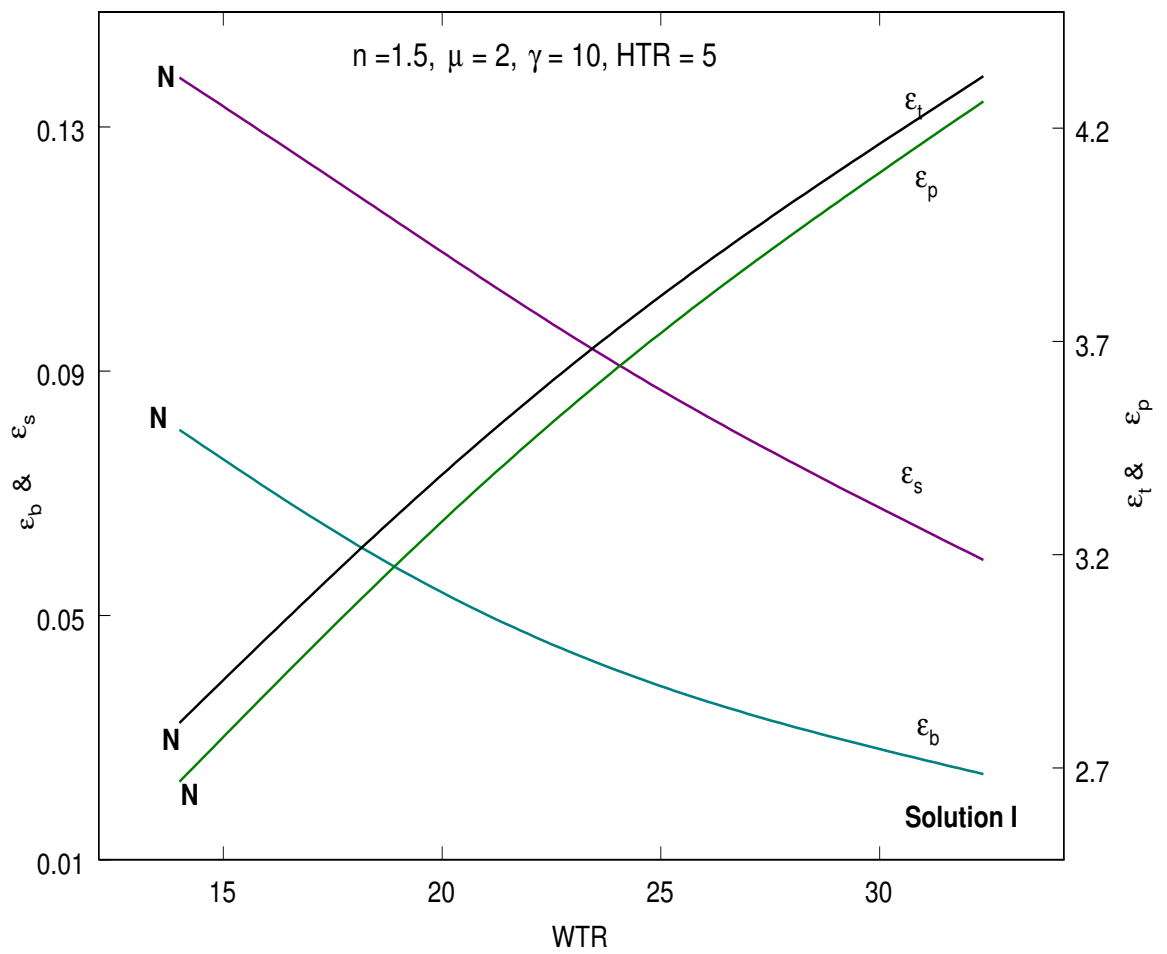


Fig. 3.20: Variation of ϵ_t , ϵ_p , ϵ_s and ϵ_b with chip-breaker position, N= Negative friction angle limit

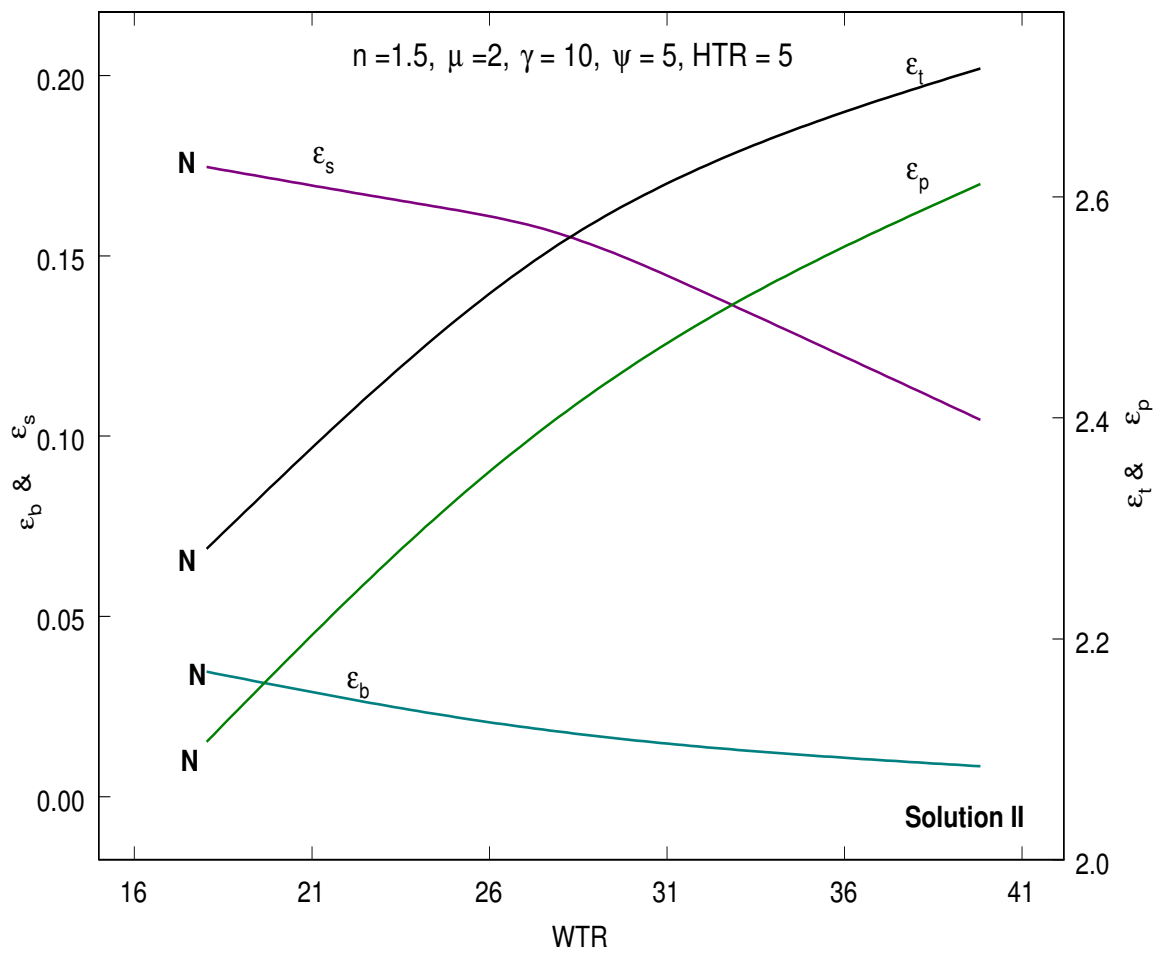


Fig. 3.21: Variation of ϵ_t , ϵ_p , ϵ_s and ϵ_b with chip-breaker position, N= Negative friction angle limit

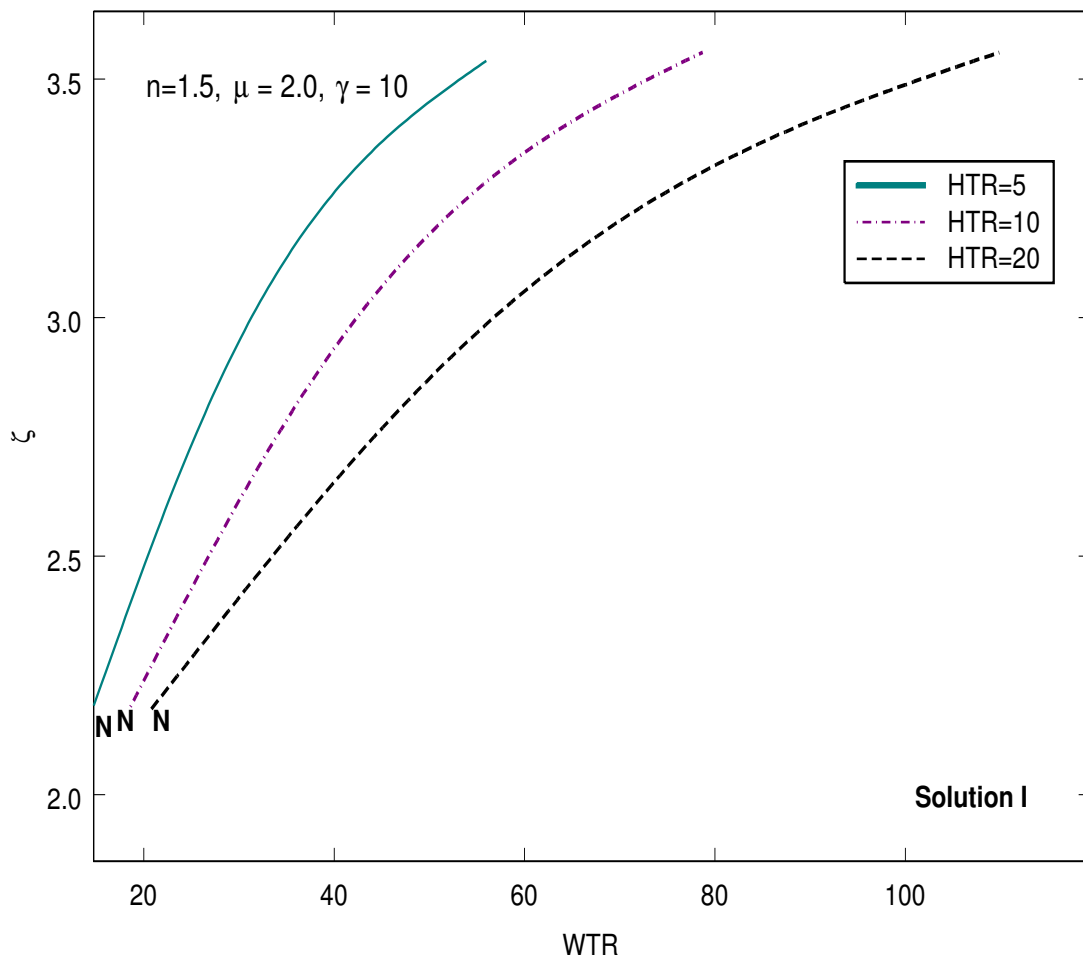


Fig. 3.22: Variation of cutting ratio ζ with chip-breaker position and feed, N= Negative friction angle limit

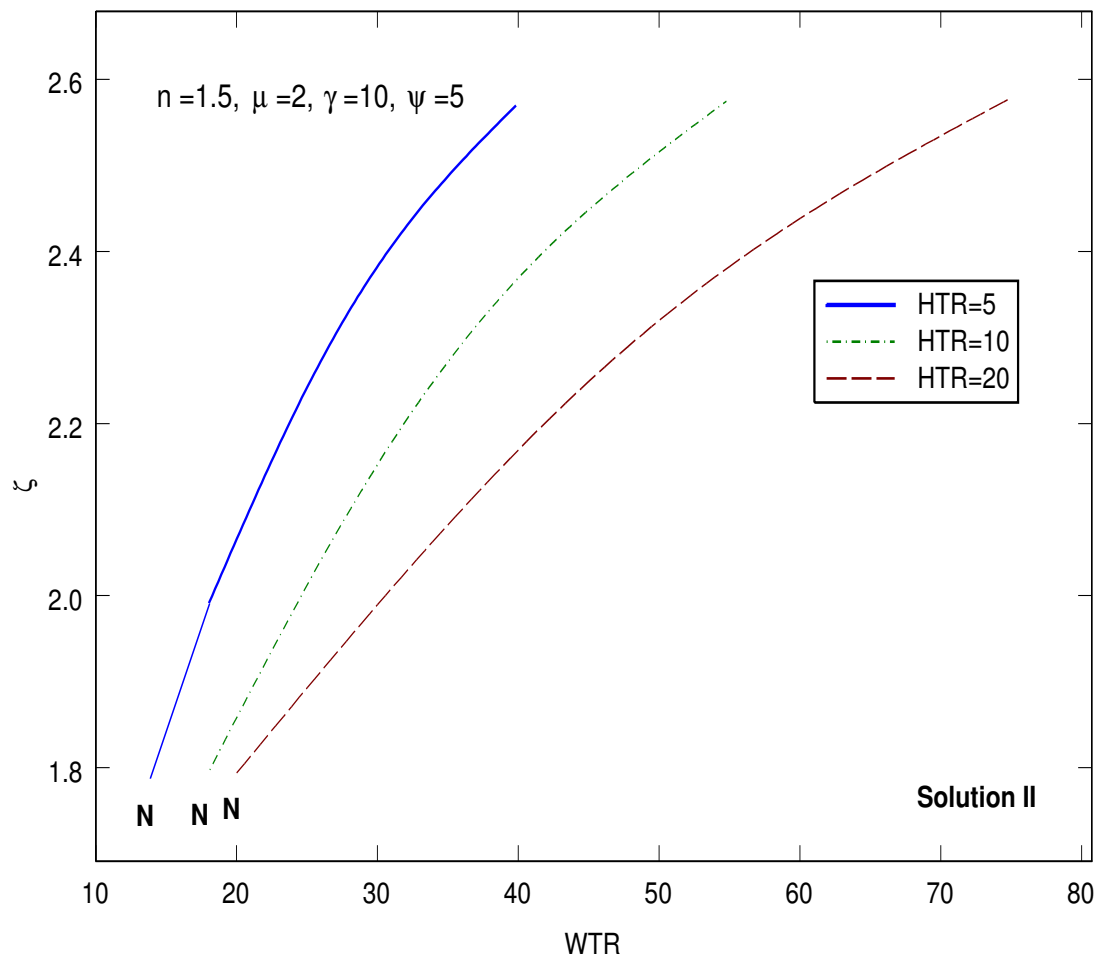


Fig. 3.23: Variation of cutting ratio ζ with chip-breaker position and feed, N= Negative friction angle limit

proposed by Athavale *et al.* [54] can be taken as a criterion to assess effectiveness of chip breaking at least within the assumption of rigid-perfectly plastic material behaviour. It is a well-known experimental observation that for any given value of feed, as the chip breaker moves away from the cutting edge, the effectiveness of chip breaking decreases. The present theoretical analysis suggest that both (F_c/t_0) and ϵ_t increases with WTR even though the chip breaker becomes less effective. Hence it appears that the bending strain ϵ_b is most likely the critical parameter in chip breaking and when this attains a certain threshold value there is likelihood of chip fracture [91]. It may further be concluded that proper positioning of a chip breaker not only decreases the energy consumption but also helps in producing effectively broken chips.

The variation of breaking strain with chip breaker position and rake angle is depicted in Fig. 3.24 for solution I. It is clear from this figure that for a fixed position of chip breaker, the increase in rake angle, decreases the breaking strain. The tendency of chip breaking thus decreases with increase in rake angle, that is, the chip breaker has to be brought nearer to the cutting edge for effective chip breaking. For the same value of feed, this also increases the breaking strain (Fig. 3.25 and Fig. 3.26).

Fig. 3.27 refers to the variation of breaking strain with chip breaker position and friction coefficient. The figure indicates that increased friction at chip/tool interface helps in chip breaking. However, with very severe friction condition ($\mu = 3$), the slip-line field solutions are found to be limited by negative friction angle. Nevertheless, the range of solutions obtained with $\mu = 2$, are well behaved and cover all the three main types of chips, i.e., under-broken, effectively-broken and over-broken.

It may be seen that the normalized radius of chip curvature R_{chip}/t_0 decreases or chip curls tightly when the chip breaker is brought nearer to the cutting edge. This helps in effective breaking of chips. However, rake angle is found to have negligible effect on chip curvature (Fig. 3.28), though it is found to be affected significantly by feed (Fig. 3.29 and 3.30). Thus, for the same position of the chip breaker, as feed increases radius of chip curl decreases which aids in chip breaking. According to Nakayama [32] feed and chip curl are two most important parameters that influence chip breaking. At low feed large chip curl radius is obtained and this results in under-breaking of chips. Chips with small curl radius are obtained when feed is increased.

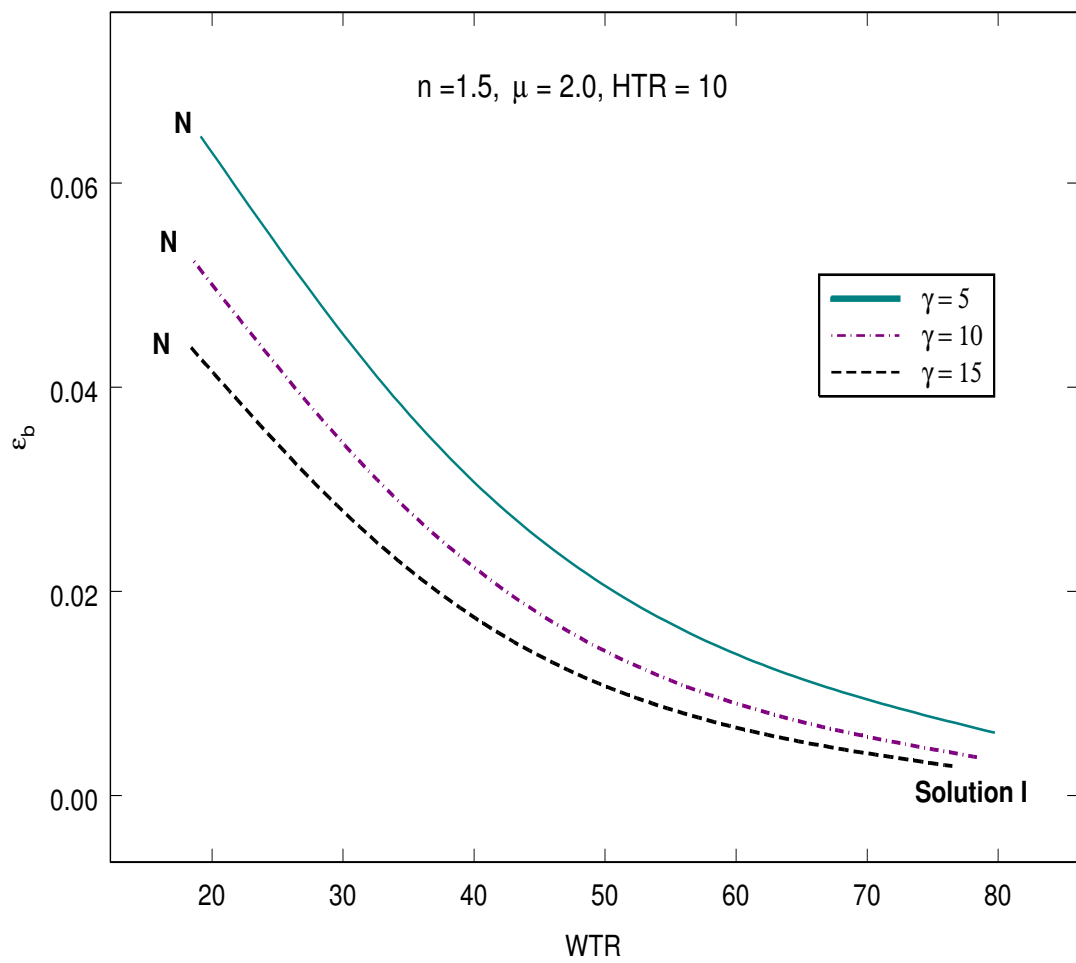


Fig. 3.24: Variation of breaking strain ϵ_b with chip-breaker position and rake angle γ , N= Negative friction angle limit

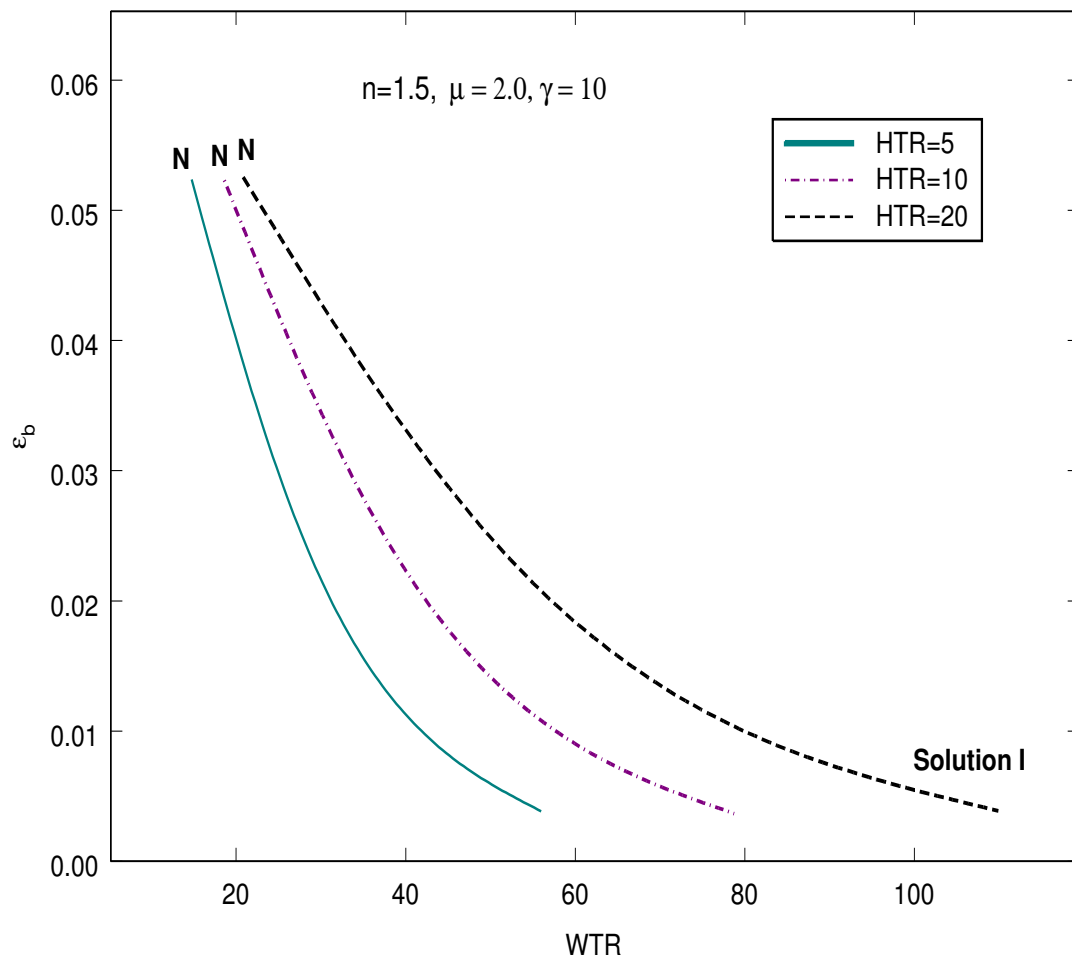


Fig. 3.25: Variation of breaking strain ϵ_b with chip-breaker position and feed, N= Negative friction angle limit

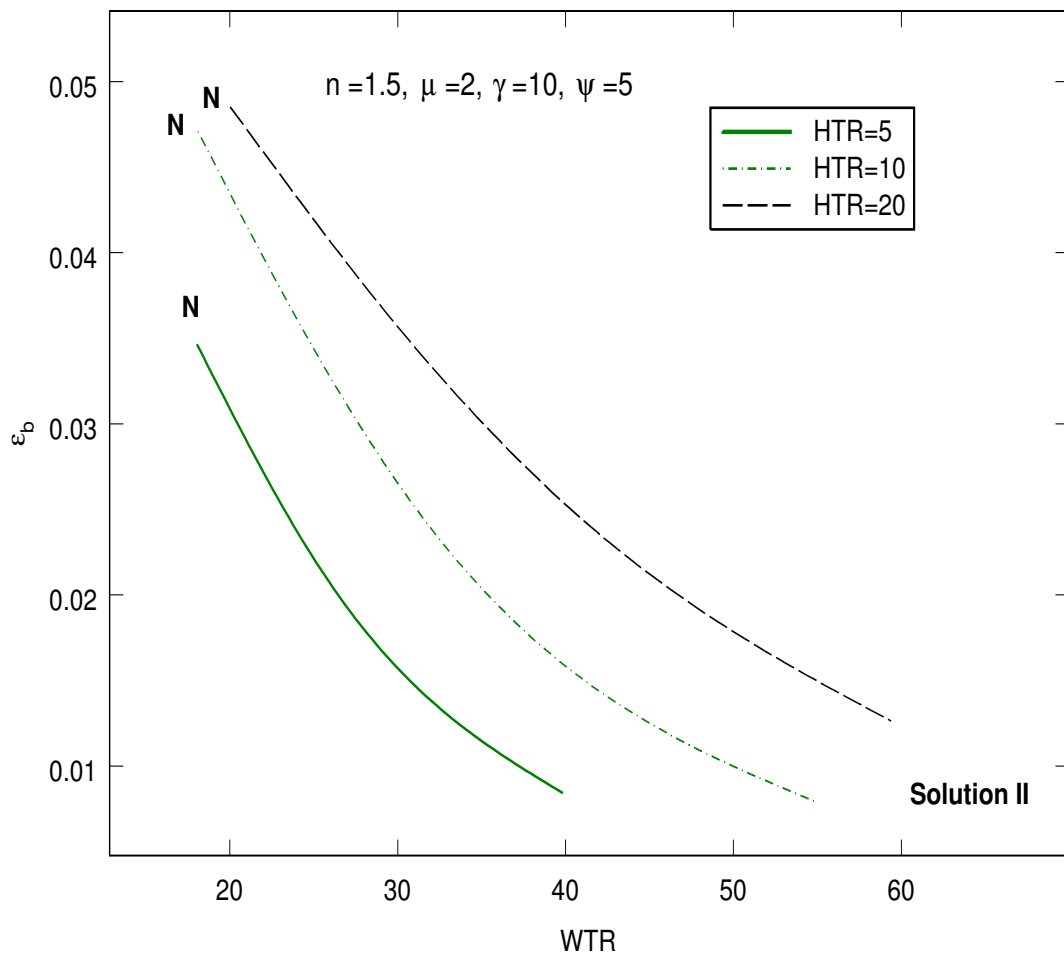


Fig. 3.26: Variation of breaking strain ϵ_b with chip-breaker position and feed, N= Negative friction angle limit

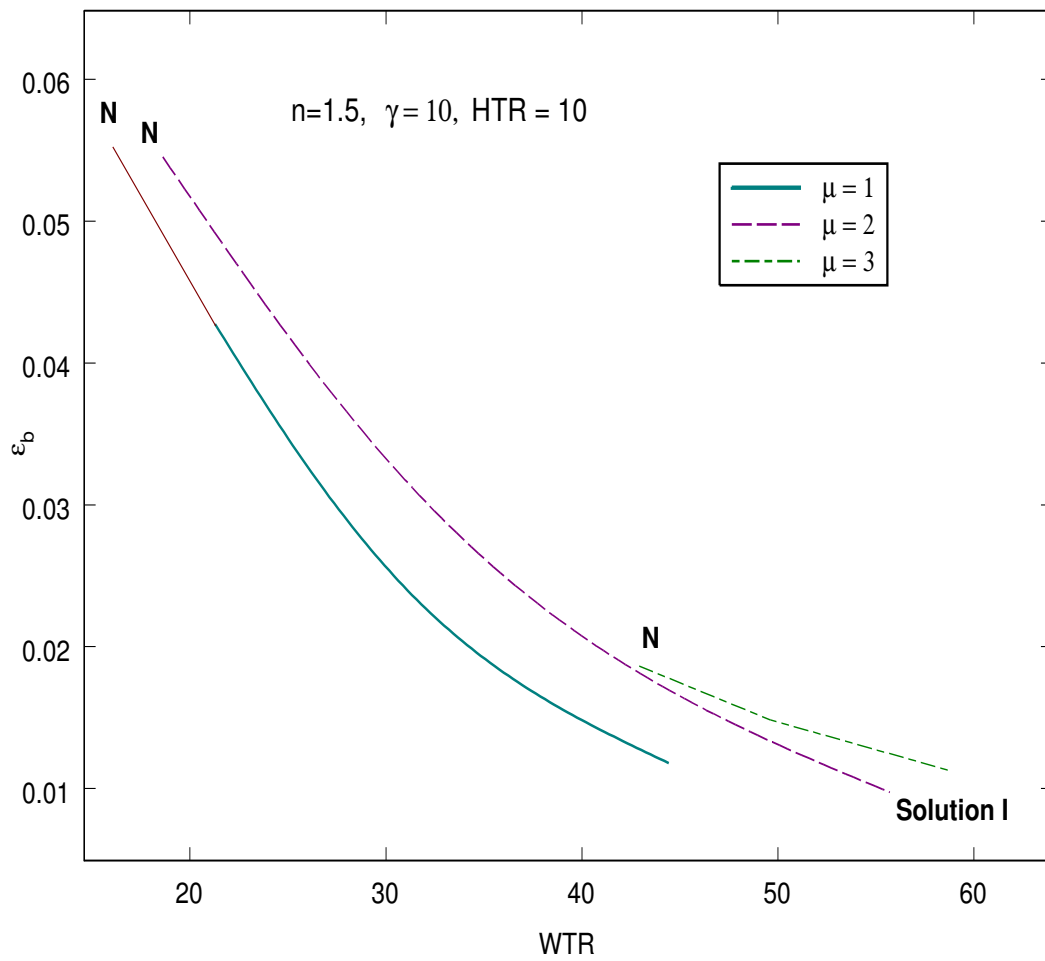


Fig. 3.27: Variation of breaking strain ϵ_b with chip-breaker position and friction coefficient, N= Negative friction angle limit μ

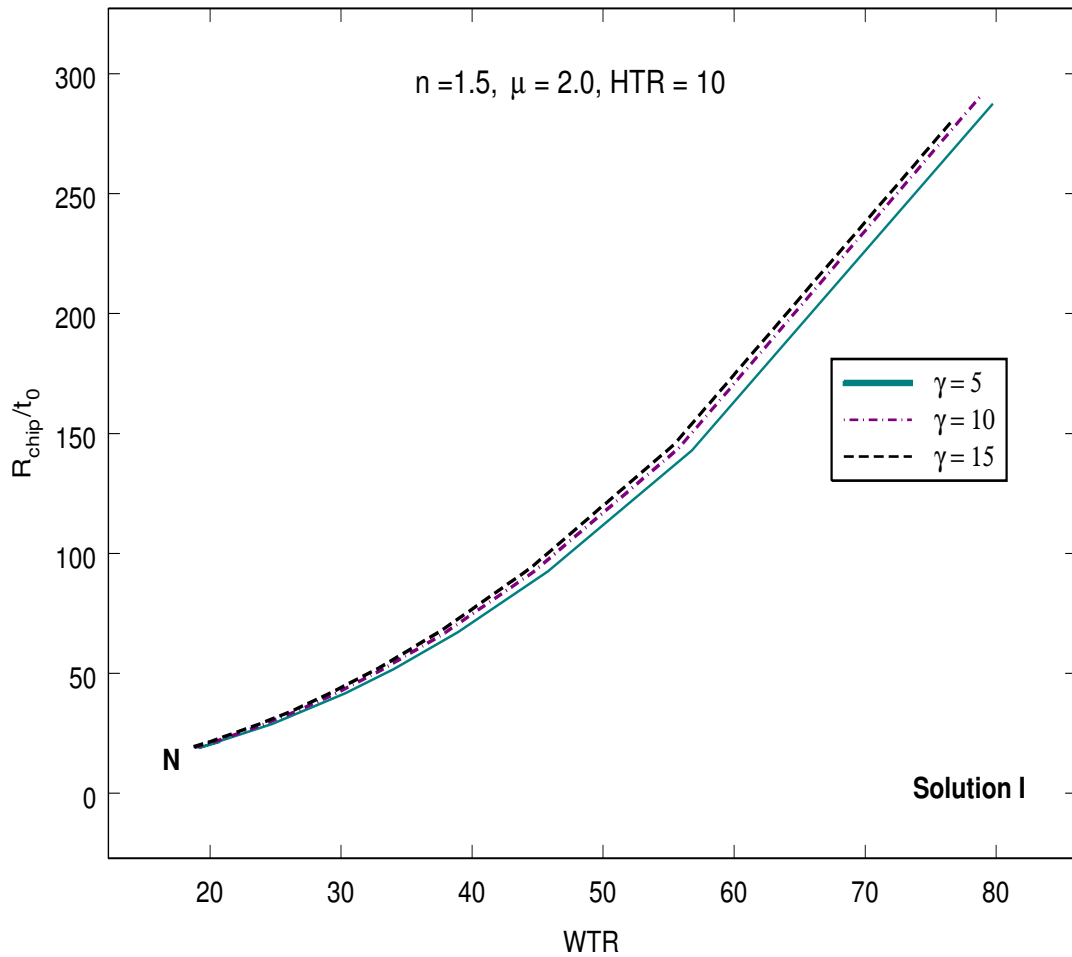


Fig. 3.28: Variation of non-dimensionalized outer radius of chip curvature with chip-breaker position and rake angle γ , N= Negative friction angle limit

This leads to effective or over-breaking of chips. This is demonstrated in Fig. 3.31 for feed t_0 equal to 0.06, 0.12 and 0.24. For W equal to 4.5, R_{chip} is found to be equal to 8.1 when feed is 0.06 and the same for feed equal to 0.24 is found as 7.2.

The variation of chip radius of curvature with total strain and feed is shown in Fig. 3.32. With increase in total strain, chip radius of curvature also increases. This finding supports/strengthens the earlier conclusion that chip breaking is not dependent on total strain.

Fig. 3.33 refers to the variation of cutting ratio with chip breaker position and rake angle. It is seen that for a particular position of chip breaker, as rake angle

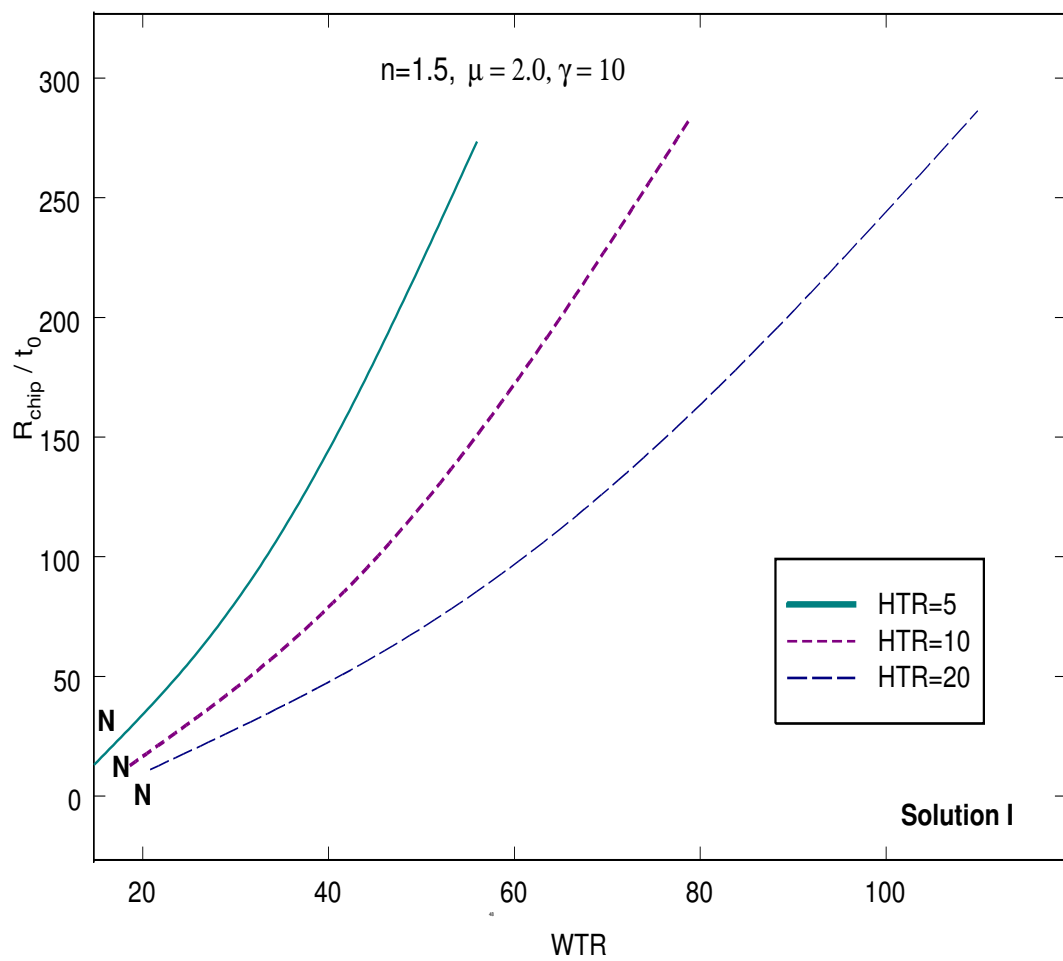


Fig. 3.29: Variation of non-dimensionalized outer radius of chip curvature with chip-breaker position and feed, N= Negative friction angle limit

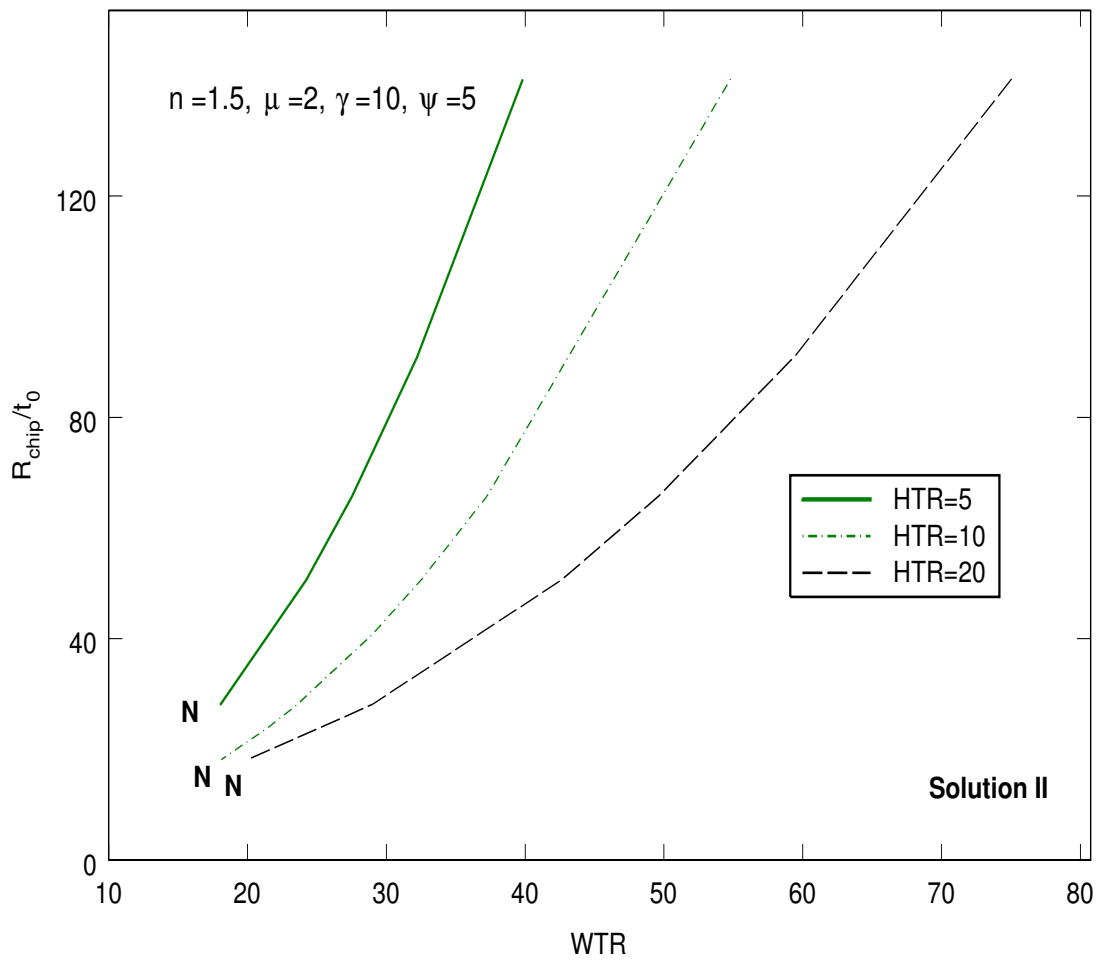


Fig. 3.30: Variation of non-dimensionalized outer radius of chip curvature with chip-breaker position and feed, N= Negative friction angle limit

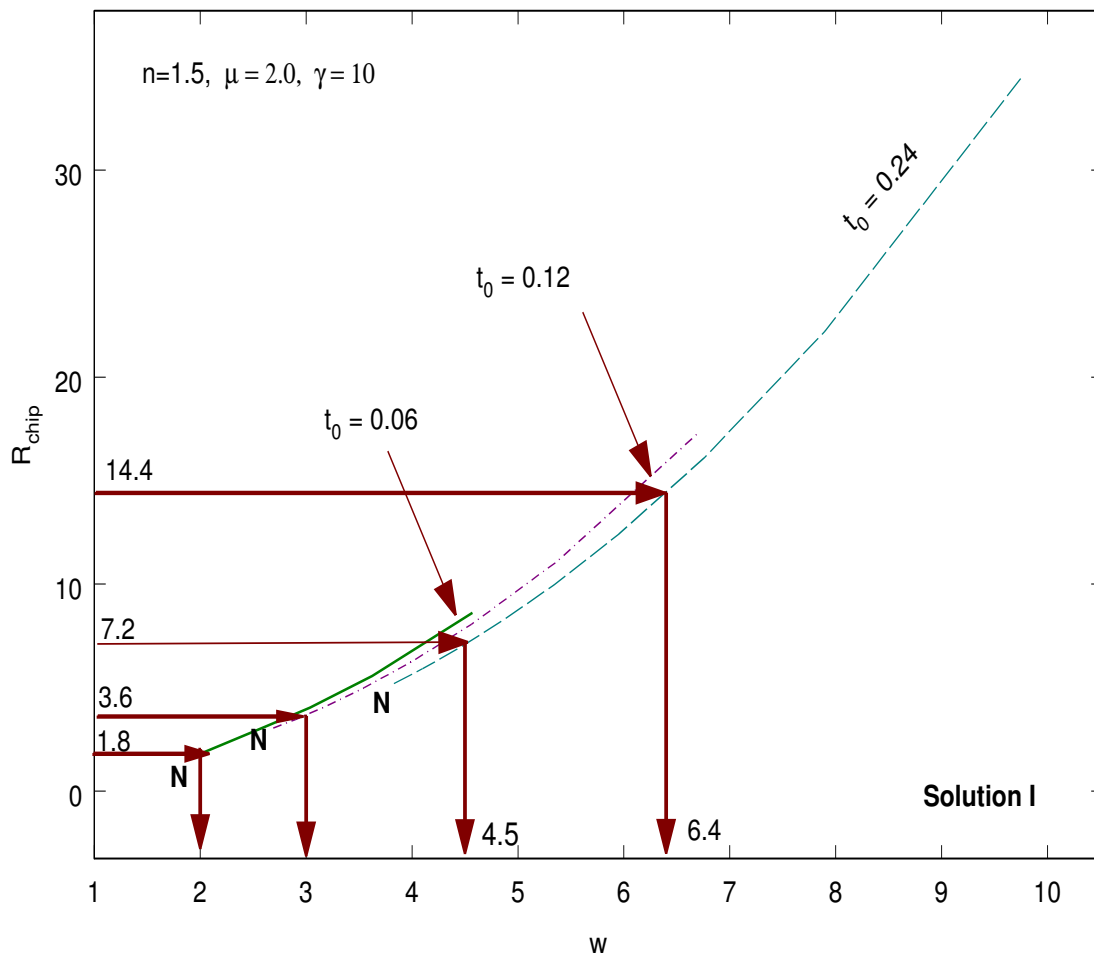


Fig. 3.31: Variation of outer radius of chip curvature with chip-breaker position and feed,
 N= Negative friction angle limit

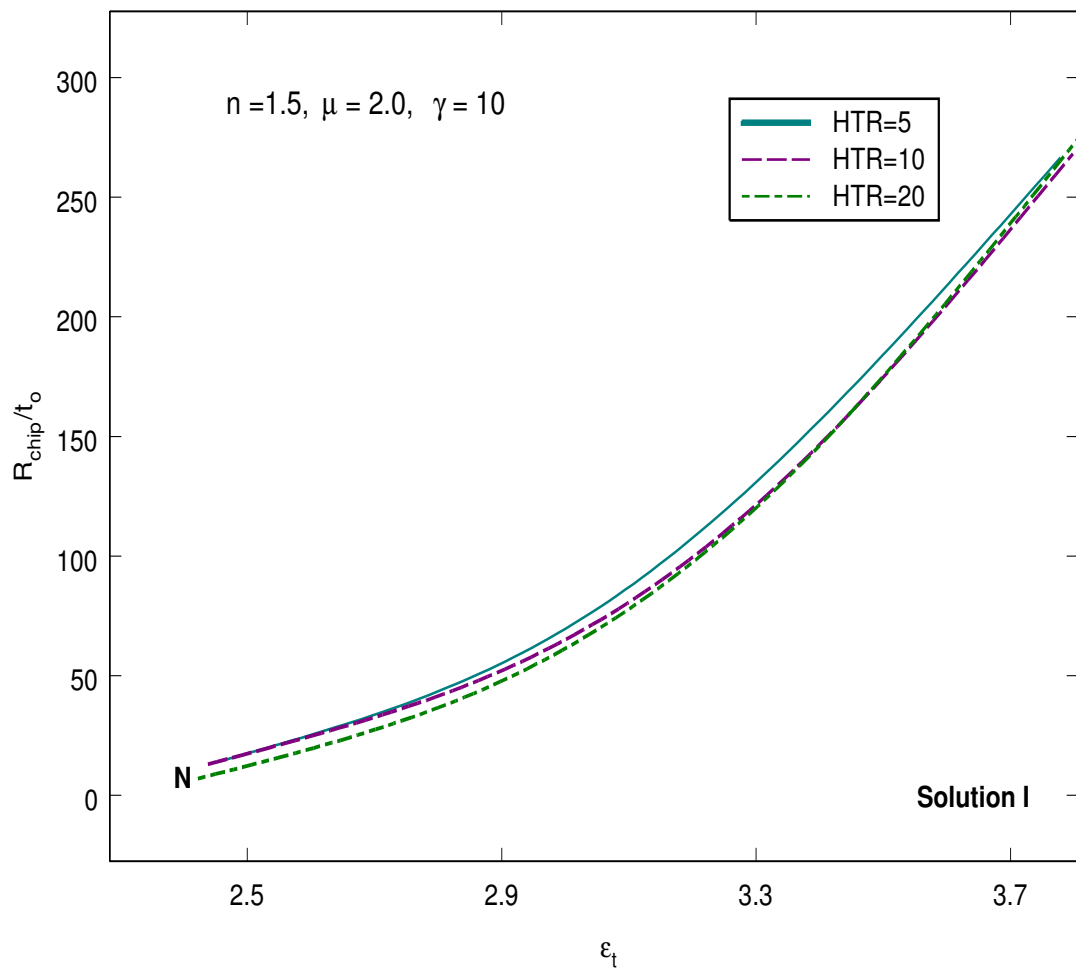


Fig. 3.32: Variation of non-dimensionalized outer radius of chip curvature with total strain ϵ_t and feed, N= Negative friction angle limit

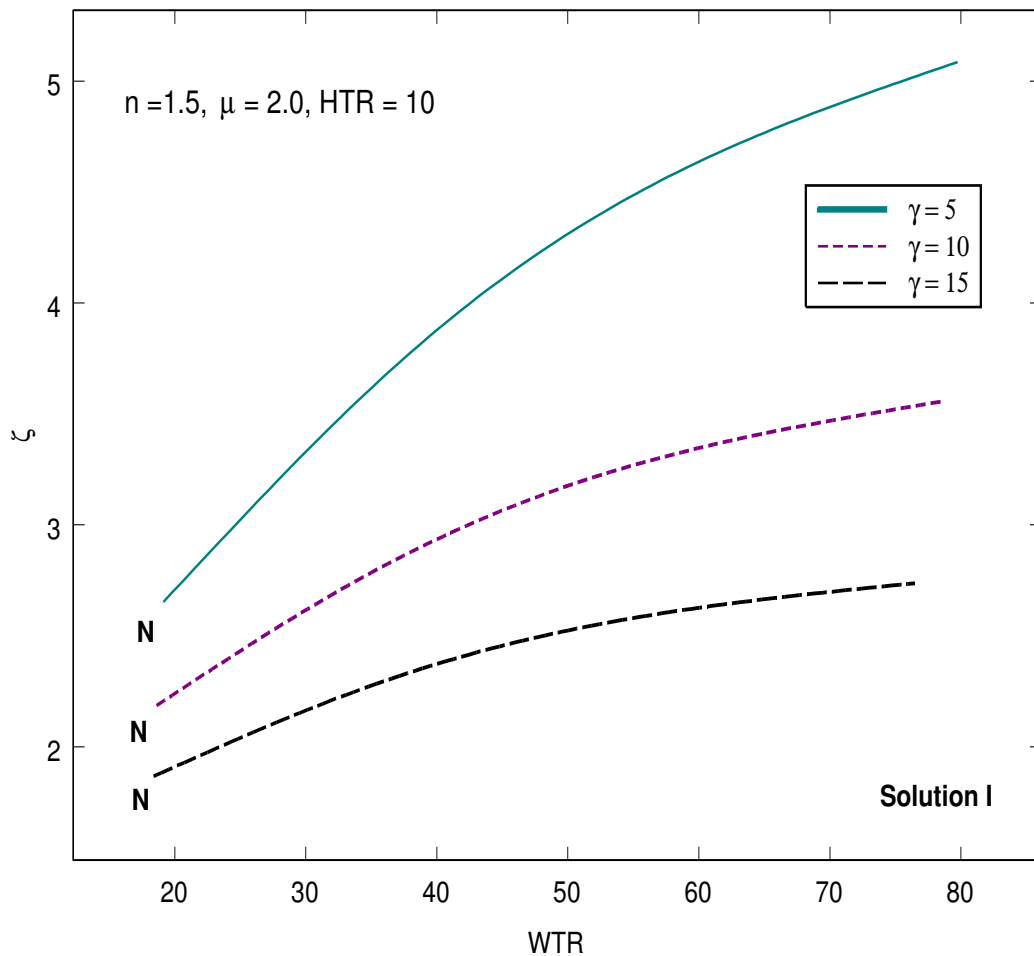


Fig. 3.33: Variation of cutting ratio ζ with chip-breaker position and rake angle γ , N= Negative friction angle limit

increases, cutting ratio and hence the chip thickness decreases.

The variation of non-dimensionalized contact length with chip breaker position as a function of tool rake angle and feed are illustrated in Fig. 3.34 and 3.35 respectively. For a constant chip breaker position, contact length decreases with increase in rake angle but increases with increase in feed.

It may be seen that the chip breaker force is a negligible fraction of the cutting force (Fig. 3.36 and 3.37). It decreases as both feed and rake angle decrease. Also as the chip breaker shifts away from cutting edge, the chip breaker force decreases whereas the cutting force increases. For a particular value of chip breaker position

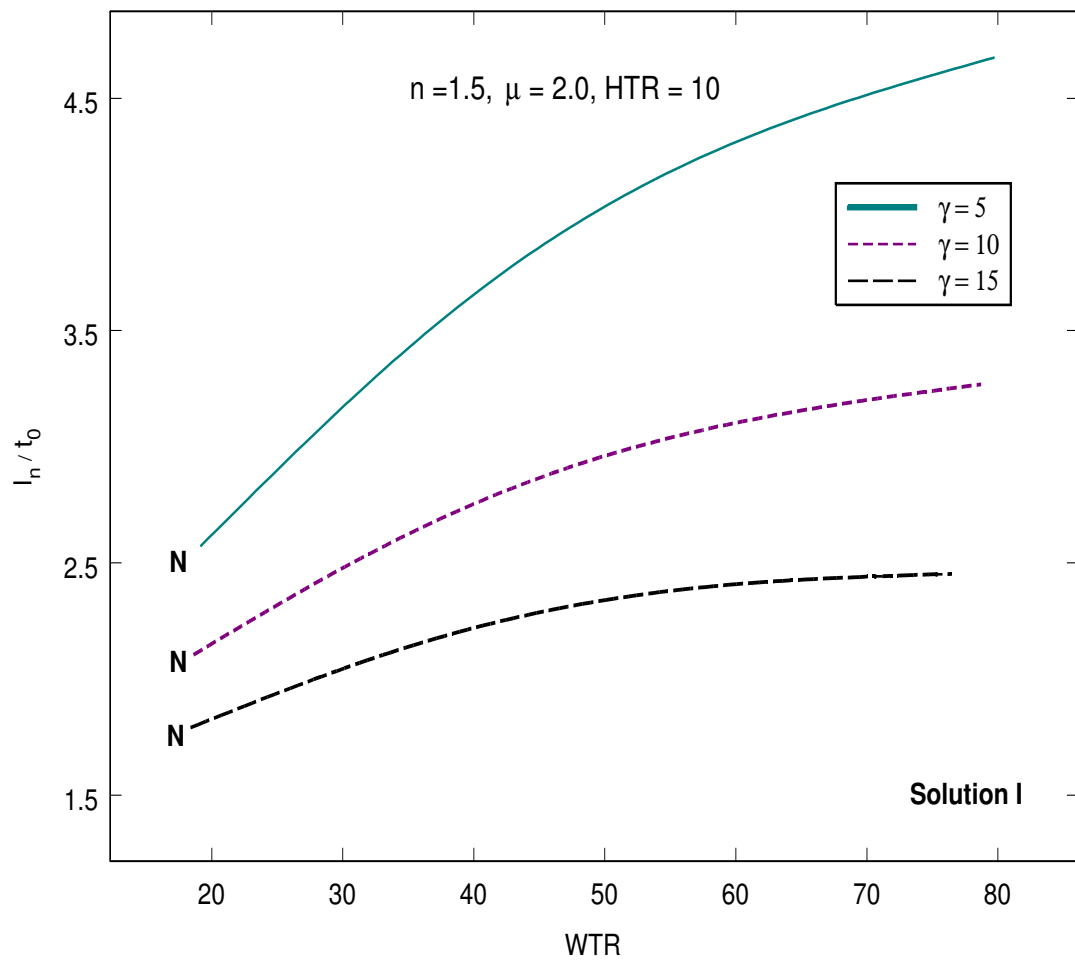


Fig. 3.34: Variation of non-dimensionalized contact length with chip-breaker position and rake angle γ , N= Negative friction angle limit

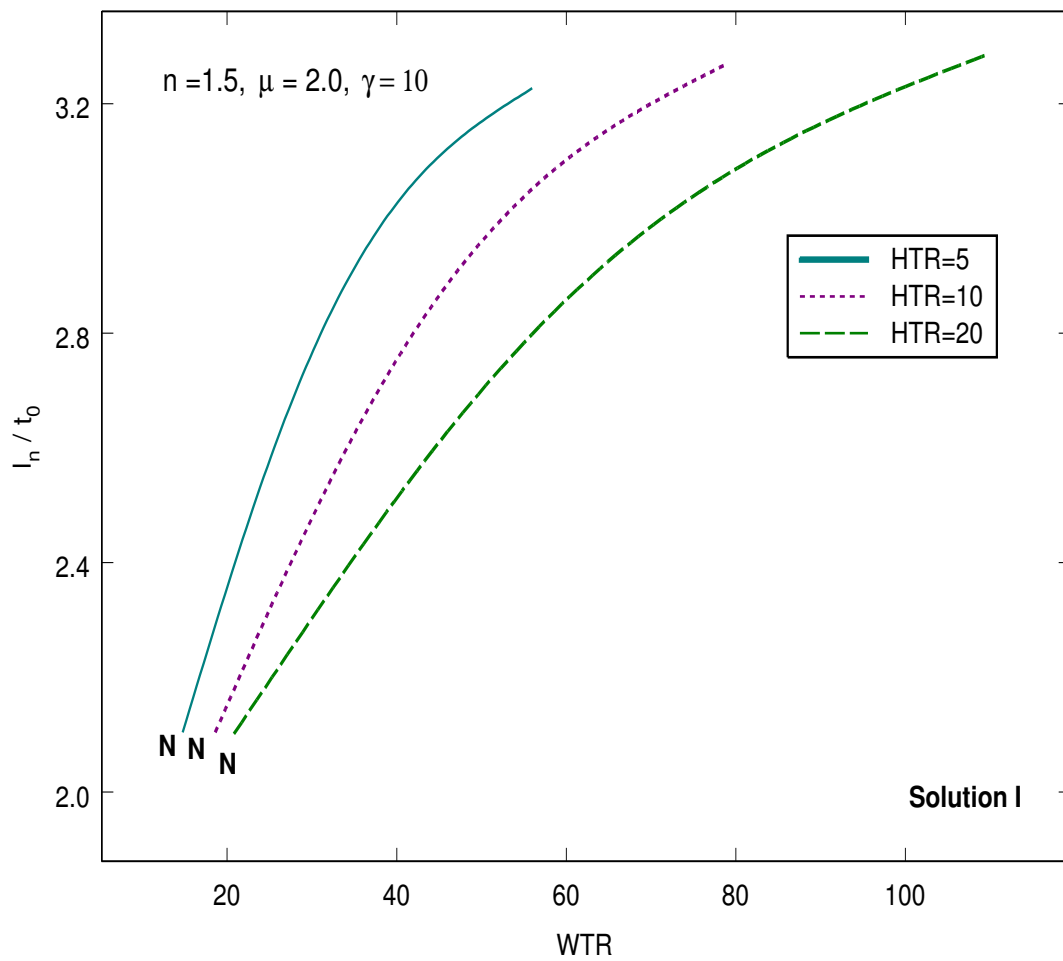


Fig. 3.35: Variation of non-dimensionalized contact length with chip-breaker position and feed, N= Negative friction angle limit

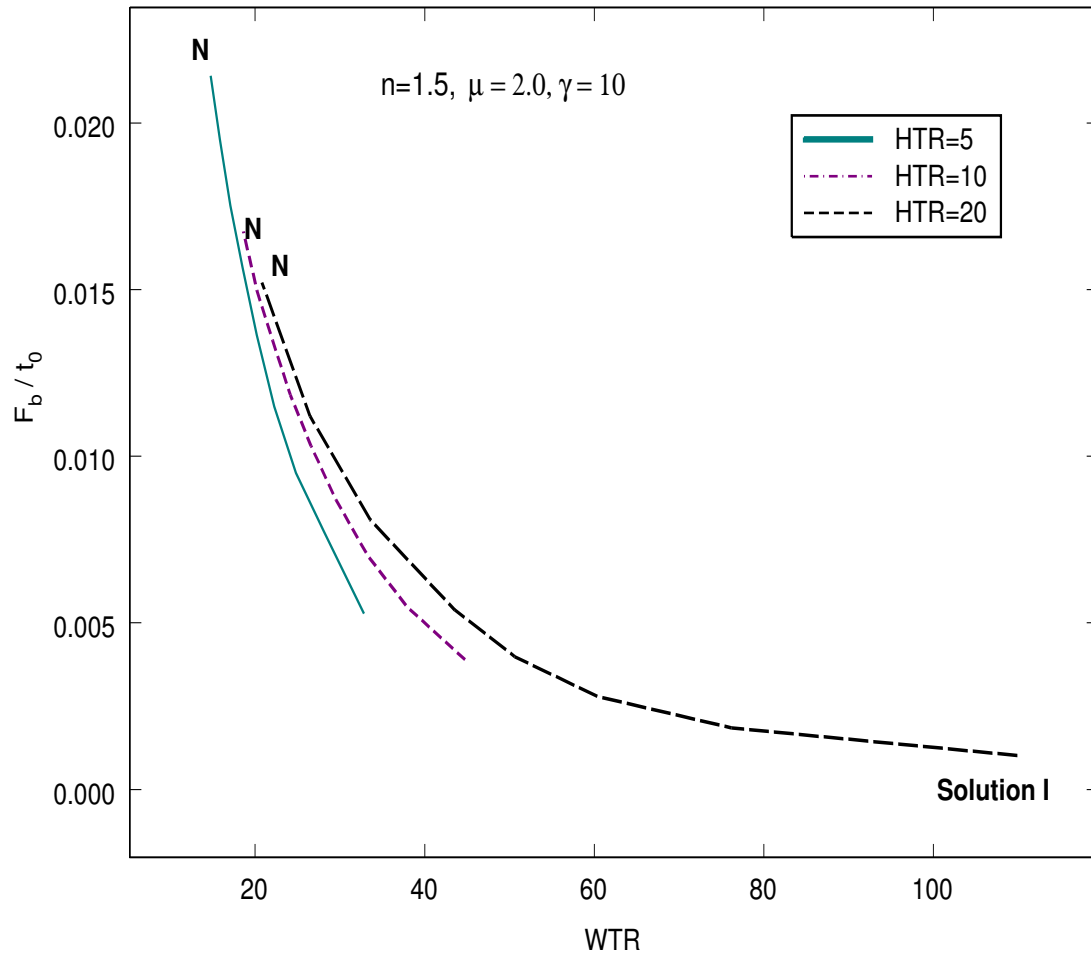


Fig. 3.36: Variation of non-dimensional chip breaker force with chip breaker position and feed, N= Negative friction angle limit

and rake angle the magnitude of chip breaker force is found to be less than one percent of cutting force. The contribution of chip breaker force is simply to decrease the curl radius of chip to enable it to break easily. This is clearly demonstrated in this figure.

3.7 Conclusions

Two slip-line field models are developed for orthogonal cutting with step type chip breaker assuming adhesion friction at chip-tool interface. For both the fields the chip curl radius, total plastic strain suffered by the material in the primary and secondary

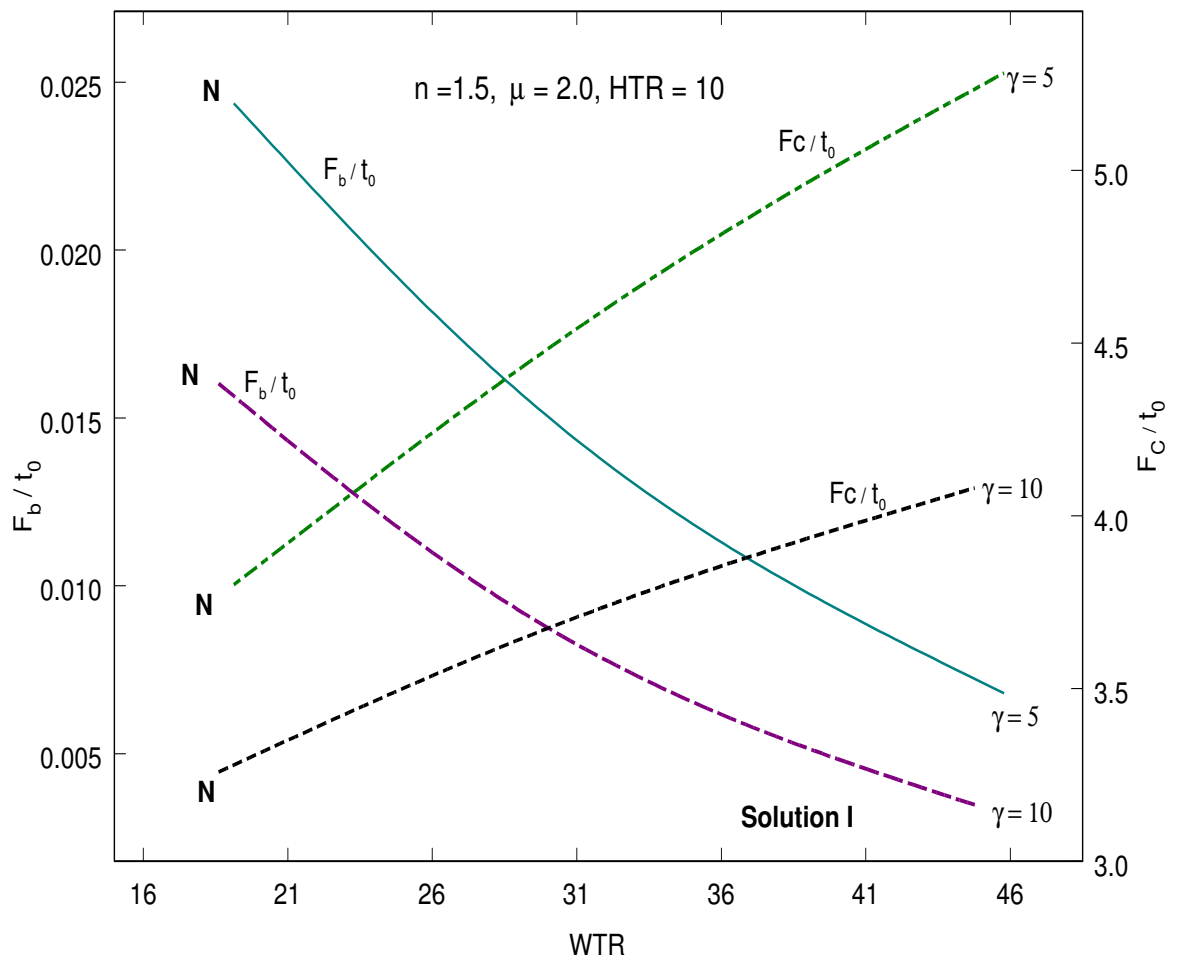


Fig. 3.37: Variation of non-dimensional chip breaker force and cutting force with chip breaker position and rake angle γ , N= Negative friction angle limit

shear zones, specific cutting energy, cutting force and chip breaker force are estimated for various chip breaker positions as a function of rake angle and feed. The breaking strain in the chip is calculated from the formula,

$$\epsilon_b = \frac{t_{chip}}{2R_{chip}} \quad (3.36)$$

by neglecting the effect of the radius of chip at fracture. It is observed that for a given feed, the chip curl radius, cutting ratio and the total strain ϵ_t increases as the chip breaker moves away from the cutting edge. The breaking strain and the secondary shear strain, however, decrease with increase in distance of the chip breaker from the cutting edge. Its also observed that the secondary strain suffered by the material is only of the order of approximately 10 to 15 % of the total strain. This observation supports the view that chip breaking is governed by the breaking strain and not by “material damage” or by specific cutting energy consumed during machining.

4. AN EVALUATION OF CHIP BREAKABILITY CRITERIA USING SLIP-LINE FIELD ANALYSIS

4.1 Introduction

Chip breaking may be defined as breaking up of long chips into manageable size in a metal removal process where continuous chips are being produced. This is usually accomplished by chip breakers/formers that control the radius of the chip and direct it in such a manner that its free end anchors onto the machined surface or the tool flank imposing additional strains on the chip resulting in its breakage. Chip breakability depends on a number of factors such as the chip thickness, mechanical properties of the chip and the chip curl radius and many researchers have attempted to correlate these parameters with none fully succeeding because of the complex nature of the problem of chip breaking. In most cases these criteria have a post-process nature rather than helping in making pre-process decisions about chip breaking. Hence, chip breaking in metal cutting remains one of the fundamental problems that has to be solved for further advance in automated manufacturing.

During the last four decades, a number of researchers have tried to study the mechanism of chip breaking and have established chip breakability criterion with limited success. The early chip-breakability criteria have been largely based on the chip thickness-to-radius ratio. Chip control tools were assumed to be effective if the chips produced with these tools were tightly curled. Henriksen [30, 48, 49] and Okushima *et al.* [50] found that the degree of chip breaking is dependent on the feed rate or undeformed chip thickness and on the radius of chip curvature imposed by the action of the chip former. It was reported that the chip breaking increased as the radius of chip curvature decreased or as the feed increased.

According to Okushima *et al.* [50] the degree of chip breaking can be represented by the value of the parameter 'a', which is the ratio of square of feed to final chip curl

radius. They determined the ranges for 'a' for the three groups of chip breaking for medium-carbon grade steel. They found that the value of 'a' for under-breaking must be less than $1 \times 10^{-2}mm$, for effective breaking it should lie between $1 \times 10^{-2}mm$ and $2 \times 10^{-2}mm$ and for over-breaking it should be greater than $2 \times 10^{-2}mm$.

Experimental investigation using a step type chip breaker has been reported by Nakayama [32], Trim and Boothroyd [92] and Subramanian *et al.* [93]. A criterion for chip breaking based on chip strain analysis was first presented by Nakayama [51]. He showed that the chip breaks when the strain on the chip surface exceeds the fracture strain of the chip material. For medium carbon steel this strain was reported to be equal to or greater than 0.05. Takayama *et al.* [52] and Jawahir [53], however, found the corresponding values of breaking strain to be 0.046-0.052 and 0.036-0.048, respectively. Spaans and Goedemondt [94] also investigated strains in chips. The results obtained by these authors seem to show some disparity probably because the testing conditions were not easily controlled [95]. A hybrid algorithm based model for predicting chip breakability for various chip shapes and sizes has been proposed by Fang, Fie and Jawahir [36].

Worthington *et al.* [41, 40, 96, 33], used the model suggested by Nakayama for groove-type chip breakers. The critical range of the chip thickness-to-radius ratio for effective chip-breaking was found by them to be between 0.06 and 0.17.

In an experimental investigation using restricted contact tools, a new chip breakability criteria, based on control factor K, (ratio of restricted to natural contact length) was reported by Sadik and Lindstrom [5], for turning of carbon steel. They found that in case of low feeds under-controlled chips were obtained when the value of K is greater than unity. 'Acceptable chip form' or controlled chips were obtained and long tool life was observed when the value of 'K' was between 0.5 and 1. Over-controlled chips in the form of short, separate or connected segments of a dark blue colour was found for the value of 'K' less than 0.5.

Shinozuka *et al.* [42] simulated chip breaking mechanism using thermo-elastic plastic FEM. They verified the chip-breakability criteria suggested by Nakayama and proposed a very useful criterion for the design of chip breakers. In their study they introduced the concept of aspect ratio R_{as} which is the ratio of the length of the chip that has come out of the chip breaker groove with its free end just touching the work

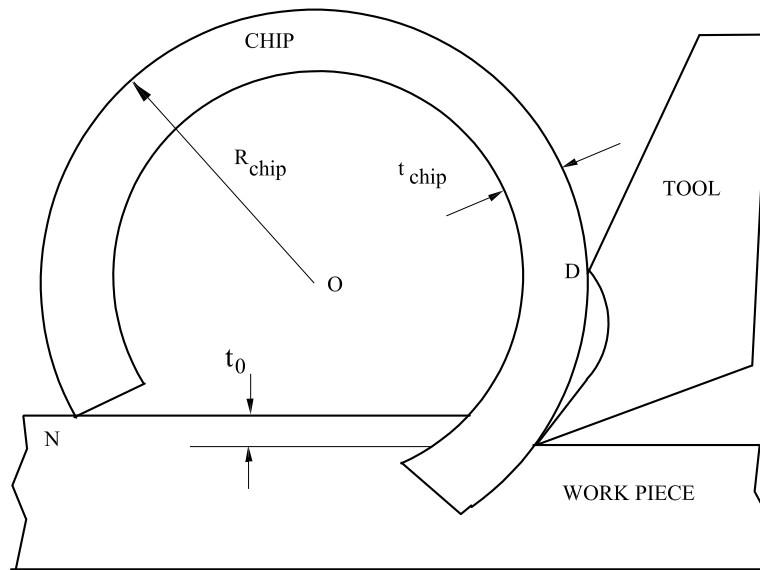


Fig. 4.1: Aspect ratio

piece surface to chip thickness Fig. 4.1. According to them chip breakability is good when aspect ratio is less than 20.

Using Eulerian finite element technique, a ‘material damage-based model’ for predicting chip breakability was presented by Athavale and Strenkowski [54]. They concluded that a chip will break or not depends upon the ductility remaining in the chip and the subsequent stresses placed upon it. After leaving the shear zone, the chip is subjected to high tensile stresses as it is bent and twisted by the chip breaker. The tensile stresses produced during opening up of the chip must be large enough to cause fracture. They found that the chips with a higher thickness-to-radius ratio and lower normalized accumulated damage factor broke more readily.

An energy approach to chip breaking while machining with grooved tool inserts has been suggested by Grzesik and Kwiatkowska [55]. These authors correlated the specific cutting energy consumed during machining with different types of chip forms. In a recent study, Yang *et al.* [56, 57], calculated the energy expended per unit length of the chip as it passed through the shear zone. They observed that chips imparted with higher energy per unit length are more likely to break.

These chip breakability criteria are shown arranged in chronological order in Table 4.1.

Tab. 4.1: Chip Breakability Criterion

Sl.No.	YEAR	AUTHORS	CRITERIA	APPROACH	UNDER-BROKEN	EFFECTIVE-BROKEN	OVER-BROKEN
1	1954	Hendriksen [30, 48, 49]	feed, t_0	expt		Inversely proportional to radius of curvature	
2	1960	Okushima, Hoshi and Fujinawa [50]	$(t_0)^2 / R_{chip}$	expt		Proportional to feed, $0.01 \leq a \leq 0.02$	
3	1963	Nakayama [51]	Breaking Strain, ϵ_b	expt		≥ 0.05	
4	1968	Trim and Boothroyd [92]	chip-tool contact length and t_{chip}	expt		proportional to chip-tool contact length and t_{chip}	
5	1970	Takayama [52]	$R_{chip \text{ on leaving groove}} / R_{chip \text{ original}}$	expt	1.2 - 2.0		
6	1970	Takayama [52]	Breaking Strain, ϵ_b	expt		0.046 - 0.052	
7	1979	Worthington and Rahman [41]	$t_0 / R_{chip \text{ on leaving groove}}$	expt	≤ 0.06	0.06 - 0.17	0.17 - 0.25
8	1986	Jawahir [53]	Breaking Strain, ϵ_b	expt		0.036 - 0.048	

(continued on next page)

Tab. 4.1: Chip Breakability Criterion (Contd.)

Sl.No.	YEAR	AUTHORS	CRITERIA	APPROACH	UNDER-BROKEN	EFFECTIVE-BROKEN	OVER-BROKEN
9	1995	Fang, Fei and Jawahir [36]	Chip Breakability Index, C_{in}	expt		0.08-1.0	
10	1995	Zhang, Lee and Seah [97]	Chip Packing Density Index, CPDI	expt	6 - 96	131 - 301	301 - 331
11	1995	Sadik and Lindstrom [5]	Control Factor, $K=l_{rc} / l_n$	expt	$K > 1$ at low feed when $l_n < l_{rc}$	$0.5 l_{rc} \leq K < 1$	$K < 0.5 l_n$
12	1996	Shinozuka, Obikawa and Shirakashi [42]	Aspect Ratio, R_{as} = Length of chip/ t_{chip}	FEM		$R_{as} < 20$	
13	1997	Kim and Kweun [45]	Chip Breaking Performance	expt	0.3 - 0.5		

(continued on next page)

Tab. 4.1: Chip Breakability Criterion (Contd.)

Sl.No.	YEAR	AUTHORS	CRITERIA	APPROACH	UNDER-BROKEN	EFFECTIVE-BROKEN	OVER-BROKEN
14	1997	Athavale and Strenkowski [54]	Normalized Accumulated Damage Factor or Loss of Ductility	FEM	expt	Lower value of Damage Factor, ≤ 0.065 and $t_{chip}/R_{chip \text{ on leaving groove}} \geq 0.12$	
15	1997	Grzesik and Kwiatkowska [55]	Specific Cutting Energy, F_c / t_0 and Interface Control Factor, $K_{int} = l_{rc}/t_0$	expt	More F_c / t_0 is required in finish turning to break thin chips	finish turning $K_{int} = 0.50 - 0.80$, medium turning $K_{int} = 1.25 - 1.75$, rough turning $K_{int} = 0.875 - 1.75$	

In spite of all the research in this area, a lack of basic theory for three dimensional plastic flow and the complicated geometry of chip formers make it impossible to develop a pure three dimensional oblique cutting model. Hence, in all the criterion discussed above, almost every author has invariably considered the two dimensional orthogonal cutting model for suggesting a suitable chip breaking criteria [95].

Theoretical studies to evaluate performance of chip breakers using slip-line field theory has also been reported by Shi and Ramalingam [98], Fang [25] for groove type chip breakers, by Dewhurst [23] for ramp type chip breakers and by Maity and Das [87, 88] for step-type chip breakers, assuming constant friction at chip/tool interface. However, no attempt has been made to date to correlate the strain and strain energy calculated from the slip-line field analysis with effectiveness of chip breaking.

In the present chapter, a slip-line field analysis is carried out for pure orthogonal cutting using a cutting tool with a parallel step-type smooth chip breaker. The slip-line field studied is that proposed earlier by Dewhurst [23]. Adhesion friction is assumed at the chip/tool interface. The strain suffered by the chip during deformation has been calculated using the method suggested by Atkins *et al.* [75]. The total shear strain, shear strain in the secondary shear zone, strain distribution across the chip thickness, breaking strain and radius of chip curvature has been estimated for different positions of the chip breaker. The existing chip breakability criteria are compared with those obtained from the slip-line field analysis.

4.2 Slip-line field solution

The slip-line field due to Dewhurst [23, 22] for orthogonal machining with step-type chip breaker is shown in Fig. 4.2 along with its associated hodograph. Referring to this figure it may be seen that the field consists of the primary shear line AE, the secondary shear zone CDE and a singular field BCE. The material slides on the tool face DE consistent with the adhesion friction law given by equation (1.5). After emerging from the deformation region the curled chip encounters the chip breaker of height H placed on the tool face at a distance W from the cutting edge. This reduces the radius of curvature of the chip by imposing a force on it and thus helps in chip

breaking. The chip boundary for the field is defined by the convex β - line AB, concave α - line DC and the convex α - line BC.

Referring to the hodograph Fig. 4.2(b), it may be seen that the material suffers a velocity discontinuity of magnitude ρ on crossing the primary shear line. Thus, the velocity along the slip-line EBA is given by the circular arc eba and along the slip-lines BC and CD by the hodograph curves bc and cd respectively. Since the chip is rotating rigidly with angular velocity ω , the lines AB, BC and CD must also appear in the hodograph but rotated through 90 degrees in the direction of ω and multiplied by the scale factor ω i.e. $abcd$ must be geometrically similar to ABCD. Hence, slip-line BA is also a circular arc of radius ρ/ω . The column vector σ for the radius of curvature of the slip-line DC is determined from the mixed stress and velocity boundary conditions in the following manner:

$$DC = \sigma \quad (4.1)$$

$$EC = \mathbf{CL}_{\eta\phi_C}\sigma \quad (4.2)$$

$$BC = \mathbf{Q}_{\beta\psi}\mathbf{CL}_{\eta\phi_C}\sigma \quad (4.3)$$

where, \mathbf{CL} is the adhesion operator that constructs the field between the tool face and the slip-line DC consistent with the friction law given by equation (1.5) and ϕ_C is the friction angle at point C.

Referring to the hodograph (Fig. 4.2(b)) it may be seen that ec can be calculated from be and bc ($=\omega BC$). Thus,

$$ec = \mathbf{P}_{\beta\psi}be + \mathbf{Q}_{\psi\beta}\omega BC \quad (4.4)$$

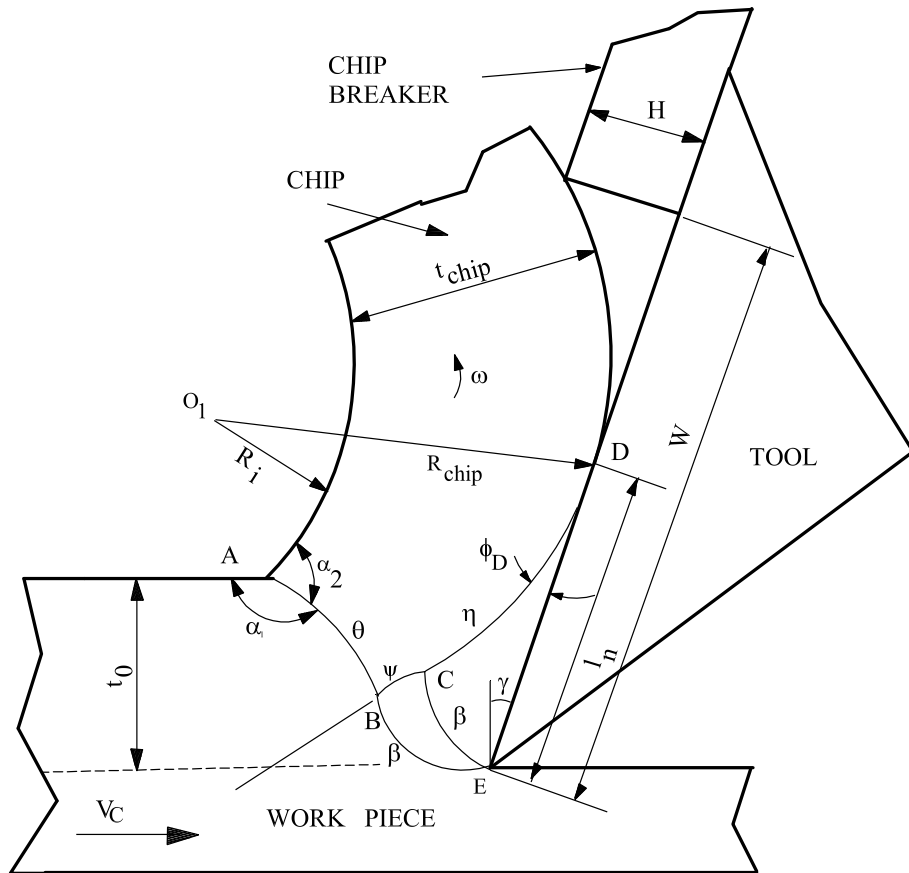
where, $be = \rho\bar{c}$ is a circular arc of radius ρ . Hence,

$$dc = \mathbf{CL}_{\beta\phi_E}ec \quad (4.5)$$

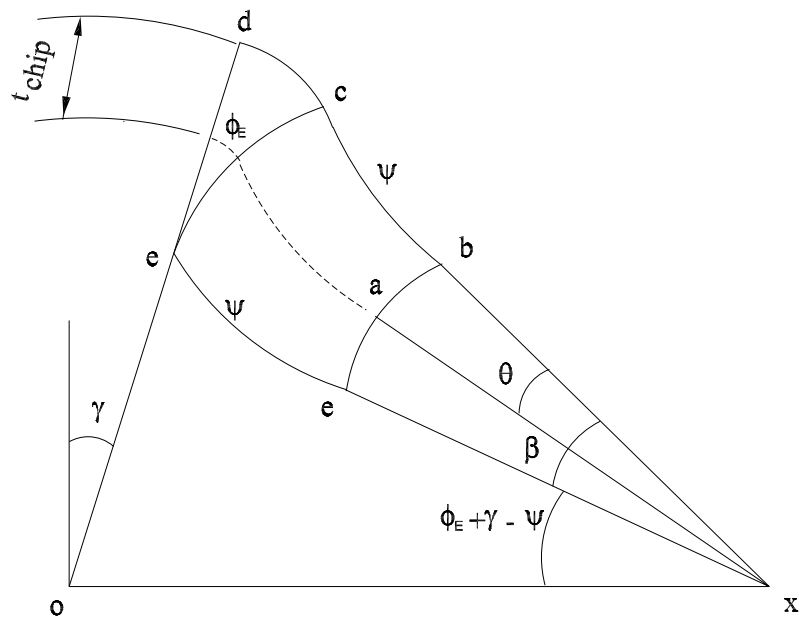
As dc is geometrically similar to its slip-line image DC, dc is also given by the relation,

$$dc = \omega DC = \omega\sigma \quad (4.6)$$

Substituting equations (4.3), (4.4) and (4.6) in (4.5) it is readily seen that in order for the slip-line field to satisfy the mixed stress and velocity boundary conditions, σ must satisfy the matrix equation,



(a)



(b)

Fig. 4.2: (a) Dewhurst's slip-line field with the geometry of chip-breaker and cutting tool
 (b) Hodograph for corresponding slip-line field (not to scale)

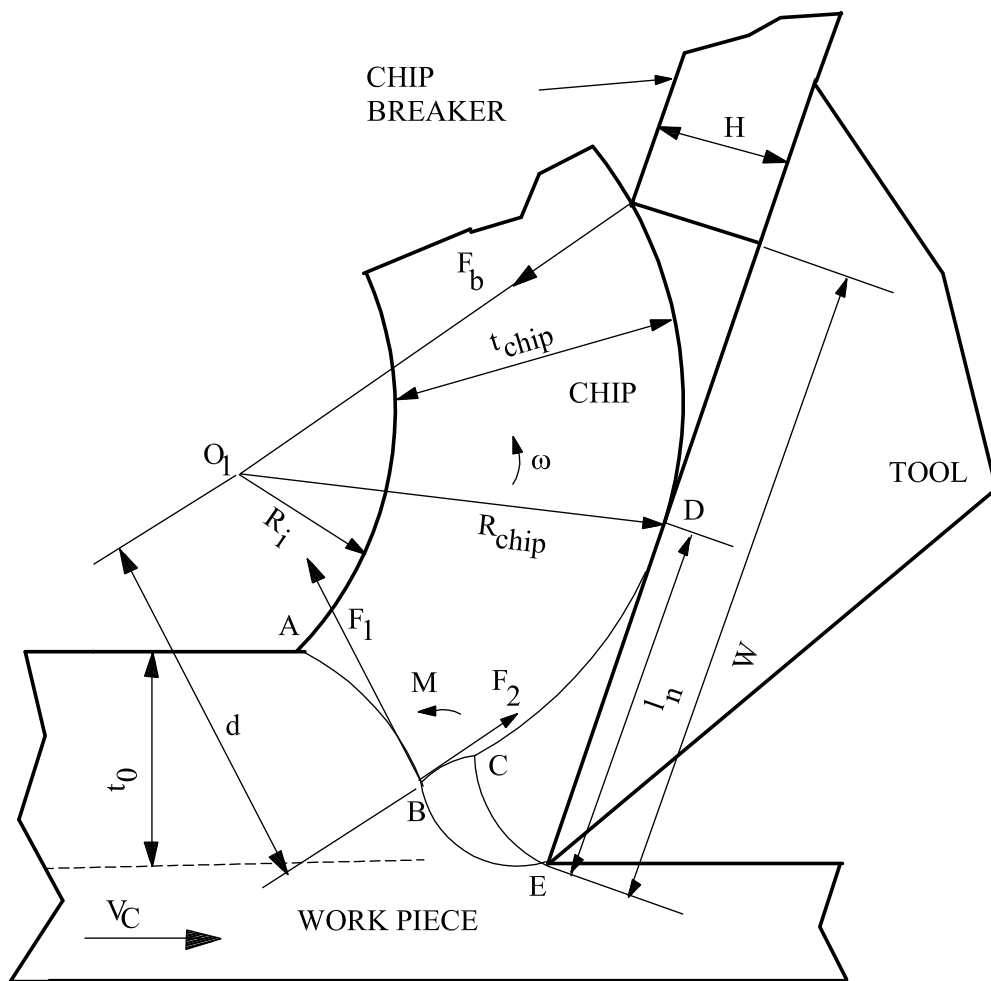


Fig. 4.3: Forces acting on chip

$$(\mathbf{I} - \mathbf{CL}_{\beta\phi_E} \mathbf{Q}_{\psi\beta} \mathbf{Q}_{\beta\psi} \mathbf{CL}_{\eta\phi_C}) DC = \left(\frac{\rho}{\omega}\right) \mathbf{CL}_{\beta\phi_E} \mathbf{P}_{\beta\psi} \bar{c} \quad (4.7)$$

where, ϕ_E is the friction angle at E, \mathbf{I} is the unit matrix and \bar{c} is a column vector representing a circle of unit radius.

In equation (4.7), \mathbf{P} and \mathbf{Q} are a set of standard matrix operators as discussed by Dewhurst and Collins [72] and \mathbf{CL} is the linear operator [73, 74]. Thus, DC can be calculated when for given value of field angles η, θ, ψ and friction angles ϕ_E and ϕ_C these matrix operators are constructed.

To derive the structure of the linear operator \mathbf{CL} , the relation between the angular coordinates η_i and β_i of any point on tool face DE was approximated by the linear relation,

$$\beta_i = m_0 \eta_i \quad (4.8)$$

m_0 in the above equation was determined by the method of linear regression analysis as explained in Appendix A. This value of m_0 was then used to construct \mathbf{CL} .

4.3 Method of solution

The slip-line field shown in Fig. 4.2(a) is of the ‘‘indirect’’ type since none of the slip-lines in the deforming zone BCDE have known shape at the outset. The shape of a first slip-line must therefore be found before the remainder can be determined ‘directly’ from it. The matrix equation that defines the shape of the slip-line DC ($=\sigma$) for given values of field angles β, ψ, η and friction angle ϕ_C is presented in equation (4.7). The problem thus reduces to determining the above field angles such that the force and geometrical constraints imposed by the chip breaker are satisfied. These conditions may be stated as,

1. The sum total of the forces and moment acting on the chip must be zero.
2. The outer radius of curvature of the chip imposed by the chip breaker must be equal to that calculated from the hodograph (Fig. 4.2(b)).

Referring to Fig. 4.3, if the forces on the chip boundary ABCD are resolved parallel and perpendicular to the chip breaker force F_b , the above condition may be stated

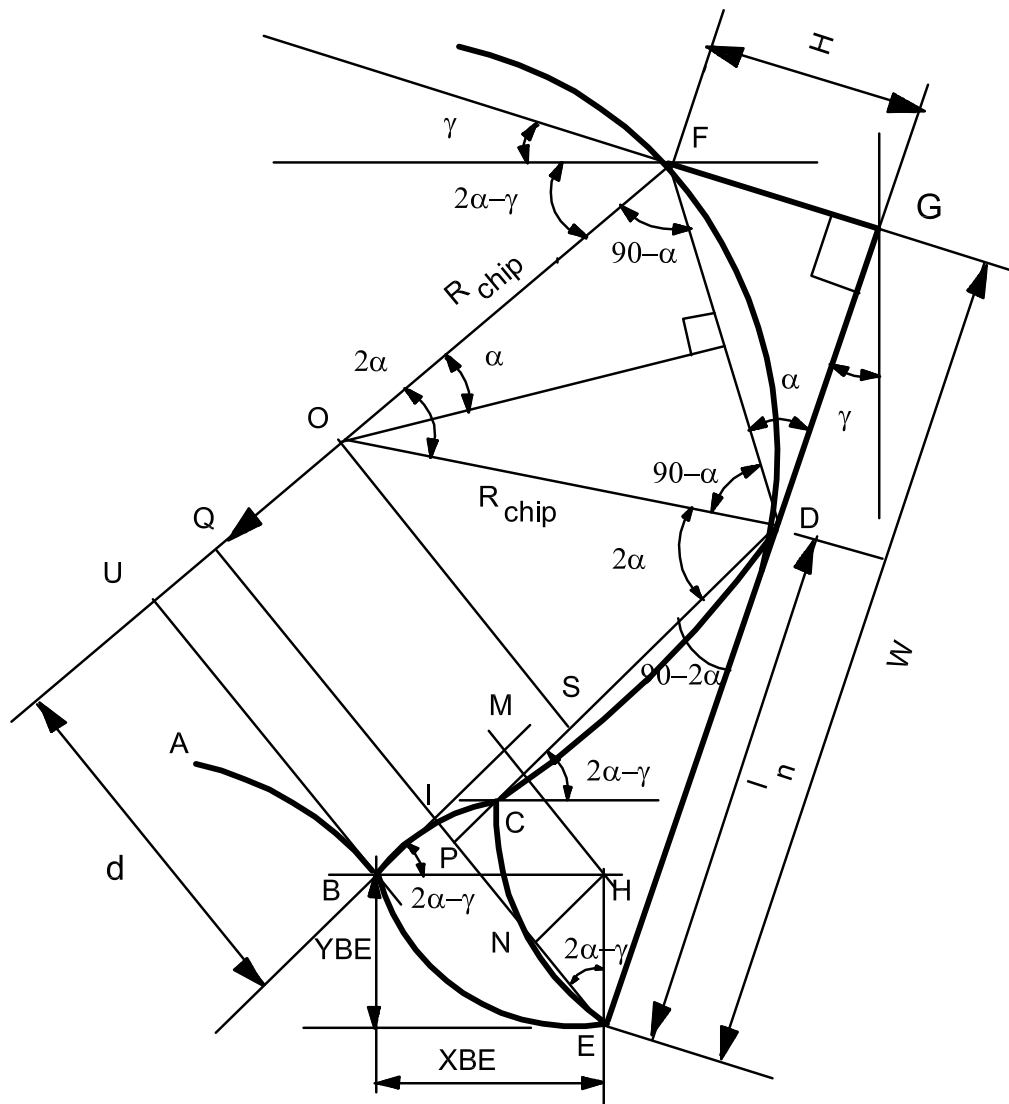


Fig. 4.4: Calculation of distance 'd' and radius of curvature R_{chip}

as,

$$E_1 = F_1 = 0 \quad (4.9)$$

$$E_2 = M + F_b \cdot d = 0 \quad (4.10)$$

where $F_b = F_2$, and

$$E_3 = R_o - R_{chip} = 0 \quad (4.11)$$

where R_{chip} is the outer radius of chip curvature and is given by

$$R_{chip} = \frac{(W - l_n)^2}{2H} + \frac{H}{2} \quad (4.12)$$

and R_o is that calculated from the hodograph (Fig. 4.2(b)). M in equation (4.10) is the anti-clockwise moment acting on the chip at B and d is the normal distance of the line of action of F_b from B. An expression for d is readily obtained from geometry. Thus, referring to Fig. 4.4, it can be seen that,

$$d = BU = EQ - EI \quad (4.13)$$

or,

$$EQ = EP + PQ = EP + OS \quad (4.14)$$

From $\triangle EPD$,

$$EP = ED \cdot \cos(2\alpha) = l_n \cdot \cos(2\alpha) \quad (4.15)$$

and, from $\triangle OSD$,

$$OS = OD \cdot \sin(2\alpha) = R_{chip} \cdot \sin(2\alpha) \quad (4.16)$$

Substituting equations (4.15) and (4.16) in equation (4.14),

$$EQ = l_n \cdot \cos(2\alpha) + R_{chip} \cdot \sin(2\alpha) \quad (4.17)$$

Similarly,

$$EI = EN + NI = EN + HM \quad (4.18)$$

From $\triangle EHN$,

$$EN = EH \cdot \cos(2\alpha - \gamma) = YBE \cdot \cos(2\alpha - \gamma) \quad (4.19)$$

and, from $\triangle BHM$,

$$HM = BH \cdot \sin(2\alpha - \gamma) = XBE \cdot \sin(2\alpha - \gamma) \quad (4.20)$$

Substituting equations (4.19) and (4.20) in equation (4.18),

$$EI = YBE \cdot \cos(2\alpha - \gamma) + XBE \cdot \sin(2\alpha - \gamma) \quad (4.21)$$

Finally, substituting equations (4.17) and (4.21) in equation (4.13),

$$d = l_n \cdot \cos(2\alpha) + R_{chip} \cdot \sin(2\alpha) - YBE \cdot \cos(2\alpha - \gamma) - XBE \cdot \sin(2\alpha - \gamma) \quad (4.22)$$

For inputs of friction parameters μ , n and for prescribed values of field angle ψ and η the FORTRAN programme used to solve the above problem first determined the shape of the slip-line DC by solution to equation (4.7). From this initial slip-line and an initial guess for the field variables θ , p_D and WTR it then calculated the force system on the chip and its radius of curvature and generated equations (4.9)-(4.11). These equations were then solved to determine θ , p_D and W, where θ represents the angular range of slip-line BA, p_D is the hydrostatic pressure at D and W is the distance of the chip breaker from the cutting edge (Fig. 4.2(a)). As the above equations are non-linear, these were solved by an iterative method developed by Powell [89] for solution to non-linear algebraic equations with unknown derivatives. The above field parameters were assumed to be correctly estimated when the sum of the square of the residuals $(E_1^2 + E_2^2 + E_3^2) \leq 10^{-10}$. These optimised field variables were then used to construct the field, plot the streamlines and estimate the strains.

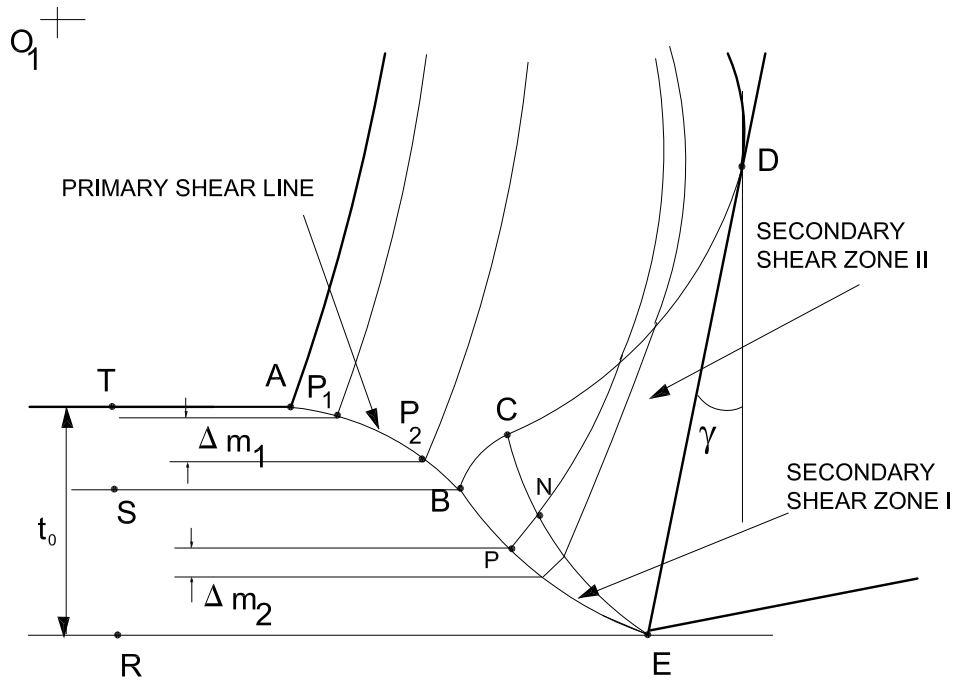
It may be seen that this field is characterised by four degrees of freedom. While, there are only three conditions to be satisfied for constructing a valid solution. Hence, the field is non-unique in nature.

4.4 Streamline Plotting and Strain Estimation

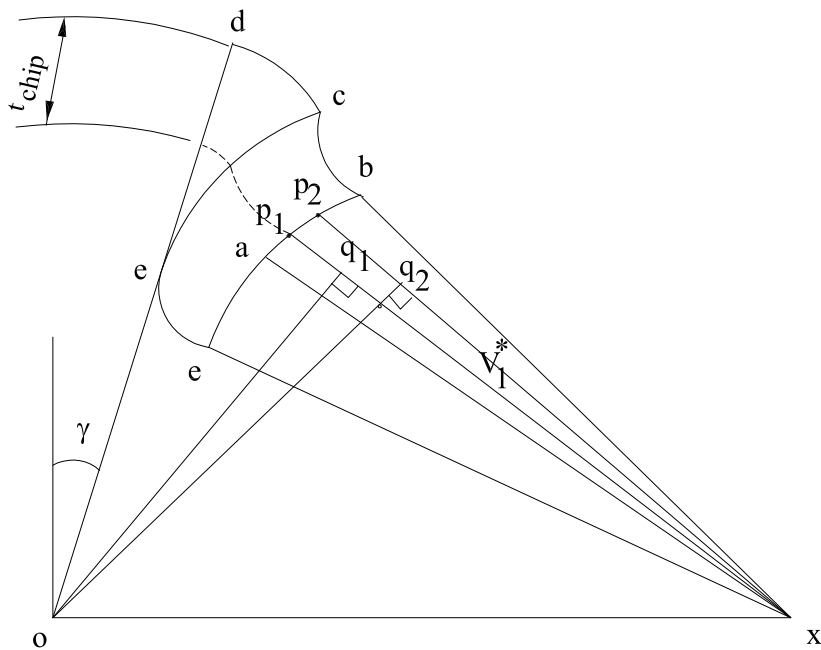
4.4.1 Plotting of Streamline

The procedure for plotting of the streamlines in the plastic deformation zones was similar to that explained in Section 3.4.

For plotting the streamlines the undeformed material of thickness t_0 was divided into two streamtubes of thickness TS and SR ($t_0=TS+SR$) such that the layer of material of thickness TS crossed the primary shear line through AB and that of thickness SR through BE.



(a)



(b)

Fig. 4.5: (a) Flow of streamlines in the workpiece and slip-line field (b) Hodograph for estimation of strain along the primary shear line (not to scale)

The streamlines are horizontal lines before the material enters the deformation zone. The mass flowing through TS is divided into 14 streamtubes with equal mass flow of Δm_1 . After crossing the line AB, the streamlines become circular arcs with centre at O_1 as shown in Fig. 4.5.

Similarly, the streamlines in the region SR are horizontal lines before crossing the line BE. Region SR is also discretised into 14 streamtubes with equal mass flow Δm_2 . The material within any streamtube in SR is initially strained on crossing the primary shear line BE. It then undergoes further deformation when it passes through the singular field BCE and the secondary shear zone CDE as shown in Fig. 4.5. The velocity and position of a particle along a streamline can be used for estimation of primary and secondary strains in the deformation zones. The method of plotting the streamlines in the secondary deformation zones was similar to that discussed in detail in Section 3.4. The streamlines become circular arcs with centre O_1 after crossing the slip-lines BC and CD. An illustrative example of the streamlines obtained by the proposed method is shown in Fig. 4.6.

4.4.2 Strain estimation

The shear strains induced in the material for any given geometry are calculated from the corresponding slip-line field configuration using the method suggested by Atkins *et al.* [75]. For computing the shear strain ϵ_p along the primary shear line AB and BE, each of these lines were discretised into 14 straight elements [91]. For each element the average normal component of velocity was obtained from the hodograph and the shear strain was calculated as the ratio of the magnitude of the velocity discontinuity to the normal velocity. On summing up the shear strains for all elements the total strain for the primary shear line was estimated.

Thus if P_1 and P_2 are points (Fig. 4.5(b)) on the primary shear line ABE, the shear strain suffered by the material on crossing these points may be written as,

$$(\delta\epsilon)_{P_1} = \frac{V_1^*}{oq_1} \quad (4.23)$$

and

$$(\delta\epsilon)_{P_2} = \frac{V_1^*}{oq_2} \quad (4.24)$$

where V_1^* is the velocity discontinuity and oq_1 and oq_2 are respectively the perpendicular distances of point 'o' from x_{p_1} and x_{p_2} as shown in Fig. 4.5(b). The strain suffered by the material passing between the points P_1 and P_2 is obtained by taking the mean of $(\delta\epsilon)_{P_1}$ and $(\delta\epsilon)_{P_2}$. The total 'damage' experienced by the deforming material on crossing the primary shear line AB and BE is therefore given by,

$$\epsilon_p = \frac{\Delta m_1}{t_0} \sum_{i=1}^{14} \left(\frac{\delta\epsilon_i + \delta\epsilon_{i+1}}{2} \right) |_{AB} + \frac{\Delta m_2}{t_0} \sum_{i=1}^{14} \left(\frac{\delta\epsilon_i + \delta\epsilon_{i+1}}{2} \right) |_{BE} \quad (4.25)$$

where $\delta\epsilon_i$ and $\delta\epsilon_{i+1}$ denote the strains for two consecutive points on ABE. The shear strain experienced by the material while flowing along a streamline passing through the secondary deformation zones BCE and CDE, the strains were similarly calculated at discrete points along this line starting from BE till it crossed the lines BC and CD. Let P and N denote two such consecutive points on the i^{th} streamline as shown in Fig. 4.5(a). The secondary strain suffered by the material while travelling from P to N can be expressed as

$$\delta\epsilon_s = \frac{V^*}{oq} \quad (4.26)$$

where V^* = velocity discontinuity pn as shown in Fig. 4.7, and oq = perpendicular distance of point 'o' from pn . The strain suffered by the material while flowing along this streamline is obtained by summing up of these elemental strains. Thus,

$$(\delta\epsilon_s)_i = \sum \frac{V^*}{oq} \quad (4.27)$$

Therefore, the secondary strain suffered by the material in a streamtube before exit from the deformation zone is obtained by taking the mean of the strains calculated for the bounding streamlines. The total secondary shear strain accumulated in the streamtubes on passing through BCE and CDE can be expressed as

$$\epsilon_s = \frac{\Delta m_2}{t_0} \sum_{i=1}^{14} \left(\frac{(\delta\epsilon_s)_i + (\delta\epsilon_s)_{i+1}}{2} \right) \quad (4.28)$$

Hence, the total strain ϵ_t experienced during chip formation can be expressed as

$$\epsilon_t = \epsilon_p + \epsilon_s \quad (4.29)$$

4.5 Results and Discussion

The results of computation from the present slip-line field analysis are shown in the following figures where, the variation of important machining parameters has been

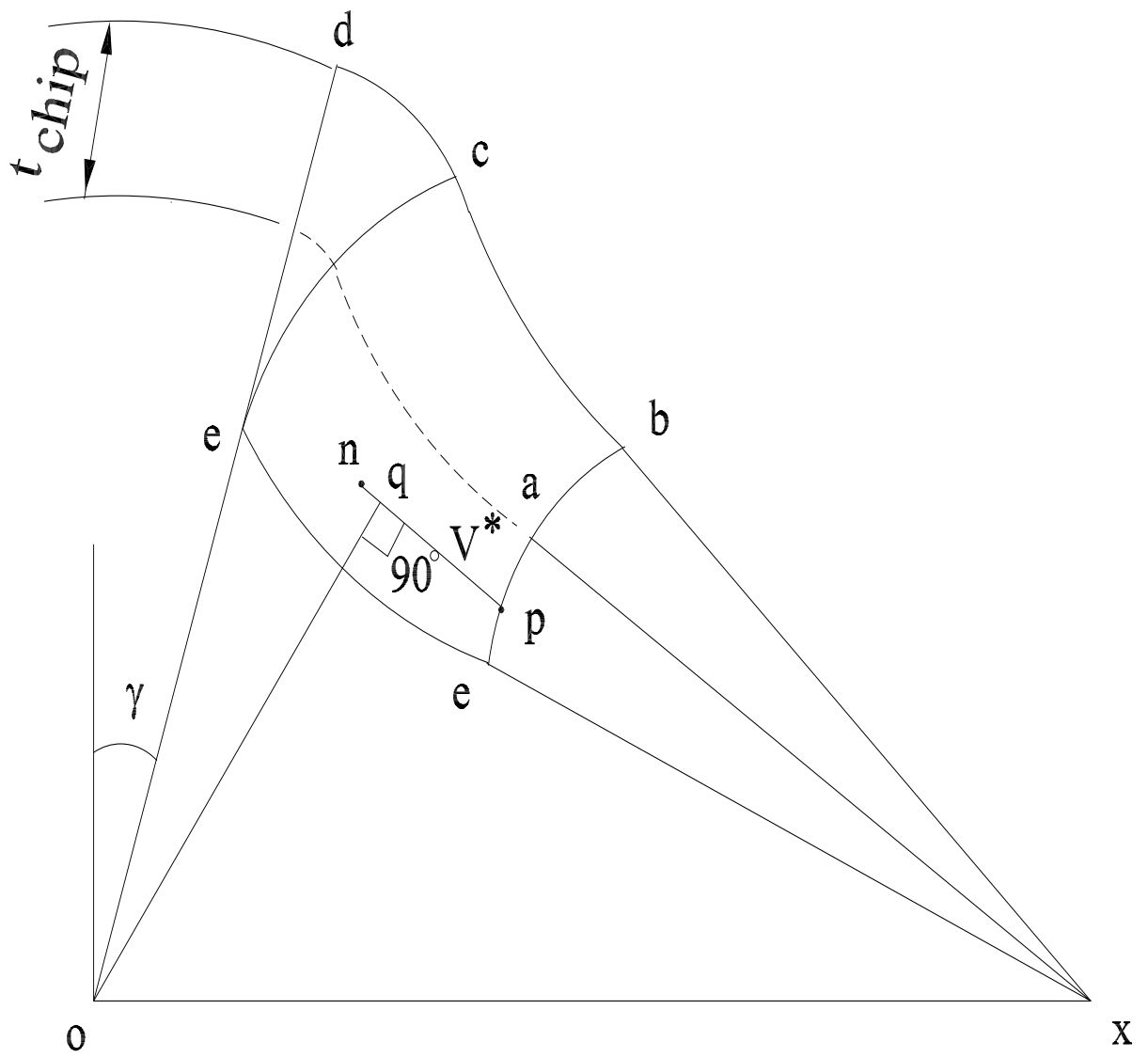


Fig. 4.7: Construction for estimation of strain in secondary deformation zone (not to scale)

Ref Fig. 4.2(a) for corresponding slip-line field

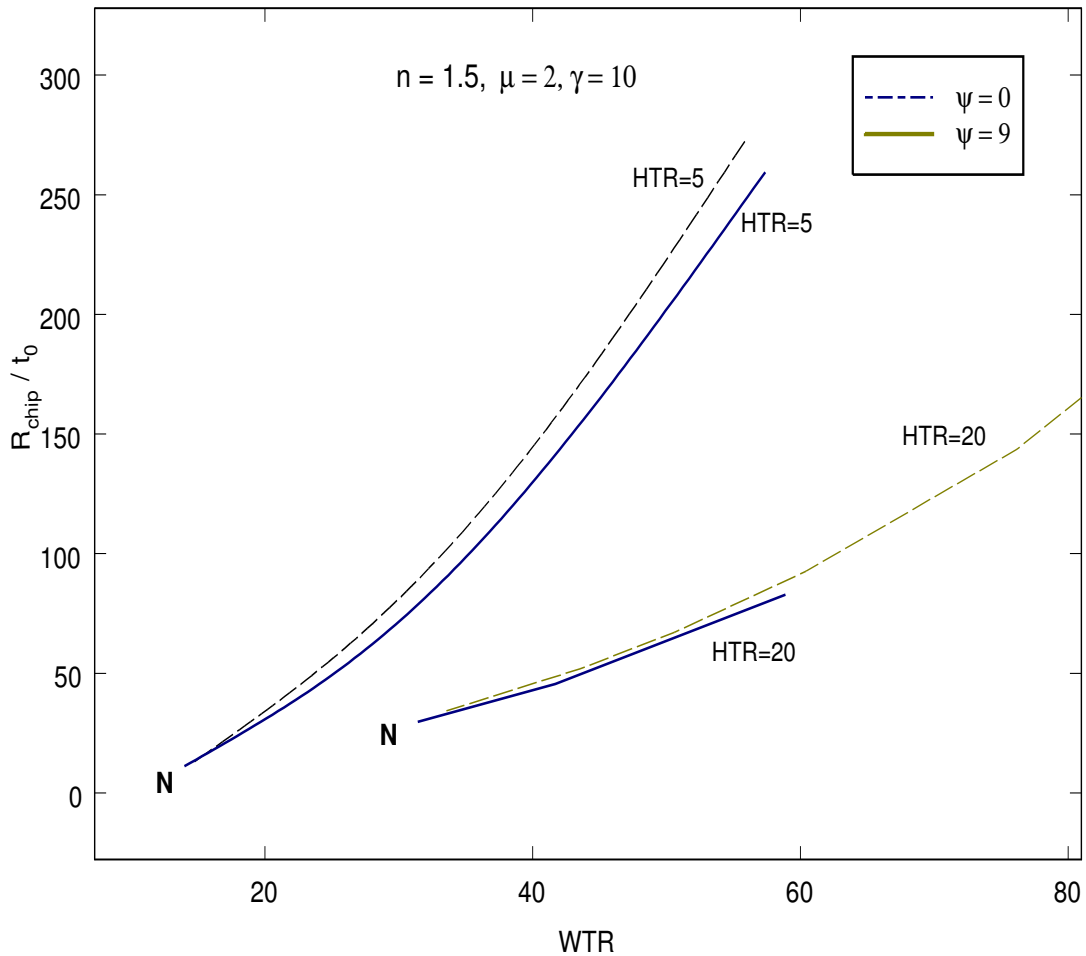


Fig. 4.8: Range of variation of radius of curvature with chip-breaker position and feed, N= Negative friction angle limit

studied as functions of chip breaker position WTR ($=W/t_0$), chip breaker height HTR ($=H/t_0$), tool rake angle γ and interface friction condition.

The variation of chip curvature (R_{chip}/t_0) as a function of chip breaker position WTR and feed is depicted in Fig. 4.8. The figure indicates that as the chip breaker moves away from the cutting edge, radius of chip curvature increases. The effect, however, is more pronounced at higher feeds than that at lower feed values. The tool-chip natural contact length (l_n/t_0) is found to increase as radius of chip flow circle increases (Fig. 4.9). The specific cutting energy (F_c/t_0), cutting ratio ζ and total strain ϵ_t in the chip also increase with chip radius and contact length though

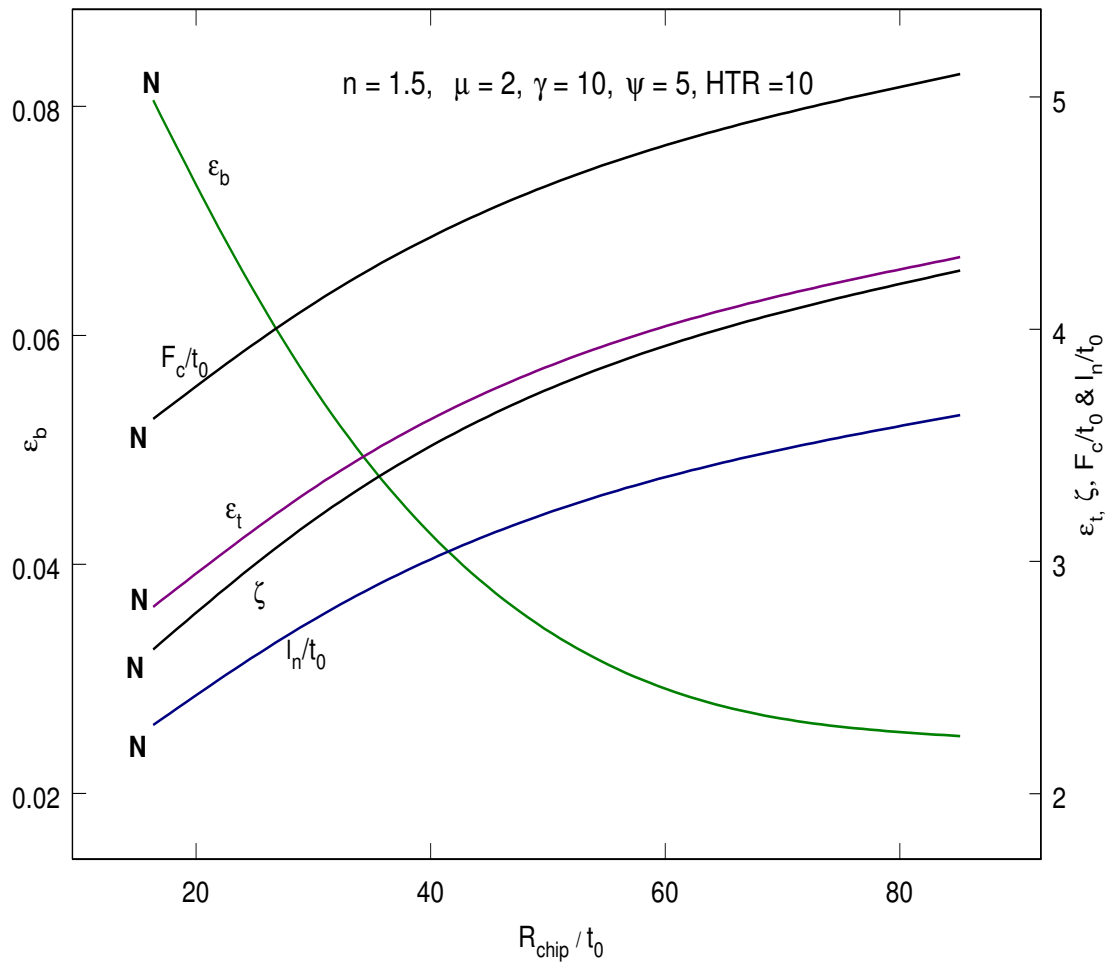


Fig. 4.9: Variation of total strain ϵ_t , breaking strain ϵ_b , specific cutting energy F_c/t_0 , cutting ratio ζ , normalized contact length l_n/t_0 with chip radius of curvature, N = Negative friction angle limit

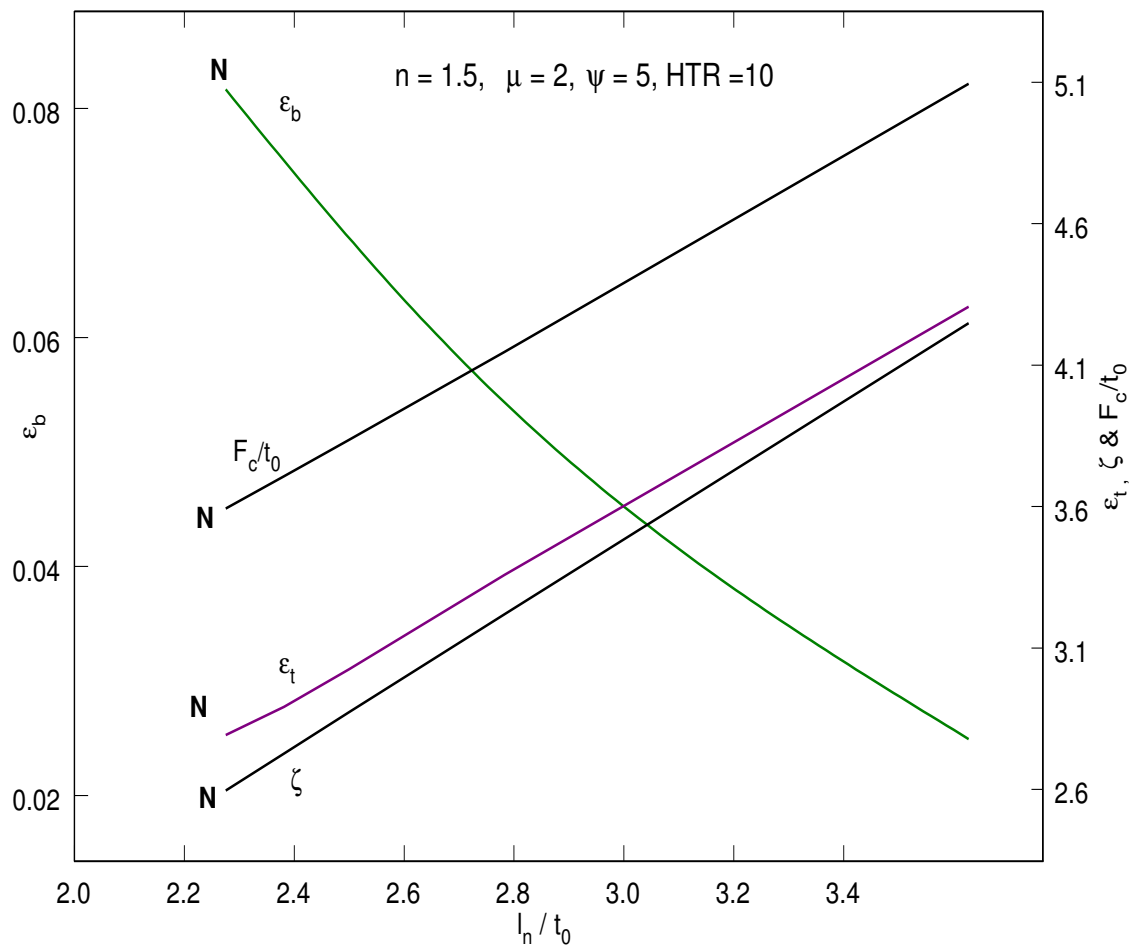


Fig. 4.10: Variation of total strain ϵ_t , breaking strain ϵ_b , specific cutting energy F_c/t_0 , cutting ratio ζ with contact length, N= Negative friction angle limit

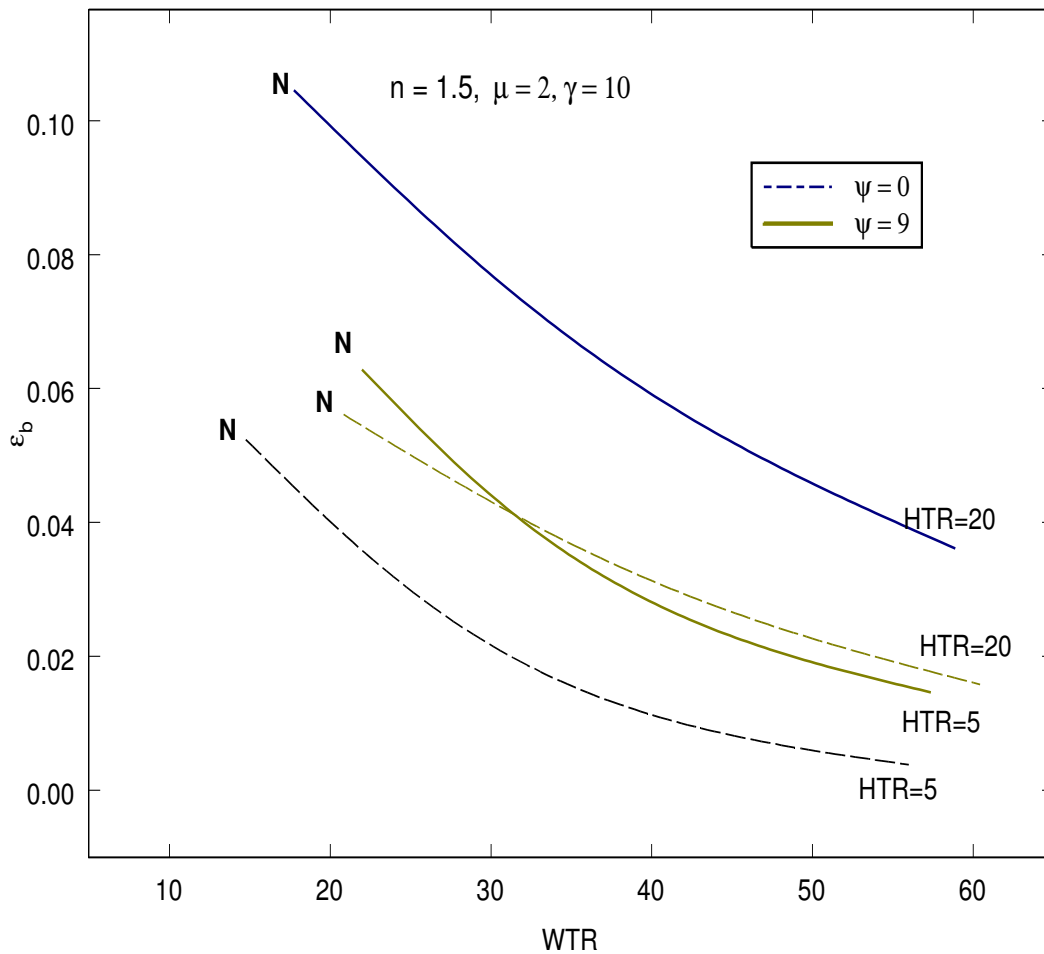


Fig. 4.11: Range of variation of breaking strain ϵ_b with chip-breaker position and feed, N= Negative friction angle limit

the breaking strain ϵ_b decreases (Fig. 4.9 and Fig. 4.10). Since in metal machining an increased value of ζ is associated with an increased shear strain, the results are compatible and agree with the findings of Dewhurst [23] for a ramp type chip breaker. Boothroyd [92] had indicated that in orthogonal machining the contact length was approximately equal to chip thickness. The present slip-line field analysis also shows a linear relationship between these parameters (Fig. 4.10) though their absolute values are not numerically equal.

The variation of breaking strain ϵ_b with chip breaker position and feed is shown in Fig. 4.11 for values of HTR equal to 5 and 20. The figure indicates that for the same

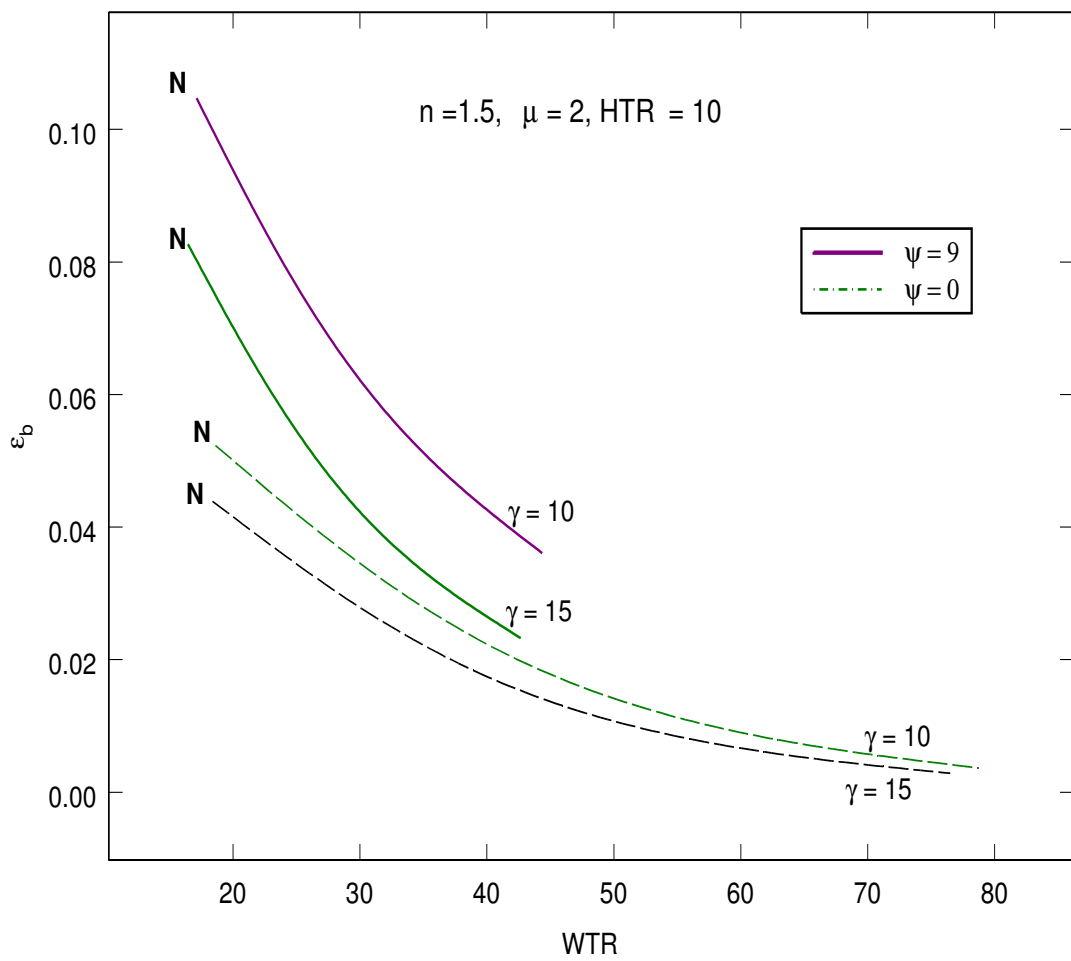


Fig. 4.12: Range of variation of breaking strain ϵ_b with chip-breaker position and rake angle γ , N= Negative friction angle limit

value of feed as the chip breaker comes closer to the cutting edge the breaking strain increases. Rake angle has a tendency to lower ϵ_b possibly due to its influence on chip thickness (Fig. 4.12). However, as indicated by Nakayama [32] rake angle does not affect chip breaking to any significant extent. For any given feed, calculated values of ϵ_b lie within a range and this is due to the non-unique nature of the machining process.

Computed values of strain suffered by the material in passing through the primary and secondary deformation zones are shown in Figs. 4.13 to 4.15 as functions of chip breaker position WTR and feed. Referring to these figures it may be seen that as the chip breaker moves away from the cutting edge both the total strain ϵ_t and the primary strain ϵ_p increase (Figs. 4.13,4.16,4.17) while, the secondary strain ϵ_s decreases (Fig. 4.14-4.15). For the same chip breaker position, an increase in feed (low HTR value) has a tendency to increase ϵ_t (Fig. 4.16) whereas the reverse happens when the rake angle increases (Fig. 4.17). It may also be noticed that for the same chip breaker position, an increase in feed and tool rake angle γ results in a decrease in the value of ϵ_s (Fig. 4.14-4.15) For all positions of the chip breaker, however ϵ_s is found to constitute only a marginal percent ($\approx 10 - 15\%$) of the total strain ϵ_t .

The variation of cutting ratio ζ and specific cutting energy (F_c/t_0) with chip breaker position WTR are shown in (Fig. 4.18-4.21). Both these parameters exhibit similar trend of variation. They increase with WTR as feed increases (Fig. 4.18 and 4.20) and decrease as rake angle increases (Fig. 4.19 and 4.21). Tool-chip interface friction results in an increase in these parameters (Fig. 4.22). These results are in agreement with the findings of Shi and Ramalingam [98] and Das and Dundur [99]. It may also be seen that the total strain ϵ_t increases as interface friction increases (Fig. 4.22), but the bending strain decreases as interface friction increases (Fig. 4.23). This may be due to the fact that increased friction usually increases chip curvature ($1/R_{chip}$) resulting in formation of chips of large curl radius [22, 24]. At low friction R_{chip} decreases and hence ϵ_b increases. At very low value of R_{chip} , however, the chip may completely escape the obstruction surface of the work piece and the tool forming continuous chips even if breaking strain ϵ_b is high [92].

It may be noticed that tool-chip natural contact length increases with WTR (Figs. 4.24 and 4.25). An increase in feed increases the contact length (Fig. 4.24)

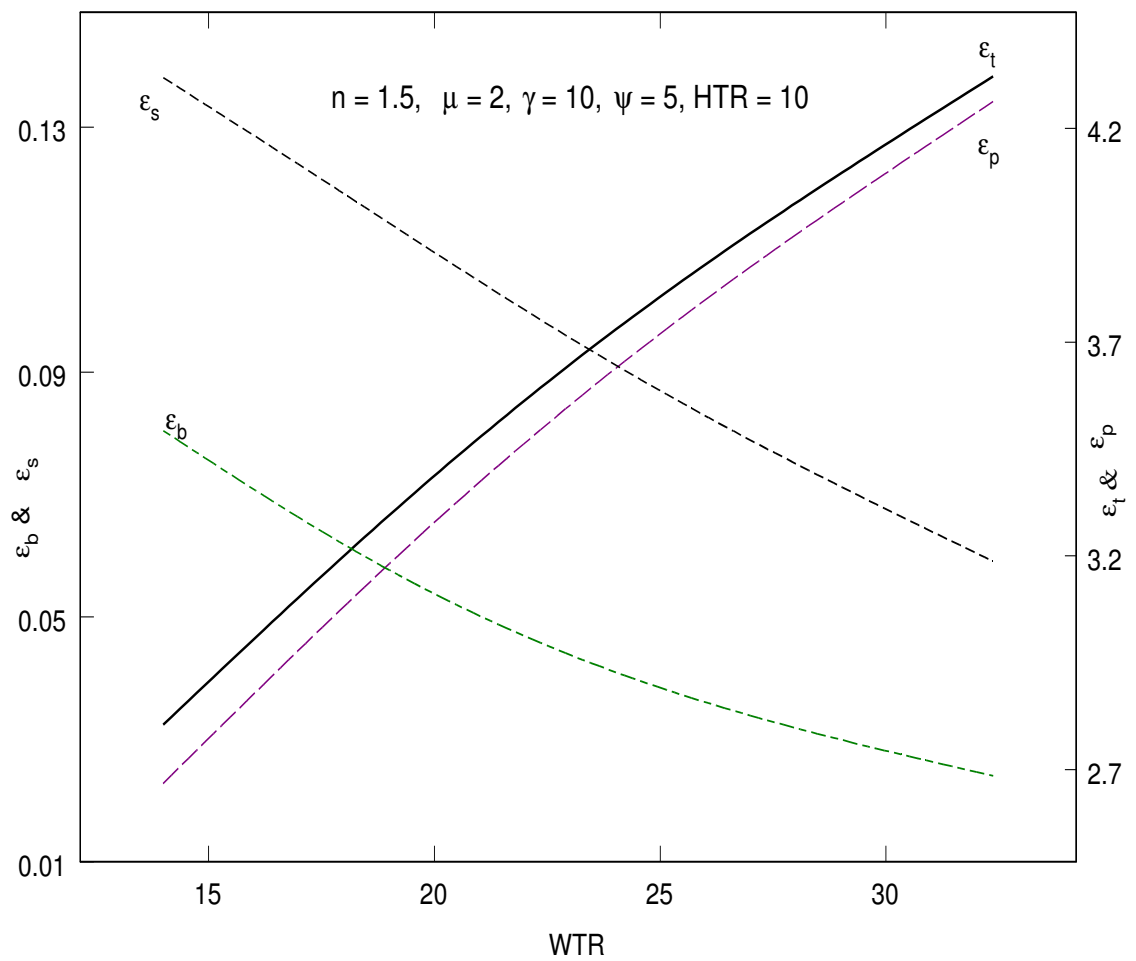


Fig. 4.13: Variation of total strain ϵ_t , primary shear strain ϵ_p , secondary zone shear strain ϵ_s and breaking strain ϵ_b with chip-breaker position, N= Negative friction angle limit

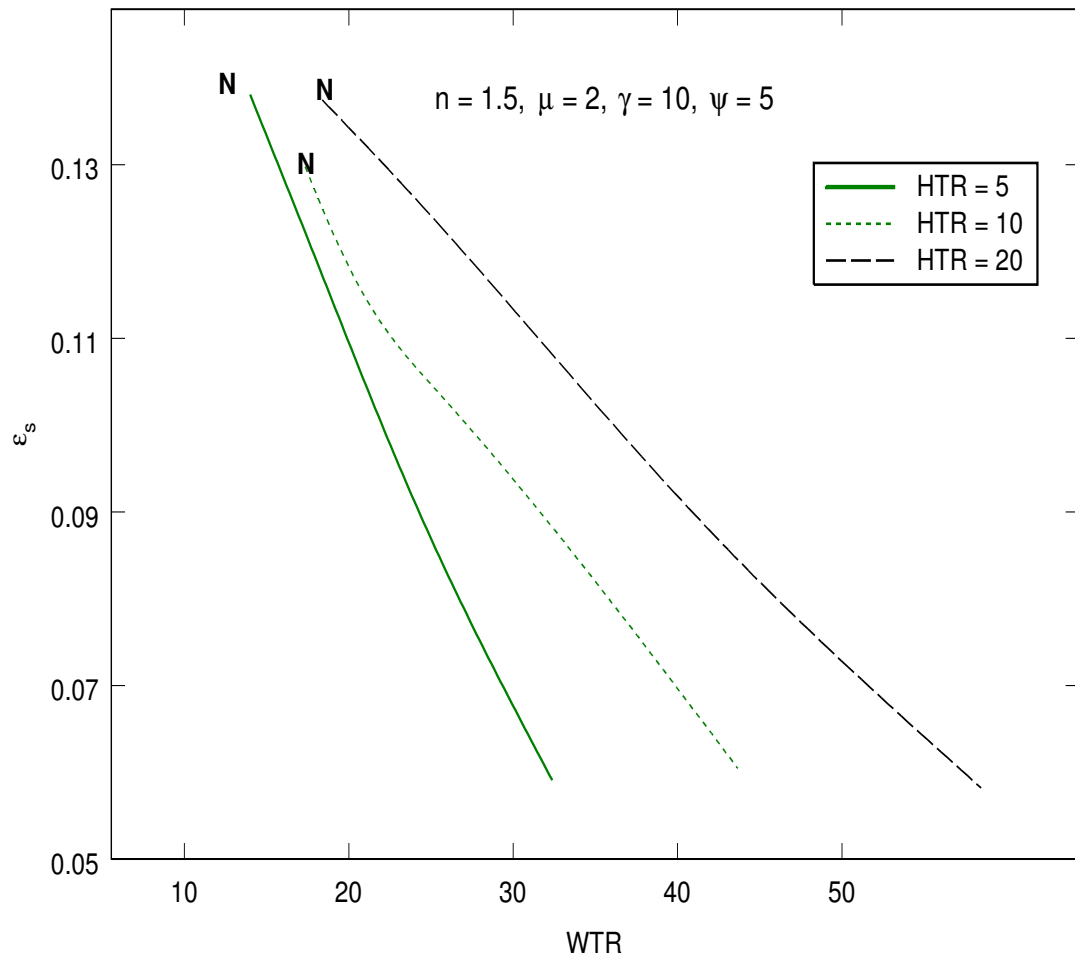


Fig. 4.14: Range of variation of secondary shear strain ϵ_s with chip-breaker position and feed, N= Negative friction angle limit

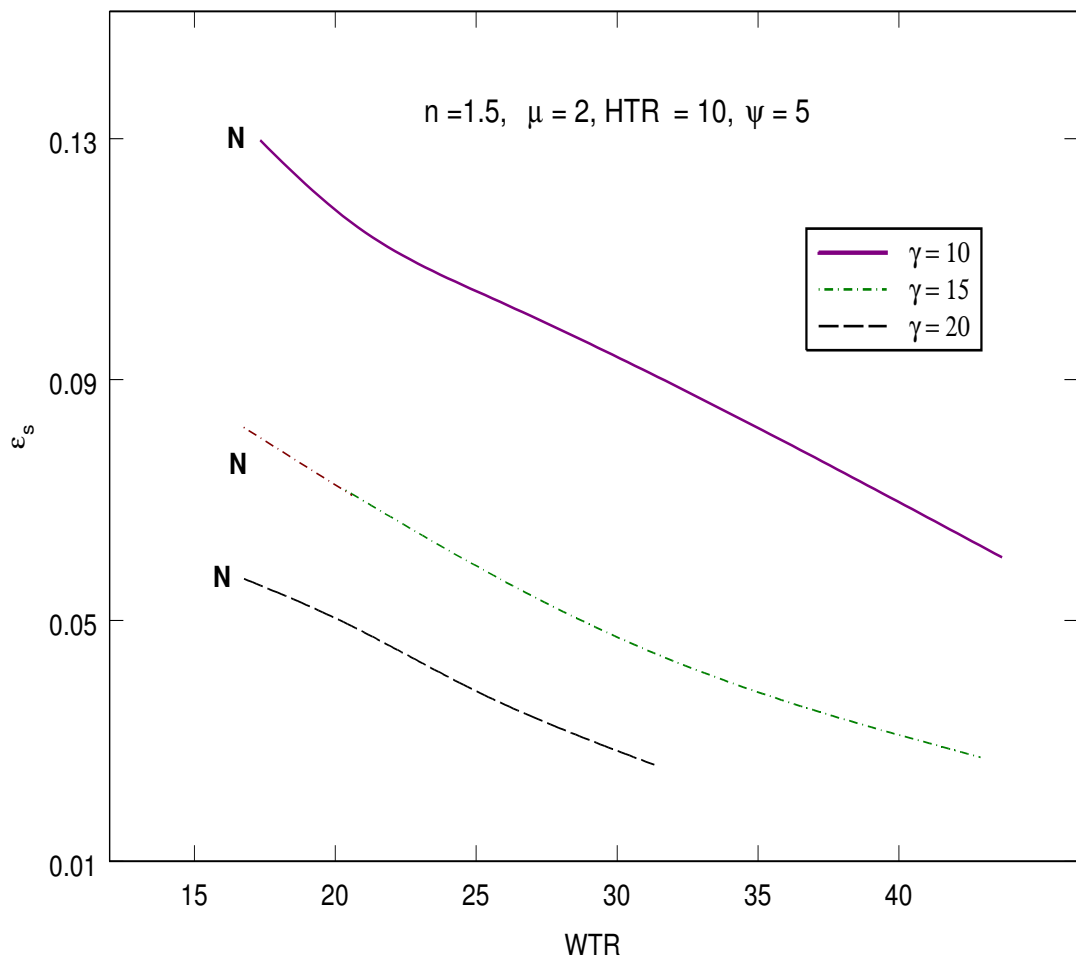


Fig. 4.15: Range of variation of secondary shear strain ϵ_s with chip-breaker position and rake angle γ , N= Negative friction angle limit

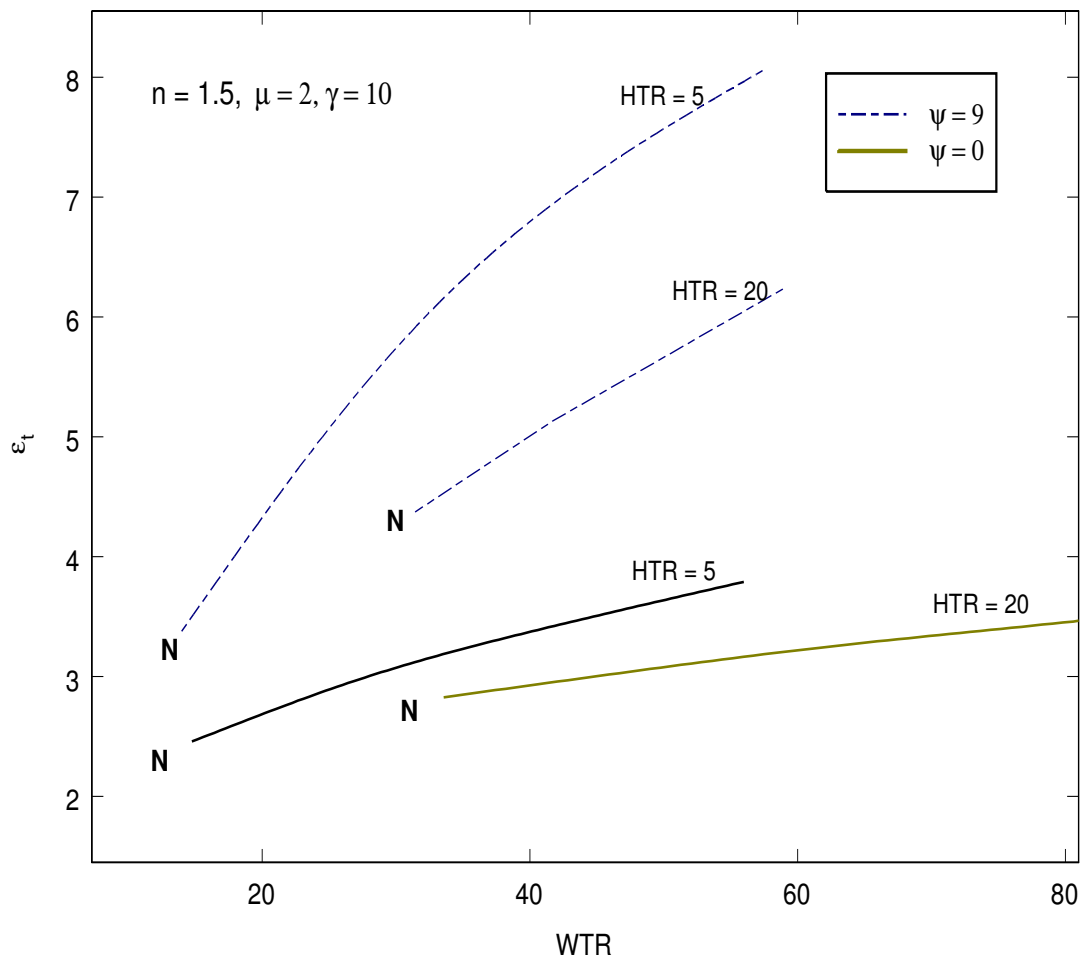


Fig. 4.16: Range of variation of total strain ϵ_t with chip-breaker position and feed, N= Negative friction angle limit

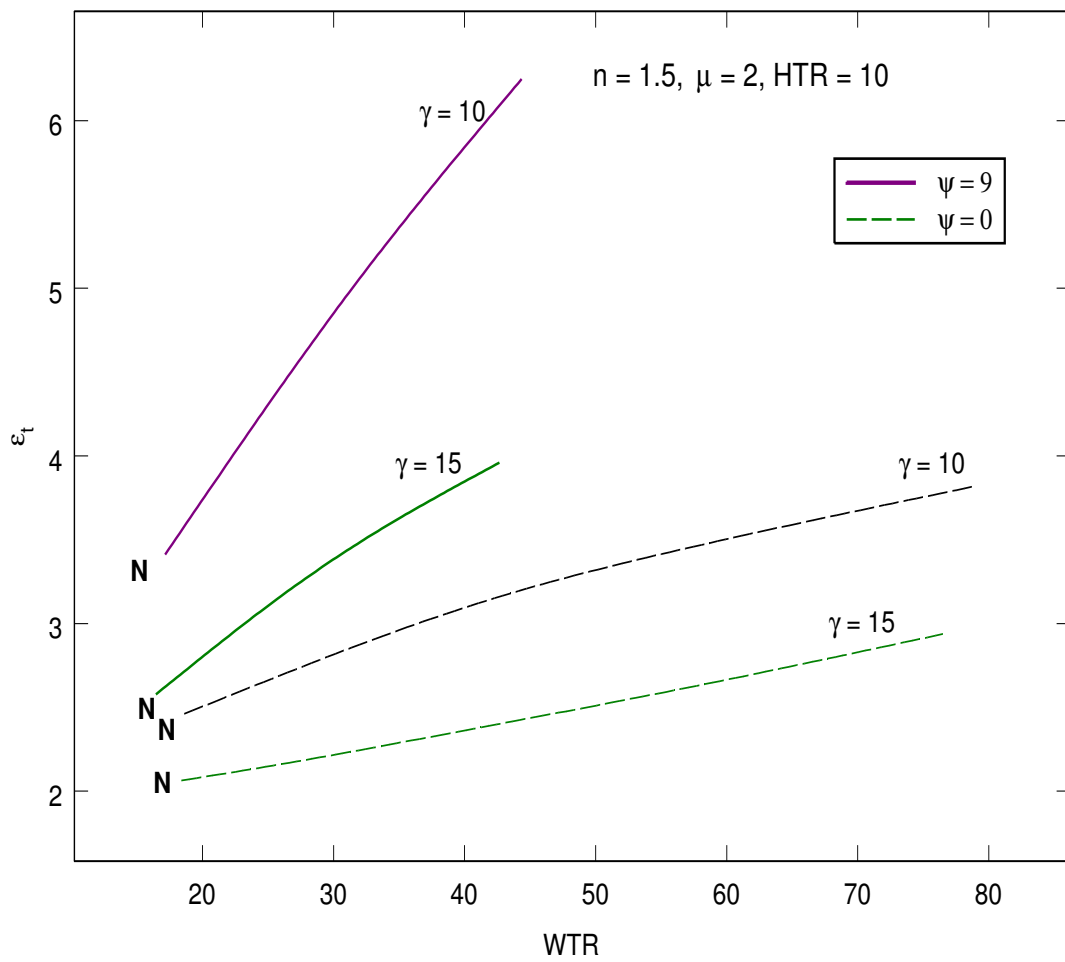


Fig. 4.17: Range of variation of total strain ϵ_t with chip-breaker position and rake angle γ ,
N= Negative friction angle limit

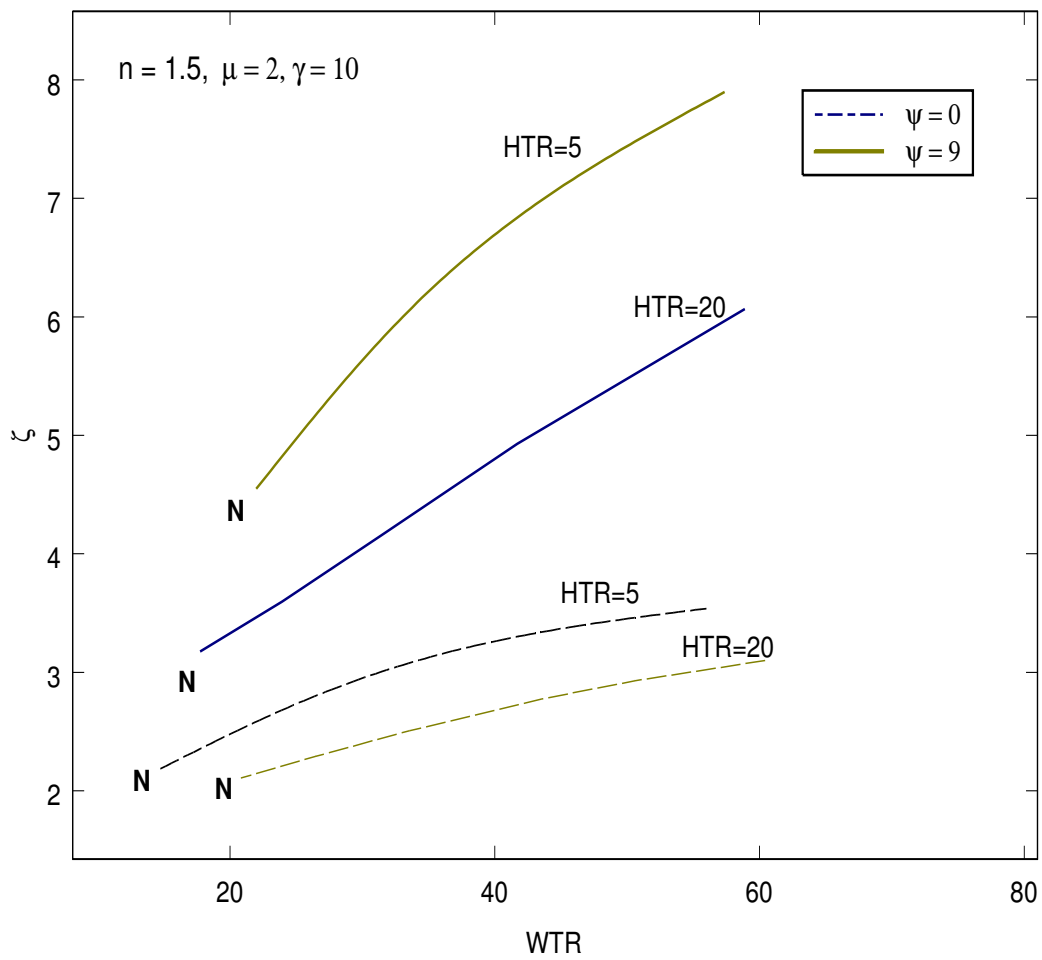


Fig. 4.18: Range of variation of cutting ratio ζ with chip-breaker position and feed, N= Negative friction angle limit

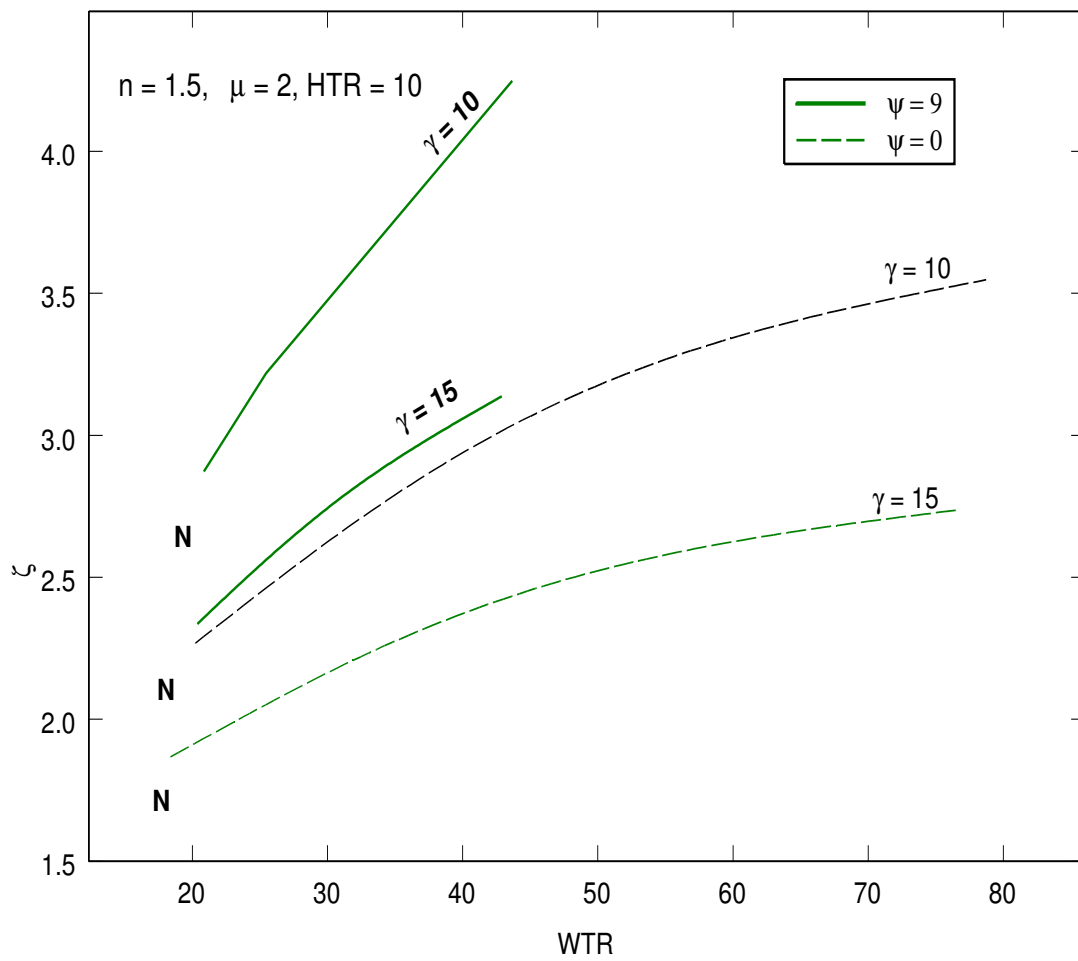


Fig. 4.19: Range of variation of cutting ratio ζ with chip-breaker position and rake angle γ , N= Negative friction angle limit

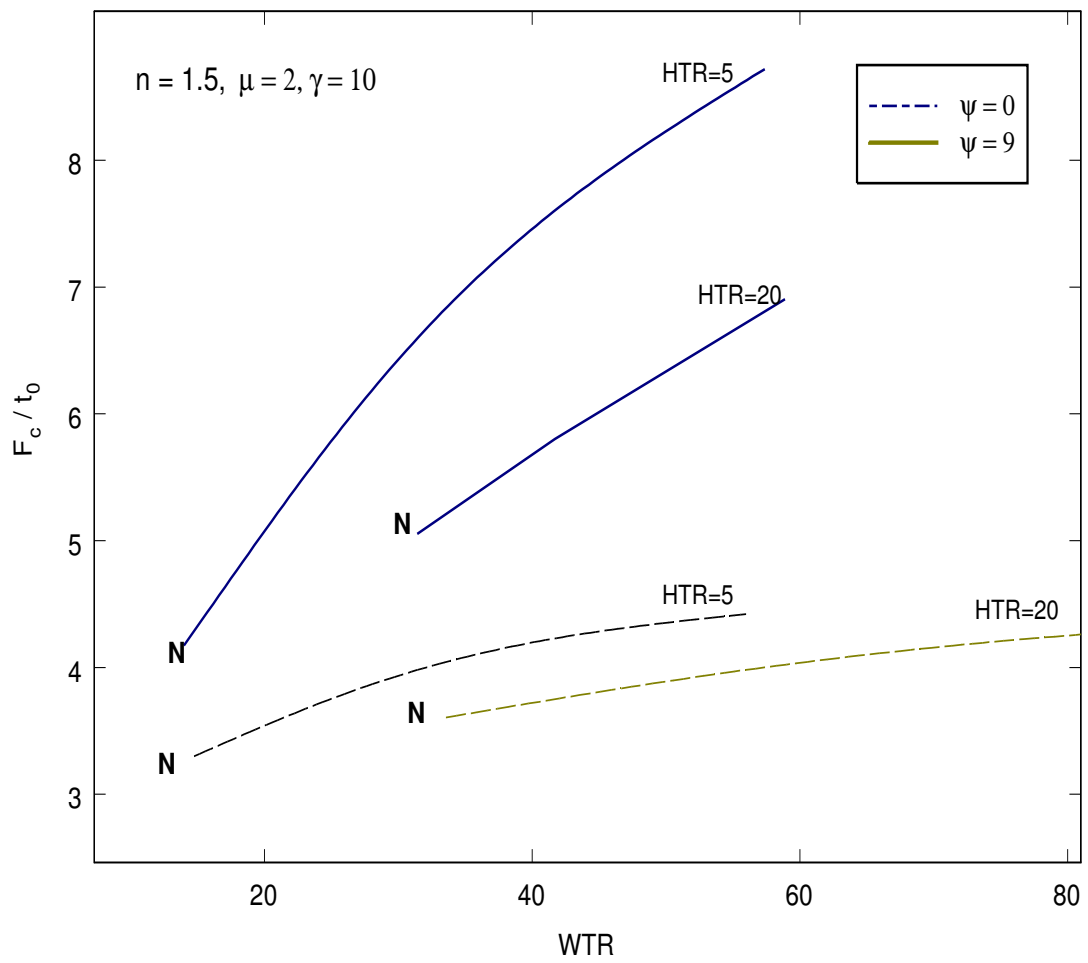


Fig. 4.20: Range of variation of specific cutting energy (F_c/t_0) with chip breaker position and feed

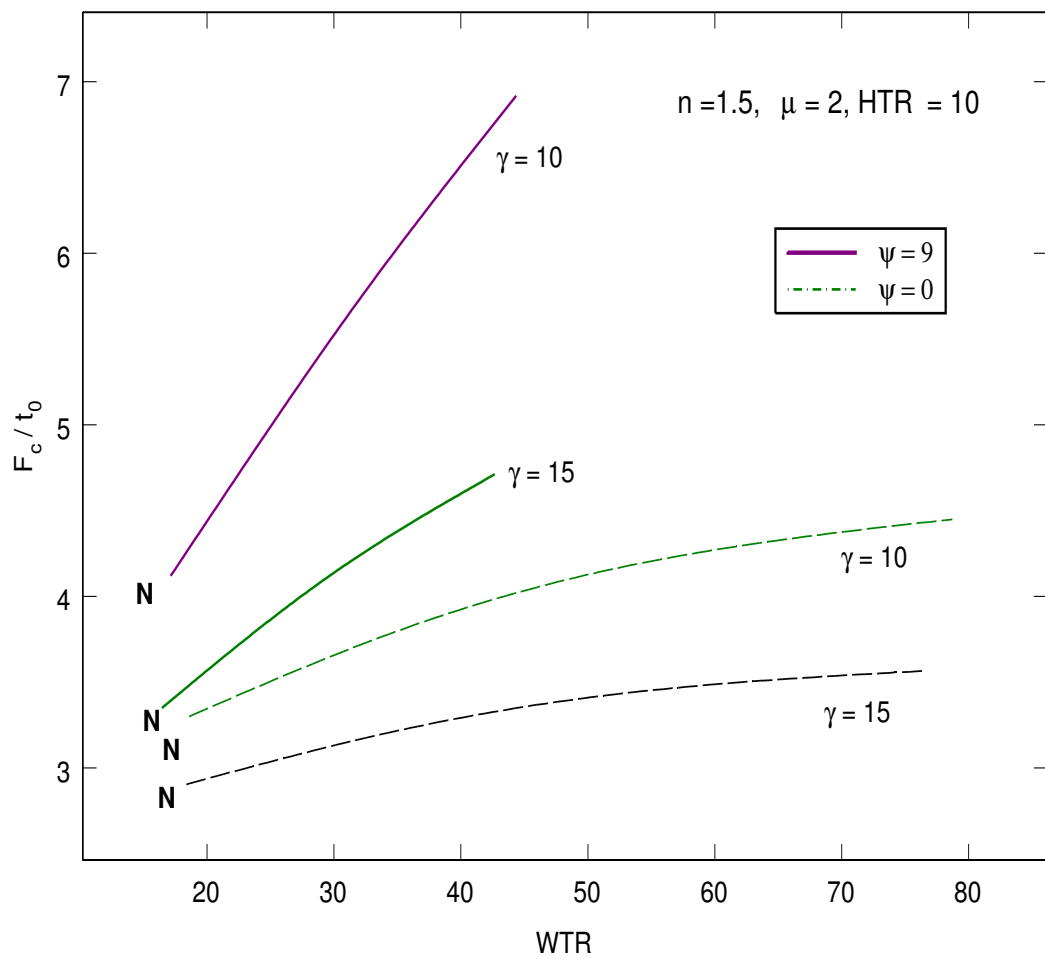


Fig. 4.21: Range of variation of specific cutting energy (F_c/t_0) with chip breaker position and rake angle γ , N= Negative friction angle limit

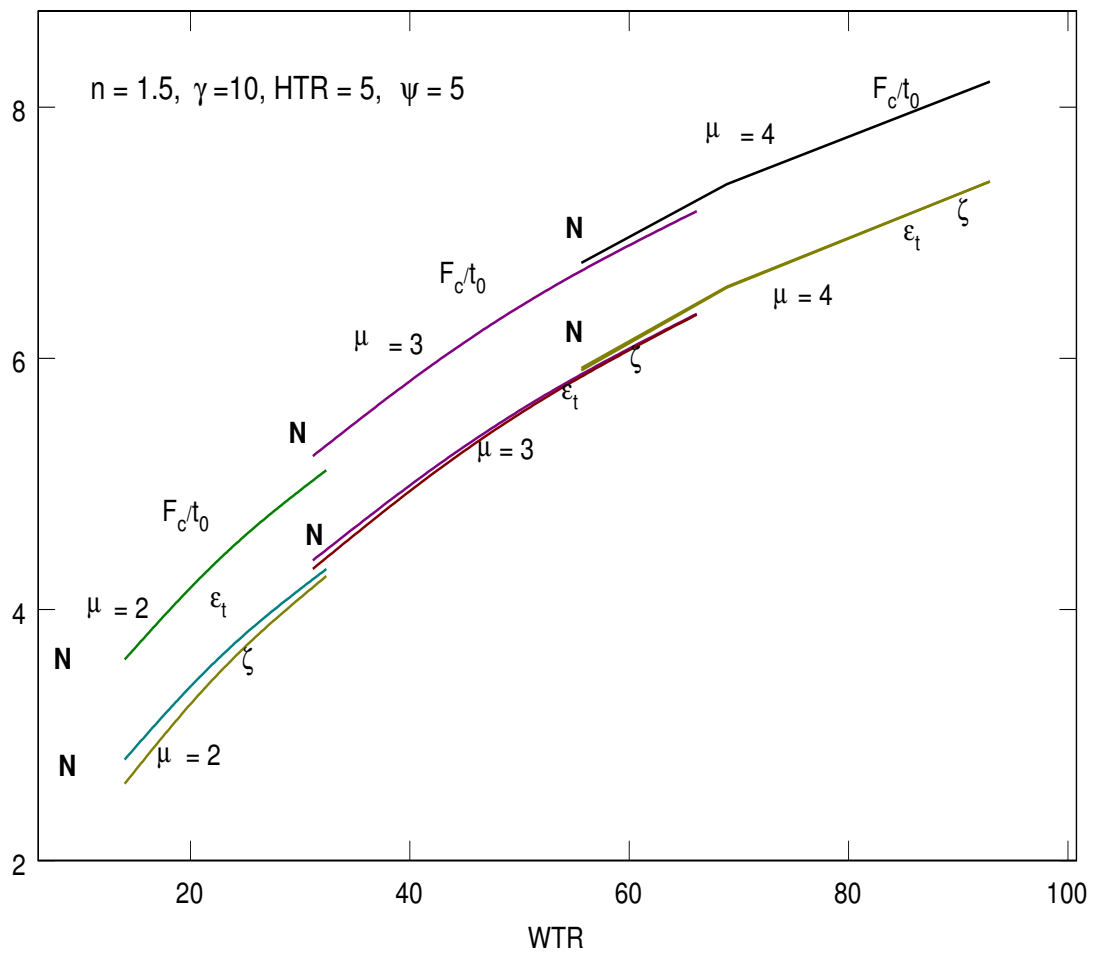


Fig. 4.22: Variation of total strain ϵ_t , cutting ratio ζ and specific cutting energy (F_c/t_0) with chip-breaker position and friction coefficient μ

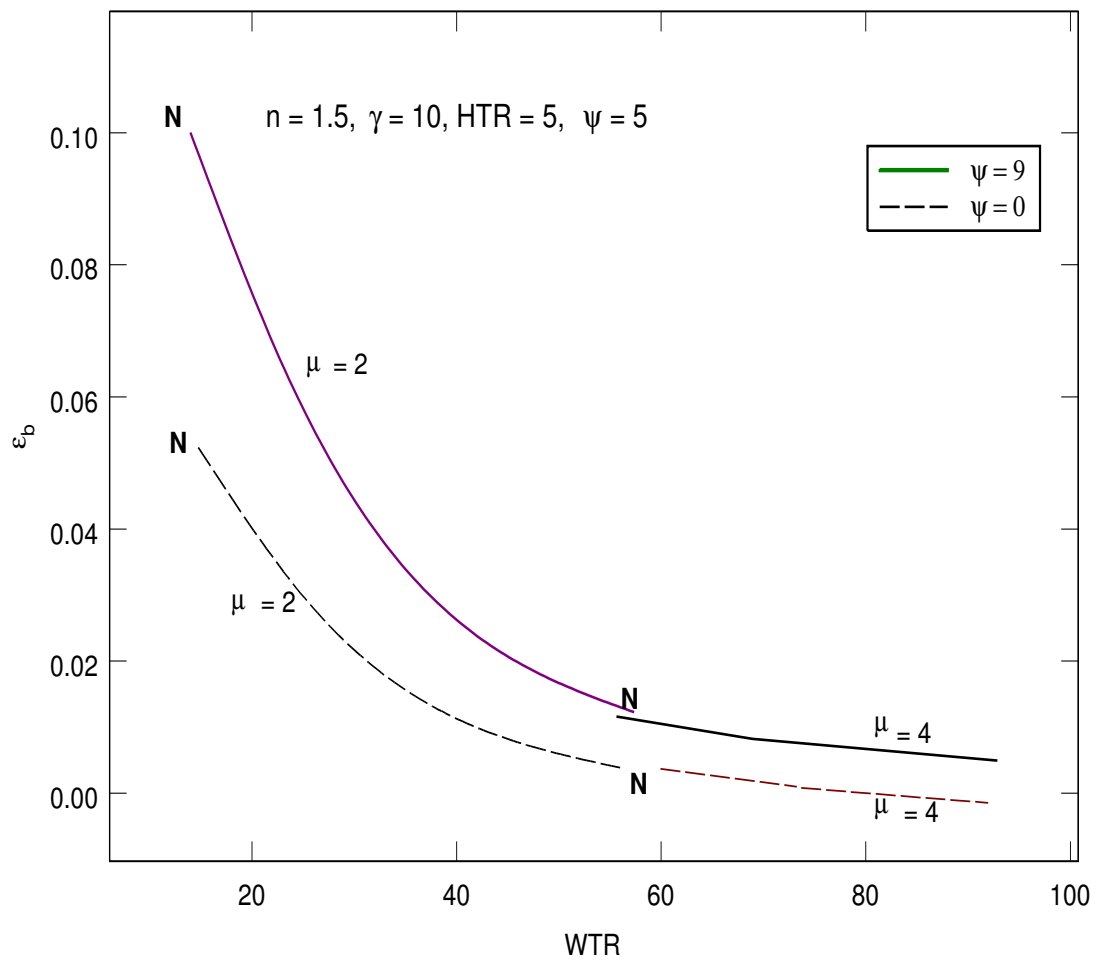


Fig. 4.23: Variation of breaking strain ϵ_b with chip-breaker position and friction coefficient μ , N= Negative friction angle limit

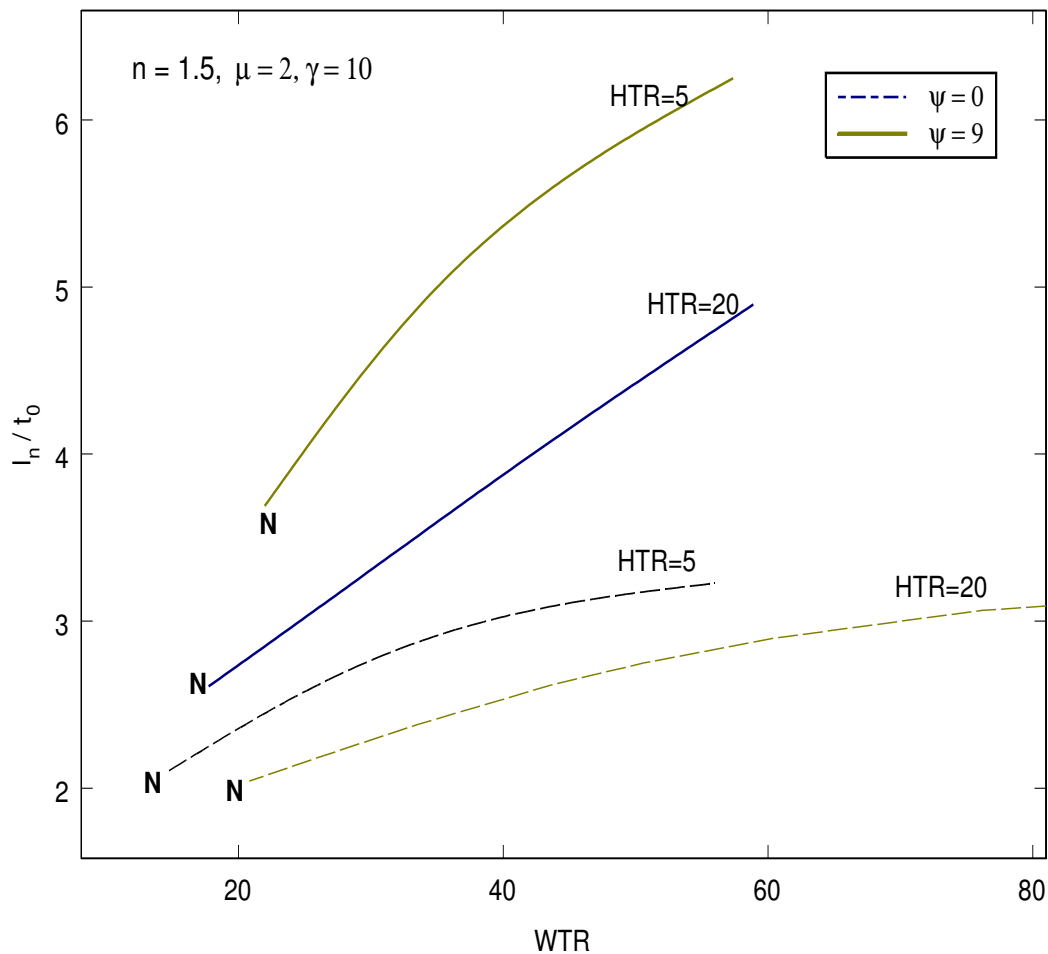


Fig. 4.24: Range of variation of non-dimensionalised contact length with chip-breaker position and feed, N= Negative friction angle limit

while the reverse happens when the rake angle increases (Fig. 4.25). As chip form is heavily dependent on natural contact length [5], variation in the position of the chip breaker may also affect chip form.

The variation of chip breaker force with chip breaker position is shown in Fig. 4.26. For the whole range of WTR values examined however, its contribution to the cutting force is less than half percent.

The variation of strain across the thickness of the chip as functions of chip breaker position and feed is shown in Figs. 4.27 and 4.28 respectively. The chip thickness in these figures is normalised between 0 and 1, so that points A,B,C and D in the above

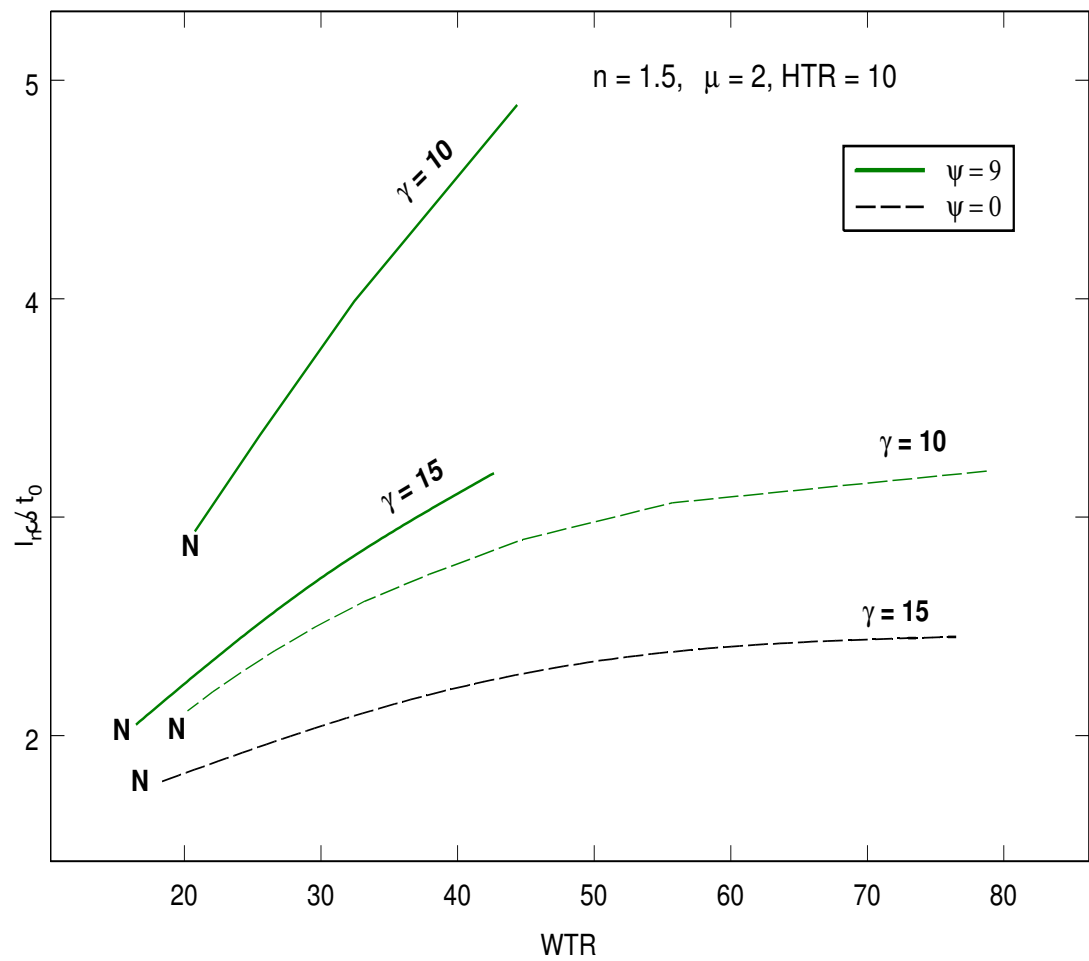


Fig. 4.25: Variation of non-dimensionalised contact length with chip-breaker position and rake angle γ , N= Negative friction angle limit

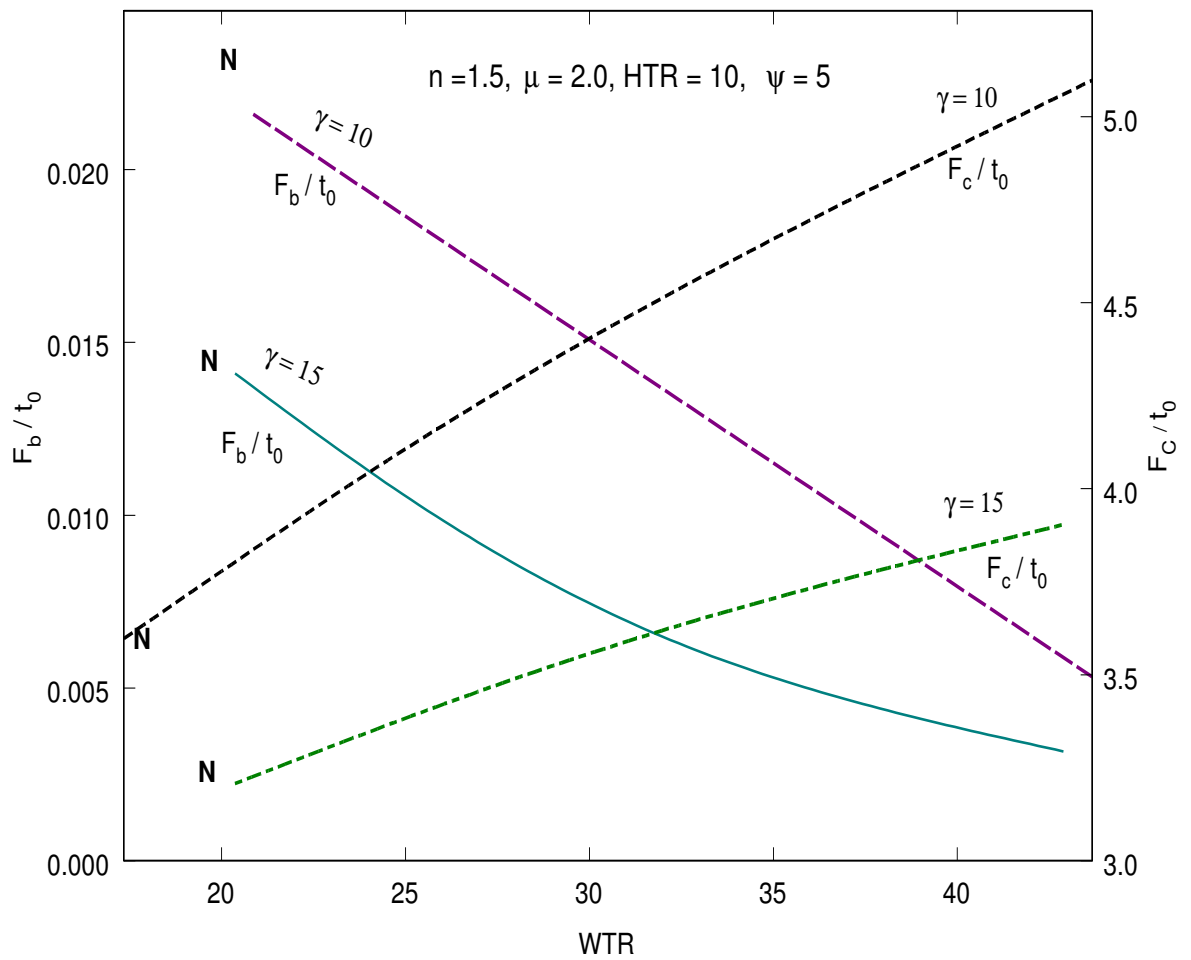


Fig. 4.26: Variation of non-dimensional chip breaker force and cutting force with chip breaker position and rake angle γ , N= Negative friction angle limit

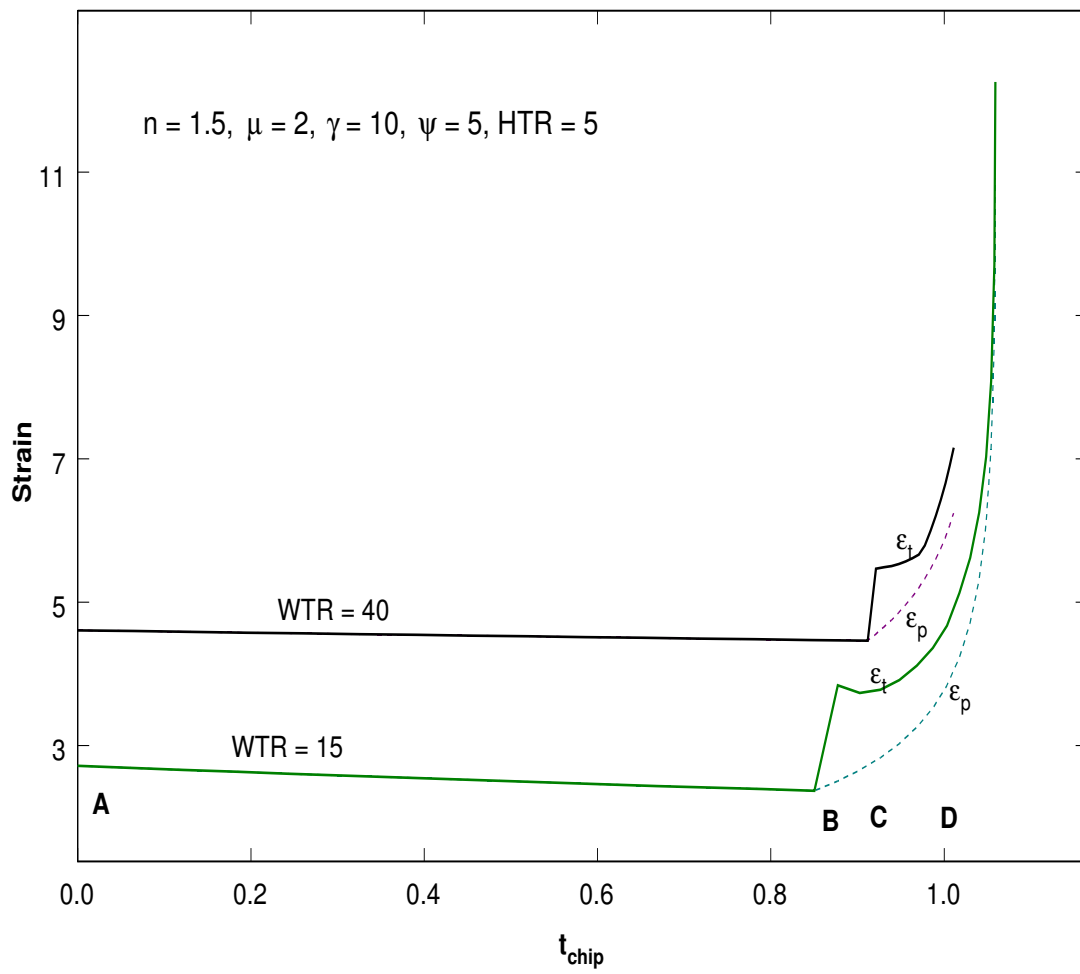


Fig. 4.27: Variation of primary and total strain across the normalized chip thickness with chip breaker position

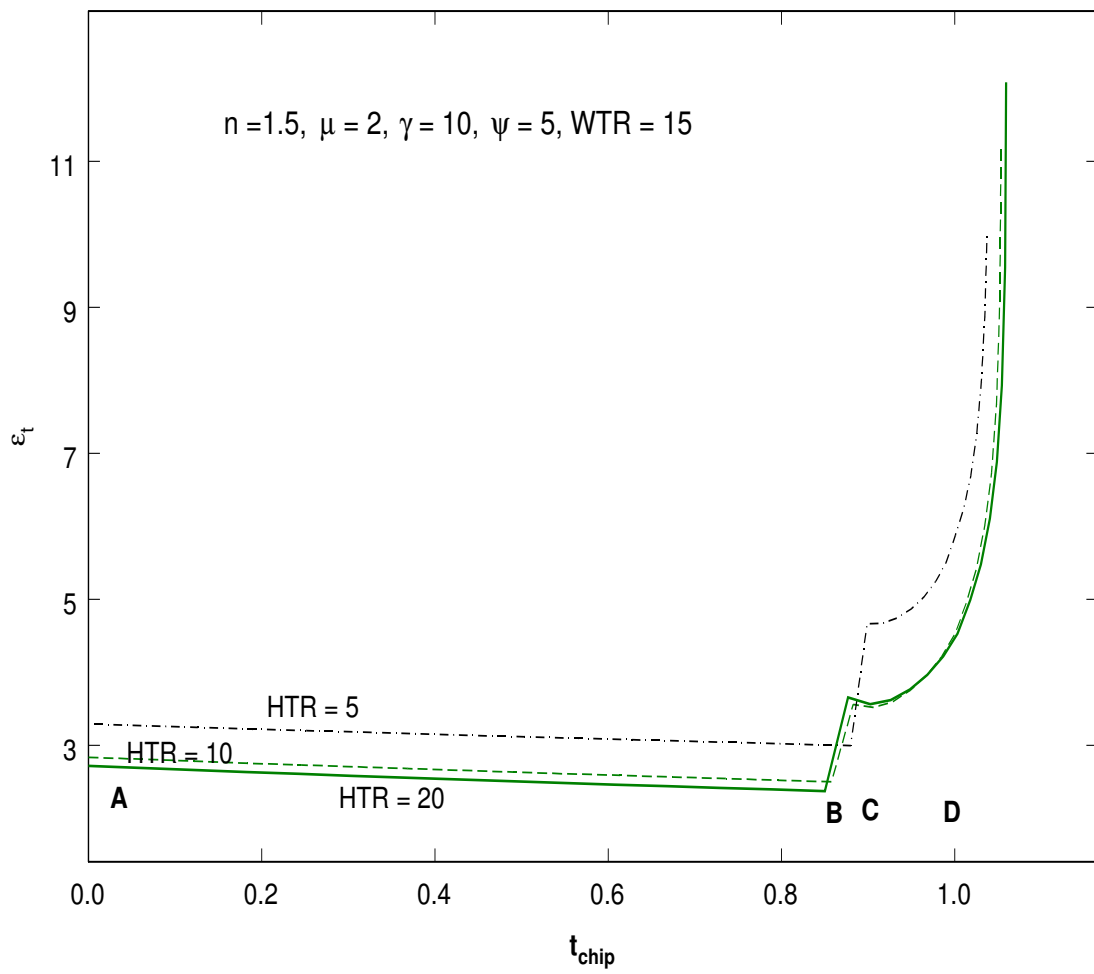


Fig. 4.28: Variation of total strain across the normalized chip thickness with feed

figures corresponds to points A,B,C and D in the slip-line field solution (Fig. 4.2). Referring to these figures it may be seen that nearly 80 % of the uncut layer of material are strained due to passage through the primary shear line only ($TS = 0.8 t_0$), only 20% of the material experience straining due to flow through both primary and secondary shear zones ($SR = 0.2 t_0$). The absolute value of strain suffered by the material flowing through the different streamtubes within TS is found to be nearly same as may be seen from the fact that line AB in the above figures is nearly horizontal. Also, strain within AB is found to be only marginally influenced by feed (Fig. 4.28) though it is affected significantly by chip breaker position (Fig. 4.27).

After B strain continuously increases due to increase in ϵ_p and also due to contribution of ϵ_s . Increase in ϵ_p is due to continuous decrease in the normal component of velocity from B to E. The overall effect is that strains of very high order of magnitude (≈ 12) is experienced by material flowing along the streamlines close to the tool face. This gives credence to the conjecture by Ponshe [18] that variation of strain across the chip thickness is the reason for chip curl. Also as the difference in strain between outermost and innermost fibre for $WTR = 15$ is higher than that for $WTR = 40$, curl radius in the former case is lower.

4.6 Evaluation of chip breakability criterion

Chip breakability criterion define the limiting conditions of chip breaking under which long continuous chips can be effectively broken into smaller pieces for easy disposal. Chip breakability depends on a number of factors. The most important ones being uncut chip thickness, chip thickness, radius of chip curvature, radius of chip before fracture and mechanical properties of the chip. As reported by Nakayama [32], radius of chip before fracture is rather difficult to determine theoretically. Also it is usually large and has less influence on chip breaking. Chips, depending on their size and radius are classified as under broken, effectively broken and over broken. It is worth noting, however, that the boundaries defining these three types of chip shapes is rather fuzzy: each investigator defining these boundaries in his own way to suit his requirements.

In Fig. 4.29 some of these criterion are plotted as function of chip breaker position

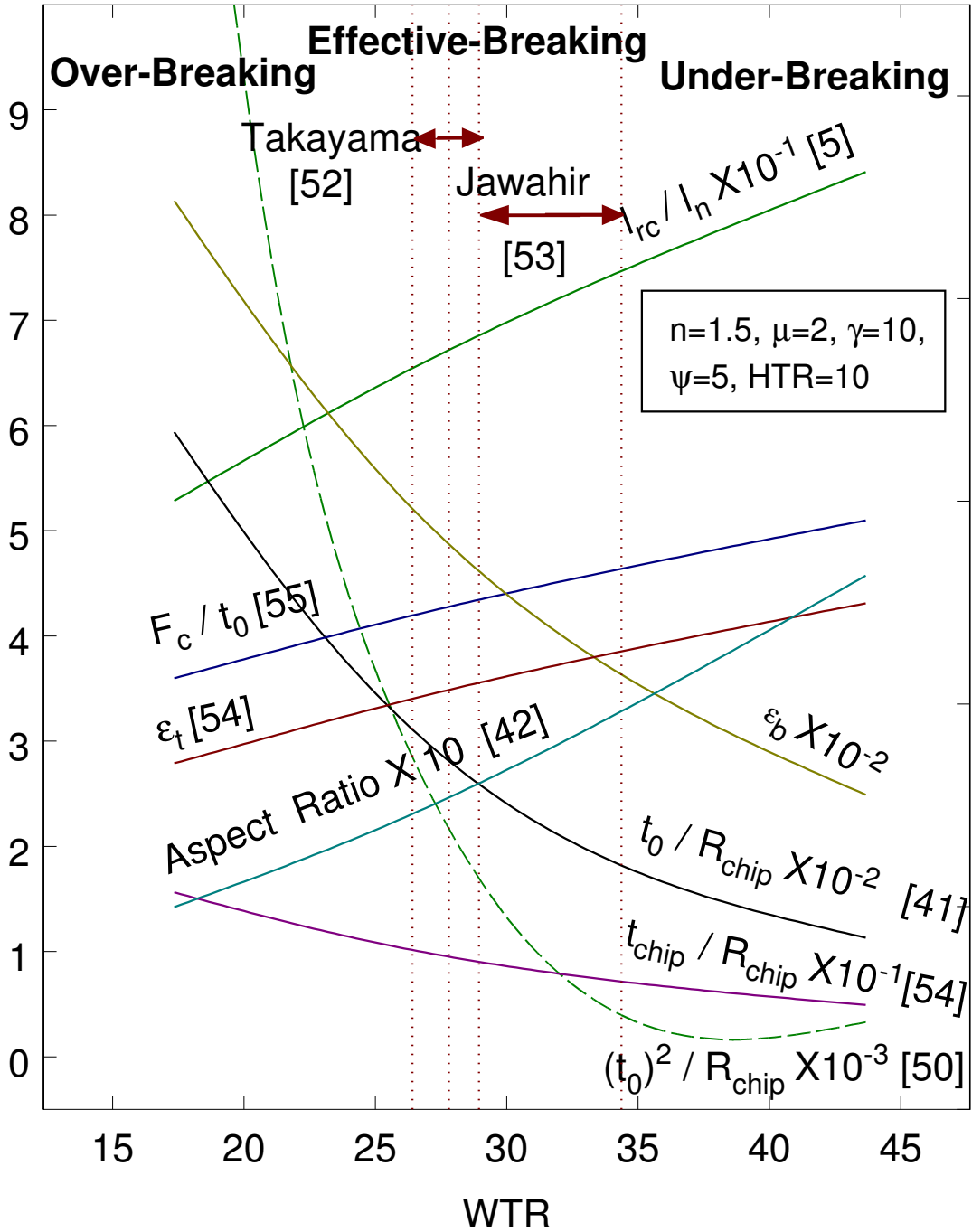


Fig. 4.29: Comparison of various Chip Breaking Criterion

WTR. It must be mentioned that except for the criterion based on total strain ϵ_t (material damage [54]) and aspect ratio [42] all other criterion were established from experimental observation. In the present case, the curves defining these criterion were computed from slip-line field analysis using Dewhurst's field with $\psi = 5$ degrees [23]. For Kudo's field (Solution I) $\psi = 0$ and for Dewhurst's field with $\psi \geq 9$ degrees, the friction angle at E becomes negative. Thus $\psi = 5$ degrees nearly defines the mean of the solution range.

In Fig. 4.29, the boundaries between under-broken, over-broken and effectively-broken chips have been established from breaking strain ϵ_b values as suggested by Takayama *et al.* [52] and Jawahir [53].

Referring to Fig. 4.29 it may be seen that a chip breaker criterion based on specific cutting energy as proposed by Grzesik *et al.* [55] nor that based on total "material damage" proposed by Athavale *et al.* [54] can be taken as criterion to assess effectiveness of chip breaking at least within the assumption of rigid-perfectly plastic material behaviour. It is well known experimental observation that for any given value of feed as the chip breaker moves away from the tool tip the effectiveness of chip breaking decreases. The present theoretical analysis suggest that both (F_C/t_0) and ϵ_t increase with WTR even though the chip breaker becomes less effective.

The criterion based on restricted contact length (l_{rc}/l_n) proposed by Sadik *et al.* [5] yields results consistent with those obtained from the slip-line field analysis for the zone between over and effective breaking though it deviates a little for the zone between under and effective breaking. The theoretical results calculated from the present slip-line field analysis (Appendix D) also agree with those obtained by Shinozuka *et al.* using FEM [42], though the present range of aspect ratio values for effective breaking are slightly higher than those suggested by these authors. The chip breakability criterion based on breaking strain appears to be most effective in assessing breakability of chips. The chip breakability criterion based on (t_0/R_{chip}) , (t_0^2/R_{chip}) and (t_{chip}/R_{chip}) show similar trend as that exhibited by breaking strain ϵ_b . They also compare favorably with present experimental observations (Discussed in detail in next chapter). These criteria, therefore can be used to assess effectiveness of chip breaking.

4.7 Conclusions

In the present chapter a slip-line field analysis has been carried out for pure orthogonal cutting using a cutting tool with a parallel step-type smooth chip breaker. The slip-line field studied is that proposed by Dewhurst [22]. Adhesion friction is assumed at the chip/tool interface and the field is analysed by the matrix operational procedure developed by Dewhurst and Collins [72] and Dewhurst [73, 74].

The shear strain suffered by the chip at the primary and secondary shear zones is estimated using the method suggested by Atkins *et al.* [75]. Strain variation across the thickness of the chip is also calculated as a function of the chip breaker height and its distance from the cutting edge. It is shown that 80 % of the chip material suffer 'damage' due to its passage through the primary shear line only. Rest 20 % of the material experience straining due to passage through the primary and secondary deformation zones. For all feeds and rake angles, however, the secondary strain is found to constitute only 10 to 15 % of the total strain.

The results of computation indicate that for a given value of feed as the chip breaker moves away from the cutting edge, total strain and primary strain imparted to the chip increase while, the secondary strain and breaking strain decrease. Radius of chip curl, tool-chip contact length, cutting ratio and specific cutting energy also increase as the distance of the chip breaker from the cutting edge increases. For a given position of the chip breaker increasing the feed has a tendency to increase the above parameters while, the increase in the rake angle has the reverse effect. For all positions of the chip breaker, however, the chip breaker force is found to be less than half percent of the cutting force.

It is seen that chip breakability criterion based on 'material damage' or specific cutting energy can not be used to assess the effectiveness of chip breaking. On the other hand criteria based on breaking strain and the ratio of t_{chip} to R_{chip} or feed to R_{chip} exhibit similar trend of variation with WTR and can be used to assess effectiveness of chip breaking.

For any given chip breaker position, feed and rake angle, the chip parameters such as chip thickness, radius of chip flow circle and strain lie within a range and this is due to the non-uniqueness of the machining process.

5. PARTIAL EXPERIMENTAL VALIDATION OF MODEL

5.1 Introduction

Modern high powered machine tools with cutting tools of sintered carbide have increased the rate of chip formation and it has become necessary to produce properly broken chips for convenient handling and disposal. The problem attains serious proportions especially in turning and boring operation where, the tool removes metal for a considerable period and the chips produced in the form of long ribbons can present serious hazard to the machine tool, machine operator and also damage the machined surface by scuffing. This has made it necessary to have proper control on shape and size of chips by bringing into use chip breakers of various forms. The main purpose of these devices is to produce tightly curling chips and direct them in such a manner that they strike the work piece or flank face of the cutting tool resulting in intermittent fracturing of chips.

The mechanism of chip breaking by ramp and step-type chip breakers has been investigated experimentally by Nakayama [32], Trim and Boothroyd [92], Henriksen [30, 48] and Subramanian *et al.* [93]. The action of a groove-type chip breaker has been studied by Worthington and Redford [33], Worthington [40], Worthington and Rahman [41]. Chip breakability criteria based on breaking strain has been suggested by Nakayama [51], Takayama *et al.* [52], Jawahir [53] and Worthington *et al.* [40] and those based on feed and radius of chip flow circle has been proposed by Henriksen [30, 48, 49, 100], Okushima *et al.* [50] and Shinozuka *et al.* [42]. Criterion based on cutting energy has also been established by Athavale and Strenkowski [54], Grzesik and Kwiatkowska [55], Yang *et al.* [56, 57]. The aim of these investigations has been to determine conditions for breaking of chips into optimum sized pieces for ease of removal. However, the validity of any recommended condition for effective chip breaking depends upon the repeatability or otherwise of the process.

In the present investigation experimental studies were carried out to validate the theoretical predictions from slip-line field analysis. Orthogonal cutting tests were carried out on a copying lathe using HSS (High Speed Steel) tools fitted with step-type chip breakers. Important chip features such as thickness, radius of curvature and length were measured for different feeds and chip breaker positions. Cutting ratio, breaking strain and some important chip breakability parameters were computed from the experimental data and these were compared with those obtained from the theoretical models.

5.2 Experimental Setup and Procedure

Orthogonal turning tests were carried out on a HMT copying lathe with automatic feed system (Fig. 5.1). Mild steel tubes of 40 mm outside diameter and 5 mm thickness were used as work-pieces. One end of these tubes was supported by the three jaw self-centering chuck and the other end was left unsupported. To remove any eccentricity in the work-piece these tubes were first subjected to a skin pass. A high speed steel (HSS) cutting tool with 10 degree orthogonal rake angle and zero degree inclination angle was used in the cutting tests. On the tool angles were ground by using a CNC surface grinder (Fig. 5.2). A step-type chip breaker of HSS was welded on to the rake face of the tool by Tungsten Inert Gas (TIG) welding (Fig. 5.3). Detailed specifications of the items relating to the present experimental investigations are presented in Table 5.1.

Cutting tests were carried out at cutting speeds between 40 to 50 m/min and feed values between 0.06 to 0.32 mm/revolution. For the chip breaker the height to feed ratio (HTR) was set at 5, 10 and 20 and the width to feed ratio (WTR) was varied between 12 and 75. The tests were conducted dry (without coolant). These experimental observations are tabulated in Table 5.2. From 34 experimental runs, four representative chip samples indicated by same 'Pkt No.', were collected for measurement of chip thickness, chip length and radius of chip curvature using an image analyser (Fig. 5.4). The radius of curvature after spring back correction R_{chip}/t_0 and cutting ratio ζ were then computed from these measured data. These data for the representative chip samples are provided in the above table.

Fig. 5.5 presents various chip forms obtained from these experiments for various feeds and chip breaker positions. It can be seen from this figure, that for the same feed, smaller chips are obtained as the chip breaker comes closer to the cutting edge.

Tab. 5.1: Specifications of items related with experimental work

Item	Parameter	Specification
Cutting tool:		
	Material of cutting tool	High Speed Steel with 10% Cobalt
	Length of cutting tool	60 mm
	Cross-section of tool	15x15 mm
	Orthogonal rake angle (γ)	10.0 degree
	Inclination angle (λ)	0.0 degree
	Principal cutting edge angle (ϕ_p)	90 degree
Work Piece:		
	Material	Mild Steel
	Outer diameter of tube	40 mm
	thickness of tube	5 mm
Grinding Machine:		
	Type	Surface Grinder
	Make	Praga
	Model	452 CNC
	Wheel Speed	2800 RPM
	Surface Finish	0.2 to 0.4 ra
Welding Machine:		
	Type	Tungsten Inert Gas (TIG)
	Make	Kuper Max

(continued on next page)

Tab. 5.1: Specifications of items related with experimental work (Contd.)

Item	Parameter	Specification
Machine Tool:		
	Type	Heavy Duty Copying Lathe
	Make	HMT
	Model	NL-26
	Feed Range	0.04 to 1.12 mm/rev
	Spindle speed	40 to 2040 RPM
Measuring Instrument:		
	Type	Tool Makers Microscope
	Make	Carl Zeiss, Germany
	Accuracy	0.001 mm

5.3 Correction due to spring back

The chip breaker operates by reducing the radius of curvature of the chip and directing it in such a manner that it strikes the surface of the work and breaks. On fracture elastic strains in the chip are released and the radius of curvature of the chip increases due to elastic spring back (Fig. 5.6). The measured radius R_{chip}^* (Table 5.2) is therefore higher than the true radius of curvature R_{chip} imposed by the chip breaker. R_{chip} can be calculated from R_{chip}^* by incorporating correction for spring back as suggested by Gardiner [101]. This may be written as,

$$\frac{R_{chip}}{R_{chip}^*} = 4 \left(\frac{R_{chip} \sigma_0}{E t_{chip}} \right)^3 - 3 \left(\frac{R_{chip} \sigma_0}{E t_{chip}} \right) + 1 \quad (5.1)$$

where, σ_0 is the yield stress and E is the modulus of elasticity of work piece.

After applying the correction due to spring back effect to the radius of curvature of chip, there was excellent match between the experimental and the theoretical values obtained from analysis of Dewhurst's field (Fig. 5.13). A reduction of 10 to 20 % in R_{chip} was noticed with spring back correction. Correct estimation of chip radius of curvature yielded the value of breaking strain ϵ_b more precisely using equation (3.35).

Fig. 5.1: Turning operation on HMT Lathe

Fig. 5.2: Grinding of tools rake face on CNC surface grinder

Fig. 5.3: Welding of chip breaker on tool rake face

Fig. 5.4: Measurement of chip features

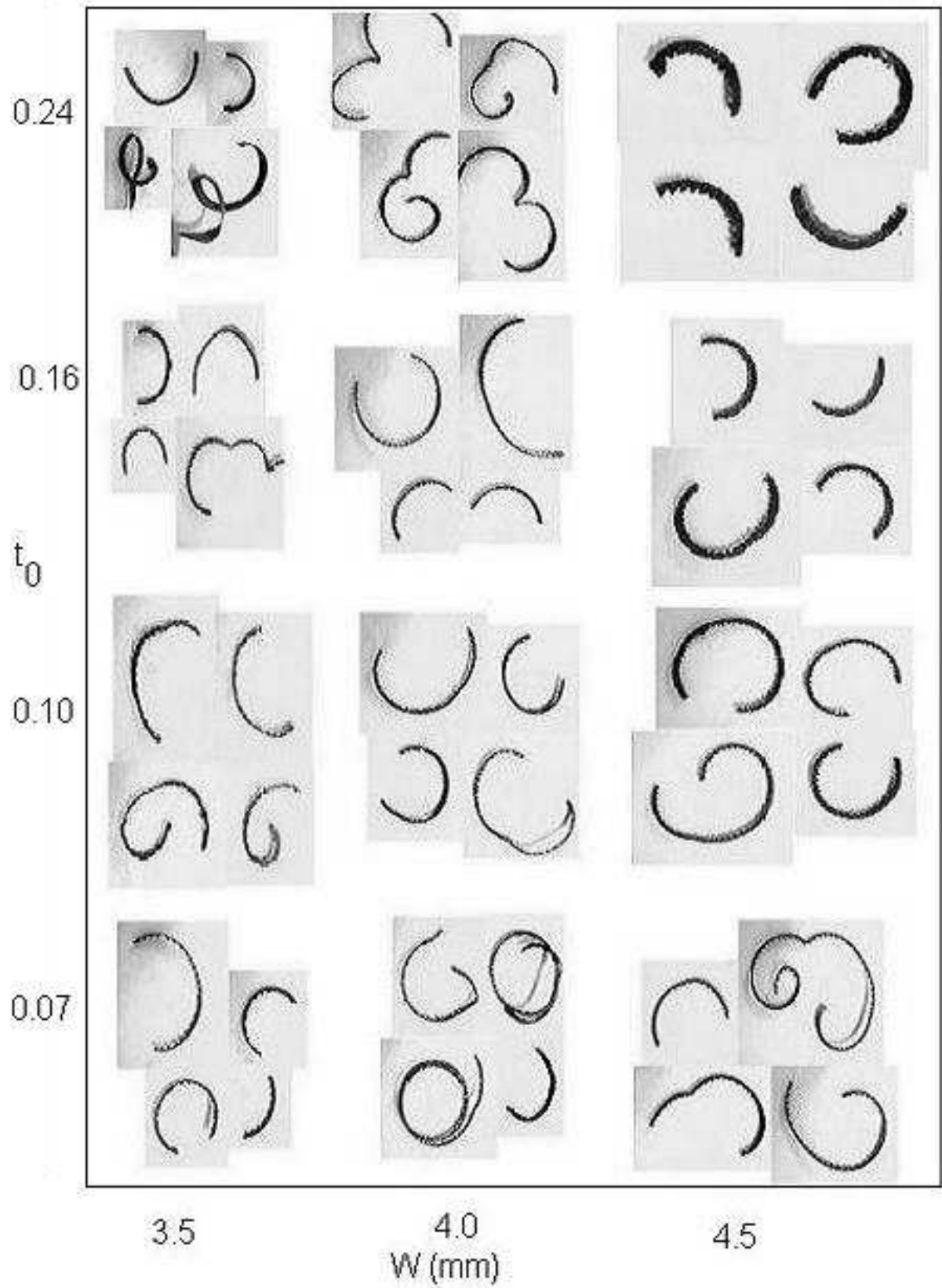


Fig. 5.5: Chip forms produced in machining operations

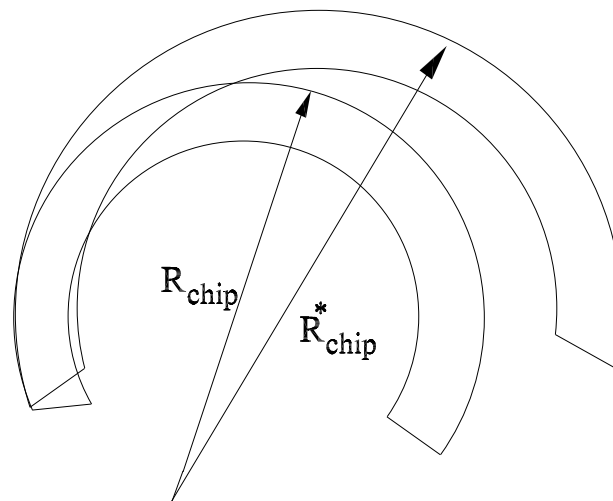


Fig. 5.6: Chip radius of curvature with and without spring back

There was an increase of 15 to 30 % in breaking strain on incorporation of spring back correction which was quite significant (See Fig. 5.11).

5.4 Correction due to shifting of neutral axis

During bending of curved beams the neutral axis of the beam gets shifted from the centroid towards the centre of curvature requiring correction of the breaking strain value calculated from (equation (C.10)). In Appendix C, the modified expression for calculation of breaking strain considering shifting of the neutral axis is discussed. Representative values of breaking strain calculated with and without this correction is also provided in Table 5.3. Referring to this table, it may be seen that the effect of the shift of the neutral axis on breaking strain is insignificant. Hence, this correction was not considered for calculation of breaking strain.

5.5 Results and discussion

Experimentally determined machining parameters are compared with those obtained from slip-line field analysis in the following figures. The experimental data in these figures were collected from representative chip samples as discussed earlier.

The variation of cutting ratio ζ with chip breaker position is illustrated in Figs. 5.7

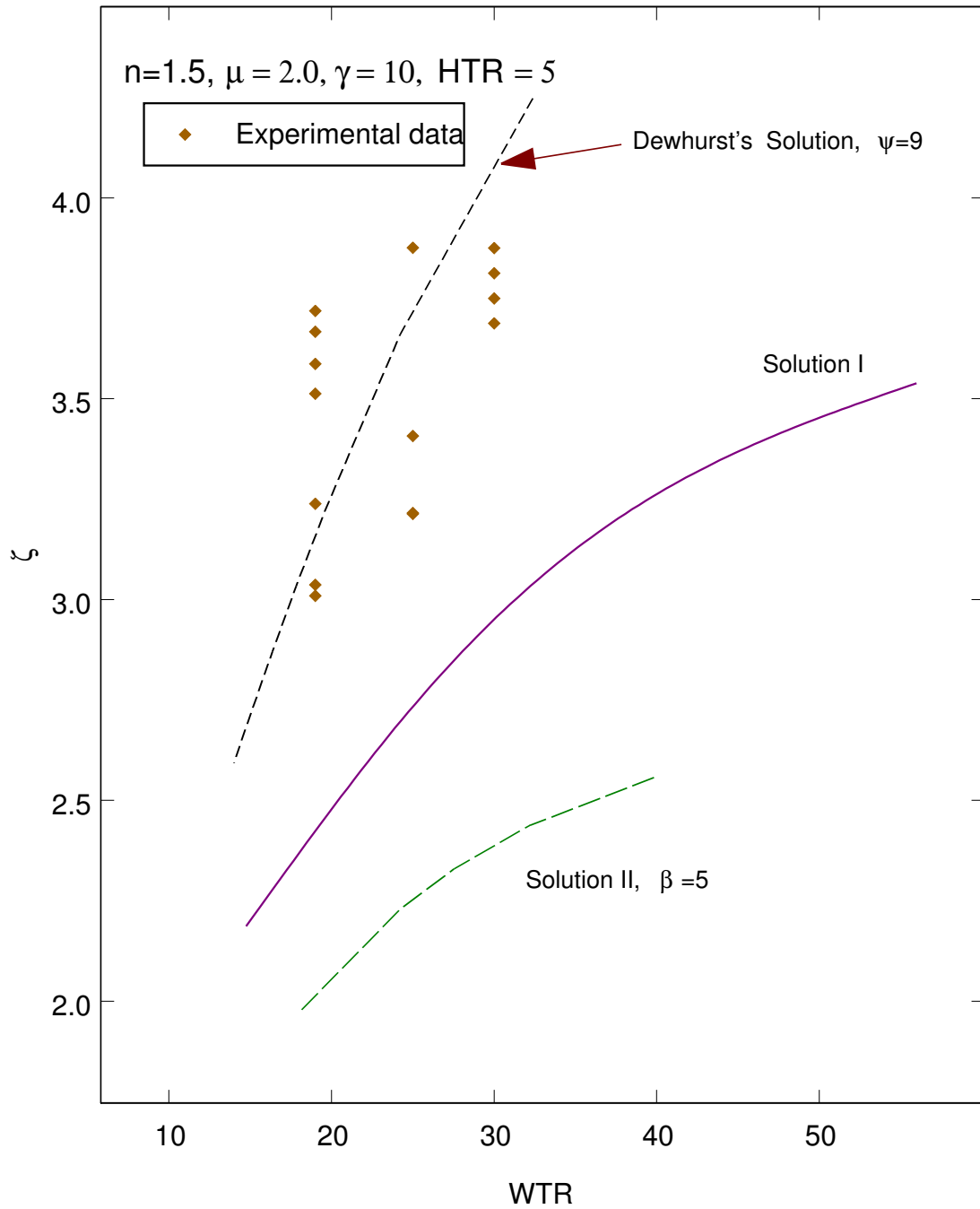


Fig. 5.7: Variation of cutting ratio ζ with chip-breaker position for higher feed

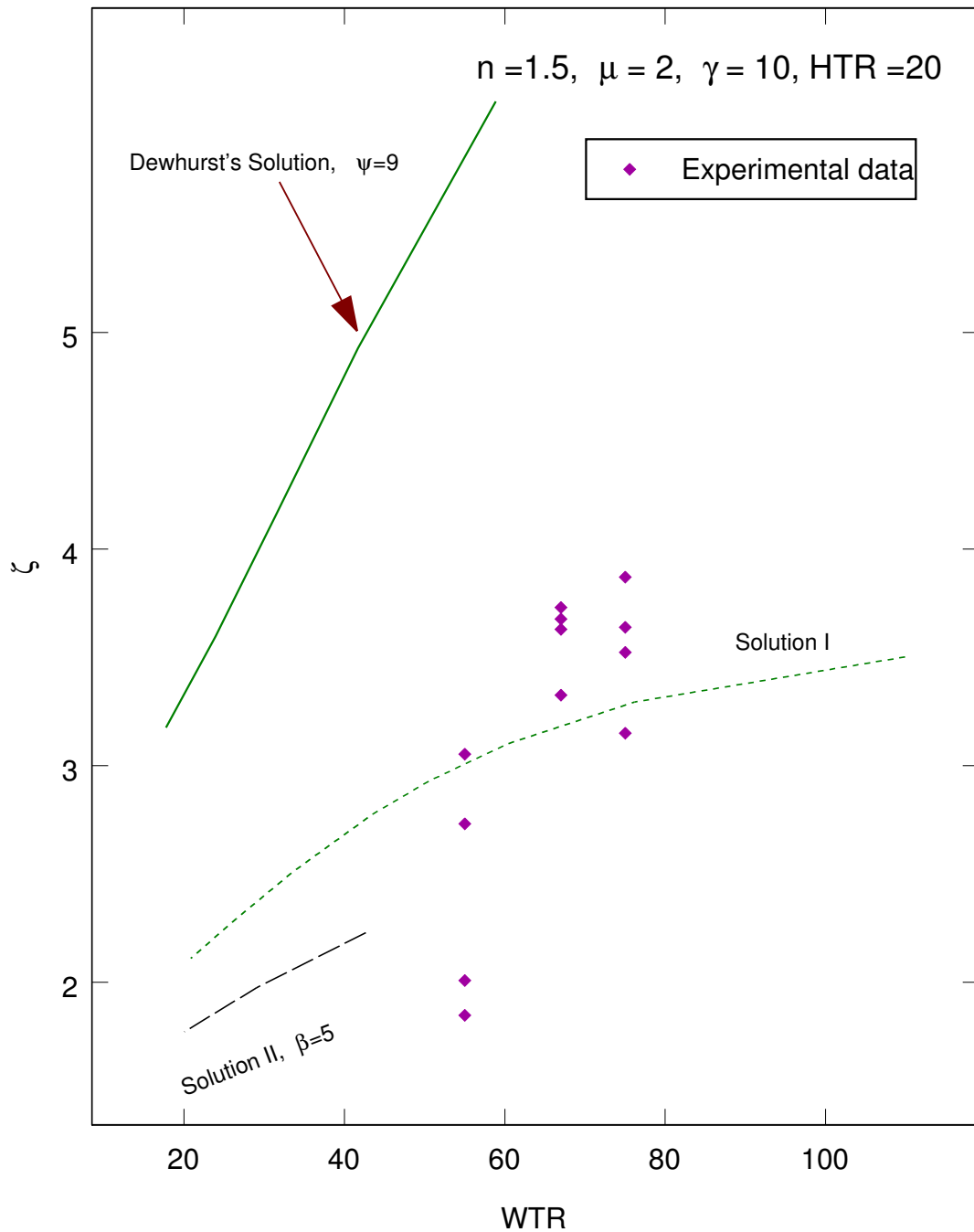


Fig. 5.8: Variation of cutting ratio ζ with chip-breaker position for lower feed

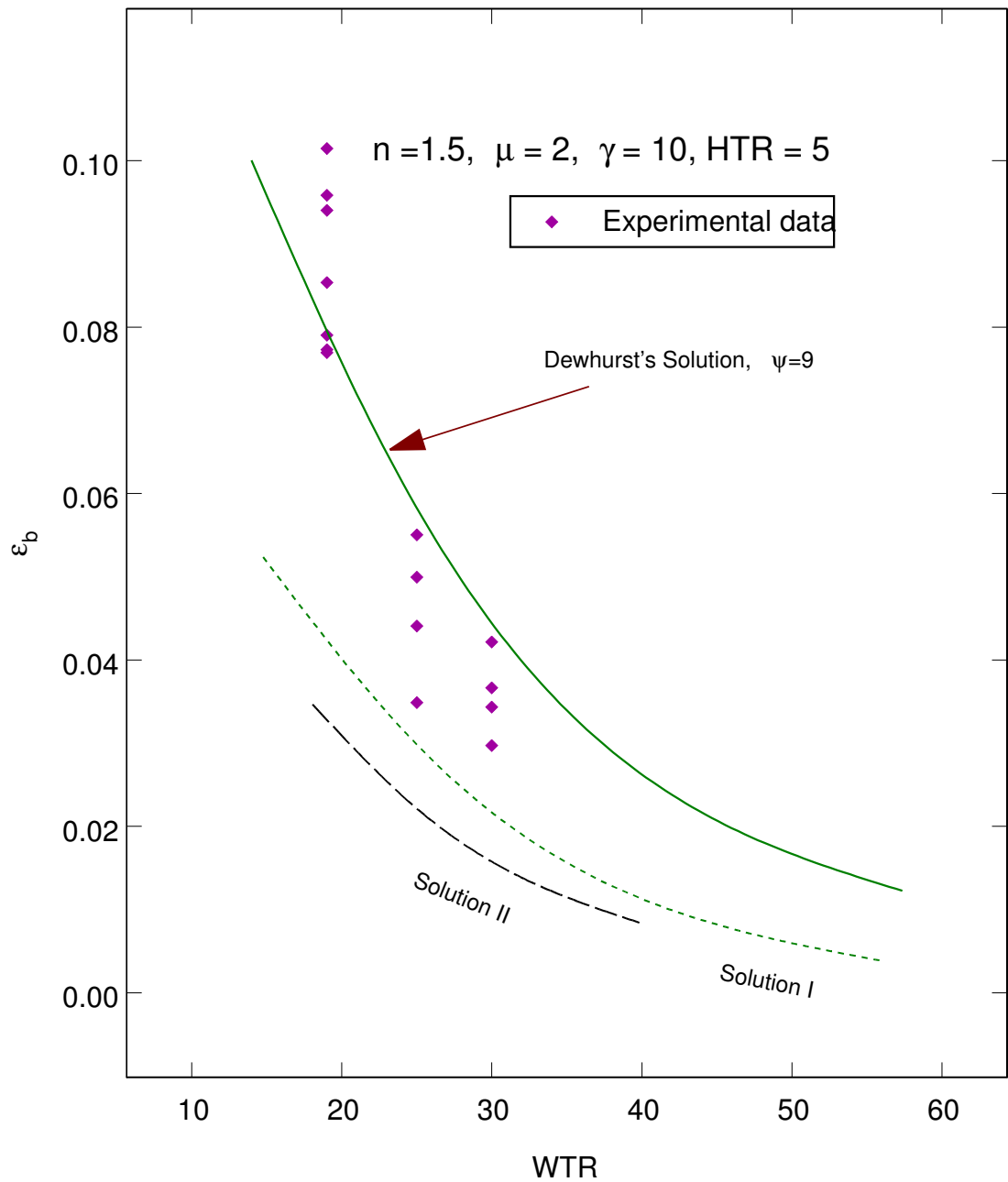


Fig. 5.9: Variation of breaking strain ϵ_b with chip-breaker position for higher feed

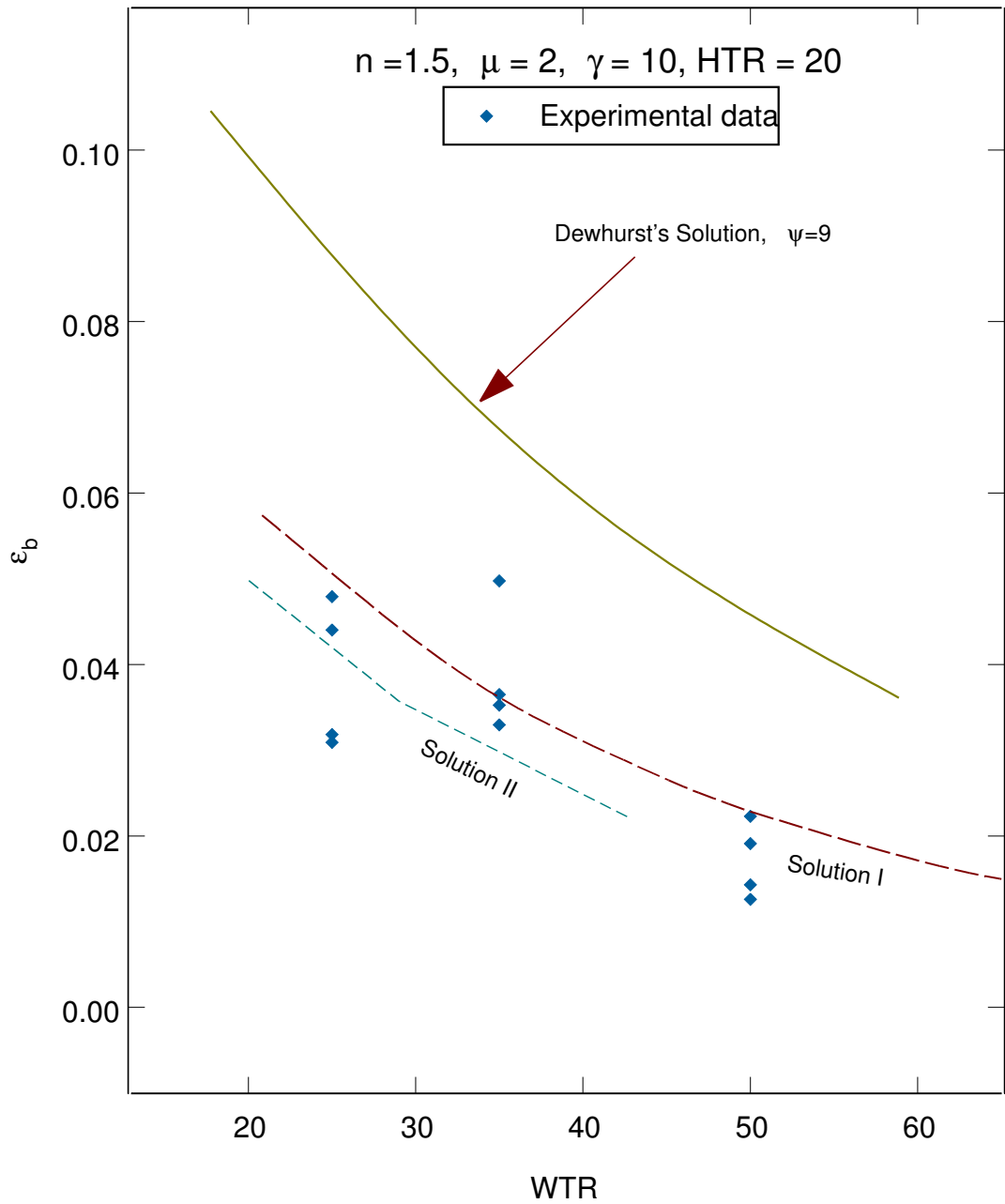
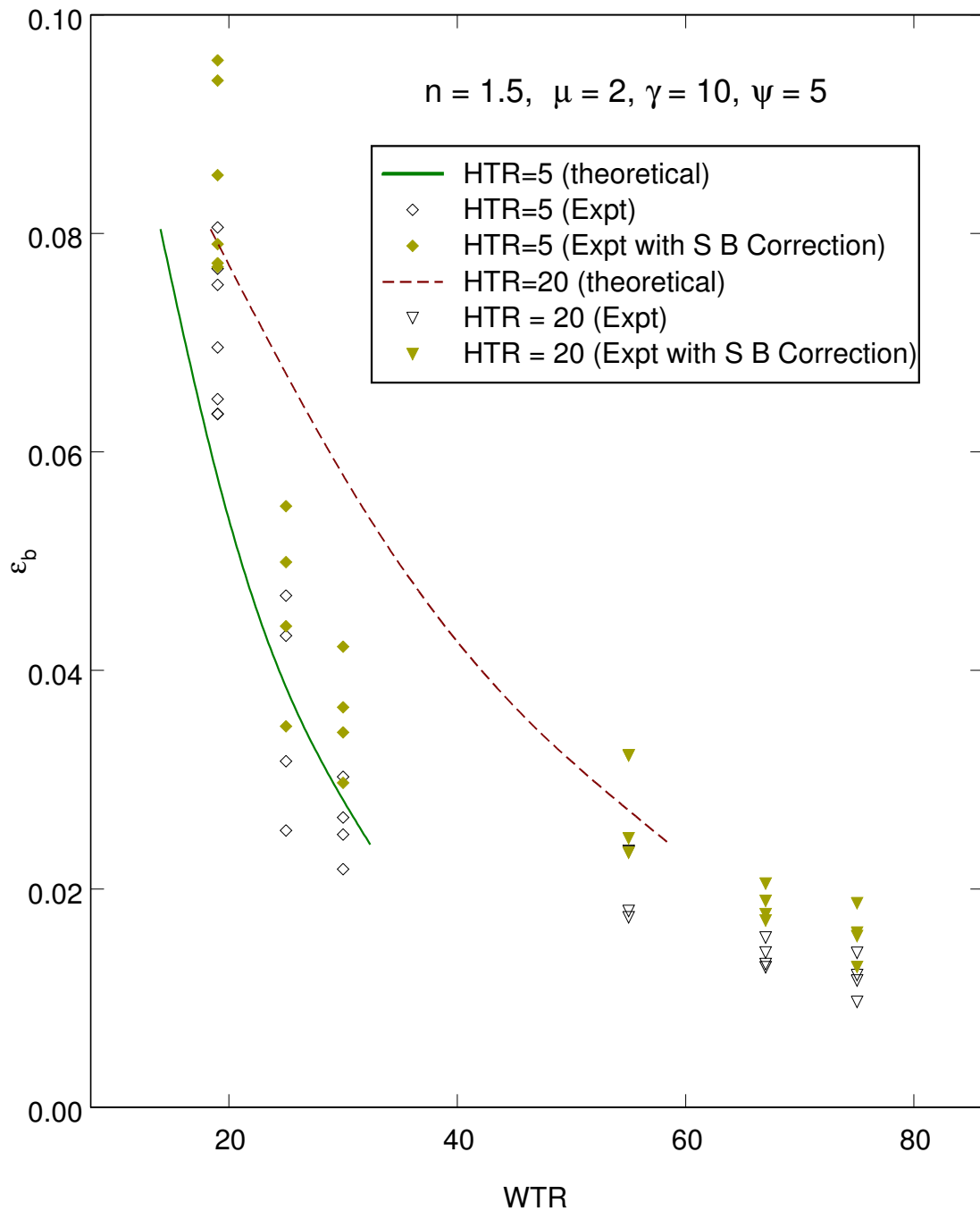


Fig. 5.10: Variation of breaking strain ϵ_b with chip-breaker position for lower feed



◆
 Fig. 5.11: Variation of breaking strain ϵ_b with chip-breaker position with and without spring back (SB) correction

and 5.8 for HTR values equal to 5 and 20 respectively along with the present experimental results. The figures indicate that the experimentally determined values of cutting ratio for higher feeds (HTR=5) have better agreement with the theoretical results computed from Dewhurst's field (Fig. 5.7), where as at lower feeds (HTR=20) the experimental values show better match with those obtained from Kudo's first solution (Fig. 5.8). Similar trend is also noticed when variation of breaking strain ϵ_b with WTR is considered (Fig. 5.9 and Fig. 5.10). It may also be seen that there is better agreement between theory and experiment when effect of spring back is taken into account (Fig. 5.11).

The variation of chip radius of curvature (R_{chip}/t_0) with WTR is shown in Figs. 5.12 and 5.13 where a comparison has been made between theoretically estimated values with those obtained from the present experimental investigation. The results again show better match when the correction due to spring back effect is incorporated. An excellent agreement between theory and experiment is also observed when variation of breaking strain ϵ_b with chip curvature (R_{chip}/t_0) is analysed as may be seen from Fig. 5.14. Most of the experimental points lie within the solution range defined by Dewhurst's field and Kudo's second field with Dewhurst's solution forming the upper limit and Kudo's solution the lower limit.

A comparison between theoretically estimated and experimentally observed chip breakability parameters (Table 5.4) has been made in Figs. 5.15 and 5.16, where these have been plotted as functions of WTR and feed respectively. The theoretical results in the above figures have been computed from Dewhurst's field (Fig. 4.2) with $\psi=5$ degrees. Thus the results shown in the above figures represent those corresponding to the mean of the solution range between $\psi=0$ when Dewhurst's field reduces to that suggested by Kudo and $\psi=9$ degrees when friction angle at E becomes negative and the field is no more applicable.

Chips in Fig. 5.15 were assumed to be effectively broken when $R_{chip} = 6\text{mm}$ and when bending strains in the chips were equal to those suggested by Takayama *et al.* [52] and Jawahir [53]. The chips in the present experimental investigation were considered to be under-broken as $R_{chip} > 6\text{mm}$. Referring to Figs. 5.15 and 5.16 it may be seen that there is excellent agreement between theory and experiment indicating that chip breakability criteria based on t_0 , t_{chip} and R_{chip} predict effectiveness of chip breaking

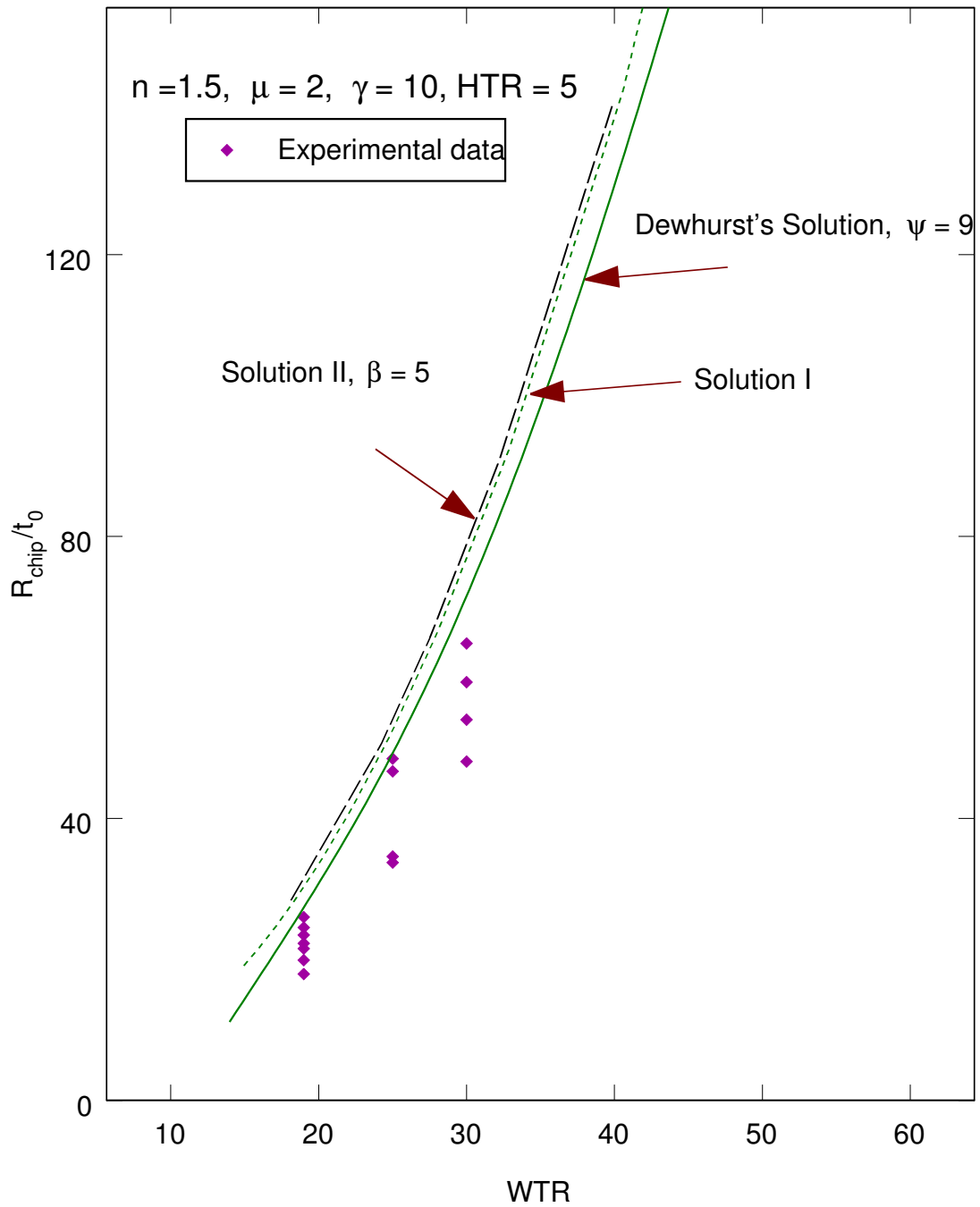


Fig. 5.12: Variation of normalized chip radius of curvature with chip-breaker position

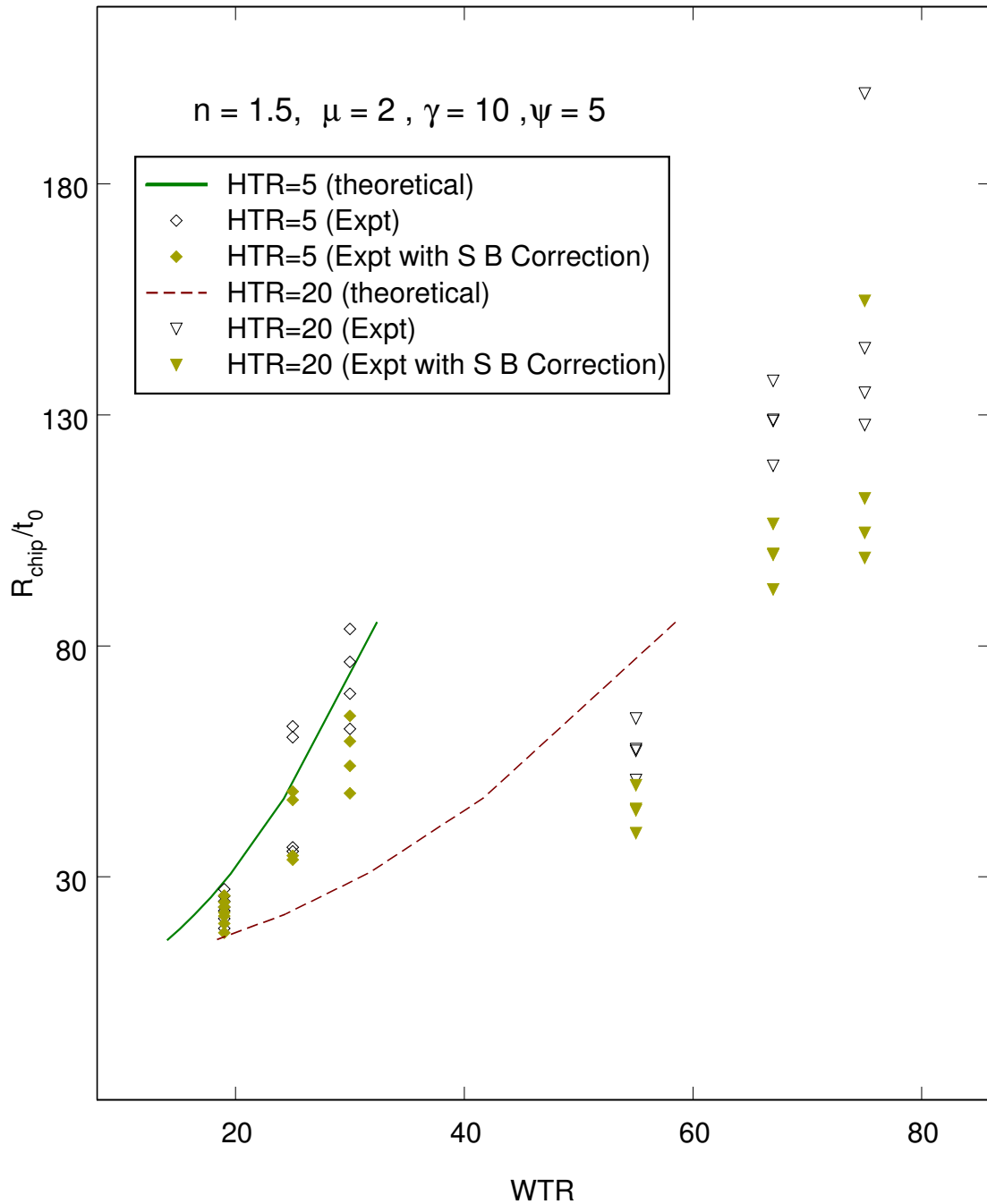


Fig. 5.13: Variation of chip radius of curvature with chip-breaker position with and without spring back (SB) correction

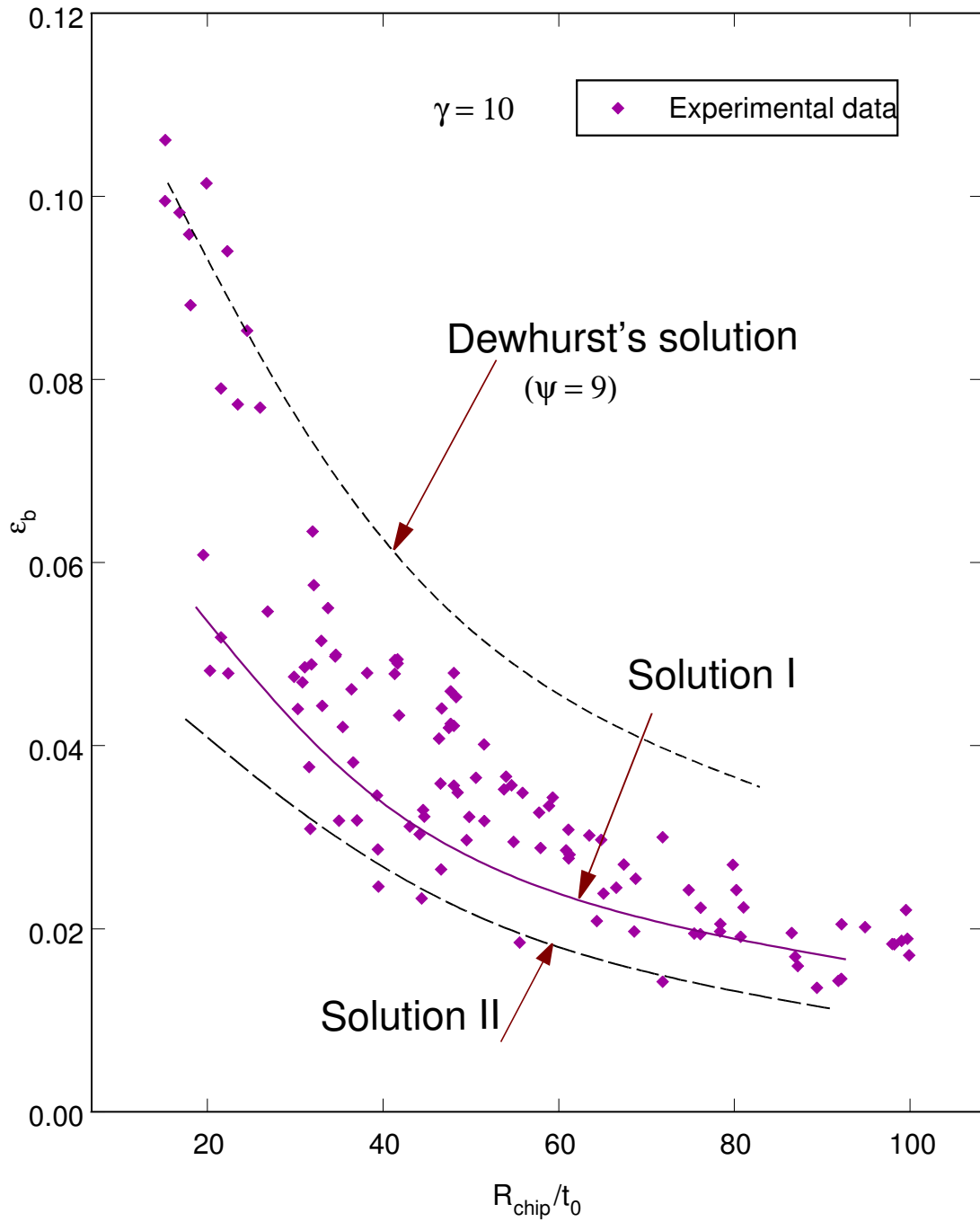


Fig. 5.14: Variation of breaking strain ϵ_b with normalized chip radius of curvature, considering all three fields

more accurately than any other criterion.

5.6 Chip breaker design

Fang *et al.* [36] have suggested classification of chips using fuzzy logic technique. These authors reported that in case of orthogonal cutting, spiral and circular chips, with their radius of curvature ‘about’ 6 mm (Fig. 5.5) can be considered as ‘excellent’ and ‘good’ respectively from chip breakability point of view. Hence, the chips with fractional turn and radius of curvature of ‘about’ 6 mm are termed as ‘effectively broken chips’. The chips with radius of curvature ‘much less than’ or ‘much greater than’ 6 mm were considered as ‘over-broken’ or ‘under- broken’ chips, respectively.

In the present case, it was observed that ‘effective breaking’ was obtained while machining with feed values of 0.12 and 0.24 mm/rev. The normalised radii of curvature, R_{chip}/t_0 for these feed values were about 25 ($=6/0.24$) and 50 ($=6/0.12$), respectively. Fig. 5.17 shows the variation of breaking strain and normalised radius of chip curvature with chip breaker positions for HTR equal to 5 and 10. These values were obtained from Dewhurst’s field with field angle $\psi = 5$. It may be seen that for R_{chip}/t_0 equal to 25 (HTR=5), the corresponding WTR is 18 and the breaking strain is found to be 0.065. Similarly, for R_{chip}/t_0 equal to 50 (HTR=10), WTR is equal to 33 and the corresponding breaking strain is 0.039, which are quite close to those suggested by Takayama *et al.* [52] and Jawahir [53]. The range of chip breaker position for effective breaking can be calculated as 3.96 ($=33*0.12$) and 4.32 ($=18*0.24$) for the feed values 0.12 and 0.24 mm/rev respectively. This approach of chip breaker design, with the help of Fig. 5.17, is an easier and quicker one to find the position of chip breaker for any given feed range and to estimate the value of the breaking strains.

5.7 Conclusions

Orthogonal machining tests were carried out on mild steel tubes using HSS tools with 10 % cobalt. Chip breaking was accomplished using a step-type chip breaker. Chip thickness and chip curl radius were measured using an image analyser. Breaking strain

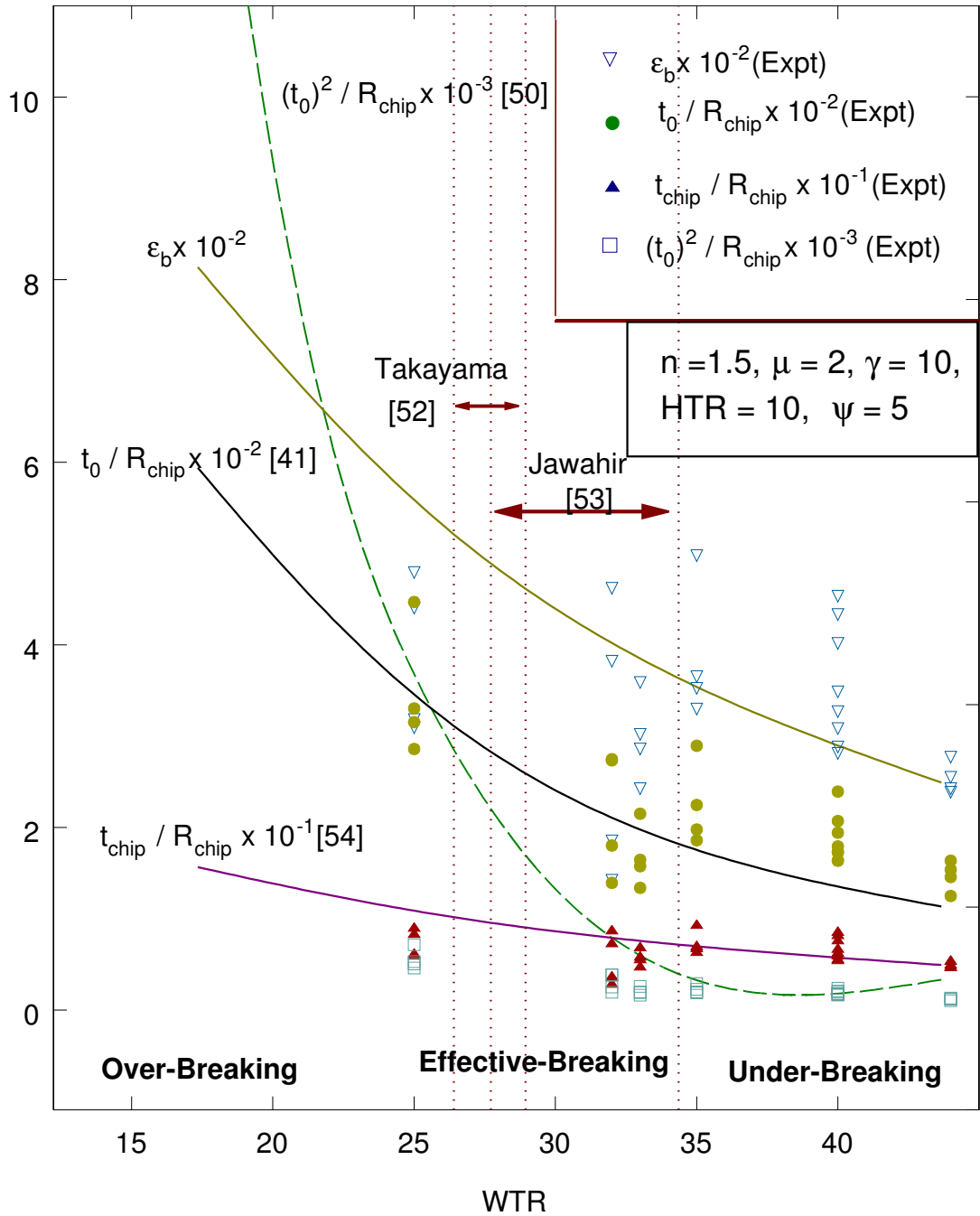


Fig. 5.15: Variation of chip breakability parameters with chip breaker position

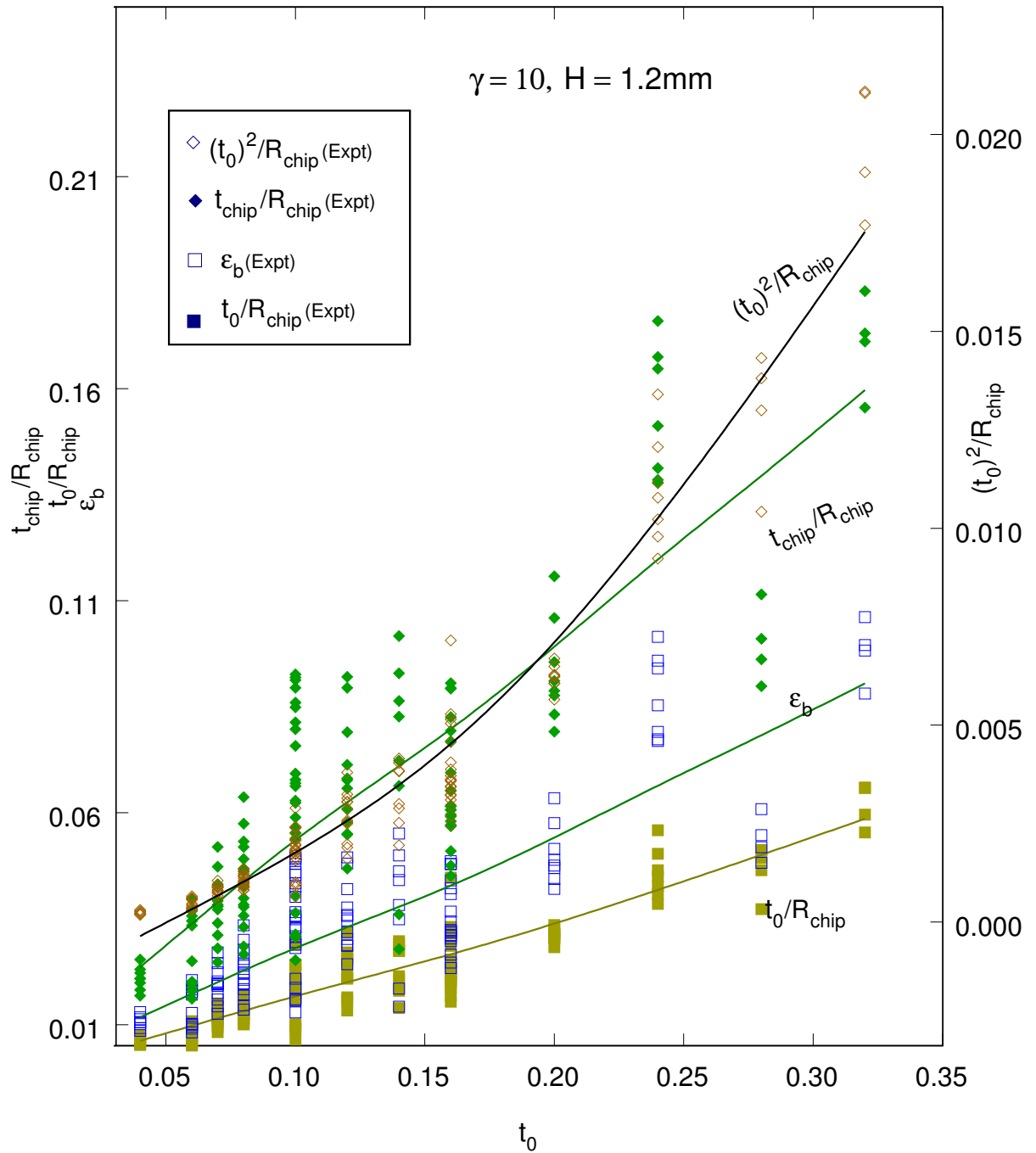


Fig. 5.16: Variation of chip breakability parameters with feed

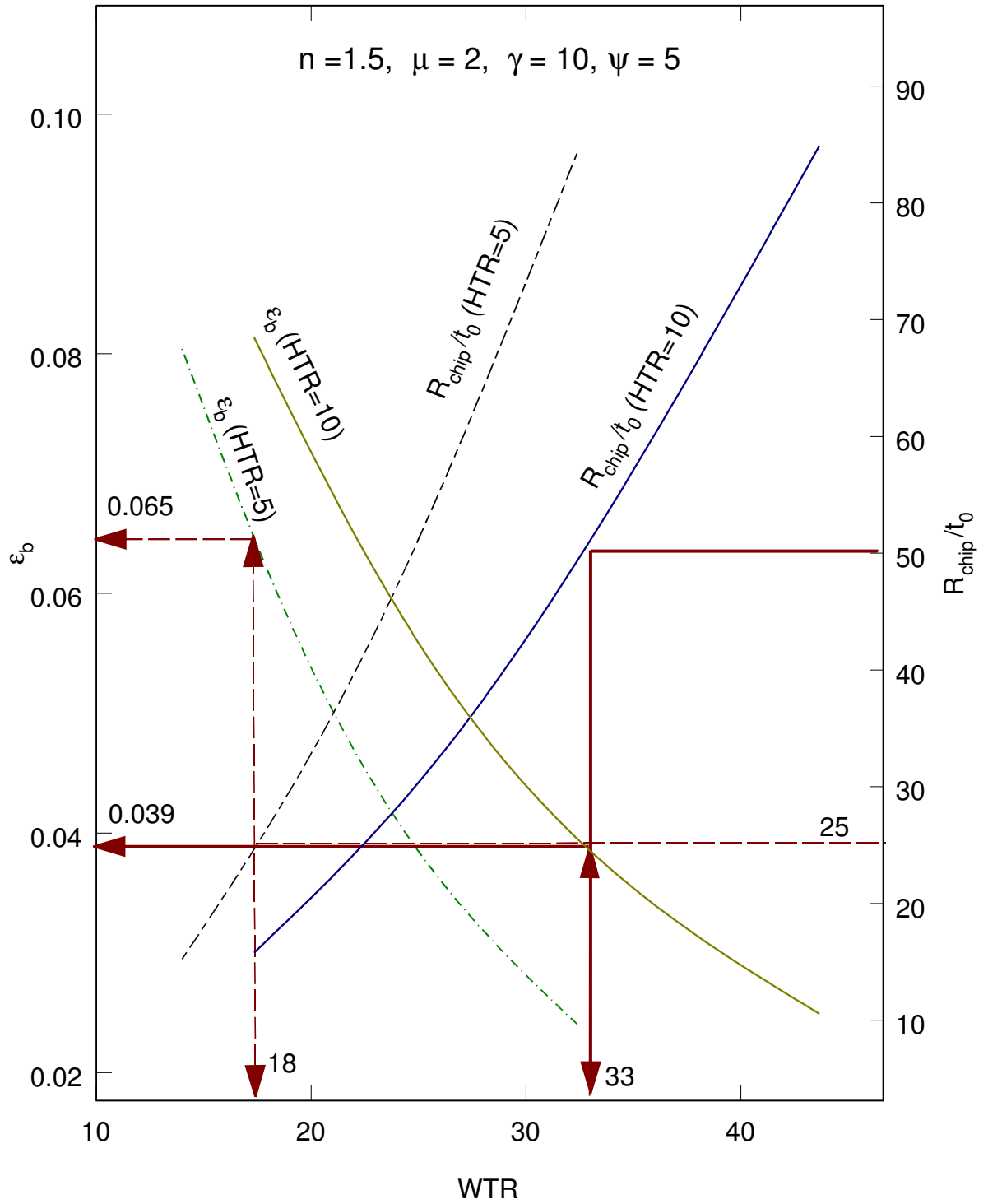


Fig. 5.17: Variation of breaking strain ϵ_b and radius of curvature with chip-breaker position

was calculated from a simplified formula, $\epsilon_b = t_{chip}/(2R_{chip})$ and this was correlated with the degree of chip breaking. It is seen that experimentally determined values of cutting ratio and R_{chip}/t_0 have better agreements with theoretical values computed from Dewhurst's field at higher feeds, whereas, at lower feeds experimental values show better match with those obtained from Kudo's first solution. There is better match between theory and experiments when spring back correction is taken into account. The variation of ϵ_b with R_{chip}/t_0 determined experimentally lie within the region defined by Dewhurst's field and Kudo's second solution. Chip breakability criteria based on ϵ_b , t_{chip} , t_0 and R_{chip} shows similar trend with WTR and can be used to assess chip breaking.

Tab. 5.2: Experimental observations

Pkt. No.	γ deg	V_c m/min	t_0 mm/rev	d mm	W mm	H mm	t_{chip} mm	l_{chip} mm	R_{chip}^* mm	R_{chip} mm	$\frac{R_{chip}^*}{t_0}$	$\frac{R_{chip}}{t_0}$	ζ
1.06	10	40	0.14	1.90	4.48	1.26	0.37	14.10	6.610	5.123	47.214	36.591	2.64
1.06	10	40	0.14	1.90	4.48	1.26	0.28	19.21	10.035	7.777	71.679	55.551	2.00
1.06	10	40	0.14	1.90	4.48	1.26	0.28	25.48	12.980	10.060	92.714	71.854	2.00
1.06	10	40	0.14	1.90	4.48	1.26	0.44	15.00	6.575	5.096	46.964	36.397	3.14
1.07	10	40	0.16	1.90	4.48	1.28	0.50	21.55	10.640	8.246	66.500	51.538	3.13
1.07	10	40	0.16	1.90	4.48	1.28	0.41	17.40	8.885	6.886	55.531	43.037	2.56
1.07	10	40	0.16	1.90	4.48	1.28	0.41	18.40	9.120	7.068	57.000	44.175	2.56
1.07	10	40	0.16	1.90	4.48	1.28	0.38	18.80	9.625	7.459	60.156	46.621	2.38
1.08	10	40	0.20	1.90	4.60	1.20	0.74	14.40	6.730	6.394	33.650	31.968	3.70
1.08	10	40	0.20	1.90	4.60	1.20	0.63	17.05	8.510	6.595	42.550	32.976	3.15
1.08	10	40	0.20	1.90	4.60	1.20	0.56	19.18	9.135	7.080	45.675	35.398	2.80
1.08	10	40	0.20	1.90	4.60	1.20	0.68	14.93	6.760	6.422	33.800	32.110	3.40
1.09	10	40	0.24	1.90	4.56	1.20	0.86	13.74	6.565	6.237	27.354	25.986	3.58
1.09	10	40	0.24	1.90	4.56	1.20	0.84	11.17	5.025	4.774	20.938	19.891	3.50
1.09	10	40	0.24	1.90	4.56	1.20	0.72	9.09	4.525	4.299	18.854	17.911	3.00
1.09	10	40	0.24	1.90	4.56	1.20	0.80	9.09	4.525	4.299	18.854	17.911	3.33
2.16	10	50	0.16	1.90	4.48	1.28	0.59	18.86	8.530	6.611	53.313	41.317	3.69
2.16	10	50	0.16	1.90	4.48	1.28	0.45	18.72	6.415	4.972	40.094	31.073	2.81
2.16	10	50	0.16	1.90	4.48	1.28	0.57	20.74	9.575	7.421	59.844	46.379	3.56
2.16	10	50	0.16	1.90	4.48	1.28	0.45	22.14	10.220	7.921	63.875	49.503	2.81

(continued on next page)

Tab. 5.2: Experimental observations (Contd.)

Pkt. No.	γ deg	V_c m/min	t_0 mm/rev	d mm	W mm	H mm	t_{chip} mm	l_{chip} mm	R_{chip}^* mm	R_{chip} mm	$\frac{R_{chip}^*}{t_0}$	$\frac{R_{chip}}{t_0}$	ζ
2.17	10	50	0.20	1.90	4.60	1.20	0.55	15.16	6.960	6.612	34.800	33.060	2.75
2.17	10	50	0.20	1.90	4.60	1.20	0.53	15.48	7.710	5.975	38.550	29.876	2.65
2.17	10	50	0.20	1.90	4.60	1.20	0.54	15.13	7.950	6.161	39.750	30.806	2.70
2.17	10	50	0.20	1.90	4.60	1.20	0.58	14.24	6.705	6.370	33.525	31.849	2.90
2.18	10	50	0.24	1.90	4.56	1.20	0.89	13.27	6.195	5.885	25.813	24.522	3.71
2.18	10	50	0.24	1.90	4.56	1.20	0.78	12.74	5.930	5.634	24.708	23.473	3.25
2.18	10	50	0.24	1.90	4.56	1.20	0.88	12.51	5.625	5.344	23.438	22.266	3.67
2.18	10	50	0.24	1.90	4.56	1.20	0.73	10.81	5.440	5.168	22.667	21.533	3.04
2.19	10	50	0.28	1.90	4.48	1.12	0.61	14.14	5.760	5.472	20.571	19.543	2.18
2.19	10	50	0.28	1.90	4.48	1.12	0.51	16.68	5.975	5.676	21.339	20.272	1.82
2.19	10	50	0.28	1.90	4.48	1.12	0.58	13.68	6.350	6.033	22.679	21.545	2.07
2.19	10	50	0.28	1.90	4.48	1.12	0.76	16.13	7.920	7.524	28.286	26.871	2.71
2.20	10	50	0.32	1.90	4.48	1.28	0.90	12.74	6.090	5.786	19.031	18.080	2.81
2.20	10	50	0.32	1.90	4.48	1.28	0.92	11.97	5.660	5.377	17.688	16.803	2.88
2.20	10	50	0.32	1.90	4.48	1.28	0.84	11.29	5.110	4.855	15.969	15.170	2.63
2.20	10	50	0.32	1.90	4.48	1.28	0.89	11.06	5.120	4.864	16.000	15.200	2.78
3.23	10	40	0.10	1.90	3.50	1.00	0.28	22.35	5.750	4.456	57.500	44.563	2.80
3.23	10	40	0.10	1.90	3.50	1.00	0.36	14.33	6.940	5.379	69.400	53.785	3.60
3.23	10	40	0.10	1.90	3.50	1.00	0.32	15.79	4.460	3.457	44.600	34.565	3.20
3.23	10	40	0.10	1.90	3.50	1.00	0.35	13.65	6.525	5.057	65.250	50.569	3.50

(continued on next page)

Tab. 5.2: Experimental observations (Contd.)

Pkt. No.	γ deg	V_c m/min	t_0 mm/rev	d mm	W mm	H mm	t_{chip} mm	l_{chip} mm	R_{chip}^* mm	R_{chip} mm	$\frac{R_{chip}^*}{t_0}$	$\frac{R_{chip}}{t_0}$	ζ
3.24	10	40	0.07	1.90	3.50	0.70	0.21	22.35	10.970	8.502	156.714	121.454	3.00
3.24	10	40	0.07	1.90	3.50	0.70	0.23	14.33	6.880	5.332	98.286	76.171	3.29
3.24	10	40	0.07	1.90	3.50	0.70	0.21	15.79	7.290	5.650	104.143	80.711	3.00
3.24	10	40	0.07	1.90	3.50	0.70	0.18	20.57	8.295	6.429	118.500	91.838	2.57
3.25	10	40	0.08	1.90	3.52	0.72	0.30	10.54	8.280	6.417	103.500	80.213	3.75
3.25	10	40	0.08	1.90	3.52	0.72	0.24	14.08	6.720	5.208	84.000	65.100	3.00
3.25	10	40	0.08	1.90	3.52	0.72	0.27	15.36	7.100	5.503	88.750	68.781	3.38
3.25	10	40	0.08	1.90	3.52	0.72	0.26	16.01	6.310	4.890	78.875	61.128	3.25
3.26	10	40	0.10	1.90	3.50	0.70	0.31	14.56	7.080	5.487	70.800	54.870	3.10
3.26	10	40	0.10	1.90	3.50	0.70	0.38	14.32	5.335	4.135	53.350	41.346	3.80
3.26	10	40	0.10	1.90	3.50	0.70	0.41	13.95	6.155	4.770	61.550	47.701	4.10
3.26	10	40	0.10	1.90	3.50	0.70	0.26	16.39	8.300	6.433	83.000	64.325	2.60
4.31	10	50	0.10	1.90	3.50	0.70	0.38	9.72	5.375	4.166	53.750	41.656	3.80
4.31	10	50	0.10	1.90	3.50	0.70	0.38	10.43	5.020	4.769	50.200	47.690	3.80
4.31	10	50	0.10	1.90	3.50	0.70	0.37	15.10	7.050	5.464	70.500	54.638	3.70
4.31	10	50	0.10	1.90	3.50	0.70	0.43	11.20	5.060	4.807	50.600	48.070	4.30
4.32	10	50	0.12	1.90	3.48	0.72	0.46	14.57	6.450	4.999	53.750	41.656	3.83
4.32	10	50	0.12	1.90	3.48	0.72	0.39	14.90	7.440	5.766	62.000	48.050	3.25
4.32	10	50	0.12	1.90	3.48	0.72	0.45	14.82	7.355	5.700	61.292	47.501	3.75
4.32	10	50	0.12	1.90	3.48	0.72	0.41	13.07	5.915	4.584	49.292	38.201	3.42

(continued on next page)

Tab. 5.2: Experimental observations (Contd.)

Pkt. No.	γ deg	V_c m/min	t_0 mm/rev	d mm	W mm	H mm	t_{chip} mm	l_{chip} mm	R_{chip}^* mm	R_{chip} mm	$\frac{R_{chip}^*}{t_0}$	$\frac{R_{chip}}{t_0}$	ζ
4.33	10	50	0.14	1.90	3.50	0.70	0.45	18.05	8.760	6.789	62.571	48.493	3.21
4.33	10	50	0.14	1.90	3.50	0.70	0.54	15.78	8.430	6.533	60.214	46.666	3.86
4.33	10	50	0.14	1.90	3.50	0.70	0.45	11.44	5.100	4.845	36.429	34.607	3.21
4.33	10	50	0.14	1.90	3.50	0.70	0.48	10.43	4.970	4.722	35.500	33.725	3.43
5.35	10	40	0.06	1.90	4.02	1.02	0.17	22.13	10.990	8.517	183.167	141.954	2.83
5.35	10	40	0.06	1.90	4.02	1.02	0.24	24.32	12.400	9.610	206.667	160.167	4.00
5.35	10	40	0.06	1.90	4.02	1.02	0.21	15.90	7.605	5.894	126.750	98.231	3.50
5.35	10	40	0.06	1.90	4.02	1.02	0.14	22.16	11.410	7.844	190.167	130.740	2.33
5.36	10	40	0.08	1.90	4.00	1.04	0.19	17.85	9.230	7.153	115.375	89.416	2.38
5.36	10	40	0.08	1.90	4.00	1.04	0.25	16.10	8.095	6.274	101.188	78.420	3.13
5.36	10	40	0.08	1.90	4.00	1.04	0.34	18.11	10.275	7.963	128.438	99.539	4.25
5.36	10	40	0.08	1.90	4.00	1.04	0.28	20.95	10.115	7.839	126.438	97.989	3.50
5.38	10	40	0.12	1.90	3.96	1.08	0.42	18.24	11.585	8.978	96.542	74.820	3.50
5.38	10	40	0.12	1.90	3.96	1.08	0.44	18.89	9.830	7.618	81.917	63.485	3.67
5.38	10	40	0.12	1.90	3.96	1.08	0.40	17.77	9.420	7.301	78.500	60.838	3.33
5.38	10	40	0.12	1.90	3.96	1.08	0.38	15.95	7.205	5.584	60.042	46.532	3.17
6.39	10	40	0.04	1.90	4.00	1.20	0.11	14.70	6.785	5.258	169.625	131.459	2.75
6.39	10	40	0.04	1.90	4.00	1.20	0.13	9.96	7.570	5.867	189.250	146.669	3.25
6.39	10	40	0.04	1.90	4.00	1.20	0.14	18.37	7.845	6.080	196.125	151.997	3.50
6.39	10	40	0.04	1.90	4.00	1.20	0.15	18.99	7.635	5.917	190.875	147.928	3.75

(continued on next page)

Tab. 5.2: Experimental observations (Contd.)

Pkt. No.	γ deg	V_c m/min	t_0 mm/rev	d mm	W mm	H mm	t_{chip} mm	l_{chip} mm	R_{chip}^* mm	R_{chip} mm	$\frac{R_{chip}^*}{t_0}$	$\frac{R_{chip}}{t_0}$	ζ
6.40	10	40	0.06	1.90	4.02	1.20	0.22	14.80	7.140	5.534	119.000	92.225	3.67
6.40	10	40	0.06	1.90	4.02	1.20	0.22	15.30	7.720	5.983	128.667	99.717	3.67
6.40	10	40	0.06	1.90	4.02	1.20	0.22	15.61	8.240	6.386	137.333	106.433	3.67
6.40	10	40	0.06	1.90	4.02	1.20	0.20	15.73	7.734	5.994	128.900	99.898	3.33
6.41	10	40	0.07	1.90	3.99	1.19	0.25	16.82	9.495	7.359	135.643	105.123	3.57
6.41	10	40	0.07	1.90	3.99	1.19	0.23	16.25	7.815	6.057	111.643	86.523	3.29
6.41	10	40	0.07	1.90	3.99	1.19	0.19	14.65	7.880	6.107	112.571	87.243	2.71
6.41	10	40	0.07	1.90	3.99	1.19	0.21	14.62	7.080	5.487	101.143	78.386	3.00
6.42	10	40	0.08	1.90	4.00	1.20	0.33	16.53	7.415	5.747	92.688	71.833	4.13
6.42	10	40	0.08	1.90	4.00	1.20	0.28	13.70	6.960	5.394	87.000	67.425	3.50
6.42	10	40	0.08	1.90	4.00	1.20	0.23	16.40	7.860	6.092	98.250	76.144	2.88
6.42	10	40	0.08	1.90	4.00	1.20	0.30	12.94	6.080	4.712	76.000	58.900	3.75
6.43	10	40	0.10	1.90	4.00	1.20	0.36	14.33	7.455	5.778	74.550	57.776	3.60
6.43	10	40	0.10	1.90	4.00	1.20	0.41	13.55	6.235	4.832	62.350	48.321	4.10
6.43	10	40	0.10	1.90	4.00	1.20	0.37	14.76	7.210	5.588	72.100	55.878	3.70
6.43	10	40	0.10	1.90	4.00	1.20	0.39	14.96	6.645	5.150	66.450	51.499	3.90
7.44	10	50	0.04	1.90	4.00	1.20	0.14	20.08	11.220	7.714	280.500	192.844	3.50
7.44	10	50	0.04	1.90	4.00	1.20	0.14	14.54	9.100	7.053	227.500	176.313	3.50
7.44	10	50	0.04	1.90	4.00	1.20	0.15	20.48	9.300	7.208	232.500	180.188	3.75
7.44	10	50	0.04	1.90	4.00	1.20	0.15	25.59	12.965	8.913	324.125	222.836	3.75

(continued on next page)

Tab. 5.2: Experimental observations (Contd.)

Pkt. No.	γ deg	V_c m/min	t_0 mm/rev	d mm	W mm	H mm	t_{chip} mm	l_{chip} mm	R_{chip}^* mm	R_{chip} mm	$\frac{R_{chip}^*}{t_0}$	$\frac{R_{chip}}{t_0}$	ζ
7.45	10	50	0.07	1.90	3.99	1.19	0.22	9.86	6.010	4.658	85.857	66.539	3.14
7.45	10	50	0.07	1.90	3.99	1.19	0.20	12.96	6.815	5.282	97.357	75.452	2.86
7.45	10	50	0.07	1.90	3.99	1.19	0.29	16.95	7.210	5.588	103.000	79.825	4.14
7.45	10	50	0.07	1.90	3.99	1.19	0.26	17.08	8.570	6.642	122.429	94.882	3.71
7.46	10	50	0.08	1.90	4.00	1.20	0.23	18.83	8.975	6.956	112.188	86.945	2.88
7.46	10	50	0.08	1.90	4.00	1.20	0.28	16.18	8.365	6.483	104.563	81.036	3.50
7.46	10	50	0.08	1.90	4.00	1.20	0.21	19.76	9.515	7.374	118.938	92.177	2.63
7.46	10	50	0.08	1.90	4.00	1.20	0.21	15.74	7.080	5.487	88.500	68.588	2.63
7.47	10	50	0.10	1.90	4.00	1.20	0.36	16.60	7.885	6.111	78.850	61.109	3.60
7.47	10	50	0.10	1.90	4.00	1.20	0.32	16.05	7.475	5.793	74.750	57.931	3.20
7.47	10	50	0.10	1.90	4.00	1.20	0.34	12.81	5.395	4.181	53.950	41.811	3.40
7.47	10	50	0.10	1.90	4.00	1.20	0.33	18.39	7.900	6.122	79.000	61.225	3.30
7.48	10	50	0.12	1.90	4.20	1.80	0.27	18.83	5.735	4.445	47.792	37.039	2.25
7.48	10	50	0.12	1.90	4.20	1.80	0.31	16.18	6.085	4.716	50.708	39.299	2.58
7.48	10	50	0.12	1.90	4.20	1.80	0.26	14.75	6.100	4.728	50.833	39.396	2.17
7.48	10	50	0.12	1.90	4.20	1.80	0.27	15.74	4.888	3.788	40.733	31.568	2.25
8.49	10	50	0.16	1.90	4.80	0.80	0.59	18.05	13.385	10.373	83.656	64.834	3.69
8.49	10	50	0.16	1.90	4.80	0.80	0.62	17.89	12.250	9.494	76.563	59.336	3.88
8.49	10	50	0.16	1.90	4.80	0.80	0.60	12.67	11.150	8.641	69.688	54.008	3.75
8.49	10	50	0.16	1.90	4.80	0.80	0.61	13.79	9.925	7.692	62.031	48.074	3.81

(continued on next page)

Tab. 5.2: Experimental observations (Contd.)

Pkt. No.	γ deg	V_c m/min	t_0 mm/rev	d mm	W mm	H mm	t_{chip} mm	l_{chip} mm	R_{chip}^* mm	R_{chip} mm	$\frac{R_{chip}^*}{t_0}$	$\frac{R_{chip}}{t_0}$	ζ
8.50	10	50	0.06	1.90	4.80	0.90	0.16	18.83	12.410	8.532	206.833	142.198	2.67
8.50	10	50	0.06	1.90	4.80	0.90	0.21	16.18	13.485	10.451	224.750	174.181	3.50
8.50	10	50	0.06	1.90	4.80	0.90	0.19	19.76	17.145	11.787	285.750	196.453	3.17
8.50	10	50	0.06	1.90	4.80	0.90	0.22	17.83	14.410	11.168	240.167	186.129	3.67
9.51	10	40	0.16	1.90	4.00	1.60	0.40	15.73	5.100	4.845	31.875	30.281	2.50
9.51	10	40	0.16	1.90	4.00	1.60	0.32	14.33	4.620	3.581	28.875	22.378	2.00
9.51	10	40	0.16	1.90	4.00	1.60	0.34	15.79	7.225	5.599	45.156	34.996	2.13
9.51	10	40	0.16	1.90	4.00	1.60	0.30	17.35	6.550	5.076	40.938	31.727	1.88
9.52	10	40	0.10	1.90	7.50	2.00	0.39	20.16	19.955	15.465	199.550	154.651	3.90
9.52	10	40	0.10	1.90	7.50	2.00	0.36	17.43	12.780	9.904	127.800	99.045	3.60
9.52	10	40	0.10	1.90	7.50	2.00	0.35	19.34	14.445	11.195	144.450	111.949	3.50
9.52	10	40	0.10	1.90	7.50	2.00	0.32	21.44	13.480	10.447	134.800	104.470	3.20
9.53	10	40	0.16	1.90	8.80	3.20	0.30	17.22	8.150	6.316	50.938	39.477	1.88
9.53	10	40	0.16	1.90	8.80	3.20	0.32	15.30	9.164	7.102	57.275	44.388	2.00
9.53	10	40	0.16	1.90	8.80	3.20	0.44	15.61	9.230	7.153	57.688	44.708	2.75
9.53	10	40	0.16	1.90	8.80	3.20	0.49	21.44	10.285	7.971	64.281	49.818	3.06

Tab. 5.3: Comparison of results of breaking strain ϵ_b with and without correction due to neutral axis shift

HTR	WTR	t_0	t_{chip}	R_{chip}	ϵ_b	e	ϵ_b with correction	% error
5	40.61	0.002	0.0071	0.3111	0.0115	0.00001	0.0115	0.39
5	32.85	0.004	0.0111	0.3324	0.0169	0.00003	0.0168	0.57
5	28.10	0.005	0.0155	0.3539	0.0221	0.00006	0.0219	0.74
5	24.80	0.007	0.0202	0.3755	0.0272	0.00009	0.0269	0.92
5	22.25	0.010	0.0252	0.3974	0.0323	0.00014	0.0319	1.10
5	20.20	0.012	0.0308	0.4195	0.0374	0.00019	0.0369	1.28
5	18.51	0.015	0.0367	0.4418	0.0425	0.00026	0.0419	1.46
5	17.08	0.019	0.0432	0.4643	0.0476	0.00035	0.0468	1.65
5	15.85	0.023	0.0501	0.4871	0.0528	0.00045	0.0519	1.84
10	55.71	0.002	0.0071	0.3110	0.0115	0.00001	0.0115	0.38
10	44.77	0.004	0.0111	0.3324	0.0169	0.00003	0.0168	0.57
10	37.93	0.005	0.0154	0.3538	0.0221	0.00006	0.0219	0.74
10	33.21	0.007	0.0201	0.3755	0.0272	0.00009	0.0269	0.92
10	29.55	0.010	0.0252	0.3973	0.0322	0.00014	0.0319	1.10
10	26.60	0.012	0.0307	0.4193	0.0373	0.00019	0.0368	1.28
10	24.15	0.015	0.0366	0.4416	0.0424	0.00026	0.0418	1.46
10	22.06	0.019	0.0431	0.4641	0.0475	0.00035	0.0467	1.64
20	76.16	0.002	0.0071	0.3110	0.0115	0.00001	0.0115	0.39
20	60.42	0.004	0.0111	0.3324	0.0169	0.00003	0.0168	0.57
20	50.58	0.005	0.0154	0.3538	0.0220	0.00006	0.0219	0.75
20	43.54	0.007	0.0201	0.3754	0.0271	0.00009	0.0269	0.92
25	122.22	0.001	0.0034	0.2899	0.0060	0.00000	0.0059	0.20
25	84.03	0.002	0.0071	0.3110	0.0115	0.00001	0.0115	0.39

Tab. 5.4: Experimentally determined chip breaking parameters

Pkt. No.	γ deg	V_c m/ min	t_0 mm/rev	d mm	t_{chip} mm	R_{chip} mm	$\frac{t_{chip}}{R_{chip}}$	$\frac{t_0^2}{R_{chip}}$ mm	$\frac{t_0}{R_{chip}}$	ϵ_b
1.06	10	40	0.14	1.90	0.37	5.123	0.722	3.826	2.733	3.611
1.06	10	40	0.14	1.90	0.28	7.777	0.360	2.520	1.800	1.800
1.06	10	40	0.14	1.90	0.28	10.060	0.278	1.948	1.392	1.392
1.06	10	40	0.14	1.90	0.44	5.096	0.863	3.846	2.747	4.317
1.07	10	40	0.16	1.90	0.50	8.246	0.606	3.105	1.940	3.032
1.07	10	40	0.16	1.90	0.41	6.886	0.595	3.718	2.324	2.977
1.07	10	40	0.16	1.90	0.41	7.068	0.580	3.622	2.264	2.900
1.07	10	40	0.16	1.90	0.38	7.459	0.509	3.432	2.145	2.547
1.08	10	40	0.20	1.90	0.74	6.394	1.157	6.256	3.128	5.787
1.08	10	40	0.20	1.90	0.63	6.595	0.955	6.065	3.032	4.776
1.08	10	40	0.20	1.90	0.56	7.080	0.791	5.650	2.825	3.955
1.08	10	40	0.20	1.90	0.68	6.422	1.059	6.229	3.114	5.294
1.09	10	40	0.24	1.90	0.86	6.237	1.379	9.236	3.848	6.895
1.09	10	40	0.24	1.90	0.84	4.774	1.760	12.066	5.027	8.798
1.09	10	40	0.24	1.90	0.72	4.299	1.675	13.399	5.583	8.375
1.09	10	40	0.24	1.90	0.80	4.299	1.861	13.399	5.583	9.305
2.16	10	50	0.16	1.90	0.59	6.611	0.892	3.872	2.420	4.462
2.16	10	50	0.16	1.90	0.45	4.972	0.905	5.149	3.218	4.526
2.16	10	50	0.16	1.90	0.57	7.421	0.768	3.450	2.156	3.841
2.16	10	50	0.16	1.90	0.45	7.921	0.568	3.232	2.020	2.841
2.17	10	50	0.20	1.90	0.55	6.612	0.832	6.050	3.025	4.159
2.17	10	50	0.20	1.90	0.53	5.975	0.887	6.694	3.347	4.435
2.17	10	50	0.20	1.90	0.54	6.161	0.876	6.492	3.246	4.382
2.17	10	50	0.20	1.90	0.58	6.370	0.911	6.280	3.140	4.553
2.18	10	50	0.24	1.90	0.89	5.885	1.512	9.787	4.078	7.561
2.18	10	50	0.24	1.90	0.78	5.634	1.385	10.225	4.260	6.923
2.18	10	50	0.24	1.90	0.88	5.344	1.647	10.779	4.491	8.234
2.18	10	50	0.24	1.90	0.73	5.168	1.413	11.146	4.644	7.063
2.19	10	50	0.28	1.90	0.61	5.472	1.115	14.327	5.117	5.574
2.19	10	50	0.28	1.90	0.51	5.676	0.898	13.812	4.933	4.492
2.19	10	50	0.28	1.90	0.58	6.033	0.961	12.996	4.642	4.807
2.19	10	50	0.28	1.90	0.76	7.524	1.010	10.420	3.721	5.051
2.20	10	50	0.32	1.90	0.90	5.786	1.556	17.699	5.531	7.778
2.20	10	50	0.32	1.90	0.92	5.377	1.711	19.044	5.951	8.555
2.20	10	50	0.32	1.90	0.84	4.855	1.730	21.094	6.592	8.652
2.20	10	50	0.32	1.90	0.89	4.864	1.830	21.053	6.579	9.149

(continued on next page)

Tab. 5.4: Experimentally determined chip breaking parameters (Contd.)

Pkt. No.	γ deg	V_c m/ min	t_0 mm/rev	d mm	t_{chip} mm	R_{chip} mm	$\frac{t_{chip}}{R_{chip}}$	$\frac{t_0^2}{R_{chip}}$ mm	$\frac{t_0}{R_{chip}}$	ϵ_b
3.23	10	40	0.10	1.90	0.28	4.456	0.628	2.244	2.244	3.142
3.23	10	40	0.10	1.90	0.36	5.379	0.669	1.859	1.859	3.347
3.23	10	40	0.10	1.90	0.32	3.457	0.926	2.893	2.893	4.629
3.23	10	40	0.10	1.90	0.35	5.057	0.692	1.978	1.978	3.461
3.24	10	40	0.07	1.90	0.21	8.502	0.247	0.576	0.823	1.235
3.24	10	40	0.07	1.90	0.23	5.332	0.431	0.919	1.313	2.157
3.24	10	40	0.07	1.90	0.21	5.650	0.372	0.867	1.239	1.858
3.24	10	40	0.07	1.90	0.18	6.429	0.280	0.762	1.089	1.400
3.25	10	40	0.08	1.90	0.30	6.417	0.468	0.997	1.247	2.338
3.25	10	40	0.08	1.90	0.24	5.208	0.461	1.229	1.536	2.304
3.25	10	40	0.08	1.90	0.27	5.503	0.491	1.163	1.454	2.453
3.25	10	40	0.08	1.90	0.26	4.890	0.532	1.309	1.636	2.658
3.26	10	40	0.10	1.90	0.31	5.487	0.565	1.822	1.822	2.825
3.26	10	40	0.10	1.90	0.38	4.135	0.919	2.419	2.419	4.595
3.26	10	40	0.10	1.90	0.41	4.770	0.860	2.096	2.096	4.298
3.26	10	40	0.10	1.90	0.26	6.433	0.404	1.555	1.555	2.021
4.31	10	50	0.10	1.90	0.38	4.166	0.912	2.401	2.401	4.561
4.31	10	50	0.10	1.90	0.38	4.769	0.797	2.097	2.097	3.984
4.31	10	50	0.10	1.90	0.37	5.464	0.677	1.830	1.830	3.386
4.31	10	50	0.10	1.90	0.43	4.807	0.895	2.080	2.080	4.473
4.32	10	50	0.12	1.90	0.46	4.999	0.920	2.881	2.401	4.601
4.32	10	50	0.12	1.90	0.39	5.766	0.676	2.497	2.081	3.382
4.32	10	50	0.12	1.90	0.45	5.700	0.789	2.526	2.105	3.947
4.32	10	50	0.12	1.90	0.41	4.584	0.894	3.141	2.618	4.472
4.33	10	50	0.14	1.90	0.45	6.789	0.663	2.887	2.062	3.314
4.33	10	50	0.14	1.90	0.54	6.533	0.827	3.000	2.143	4.133
4.33	10	50	0.14	1.90	0.45	4.845	0.929	4.045	2.890	4.644
4.33	10	50	0.14	1.90	0.48	4.722	1.017	4.151	2.965	5.083
5.35	10	40	0.06	1.90	0.17	8.517	0.200	0.423	0.704	0.998
5.35	10	40	0.06	1.90	0.24	9.610	0.250	0.375	0.624	1.249
5.35	10	40	0.06	1.90	0.21	5.894	0.356	0.611	1.018	1.782
5.35	10	40	0.06	1.90	0.14	7.844	0.178	0.459	0.765	0.892
5.36	10	40	0.08	1.90	0.19	7.153	0.266	0.895	1.118	1.328
5.36	10	40	0.08	1.90	0.25	6.274	0.398	1.020	1.275	1.992
5.36	10	40	0.08	1.90	0.34	7.963	0.427	0.804	1.005	2.135
5.36	10	40	0.08	1.90	0.28	7.839	0.357	0.816	1.021	1.786

(continued on next page)

Tab. 5.4: Experimentally determined chip breaking parameters (Contd.)

Pkt. No.	γ deg	V_c m/min	t_0 mm/rev	d mm	t_{chip} mm	R_{chip} mm	$\frac{t_{chip}}{R_{chip}}$	$\frac{t_0^2}{R_{chip}}$ mm	$\frac{t_0}{R_{chip}}$	ϵ_b
5.38	10	40	0.12	1.90	0.42	8.978	0.468	1.604	1.337	2.339
5.38	10	40	0.12	1.90	0.44	7.618	0.578	1.890	1.575	2.888
5.38	10	40	0.12	1.90	0.40	7.301	0.548	1.972	1.644	2.740
5.38	10	40	0.12	1.90	0.38	5.584	0.681	2.579	2.149	3.403
6.39	10	40	0.04	1.90	0.11	5.258	0.209	0.304	0.761	1.046
6.39	10	40	0.04	1.90	0.13	5.867	0.222	0.273	0.682	1.108
6.39	10	40	0.04	1.90	0.14	6.080	0.230	0.263	0.658	1.151
6.39	10	40	0.04	1.90	0.15	5.917	0.254	0.270	0.676	1.268
6.40	10	40	0.06	1.90	0.22	5.534	0.398	0.651	1.084	1.988
6.40	10	40	0.06	1.90	0.22	5.983	0.368	0.602	1.003	1.839
6.40	10	40	0.06	1.90	0.22	6.386	0.345	0.564	0.940	1.723
6.40	10	40	0.06	1.90	0.20	5.994	0.334	0.601	1.001	1.668
6.41	10	40	0.07	1.90	0.25	7.359	0.340	0.666	0.951	1.699
6.41	10	40	0.07	1.90	0.23	6.057	0.380	0.809	1.156	1.899
6.41	10	40	0.07	1.90	0.19	6.107	0.311	0.802	1.146	1.556
6.41	10	40	0.07	1.90	0.21	5.487	0.383	0.893	1.276	1.914
6.42	10	40	0.08	1.90	0.33	5.747	0.574	1.114	1.392	2.871
6.42	10	40	0.08	1.90	0.28	5.394	0.519	1.187	1.483	2.595
6.42	10	40	0.08	1.90	0.23	6.092	0.378	1.051	1.313	1.888
6.42	10	40	0.08	1.90	0.30	4.712	0.637	1.358	1.698	3.183
6.43	10	40	0.10	1.90	0.36	5.778	0.623	1.731	1.731	3.115
6.43	10	40	0.10	1.90	0.41	4.832	0.848	2.069	2.069	4.242
6.43	10	40	0.10	1.90	0.37	5.588	0.662	1.790	1.790	3.311
6.43	10	40	0.10	1.90	0.39	5.150	0.757	1.942	1.942	3.786
7.44	10	50	0.04	1.90	0.14	7.714	0.181	0.207	0.519	0.907
7.44	10	50	0.04	1.90	0.14	7.053	0.199	0.227	0.567	0.993
7.44	10	50	0.04	1.90	0.15	7.208	0.208	0.222	0.555	1.041
7.44	10	50	0.04	1.90	0.15	8.913	0.168	0.180	0.449	0.841
7.45	10	50	0.07	1.90	0.22	4.658	0.472	1.052	1.503	2.362
7.45	10	50	0.07	1.90	0.20	5.282	0.379	0.928	1.325	1.893
7.45	10	50	0.07	1.90	0.29	5.588	0.519	0.877	1.253	2.595
7.45	10	50	0.07	1.90	0.26	6.642	0.391	0.738	1.054	1.957
7.46	10	50	0.08	1.90	0.23	6.956	0.331	0.920	1.150	1.653
7.46	10	50	0.08	1.90	0.28	6.483	0.432	0.987	1.234	2.160
7.46	10	50	0.08	1.90	0.21	7.374	0.285	0.868	1.085	1.424
7.46	10	50	0.08	1.90	0.21	5.487	0.383	1.166	1.458	1.914

(continued on next page)

Tab. 5.4: Experimentally determined chip breaking parameters (Contd.)

Pkt. No.	γ deg	V_c m/ min	t_0 mm/rev	d mm	t_{chip} mm	R_{chip} mm	$\frac{t_{chip}}{R_{chip}}$	$\frac{t_0^2}{R_{chip}}$ mm	$\frac{t_0}{R_{chip}}$	ϵ_b
7.47	10	50	0.10	1.90	0.36	6.111	0.589	1.636	1.636	2.946
7.47	10	50	0.10	1.90	0.32	5.793	0.552	1.726	1.726	2.762
7.47	10	50	0.10	1.90	0.34	4.181	0.813	2.392	2.392	4.066
7.47	10	50	0.10	1.90	0.33	6.122	0.539	1.633	1.633	2.695
7.48	10	50	0.12	1.90	0.27	4.445	0.607	3.240	2.700	3.037
7.48	10	50	0.12	1.90	0.31	4.716	0.657	3.054	2.545	3.287
7.48	10	50	0.12	1.90	0.26	4.728	0.550	3.046	2.538	2.750
7.48	10	50	0.12	1.90	0.27	3.788	0.713	3.801	3.168	3.564
8.49	10	50	0.16	1.90	0.59	10.373	0.569	2.468	1.542	2.844
8.49	10	50	0.16	1.90	0.62	9.494	0.653	2.697	1.685	3.265
8.49	10	50	0.16	1.90	0.60	8.641	0.694	2.963	1.852	3.472
8.49	10	50	0.16	1.90	0.61	7.692	0.793	3.328	2.080	3.965
8.50	10	50	0.06	1.90	0.16	8.532	0.188	0.422	0.703	0.938
8.50	10	50	0.06	1.90	0.21	10.451	0.201	0.344	0.574	1.005
8.50	10	50	0.06	1.90	0.19	11.787	0.161	0.305	0.509	0.806
8.50	10	50	0.06	1.90	0.22	11.168	0.197	0.322	0.537	0.985
9.51	10	40	0.16	1.90	0.40	4.845	0.826	5.284	3.302	4.128
9.51	10	40	0.16	1.90	0.32	3.581	0.894	7.150	4.469	4.469
9.51	10	40	0.16	1.90	0.34	5.599	0.607	4.572	2.857	3.036
9.51	10	40	0.16	1.90	0.30	5.076	0.591	5.043	3.152	2.955
9.52	10	40	0.10	1.90	0.39	15.465	0.252	0.647	0.647	1.261
9.52	10	40	0.10	1.90	0.36	9.904	0.363	1.010	1.010	1.817
9.52	10	40	0.10	1.90	0.35	11.195	0.313	0.893	0.893	1.563
9.52	10	40	0.10	1.90	0.32	10.447	0.306	0.957	0.957	1.532
9.53	10	40	0.16	1.90	0.30	6.316	0.475	4.053	2.533	2.375
9.53	10	40	0.16	1.90	0.32	7.102	0.451	3.605	2.253	2.253
9.53	10	40	0.16	1.90	0.44	7.153	0.615	3.579	2.237	3.076
9.53	10	40	0.16	1.90	0.49	7.971	0.615	3.212	2.007	3.074

6. CONCLUSIONS

In the present investigation an attempt has been made to examine chip breakability by a smooth step-type chip breaker using the rigid-perfectly plastic slip-line field theory. Orthogonal machining is assumed and the deformation mode is analysed using the solutions proposed earlier by Kudo [21] and Dewhurst [23]. The rake face friction is represented by the adhesion friction law proposed by Maekawa *et al.* [70]. The fields are constructed by the matrix operational procedure developed by Dewhurst and Collins [72] and Dewhurst [73, 74] assuming a linear relation between the field coordinates within the secondary shear zone.

The strain in the chip has been estimated by assuming the flow of material in the deformation zone to take place along a finite number of elemental streamtubes. From the velocity of particles at discrete points along the bounding streamlines the shear strain suffered by the material in a streamtube is calculated by the method suggested by Atkins *et al.* [75]. This strain is then summed up over all the streamtubes constituting the deformation zone to calculate the total strain imparted to the material during the chip forming process.

It is shown that 80% of the chip material suffer ‘damage’ due to its flow through the primary shear line. Only 20% of the material experience straining due to passage through both primary and secondary deformation zones. However, for the feed range and rake angles examined the secondary strain is found to constitute only 10 to 15 % of the total strain. It is further observed that the strain distribution across the chip is influenced more by the chip breaker position than by the feed value. The results of computation also indicate that for a given value of feed as the chip breaker moves away from the cutting edge, the total strain and primary strain imparted to the chip increase while the secondary strain and breaking strain decrease.

It is demonstrated that as the chip breaker moves away from the cutting edge the radius of chip curvature (R_{chip}/t_0), tool-chip contact length (l_n/t_0), specific cutting

energy (F_c/t_0), cutting ratio ζ and total strain ϵ_t in the chip increase while the breaking strain and the secondary strain decrease. This observation is found to be influenced both by uncut chip thickness t_0 and tool rake angle γ . Tool-chip interface friction increases (R_{chip}/t_0), (F_c/t_0), ζ and ϵ_t but lowers the breaking strain ϵ_b .

The cutting force increases as WTR increases and rake angle γ decreases. The reverse trend is exhibited by chip breaker force F_b . However, for the whole range of chip breaker positions examined, chip breaker force is found to be of the order of half a percent of the cutting force.

The chips depending on their length and thickness can be classified as under-broken, effectively-broken and over-broken. The boundaries defining these chip shapes are however fuzzy. It is seen that both specific cutting energy (F_c/t_0) and total strain ϵ_t increase as chip breaker moves away from the cutting edge. Hence, these parameters possibly can not be used to define effectiveness of chip breaking. On the other hand ϵ_b , (t_0/R_{chip}) and (t_{chip}/R_{chip}) decrease as chip breaker moves away from the cutting edge. Since it is common experimental observation that moving the chip breaker away from the cutting edge reduces the tendency for chip breaking, chip breakability criteria based on ϵ_b , (t_0/R_{chip}) and (t_{chip}/R_{chip}) can be used to assess breaking of chips more effectively. However, the boundaries between under-breaking, effective-breaking and over-breaking as determined from the present slip-line field analysis do not exactly match with those determined by other investigators.

It is seen that experimentally determined chip parameters such as R_{chip} and ϵ_b show excellent match with those determined from Dewhurst's field at high feeds. At low feeds, however, the match with Kudo's field is better. A reduction of 10 to 20% in the value of R_{chip} is noticed when spring back correction due to elastic recovery is taken in to account. However, correction in the values of ϵ_b due to shift in neutral axis is found to be insignificant. The variation of ϵ_b with (R_{chip}/t_0) also shows excellent match between theory and experiment.

For a given value of feed, the chip breaker is found to be effective only over a given range of positions. The effectiveness of a chip breaker can be determined from a plot of ϵ_b with WTR as a function of feed as shown in Fig. 5.17. For any given chip breaker position, feed and rake angle, the chip parameters such as t_{chip} , R_{chip} and ϵ_b lie within a range and this is due to the non-uniqueness of the machining process.

APPENDIX

A. DETERMINATION OF LINEAR COEFFICIENT

Equation for the adhesion friction condition at chip-tool interface can be stated as

$$\tau = k \left[1 - e^{-\left(\frac{\mu\sigma_n}{\kappa}\right)^n} \right]^{\frac{1}{n}} \quad (\text{A.1})$$

where, τ is the shear stress, κ is the yield stress in shear of the work material, σ_n is the normal stress, μ is the low stress level coefficient of friction, and n is a constant whose value depends on tool-work material combination.

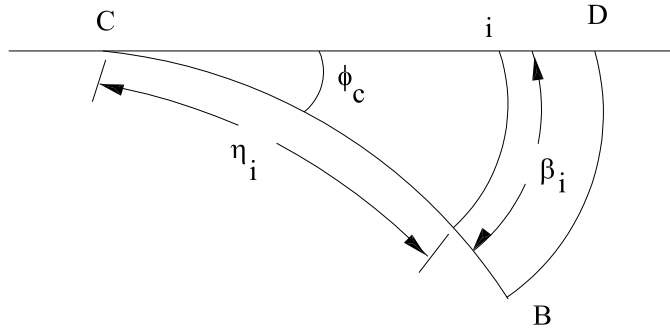


Fig. A.1: Angular coordinates of any point on the tool face

Let σ_i and τ_i denote normal stress and shear stress at any point i on the tool face CD with angular coordinates η_i and β_i (Fig. A.1). Hence

$$\sigma_i = p_C + 2(\eta_i + \beta_i) + \kappa \sin[2\phi_C + \eta_i - \beta_i] \quad (\text{A.2})$$

$$\tau_i = \kappa \cos[2(\phi_C + \eta_i - \beta_i)] \quad (\text{A.3})$$

where p_C and ϕ_C are the hydrostatic pressure and friction angle respectively at C. Substituting equations (A.2) and (A.3) into equation (A.1), we get

$$\left(1 - e^{-\{\mu\{p_C + 2(\eta_i + \beta_i) + \sin[2(\phi_C + \eta_i - \beta_i)]\}\}^n}\right)^{\frac{1}{n}} - \cos[2(\phi_C + \eta_i - \beta_i)] = 0 \quad (\text{A.4})$$

For given values of μ and n , equation A.4 may be solved numerically to determine the true value of β_i for any given value of η_i .

If the above non-linear relation between η_i and β_i is approximated by the linear relation [73, 74]

$$\beta = m_0 \eta \quad (\text{A.5})$$

the error e_i between the true and approximate value may be expressed as

$$e_i = \beta_i - m_0 \eta_i \quad (\text{A.6})$$

When the calculation is carried out over n number of points on CD, the sum of the square of the errors is given as

$$\sum_{i=1}^n e_i^2 = \sum_{i=1}^n (\beta_i - m_0 \eta_i)^2 \quad (\text{A.7})$$

For the best linear fit

$$\frac{d \sum e_i^2}{d m_0} = 0 \quad (\text{A.8})$$

Hence

$$m_0 = \frac{\sum_{i=1}^n \eta_i^2}{\sum_{i=1}^n \beta_i \eta_i} \quad (\text{A.9})$$

At the origin C (Fig. A.1), $\eta_i = \beta_i = 0$ and equation A.4 reduces to

$$\left(1 - e^{-\{\mu\{p_C + \sin(2\phi_C)\}\}^n}\right)^{\frac{1}{n}} - \cos(2\phi_C) = 0 \quad (\text{A.10})$$

Equation (A.10) is solved to determine ϕ_C for any given value of p_C .

The program developed for determination of m_0 first evaluated ϕ_C by obtaining the solution to equation (A.10) by the Newton-Raphson method. For ten known η_i values corresponding to ten discrete points on the slip-line curve BC, the programme then determined the corresponding β_i values by obtaining the solution to equation (A.4) and evaluated the linear coefficient m_0 using equation (A.9).

B. HILL'S CRITERIA TO CHECK OVER-STRESSING OF VERTICES

All the solutions obtained from the present slip-line field are not necessarily valid. To ensure the validity of results, the stress field should be extended into both the workpiece and chip to demonstrate that the yield criterion is no where violated, i.e. it is necessary to justify that the material out side the deforming region remains rigid. Following Hill [90], it can be shown that the material at the rigid vertices at A remains rigid (Fig. B.1).

If hydrostatic pressure at point A, $p_A \leq (1 - 2 \cos(\alpha_1 - \frac{\pi}{4}))$, for $\alpha_1 \leq (\frac{3\pi}{4})$,

or

$p_A \leq (1 + 2(\alpha_1 - \frac{3\pi}{4}))$, for $\alpha_1 \geq (\frac{3\pi}{4})$,

and

if $p_A \leq (1 + 2(\alpha_2 - \frac{\pi}{4}))$, for $\alpha_2 \geq (\frac{\pi}{4})$,

or

$p_A \geq (-1 + 2 \cos(\alpha_2 - \frac{\pi}{4}))$, for $\alpha_2 \leq (\frac{3\pi}{4})$

where α_1 and α_2 are the vertex angles as shown in Fig. B.1.

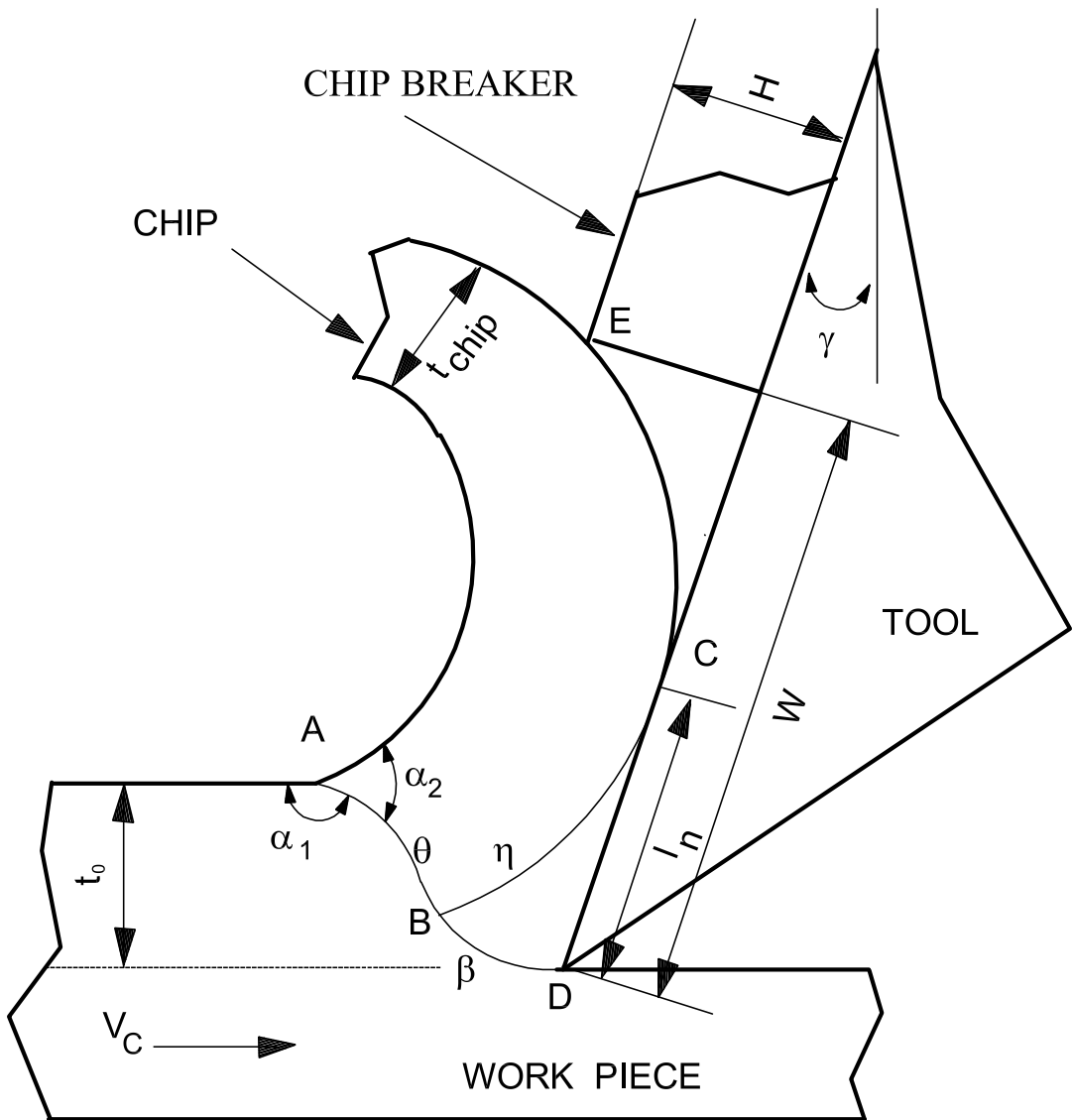


Fig. B.1: Hill's criteria to check over-stressing of vertices

C. CORRECTION OF BREAKING STRAIN DUE TO SHIFTING OF NEUTRAL AXIS

The breaking strain, ϵ_b in a chip can be determined by applying theory of bending of beams assuming that the neutral axis is passing through the center of gravity [102, 103],

$$\epsilon_b = \ln \left[\frac{l_{chip}}{l} \right] \quad (C.1)$$

In Fig C.1, for any angle δ , if l_{chip} is the length of chip at outer most layer and 'l' is the length along neutral layer, then it can be written as,

$$\delta = \frac{l_{chip}}{R_{chip}} = \frac{l}{(R_{chip} - \frac{t_{chip}}{2})} \quad (C.2)$$

or,

$$\frac{l_{chip}}{l} = \frac{R_{chip}}{(R_{chip} - \frac{t_{chip}}{2})} \quad (C.3)$$

From Equations (C.1) and (C.3), breaking strain can be written as,

$$\epsilon_b = \ln \left[\frac{R_{chip}}{(R_{chip} - \frac{t_{chip}}{2})} \right] \quad (C.4)$$

or,

$$\epsilon_b = \ln \left[\frac{1}{(1 - \frac{t_{chip}}{2R_{chip}})} \right] \quad (C.5)$$

or,

$$\epsilon_b = -\ln \left[1 - \left(\frac{t_{chip}}{2R_{chip}} \right) \right] \quad (C.6)$$

on expanding the above expression and neglecting higher terms,

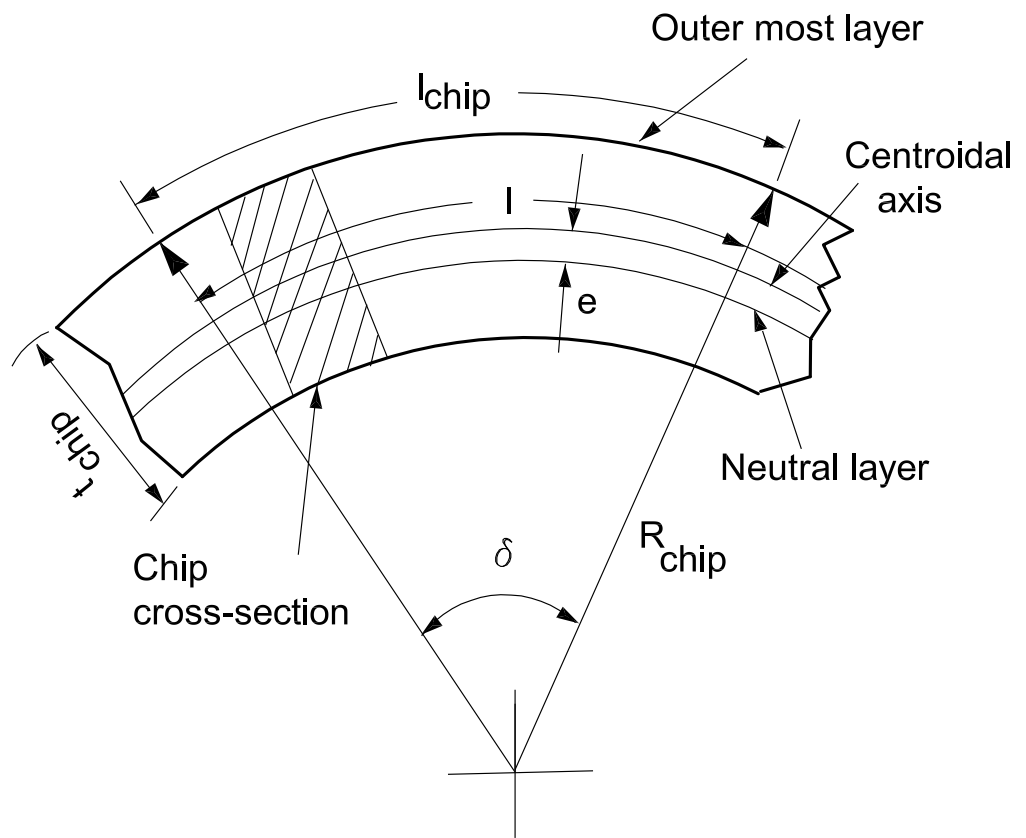


Fig. C.1: Estimation of breaking strain

$$\epsilon_b = -\left[-\left(\frac{t_{chip}}{2R_{chip}}\right)\right] \quad (C.7)$$

finally, the expression for breaking strain ϵ_b can be expressed as

$$\epsilon_b = \left[\frac{t_{chip}}{2R_{chip}} \right] \quad (C.8)$$

where R_{chip} is outer radius of the chip and t_{chip} is chip thickness. For the above calculations it was assumed that the neutral plane passes through the middle of the chip section or through centre of gravity.

Actually, in case of bending of curved beams, the value of average stresses on the concave side of beam are quite large comparing to that of convex side. Due to this the neutral axis does not pass through the C.G. of the section but shifts towards the centre of curvature of the beam. This difference in the position of neutral layer and centroidal axis of beam is shown as 'e' in the Fig C.1. The value of 'e' can be expressed as below [103]:

$$e = \left(R_{chip} - \frac{t_{chip}}{2} \right) \left[1 - \frac{1}{1 + \frac{1}{3} \left[\frac{t_{chip}}{2(R_{chip} - \frac{t_{chip}}{2})} \right]^2 + \dots} \right] \quad (C.9)$$

Incorporating the value of 'e' in equation C.4, the expression for modified breaking strain can be written as

$$\epsilon_b = \ln \left[\frac{R_{chip}}{\left(R_{chip} - \frac{t_{chip}}{2} + e \right)} \right] \quad (C.10)$$

D. DETERMINATION OF ASPECT RATIO

Shinozuka *et al.* [42] using FEM suggested a chip breakability criterion termed as ‘aspect ratio’ R_{as} to assess degree of chip breakability, which is defined as a ratio of chip length DN and chip thickness (Fig. 4.1).

The value of aspect ratio R_{as} can be calculated (Fig. D.1) as given below:

$$X_o = X_{BD} - R_{chip} \cos \gamma \quad (D.1)$$

$$Y_o = Y_{BD} + R_{chip} \sin \gamma \quad (D.2)$$

Equation of a circle having centre at a point other than the origin can be given by,

$$(X - X_o)^2 + (Y - Y_o)^2 = R_{chip}^2 \quad (D.3)$$

The coordinates of point M (X_M, Y_M) with respect to point B can be written as,

$$X_M = X_{BD} - DM \sin(\alpha - \gamma) \quad (D.4)$$

$$Y_M = Y_{BD} + DM \cos(\alpha - \gamma) \quad (D.5)$$

Equation of a line passing through a point A can be given by,

$$Y_N = Y_{BA} \quad (D.6)$$

Thus, from equation D.3

$$(X - X_o)^2 = R_{chip}^2 - (Y - Y_o)^2 \quad (D.7)$$

or,

$$X = \pm \sqrt{R_{chip}^2 - (Y - Y_o)^2} + X_o \quad (D.8)$$

Thus,

$$X_N = -\sqrt{R_{chip}^2 - (Y_{BA} - Y_o)^2} + X_o \quad (D.9)$$

$$Chord\ length\ MN = \sqrt{(X_N - X_M)^2 + (Y_N - Y_M)^2} \quad (D.10)$$

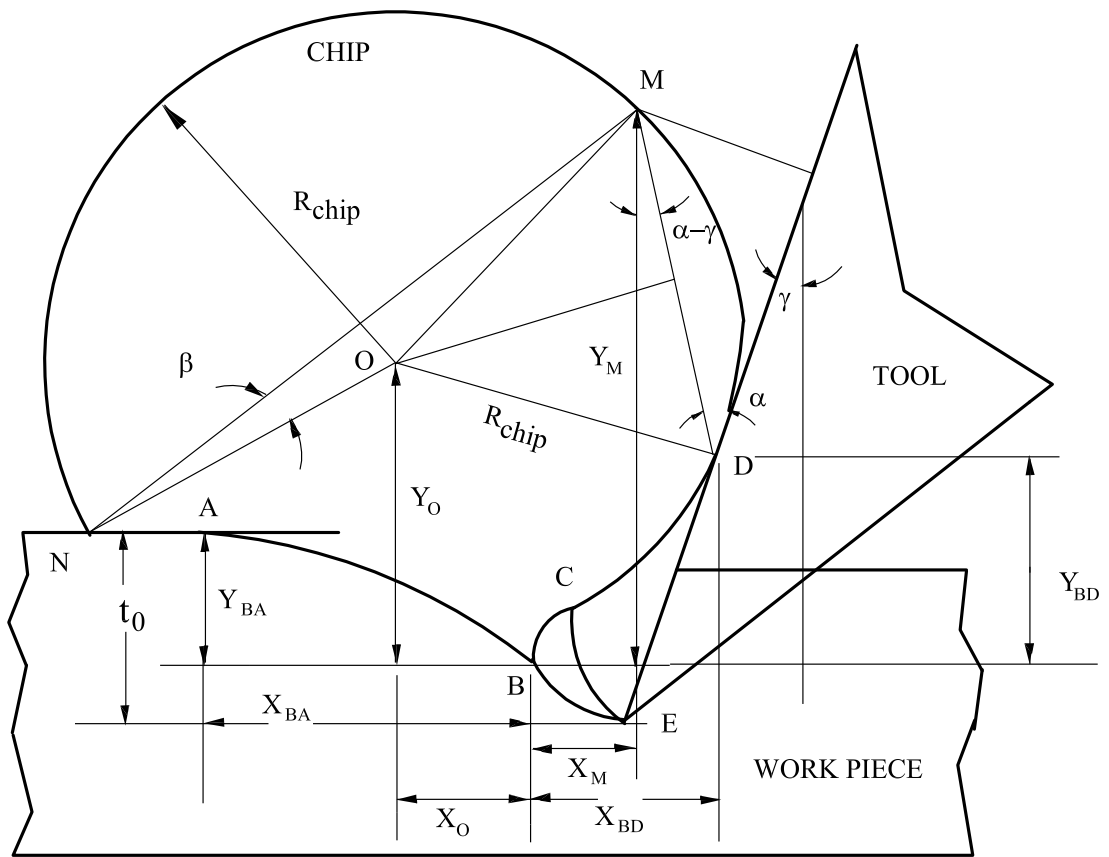


Fig. D.1: Determination of length of chip outside the chip breaker groove

$$\cos \beta = \frac{MN}{2R_{chip}} \quad (\text{D.11})$$

or,

$$\beta = \cos^{-1} \left(\frac{MN}{2R_{chip}} \right) \quad (\text{D.12})$$

Thus, the length of arc MN can be found from following equations, depending on the position of centre of circle, whether it lies on lower side of the chord MN or on the upper side,

$$\widehat{MN} = 2R_{chip} \left(\frac{3\pi}{2} - \beta \right) \quad (\text{D.13})$$

or,

$$\widehat{MN} = 2R_{chip} \left(\frac{\pi}{2} - \beta \right) \quad (\text{D.14})$$

BIBLIOGRAPHY

- [1] A. Bhattacharya, *Metal Cutting: Theory and Practice*. Central Book Publishers, 1984.
- [2] H. Ernst and M. Merchant, “Chip formation, friction and high quality machined surfaces,” *Trans. ASME*, vol. 29, no. 0, pp. 299–378, 1941.
- [3] T. N. Loladze, “Chip formation during the cutting of metals,” *Mashgiz*, 1952.
- [4] I. S. Jawahir, “Chip control literature database,” *Ann. CIRP*, vol. 42, no. 2, 1993.
- [5] M. I. Sadik and B. Lindstrom, “A simple concept to achieve a rational chip form,” *J. Materials Proc. Tech.*, vol. 54, no. 1, pp. 12–16, 1995.
- [6] A. Kharkevich and P. K. Venuvinod, “Basic geometric analysis of 3-d chip forms in metal cutting. part 1: determining up-curl and side-curl radii,” *Int. J. of Mach. Tools & Manufact.*, vol. 39, pp. 751–769, 1999.
- [7] K. Seah, M. Rahman, X. Li, and X. Zhang, “A three-dimensional model of chip flow, chip curl and chip breaking for oblique cutting,” *Int. J. of Mach. Tools & Manufact.*, vol. 36, no. 0, pp. 1385–1400, 1996.
- [8] R. J. Seethaler and I. Yellowley, “An upper bound cutting model for oblique cutting tools with nose radius,” *Int. J. of Mach. Tools & Manufact.*, vol. 37, pp. 119–134, 1997.
- [9] J. A. Arsecularatne, P. Mathew, and P. L. B. Oxley, “Prediction of chip flow direction and cutting forces in oblique machining with nose radius tools,” *Proc. I.Mech. E., J. Eng. Manuf.*, vol. 209, pp. 305–315, 1995.

-
- [10] C. Rubenstein, "The mechanics of continuous chip formation in oblique cutting in the absence of chip distortion, part - 1 theory," *Int. J. Mach. Tool Des. and Res.*, vol. 23, no. 1, pp. 11–20, 1981.
- [11] W. S. Lau and C. Rubenstein, "The mechanics of continuous chip formation in oblique cutting in the absence of chip distortion, part ii - comparison of experimental data with deductions from theory," *Int. J. Mach. Tool Des. and Res.*, vol. 21, no. 1, pp. 21–38, 1981.
- [12] K. Nakayama, "Comprehensive chip form classification based on the cutting mechanism," *Ann. CIRP*, vol. 41, no. 1, pp. 71–74, 1992.
- [13] H. Takayama and K. Nakayama, "Basic rules on the form of chip in metal cutting," *Ann. CIRP*, vol. 27, no. 1, pp. 17–21, 1978.
- [14] N. Fang, "Kinematic characterization of chip lateral curl- the third pattern of chip curl in machining," *J. of Manuf. Sc. and Eng.*, vol. 124, pp. 667–675, 2002.
- [15] E. H. Lee and B. W. Shaffer, "The theory of plasticity applied to a problem of machining," *J. App. Mech. Tran. ASME*, vol. 18, pp. 405–413, Dec 1951.
- [16] R. Hahn, "Some observations on chip curl in the metal cutting process under orthogonal cutting conditions," *Trans. ASME, Ser. B.*, vol. 73, pp. 581–591, 1953.
- [17] K. Nakayama, M. Arai, T. Kondo, and H. Suzuki, "Cutting tool with curved rake face- 'a means for breaking thin chips'," *Ann. CIRP*, vol. 30, pp. 5–8, 1981.
- [18] G. R. Ponshe, "A new explanation of the phenomenon of chip curling during machining," *ASME J. of Eng. For Ind.*, pp. 376–379, May 1967.
- [19] C. Rubenstein and C. C. Dawe, "Analysis of chip curvature," *10th Int. MTDR Conf.*, September 1969.
- [20] P. Albrecht, "New developments in the theory of the metal-cutting process," *Trans. ASME. J. of Eng. for Industry*, pp. 348–358, November 1960.

-
- [21] H. Kudo, "Some new slip-line solutions for two dimensional steady state machining," *Int. J. of Mech. Sc.*, vol. 7, pp. 43–55, 1965.
- [22] P. Dewhurst, "On the non-uniqueness of the machining process," *Proc. R. Soci. (London)*, vol. Ser A-360, pp. 587–610, 1978.
- [23] P. Dewhurst, "The effect of chip breaker constraints on the mechanics of the machining process," *Ann. CIRP*, vol. 28, no. 1, pp. 1–5, 1979.
- [24] K. P. Maithy and N. S. Das, "A class of slip-line field solutions for metal machining with slipping and sticking contact at the chip-tool interface," *Int. J. of Mech. Sci.*, vol. 43, pp. 2435–2452, 2001.
- [25] N. Fang, "Slipline modelling of machining with a rounded-edge tool, part i: New model and theory," *J. of Mech. Phys.Solids*, vol. 51, pp. 715–742, 2003.
- [26] N. Fang and I. S. Jawahir, "Analytical predictions and experimental validation of cutting force ratio, chip thickness and chip back-flow angle in restricted contact machining using the universal slip-line model," *Int. J. of Mach. Tools & Manufact.*, vol. 42, pp. 681–694, 2002.
- [27] N. Fang, "Machining with tool-chip contact on the tool secondary rake face-part i, a new slip-line model," *Int. J. of Mech. Sc.*, vol. 44, pp. 2337–2354, 2002.
- [28] N. Fang, "Machining with tool-chip contact on the tool secondary rake face-part ii, analysis and discussion," *Int. J. of Mech. Sc.*, vol. 44, pp. 2355–2368, 2002.
- [29] T. Shi and S. Ramalingam, "Slip-line solution for orthogonal cutting with a chip breaker and flank wear," *Int. J. of Mech.Sc.*, vol. 33, no. 9, pp. 689–704, 1991.
- [30] E. Henriksen, "Chip breaking-a study of three dimensional chip flow," *Trans. ASME, Ser B*, vol. 53, pp. 5–9, 1953.
- [31] I. S. Jawahir and P. L. B. Oxley, "Efficient chip control at reduced power consumption: An experimental analysis," *4t Int. Conf. Manuf. Eng.*, pp. 97–102, 1988.

-
- [32] K. Nakayama, "A study on chip-breaker," *JSME*, vol. 5, no. 17, pp. 142–150, 1962.
- [33] B. Worthington and A. Redford, "Chip curl and the action of the groove type chip former," *Int. J. Mach. Tool Des. and Res.*, vol. 13, pp. 257–270, 1973.
- [34] B. Bhaktavachalam and P. K. Venuvinod, "Side curl of chips - its importance and prediction in metal cutting," *6th All India MMTDR Conf.*, pp. 235–242, 1973.
- [35] G. Boothroyd, *Fundamentals of Metal Machining and Machine Tools*. McGraw-Hill, 1981.
- [36] X. D. Fang, J. Fie, and I. S. Jawahir, "A hybrid algorithm for predicting chip form/chip breakability in machining," *Int. J. of Mach. Tools and Manuf.*, vol. 36, no. 10, pp. 1093–1107, 1996.
- [37] W. Kluft, W. Konig, C. A. van Luttervelt, K. Nakayama, and A. J. Pekelharing, "Present knowledge of chip control," *Ann. CIRP*, vol. 28, no. 2, pp. 441–455, 1979.
- [38] Y. L. Yao and X. D. Fang, "Assessment of chip forming patterns with tool wear progression in machining via neural networks," *Int. J. of Mach. Tools & Manufact.*, vol. 31, no. 1, pp. 89–101, 1993.
- [39] V. P. Astakhov, S. V. Shevets, and M. O. M. Osman, "Chip structure classification based on mechanics of its formation," *J. of Mat. Proc. Tech.*, vol. 71, pp. 247–257, 1997.
- [40] B. Worthington, "The operation and performance of groove-type chip forming device," *Int. J. Prod. Res.*, vol. 14, no. 5, pp. 529–558, 1976.
- [41] B. Worthington and M. H. Rahman, "Predicting breaking with groove type breakers," *Int. J. Mach. Tool Des. and Res.*, vol. 19, pp. 121–132, 1979.
- [42] J. Shinozuka, T. Obikawa, and T. Shirakashi, "Chip breaking analysis from the view point of the optimum cutting tool geometry design," *J. of Mat. Proc. Tech.*, vol. 62, pp. 345–351, 1996.

-
- [43] B. Worthington, "The effect of rake face configuration on the curvature of the chip in metal cutting," *Int. J. Mach. Tool Des. Res.*, vol. 15, pp. 223–239, 1975.
- [44] X. D. Fang and I. S. Jawahir, "An analytical model for cyclic chip formation in 2-d machining with chip breaking," *Ann. CIRP*, vol. 45, no. 1, pp. 53–58, 1996.
- [45] J. D. Kim and O. B. Kweun, "A chip breaking system for mild steel in turning," *Int. J. of Mach. Tools & Manufact.*, vol. 37, no. 5, pp. 607–617, 1997.
- [46] J. L. Andreasen and L. D. Chiffre, "An automatic system for elaborationn of chip breaking diagrams," *Ann. CIRP*, vol. 47, no. 1, pp. 35–40, 1998.
- [47] P. K. Venuvinod and A. Djordjevich, "Towards active chip control," *Ann. CIRP*, vol. 45, no. 1, pp. 83–86, 1996.
- [48] E. Henriksen, "Right chip breaker-metal cutting must," *Steel*, vol. 17, p. 134, 1954.
- [49] E. Henriksen, "Chip breaker dimensions are critical in taming chips," *American Machinist*, vol. 98, no. 9, p. 117, 1954.
- [50] K. Okushima, T. Hoshi, and T. Fujinawa, "On the behaviour of chip in steel cutting- the case of the parallel type chip breaker," *JSME*, vol. 3, no. 10, p. 199, 1960.
- [51] K. Nakayama, "Pure bending test of chip- an approach to the prediction cutting force," *Bul. of the Faculty of Engg., Yokohama Nat. University*, pp. 83–88, 1963.
- [52] H. Takayama, H. Sekiguchi, and H. Takada, "One solution for chip hazard in turning- study on automatic programming for numerically controlled machines (first report)," *JSPE*, vol. 36, no. 2, pp. 150–156, 1970.
- [53] I. S. Jawahir, *An Experimental and Theoretical Study of the Effects of Tool Restricted Contact on Chip Breaking*. PhD thesis, University of New South Wales, 1986.

-
- [54] S. M. Athavale and J. S. Strenkowski, "Material damage based model for predicting chip breakability," *J. of Manuf. Sc. and Eng.*, vol. 119, pp. 675–680, Feb 1997.
- [55] W. Grzesik and E. Kwiatkowska, "An energy approach to chip-breaking when machining with grooved tool inserts," *Int. J. Mach. Tools and Manuf.*, vol. 37, no. 5, pp. 569–577, 1997.
- [56] J. A. Yang, S. M. Athavale, and J. S. Strenkowski, "A finite element chip breaking model for groove tools," *Mathematical Modelling and Science Computing in Sc. and Technology*, vol. 6, 1996.
- [57] J. A. Yang, *A Predictive Model of Chip Breaking for Groove - Type Tools in Orthogonal Machining of AISI 1020 Steel*. PhD thesis, North Carolina State University, 1992.
- [58] P. L. B. Oxley and W. F. Hastings, "Minimum work as a possible criterion for determining the frictional conditions at the tool/chip interface in machining," *Phil. Trans. R. Soc. Lond.*, vol. A 282, p. 565, 1976.
- [59] M. E. Merchant, "Mechanics of the metal cutting process ii, plasticity conditions in orthogonal cutting," *J App. Phys.*, vol. 16, pp. 318–324, 1945.
- [60] N. N. Zorev, "Interrelationship between shear processes occurring along tool face and on shear plane in metal cutting," *Proc. Conf. Int. Res. Production Engng., ASME, New York*, p. 42, 1963.
- [61] T. Childs, "Elastic effects in metal cutting chip formation," *Int. J. Mach. Tools and Manuf.*, vol. 22, no. 8, pp. 457–466, 1980.
- [62] T. C. H. Childs and M. I. Mahdi, "On the stress distribution between the chip and tool during metal cutting," *Ann. CIRP*, vol. 38, p. 55, 1989.
- [63] S. Kato, K. Yamaguchi, and M. Yanda, "Stress distribution at the interface between tool and chip in machining," *J. Eng. Ind., Trans. ASME*, vol. 94, pp. 683–689, 1972.

-
- [64] G. Barrow, W. Graham, T. Kurimoto, and Y. F. Leong, "Determination of rake face stress distribution in orthogonal machining," *Int.J.Mach.Tool Des.Res.*, vol. 22, pp. 75–85, 1982.
- [65] H. Chandrasekaran and D. V. Kapoor, "Photo-elastic analysis of tool -chip interface stresses," *ASME J. of Eng. for Ind.*, vol. 87, pp. 495–502, 1965.
- [66] A. Bagchi and P. K. Wright, "Stress analysis in machining with use of sapphire tools," *Proc. R. Soc. London A*, vol. 409, pp. 99–113, 1987.
- [67] T. Kattawinkel, "Untersuchungen an schneiden speanender werkzeuge mit hiffle der spannungsoptic," *Industr. Anzeiger*, vol. 37, pp. 29–33, 1957.
- [68] E. Usui and T. Shirakashi, "Mechanics of machining- from descriptive to predictive theory," *ASME PED*, vol. 7, pp. 13–35, 1982.
- [69] I. Finnie and M. C. Shaw, "The friction process in metal cutting," *Trans ASME*, vol. 78, pp. 1649–1657, 1956.
- [70] K. Maekawa, T. Kitagawa, and T. H. C. Childs, "Friction characteristics at tool-chip interface in steel machining," *23rd Leeds Lyon Symposium on Tribology*, pp. 559–567, 1997.
- [71] Wanheim, "Friction at high normal pressures," *Wear*, vol. 25, pp. 225–244, 1973.
- [72] P. Dewhurst and I. F. Collins, "A matrix method for constructing slip-line field solutions to a class of plane strain plasticity problems," *Int.J.Numer.Meth. Engng.*, vol. 7, pp. 357–378, 1973.
- [73] P. Dewhurst, "The coulomb friction boundary value problem in plain-strain slip-line field theory," *Advanced Technology of Plasticity*, vol. II, pp. 1085–1090, 1984.
- [74] P. Dewhurst, "A general matrix operator for linear boundary value problems in slip-line field theory," *Int.J. for numerical Methods in Eng.*, vol. 21, pp. 169–182, 1985.

-
- [75] A. G. Atkins, G. W. Rowe, and W. Johnson, "Shear strains and strain-rates in kinematically admissible velocity fields," *Int. J. Mech. Engg. Edu.*, vol. 10, no. 4, pp. 133–141, 1982.
- [76] J. Chakrabarty, *Theory of Plasticity*. McGraw-Hill, 1998.
- [77] R. Hill, *Mathematical Theory of Plasticity*. Oxford University Press, 1950.
- [78] W. Johnson, R. Sowerby, and R. D. Venter, *Plain strain slip-line fields for metal deformation processes*. Pergamon Press, 1982.
- [79] W. Johnson, R. Sowerby, and J. B. Haddow, *Plain strain slip-line fields- Theory and Bibliography*. Edward Arnold (Publishers) Ltd., 1986.
- [80] I. F. Collins, "The algebraic-geometry of slip-line fields with applications to boundary value problems," *Proc.Roy.Soc.*, vol. A-303, pp. 317–338, 1968.
- [81] R. D. Venter, R. L. Hewitt, and W. Johnson, "An engineering approach to the matrix operator technique for slip-line field construction," *North American Metal Working Research Conference VI*, April 1978.
- [82] D. J. F. Ewing, "A series method for constructing plastic slip-line fields," *J. Mech. Phys. Solids*, vol. 15, p. 105, 1967.
- [83] M. C. Shaw, N. H. Cook, and I. Finnie, "The shear angle relationship in metal cutting," *Trans. ASME*, vol. 75, pp. 273–288, 1953.
- [84] R. Hill, "The mechanics of machining a new approach," *J. Mech. Phys.Solids*, vol. 3, pp. 47–53, 1954.
- [85] K. Okushima and K. Hitomi, "An analysis of mechanism of orthogonal cutting and its application to discontinuous chip formation - (shear zone theory).," *Trans. ASME*, p. 545, 1961.
- [86] K. P. Maithy and N. S. Das, "A class of slip-line field solutions for metal machining with elastic contact," *J. of Mat. Proc. Tech.*, vol. 96, pp. 9–18, 1999.

-
- [87] K. P. Maithy and N. S. Das, "A slip-line solution to metal machining using a cutting tool with a step-type chip-breaker," *J. of Mat. Proc. Tech.*, vol. 79, pp. 217–223, 1998.
- [88] K. P. Maithy and N. S. Das, "A slip-line solution to metal- machining with chip- breaker assuming coulomb friction at the chip-tool interface," *J. Inst. of Engrs. (India)*, vol. 80, pp. 15–17, May 1999.
- [89] L. J. Kuester and H. J. Mize, *Optimization Techniques with Fortran*. McGraw-Hill, 1973.
- [90] R. Hill, "On the vectorial superposition of hencky-prandtl nets," *J. Mech. Phy. Solids*, vol. 15, p. 255, 1967.
- [91] N. S. Das, B. S. Chawla, and C. K. Biswas, "An analysis of strain in chip breaking using slip-line field theory with adhesion friction at chip/tool interface." Accepted for publication in *J. of Mat. Proc. Tech.*, UK.
- [92] A. R. Trim and G. Boothroyd, "Action of the obstruction type chip former," *Int. J of Prod.Res.*, vol. 6, no. 3, pp. 227–240, 1968.
- [93] T. L. Subramanian and A. Bhattacharya, "Mechanics of chip breaker," *Int. J. of Prod. Res.*, vol. 4, no. 1, pp. 227–240, 1965.
- [94] C. Spaans and A. Goedemondt, "The breakability as an aspect of machinability- a computer simulation of chip formation," *Society of Manufacturing Engineers*, vol. MR71, p. 154, 1971.
- [95] M. Rahman, K. Seah, and et al., "A three-dimensional model of chip flow, chip curl and chip breaking under the concept of equivalent parameters," *Int. J. of Mach. Tools & Manufact.*, vol. 35, no. 7, pp. 1015–1031, 1995.
- [96] B. Worthington, "Surface integrity, cutting forces and chip formation when machining with double rake angle tools," *Int. J. Mach. Tool Des. And Res.*, vol. 14, pp. 279–295, 1974.
- [97] X. D. Zhang, L. C. Lee, and K. H. W. Seah, "Knowledge base for chip management system," *J. Mat. Proc. Tech.*, vol. 48, pp. 215–221, 1995.

-
- [98] T. Shi and S. Ramalingam, “Modeling chip formation with grooved tools,” *Int. J. of Mech. Sc.*, vol. 35, no. 9, pp. 741–756, 1992.
- [99] N. S. Das and S. T. Dundur, “Slipline field solutions for metal machining with adhesion friction and elastic effects at the chip-tool contact region,” *Proc. I.Mech. E., J. Eng. Manuf.*, vol. 219, pp. 57–72, 2005.
- [100] E. Henriksen, “How to select chip breakers,” *American Machinist*, pp. 179–181, May 1954.
- [101] F. J. Gardiner, “The spring back of metals,” *ASME J. of Eng. For Ind.*, pp. 1–9, Jan 1957.
- [102] W. Johnson and P. B. Mellor, *Plasticity for Mechanical Engineers*. Van Nostrand, 1962.
- [103] K. Kumar and R. C. Ghai, *Advanced Mechanics of Materials*. Khanna Publishers, 1998.

PUBLICATIONS

Papers Accepted for Publication:

1. N S Das, B S Chawla, and C K Biswas “An analysis of strain in chip breaking using slip-line field theory with adhesion friction at chip/tool interface,” *J. of Mat. Proc. Tech.,UK*, 2005.

Papers communicated to International and National Journals:

1. N S Das, B S Chawla, and C K Biswas “An evaluation of chip breakability criteria using slip-line field analysis,” *Int. J. of Mach. Tools & Manufact.,UK*, 2005.
2. B S Chawla, C K Biswas, N S Das and I K Khanna “Analytical Prediction and Experimental Validation of Cutting Parameters and Breaking Strain, Using Slip-Line Field Analysis,” *J. of Institution of Engineers (India)* , 2005.
3. C K Biswas, E R K N K Srinivas, B S Chawla and I K Khanna “ Flank Wear Estimation by Neuro-Fuzzy System using Force Ratio,” *J. of Institution of Engineers (India)* , 2005.

BIODATA

Name: BALBEER SINGH CHAWLA
Designation : Q I P Research Scholar,
Mechanical Engineering Department,
National Institute of Technology,
ROURKELA- 769 008 (India).

Present Position: Reader and Head,
Department of Mechanical Engineering,
Government Engineering College,
BILASPUR - 495001 (India)

Academic qualifications :B. E. (Mech)(Hons), RaviShankar University,
Raipur (India),1981

M. Sc. (Engg), Sambalpur University,
Jyoti Vihar, Burla (India), 1991